Decay of bow thruster induced near-bed flow velocities at a vertical quay wall

A field measurement
J. W. T. Tukker

Decay of bow thruster induced near-bed flow velocities at a vertical quay wall

A field measurement

by

J.W.T. Tukker

in partial fulfillment of the requirements for the degree of Master of Science

at the Delft University of Technology,

to be defended publicly on Tuesday June 8, 2021 at 11:45.

Student number   4302818
Project duration: June 15, 2020 – June 8, 2021
Thesis committee: Dr. ir. B. Hofland   TU Delft
                     Ir. A.J. van der Hout   TU Delft
                     Ir. J.P. van den Bos   TU Delft
                     Ir. M. Ruijter   Rijkswaterstaat
                     Ir. C.V.A. van der Vorm-Hoek Rijkswaterstaat

TUDelft

Rijkswaterstaat
Ministerie van Infrastructuur en Waterstaat

Preface

This master thesis concludes my time as a student at Delft University of Technology and completes my Master of Science program in Civil Engineering in the track 'Hydraulic Engineering'. On June 15th, I started this project and for the first two months I mainly focused on preparing the field measurements in the North Sea Port of Gent. As the quay wall was only available for one week at the end of September, it was my job to make sure the measurement programme and set-up were ready by that time. Working together with the Rijkswaterstaat team, Boskalis divers and the crew of the Somtrans XXV during the field measurements was an amazing experience which I will remember as the highlight of my master thesis. The Dutch and Belgium COVID measures almost prohibited the field measurements but I'm glad that with the necessary safety measures we found a way to conduct the field measurements during the pandemic. Although due to the Dutch COVID restrictions I have never stepped inside the Rijkswaterstaat office in Utrecht, I'm grateful that Rijkswaterstaat provided me with the opportunity for this graduation thesis. The past 12 months have been extremely educational, interesting and pleasant. However, I had never imagined that I would be writing my thesis almost entirely from my bedroom in Rotterdam.

This master thesis would not have been possible without the help of a lot of people. First of all, I would like to thank my chair, Bas Hofland, for his enthusiasm and knowledge on bow thrusters and bed protections. Who even drove all the way to Gent for one day to give advice and assist with the measurements. I would like to thank the other committee members: Arne van der Hout, for his scientific view on the project, always asking the right questions and making sure I thoroughly understood what I was doing. Jeroen van den Bos, for his designers approach. Pushing me to think one step further about the applicability of my research and findings in the field. I would like to thank Charlotte van der Vorm-Hoek, for keeping me structured and advising me on a weekly basis. Finally, I would like to thank Michel Ruijter for guiding me through this thesis with his knowledge and practicality in measuring in the field. Making sure the instruments functioned correctly by testing them with me on a sunny day of measuring on his boat.

Being part of the CROW joint research programme, aimed at researching the knowledge gaps on propeller jets to optimize bed protections in ports and waterways, has been a great opportunity. Their advice and feedback contributed to the success of the field measurements in Gent resulting in a unique and extensive data set of full-scale bow thruster measurements.

I'd like to finish off this acknowledgement with a special thanks to my friends and family. Providing me with distractions and side activities besides my thesis. Telling me to close my laptop and enjoy the weekends, so I could start the week fresh on Mondays. And last but not least, thank you Guusje, for hearing me go on and on about bow thrusters for 12 months and for your support.

J.W.T. Tukker
Rotterdam, June 2021

Summary

During berthing operations vessels use their bow thruster(s) to improve their manoeuvrability, making them less dependent on the assistance of tugboats. The jet from a bow thruster reflects on the quay wall. It is directed towards the bottom where it reflects, causing high flow velocities over the bed. This may scour the nearby bed when it is left unprotected, leading to instability of the quay wall. Over the years, the shipping industry has been developing continuously, characterized primarily by the upscaling in size of inland- and sea-going vessels. As a result, vessels have more power and larger thruster diameters leading to higher hydraulic loads on quay walls and bed protections of berthing facilities. The most common type of bed protection is rip-rap (partially) penetrated with concrete. However, due to the complex flow field of the reflected jet, the decay profile of the near-bed flow velocities is unknown. This results in uncertainties in the design of bed protections and the required width of these protections that must be penetrated with concrete.

In this research, the decay of the near-bed flow velocity in perpendicular direction to the quay wall induced by a 4-channel bow thruster, commonly used by inland vessels, is researched. The eventual goal is to provide a better indication to what extent the bed protection must be penetrated with concrete. Field measurements have been conducted in the Port of Gent with the Somtrans XXV, one of the largest inland vessels in the Netherlands. The flow velocities near the bed, induced by the bow thruster, have been measured with Acoustic Doppler Velocimeters (ADV), Acoustic Doppler Current Profilers (ADCP) and Ott meters (Ott) placed on the bed within 10 m from the quay wall. In addition, the decay in pressure fluctuations over the quay wall and the bed has been measured with pressure sensors. The results from the flow velocity measurements have been analyzed on three main parameters: influence of the applied bow thruster power (P_t), the distance between the measurement instrument frame and the bow thruster (y_t) and quay wall clearance (L_{BT}). The results are compared with current guidelines and previous research to place the findings in perspective to literature.

The highest flow velocities are measured near the quay wall. At this location, the mean flow velocities are generally in the order of 1 m/s reaching up to a maximum of 1.8 m/s. Further away from the quay, the flow rapidly declines towards a more constant level of approximately 0.3-0.4 m/s. Close to the quay wall, the flow is highly turbulent while displaying a similar decline in standard deviation as observed for the mean flow velocity. This leads to constant relative turbulence intensities in the range of 0.3-0.6. To define the maximum load on the bed, the mean flow velocity plus three times the standard deviation is used resulting in a maximum load ranging between 1.6-2.8 times the mean horizontal flow velocity. Additionally, it was found that increasing the applied power of the bow thruster results in a higher maximum load while in general a lower maximum load is observed for larger quay wall clearances. Further results include that the largest maximum loads are not measured directly underneath the bow thruster axis but at a negative distance y_t towards the stern of the vessel.

The Dutch and German guidelines for determining the near-bed flow velocities generally overestimate the measurement results. In addition, the dependency of the Dutch method on the total travelled distance by the jet (x_s), based on the sum of the quay wall clearance (L_{BT}), the height of the bow thruster above the bed (h_t) and the distance x from the quay wall, are not reflected in the measurement results. For every measurement test, the Dutch method overestimates the measured horizontal mean flow velocity with an average discrepancy of 3.7 times the measured horizontal mean flow velocity. The German method overestimates the mean flow velocity in x-direction for small quay wall clearances while underestimating the flow velocity for larger quay wall clearances.

It is recommended that this unique data set acquired through the field measurements in Gent is further used to analyze the flow field of a reflected jet on a vertical quay wall by validating numerical and scale models. Combining these three different methodologies will contribute to a better understanding of this phenomenon with the eventual goal of optimizing the design of bed protections.

Contents

Nomenclature

α	coefficient for determining the efflux velocity V_0 of a bow thruster	-
$\Delta\phi$	phase difference between received echo's by the Doppler measurement instrument	rad
Δt	time difference	s
$\overline{V}_{\text{hor,Dutch}}$	mean near-bed flow velocity in horizontal direction for the Dutch method	m/s
$\overline{V}_{\text{x,German}}$	mean near-bed flow velocity in x-direction for the German method	m/s
$\overline{V}_{\text{x,Schmidt}}$	mean near-bed flow velocity in x-direction for the measurements by Schmidt (1998)	m/s
ρ_w	density of water	kg/m^3
σ_{hor}	standard deviation of V_{hor} defined as $\sqrt{\sigma_x^2 + \sigma_y^2}$	m/s
σ_{pres}	standard deviation of the pressure	m
σ_x	standard deviation of V_x	m/s
σ_y	standard deviation of V_y	m/s
a	coefficient for the length of the flow establishment region	-
a_L	coefficient for the German method to determine near-bed velocities	-
b	coefficient for the radial expansion of the flow field	-
C	Chezy's coefficient	$m^{1/2}/s$
C_1	coefficient for the efflux velocity of the jet	-
C_2	coefficient for the flow establishment length	-
C_{sound}	speed of sound in water	m/s
D_0	effective diameter computed with $D_p/\sqrt{2}$	m
D_p	propeller diameter	m
D_t	circular thruster diameter of the thruster outlet. For the rectangular thruster channel D_t is the equivalent thruster diameter of the outlet having the same cross-sectional area calculated with $\sqrt{4 \cdot \text{Width} \cdot \text{height}/\pi}$	m
D_{or}	orifice Diameter	m
f_p	percentage of installed engine power	-
F_{doppler}	Doppler frequency shift	Hz
F_{source}	frequency of the transmitted sound wave by the ADV/ADCP	Hz
f_{nyq}	Nyquist frequency of the measurement instrument ($f_{nyq} = fs/2$)	Hz
fs	sampling frequency of the measurement instrument	Hz
h	water depth	m
h_t	height of the thruster axis above the bed	m
K_T	thrust coefficient	-
k_t	turbulence factor	-

L	Distance between the port side of the vessel and the quay wall	m
L_{BT}	quay wall clearance between the considered bow thruster outlet and the quay wall	m
n	number of revolutions of the propeller	1/s
P_t	installed power of the bow thruster	kW
P_D	installed engine power	kW
r	radial distance from the jet axis	m
r_x	relative turbulence intensity of V_x defined as $\sigma_x/\overline{V}_x$	-
r_y	relative turbulence intensity of V_y defined as $\sigma_y/\overline{V}_y$	-
r_{hor}	relative turbulence intensity of V_{hor} defined as $\sigma_{hor}/\overline{V}_{hor}$	-
V	flow velocity	m/s
V_0	theoretical efflux velocity of the bow thruster jet. For two bow thrusters together (BT1&2) V_0 is multiplied with $\sqrt{2}$ by means of quadratic superposition	m/s
V_b	near-bed flow velocity	m/s
V_x	flow velocity in x-direction	m/s
V_y	flow velocity in y-direction	m/s
V_z	flow velocity in z-direction	m/s
$V_{max,in}$	maximum measured instantaneous horizontal flow velocity	m/s
V_{axis}	flow velocity in the axis of the jet	m/s
V_{max}	maximum horizontal flow velocity defined as $\overline{V}_{hor} + 3\sigma_{hor}$	m/s
V_{hor}	horizontal flow velocity near the bed defined as $\sqrt{V_x^2 + V_y^2}$	m/s
x	horizontal distance over the bed perpendicular to the quay wall	m
x_0	length of the flow establishment zone	m
x_s	total distance travelled by the jet defined as the sum of L_{BT}, h_t and x	m
x_t	distance x along the axis of the jet where the flow velocity is measured	m
ADCP	Acoustic Doppler Current Profiler	
ADV	Acoustic Doppler Velocimeter	

List of Figures

List of Tables

1

Introduction

1.1. Context

Over the years, maritime transport has been growing substantially to satisfy the demand in world transport. The international maritime trade has increased from 4.000 million tons loaded cargo in 1990 to more than 11.000 million in 2018. Growing with 275% in less than 30 years (UNCTAD, 2020). As a result, the shipping industry has been developing continuously, characterized primarily by the upscaling of inland- and sea-going vessels (OECD, 2015; Panteia, 2017; Looye, 2021). In a port, vessels berth at a quay wall to transfer their cargo or passengers. During berthing operations vessels use their bow thruster(s) to improve their manoeuvrability, making them less dependent on the assistance of tugboats. Bow thrusters are positioned in a duct near the bow, perpendicular to the axis of the vessel (Figure 1.1). The rotating propeller draws in water, accelerates and then discharges this water to provide a lateral thrust which allows for manoeuvring at low speed (Lam et al., 2011a). The jet from the bow thruster reflects on the quay wall and is directed towards the water surface and the bed (Figure 1.1). At the bottom, the jet reflects again causing high flow velocities above the bed directed away from the quay wall. This may scour the nearby bed, which can eventually lead to instability of the quay wall when the bed is left unprotected (Roubos and Verhagen, 2007). The bed is especially prone to scouring when vessel manoeuvres have a long duration or when a lot of vessels manoeuvre at the same location. This occurs at quay walls in ports or at mooring places nearby a lock or bridge. To prevent scour from developing, bed protections are designed based on the bow thruster induced flow velocities near the bed.
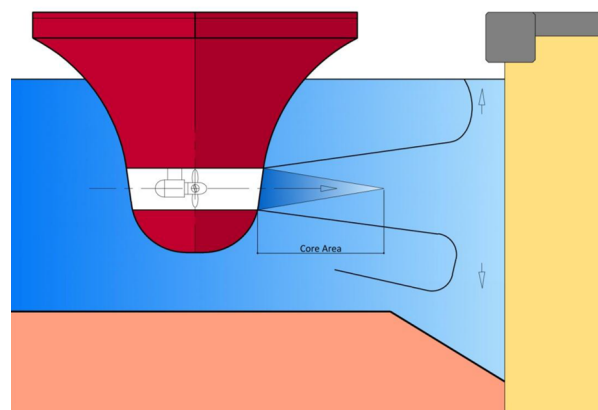
Figure 1.1: Schematization of a vessel (in red) berthing at a quay wall (in yellow) at a port while using its bow thruster. The propeller jet from the bow thruster reflects at the quay wall towards the the bed scouring the bed material(PIANC, 2015).

Throughout time the loads on harbour bottoms and quay walls have increased. The higher loads, defined as the jet flow above the bed, can be ascribed to two developments in the shipping industry. Firstly, modern vessels are equipped with bow (and stern) thrusters besides their main propulsion system. Secondly, due to upscaling in the shipping industry vessels have larger draughts, increased bow thruster diameters and more available bow thruster power (Roubos and Verhagen, 2007). During berthing, vessels with a larger draught confine the flow between the vessel and the bed causing higher flow velocities near the bed. The increased bow thruster diameter and more available bow thruster power result in higher outflow velocities (Van der Vorm, 2020).

Albertson et al. (1950) suggested a submerged jet could be investigated with a plain water jet from an orifice. This research formed the basis for all subsequent research on propeller jets (Lam et al., 2011a). However, a ships propeller jet is more complicated than a plain jet. The complex flow pattern caused by the propeller jet is characterized by mixing layers, diffusion and turbulence. Research on unconfined propeller jets has been carried out by (Fuehrer and Römisch, 1977), (Blaauw and van de Kaa, 1978), (Berger et al., 1985), (Verheij, 1983) and (Hamill, 1987) using scale models. Less attention has been given to research on confined propeller jets in close proximity of lateral restrictions, such as a vertical quay wall, the bed or the ship's hull (Wei and Chiew, 2019). Therefore, there are still several knowledge gaps on confined propeller jets (De Jong and Van Velzen, 2015). The complex flow field of a propeller jet must be fully understood to quantify scouring damage on the bed and design corresponding bed protections to prevent further damage (Hamill and Kee, 2016).

Knowledge on flow velocities near the bed, turbulence intensities and their spatial development are used as input for the bed protection design. Currently, the design of bed protection is based on empirical knowledge used to predict flow velocities and scour formation. This knowledge is based on scale models, field measurements and experience which has been documented by analytical methods with coefficients calibrated and validated on measurement results. In the PIANC (2015) guidelines, the state-of-the-art knowledge on the damaging effects of propeller jet on bed, bank and quay structures is summarized (De Jong and Van Velzen, 2015). In the guidelines two methods, the Dutch and the German, are prescribed for the design of bed protections. The German method is based on research by Fuehrer et al. (1981) and Schmidt (1998), whereas the Dutch method is based on research by Blaauw and van de Kaa (1978), Verheij (1983) and Blokland (1996). Both methods result in different outcomes for flow velocities and bed protection dimensions. Furthermore, the methods are based on limited vessel configurations and bow thruster types. Consequently, designing bed protections with these guidelines can lead to both under and over dimensioning of the bed protection.

In recent years, research on propeller jet loads gained interest starting in 2015 with SBRCURnet identifying fifteen knowledge gaps on propeller jet loads at bed and bank protections. Deltares, an independent research institute based in the Netherlands, continued on this study by researching the knowledge gap 'Reflection of transverse jets by vertical quay walls' by means of a scale model in 2015 (De Jong and Van Velzen, 2015). In 2017, on the initiative of Rijkswaterstaat, exploratory research was carried out by Deltares to prioritize the knowledge gaps defined by SBRCURnet and initiate more systematic research on propeller jet loads. The first field measurements of the research program (Section 1.4) were carried out in 2018 at the Antarticakade in the Port of Rotterdam. The objective of this research was to explore measurement techniques for measuring the flow velocity in a propeller jet (Van der Hout, 2018). Building on the experience gained by Van der Hout (2018), field measurements were conducted in June 2019 with one of the largest inland vessels in the Netherlands. Cantoni (2020) explored the flow velocities near the bed induced by the reflected propeller jet of the bow thruster by placing a measurement frame on the bed. Based on the experience and recommendations of Cantoni (2020) new field measurements were initiated by Rijkswaterstaat that took place at the end of September 2020 as part of this thesis.

1.2. Problem statement

The problem statement can be split into two parts. first, the general problem regarding the complex flow field of a reflected propeller jet on a vertical quay wall is elaborated after which the specific problem, that will be researched in this thesis, relating to the extent of the flow velocity near the bed induced by the reflected propeller jet is discussed. By researching the specific problem a contribution is made to the ongoing research on reflected propeller jets with the eventual goal of solving the general problem: understanding the complex flow field of the reflected propeller jet on a vertical quay wall to optimize the design of bed protections.

More generally, propeller jets induce complex three-dimensional flow patterns which are not yet fully understood. This is especially the case when the propeller jet is in close proximity of lateral restrictions such as a vertical quay wall, the bed or the ship's hull. These lateral restrictions of the propeller jet are present during berthing operations in ports where the propeller jet reflects on the vertical quay wall as seen in Figure 1.1. Various research has been carried out to better understand the flow field of a reflected propeller jet with the eventual goal of determining design formulas for bed protections against propeller jet induced scour in close proximity of the quay wall. Nevertheless, there is a multitude of uncertainties in the current design guidelines summarized in PIANC (2015) which provide an estimate of flow velocities near the bed and dimensions of the bed protection near a vertical quay wall. There are uncertainties in the input variables, such as the manoeuvring behaviour of the vessel and used bow thruster power, and uncertainties as a result of schematizing complex three-dimensional flow patterns in two-dimensions with simple analytical formulas based on a limited number of measurements. Besides, a limited number of ship configurations, applied power steps, propeller types, wall clearances and keel clearances have been researched. Hence, the current design methods are not necessarily describing the most common or normative hydraulic load situation on the bed during berthing procedures at a vertical quay wall. Thus, questions can be raised whether the current guidelines provide the most optimized design for bed protections near berthing structures. The uncertainties in the design guidelines give designers a lot of freedom in the design of bed protections which could lead to both under and over dimensioning of bed protections. Concluding, the complex three-dimensional flow field of a reflected propeller jet is not yet fully understood and described with analytical formulas in a two-dimensional space considering a limited range in parameter settings and ship configurations.

For the more specific problem researched in this thesis, a distinction is made between inland- and sea-going vessels. For inland shipping the bed protection costs usually make up a larger part of the total infrastructure costs in comparison to maritime shipping (Van der Hout, 2017). Therefore, the focus of the problem in this thesis is on bed protections for inland waterways, which in the Netherlands falls under the responsibility of Rijkswaterstaat. Currently, a common way of placing bed protections is applying two layers of 10-60 kg rip-rap and penetrating it with colloidal concrete. This is a robust but costly solution that is required close to the quay wall, where the highest flow velocities are expected, but not at some distance further away from the quay wall where the flow velocities near the bed have reduced (Van der Vorm, 2020). The width of the bed protection is not a variable design parameter as it depends on the width of the passive soil wedge in front of the quay wall (PIANC, 2015). However, the width of the bed protection that is penetrated with colloidal concrete and the type of rip-rap needed for the bed protections are variable design parameters (Figure 1.2. To have an indication of the width that must be penetrated with concrete the velocity decay profile in perpendicular direction from the quay wall must be known. Nonetheless, there is not much known about the decay and extent of the flow velocities over the bed in perpendicular direction from the quay wall. This results in over dimensioning of the bed protection by penetrating the majority of the bed protection with colloidal concrete.
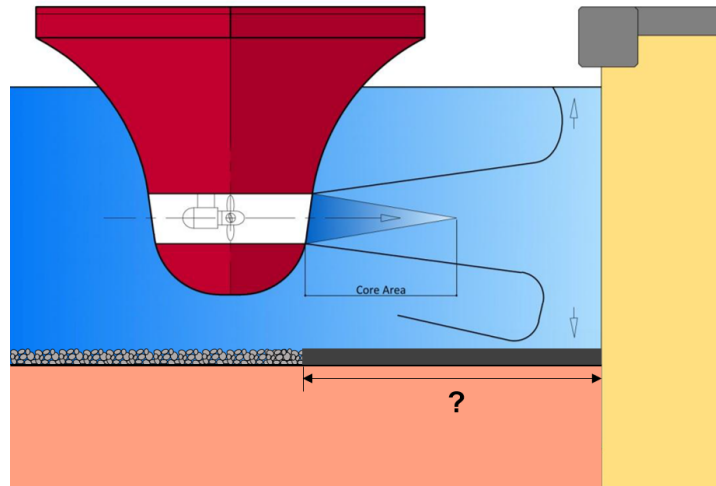
Figure 1.2: Schematization of a vessel (in red) berthing at a quay wall (in yellow) at a port while using its bow thruster. On the bed a bed protection is placed consisting out of only rip-rap on the left while on the right an undefined width (the question mark) is penetrated with colloidal concrete.

1.3. Objective
The objective of this research is to determine the decay of the near-bed flow velocities induced by a 4-channel bow thruster on a vertical quay wall. Knowledge of the flow velocity decay profile can give designers a better indication until which distance from the quay wall the bed protection must be penetrated with concrete. Thus, aiming to solve the more specific problem stated in Section 1.2. By solving the objective a contribution is made to the more general problem concerning a better understanding of the complex flow field of a propeller jet reflecting on a vertical quay wall. Investigating the decay and spatial distribution of the flow near the bed aims to give a more specific formulation of the flow velocity input to design bed protections. To achieve this objective the influence of the quay wall clearance and applied bow thruster power on the flow velocity near the bed is studied. Based on the objective, the following research question is specified:

- **How does the absolute horizontal flow velocity near the bed induced by the reflected jet of a 4-channel bow thruster on a vertical quay wall decay in perpendicular direction to the quay wall?**

Several sub-questions have to be resolved to answer the main research question:

- *What is the influence of the applied power, distance y_t, and quay wall clearance of the bow thruster on the absolute horizontal flow velocity decay near the bed?*

- *How does the proposed measurement set-up perform?*

- *What happens to the relative turbulence intensity moving from the quay wall in perpendicular direction?*

- *How do the measurement results of the flow velocity decay profile compare to previous research and guidelines?*

1.4. Background research program

This master thesis is part of a joint research program between CROW, Rijkswaterstaat, Deltares, MARIN, Boskalis, DEME, NorthSeaPorts, Loodswezen, TU Delft, BAM, Port of Rotterdam and Engineering Firm Rotterdam. The joint research project is initiated to facilitate more integral and systematic research on flow velocities and erosion caused by propeller jets. A long-term plan in the form a roadmap (Van der Vorm, 2020) is made to research the current knowledge gaps on propeller jets defined by SBRCURnet. The eventual goal of the joint research program is to improve current design guidelines and their uncertainties on bed protections as stated in the PIANC (2015). After successful field measurements in 2018 (Van der Hout, 2018) and 2020 (Cantoni, 2020), new field measurements took place in September 2020 to achieve the objective of this master thesis and gather measurement data to validate future Computational Fluid Dynamics (CFD) models and scale models. The next step after this thesis is to make a scale model (by Deltares) and a CFD model (by MARIN) based on set-up and results from the field measurement in September 2020. The three methodologies to research the near-bed flow velocities induced by a reflected propeller jet on a vertical quay wall (field measurements, scale model and CFD model) will be compared with each other and reviewed to develop a better understanding of this phenomenon.

1.5. Research method & thesis outline

To reach the objective of this master thesis field measurements are conducted with one of the largest inland vessels in the Netherlands. The vessel is equipped with a channel bow thruster system most commonly used by inland vessels in the Netherlands (Calizo Manaois, 2011). Field measurements with this kind of bow thruster system has only been carried out once before by Cantoni (2020). Following recommendations by Cantoni (2020) and members of the joint research program, a strategy for the new field measurements in September 2020 is developed.

After the introduction in this first chapter, a review of the current literature on bow thruster jets reflecting on a vertical quay wall is presented in Chapter 2 from which the knowledge gap and scope for this thesis are defined. In the literature review the different methods to determine the near-bed flow velocity are defined including the most important parameters influencing them. In Chapter 3, the measurement programme and instrument set-up for the field measurements are discussed. in Chapter 4, the data retrieved from the measurements is processed, determining the confidence level of the data sets and preparing the data for further analysing by calculating the statistical parameters for each test. The results for each measurement test are analyzed in Chapter 5 along with the influence of the applied bow thruster power, quay wall clearance and distance between the measurement instrument frame and the bow thruster axis on the near-bed flow velocities. In Chapter 6 the results are placed back in the literature framework by comparing them to previous research and guidelines. The main discussion points on the field measurements, pre-processing of the data and measurement results are elaborated in Chapter 7. To finalize, conclusions are drawn and recommendations for further research are proposed in Chapter 8.

<div align="right">

2

</div>

Literature review

In this chapter, an overview of the current literature on bow thrusters is given. Elaborating on the type of bow thrusters used during the field measurements, the flow field of the bow thruster jet, previous research on the reflection of the jet on a vertical quay wall and guidelines to determine the near-bed flow velocities induced by the reflected jet of the bow thruster.

2.1. Bow thruster

In the maritime industry, the most common used ship propulsion system is a propeller. Modern vessels are usually equipped with a main propeller to provide forward thrust and a transverse thruster which provides lateral thrust to the vessel. Transverse thrusters are usually placed in a duct perpendicular to the longitudinal axis of the ship at the bow (bow thruster) or at the stern (stern thruster), see Figure 2.1. The focus of this thesis will be on the transverse thruster placed at the bow of the ship. The bow thruster draws in water from one side of the vessel, accelerates and discharges the water on the other side of the vessel to generate a force perpendicular to the longitudinal axis of the ship. This allows for the turning and manoeuvring of the ship at very low speed without the assistance of a tugboat (Lam et al., 2011a).
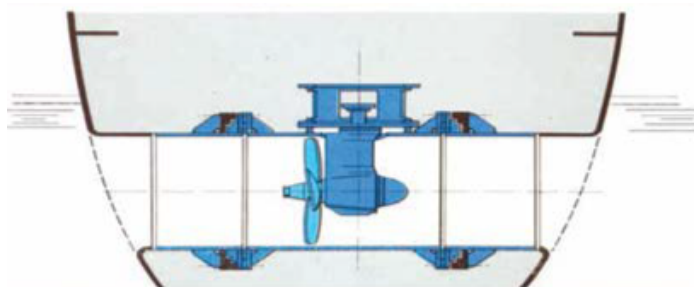
Figure 2.1: Traditional channel bow thruster mainly used for seagoing vessels (PIANC, 2015).

The bow thruster in Figure 2.1 is mostly used for seagoing vessels while inland vessels are mostly equipped with a channel bow thruster system as illustrated in Figure 2.2. The channel system bow thruster draws in water from the propeller placed in the horizontal plane underneath the vessel (Calizo Manaois, 2011). The water flows in through the horizontal propeller from where it is directed to one of the channels by a rotating drum after which it is discharged through the channel outlet providing thrust in the desired direction. The channel bow thruster has 2, 3 or 4 channels providing high manoeuvrability with 360 °of steering in case of the 4 channel bow thruster (Veth propulsion, 2020). The principle of the channel bow thruster system is elaborated in Figure 2.2.
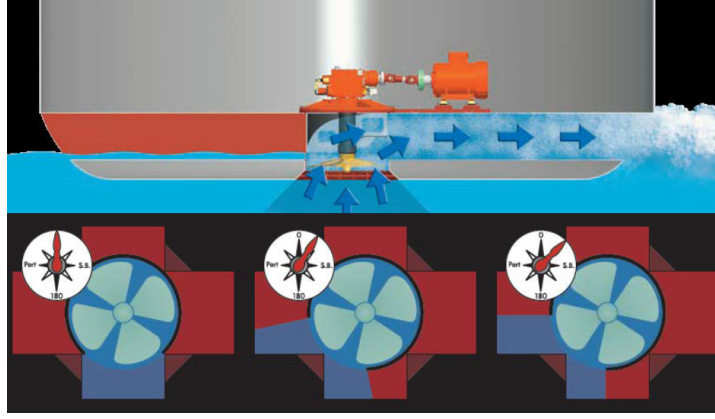
Figure 2.2: Veth Jet 4-channel bow thruster system (Veth propulsion, 2020).

2.2. Flow field unconfined propeller jet

In this section, the flow field of an unconfined propeller jet not restricted by any lateral boundaries is discussed. The propeller jet of the main propulsion system of a vessel has been researched extensively over the years and forms the basis for research on the reflected jet of a bow thruster.

2.2.1. Efflux velocity

The efflux velocity is defined as the velocity just behind the propeller or at the end of the channel in the case of a bow thruster channel system. An accurate determination of the efflux velocity for a propeller jet is of particular importance as the decay of the maximum velocity and the velocity distribution throughout the diffusing jet are related to it (Hamill et al., 2003). The efflux velocity is determined by means of *Froude's momentum theory* where the propeller is represented by an ideal actuator disc. This theory is used by both Blaauw and van de Kaa (1978) and Fuehrer and Römisch (1977) to determine the efflux velocity V_0 computed with Equation 2.1.

$$V_0 = \alpha \cdot n \cdot D_p \cdot \sqrt{K_T} \tag{2.1}$$

In Equation 2.1 α is a coefficient, n the number of revolutions of the propeller, D_p the diameter of the propeller and K_T the thrust coefficient derived from the Wageningen B- and K-series (Van Manen, 1956). Blaauw and van de Kaa (1978) and Fuehrer and Römisch (1977) found a value for α of 1.6 and 1.59 respectively. In many situations a value for the number of revolutions n or the thrust coefficient K_T is not known. Therefore, empirical relations have been derived to determine the efflux velocity such as Equation 2.2 presented by Blaauw and van de Kaa (1978) which is used in maritime engineering.

$$V_0 = C_1 \cdot \left(\frac{f_p \cdot P_D}{\rho_w \cdot D_p^2} \right)^{0.33} \tag{2.2}$$

In Equation 2.2 P_D is the installed engine power in Watt, f_p a percentage of the installed engine power, ρ_w the density of water, D_p the propeller diameter and C_1 a coefficient with a value of $C_1 = 1.17$ for ducted propellers and a value of $C_1 = 1.48$ for free propellers. For free propellers, the effective diameter can be written as $D_0 = D_p / \sqrt{2}$. Combining this with the value $C_1 = 1.48$ for free propellers results in $C_1 = 1.17$ which equals the value of $C_1 = 1.17$ for ducted propellers. As a result, Equation 2.2 can be written as Equation 2.3 for both types of propellers. In Equation 2.3 D_0 is replaced by the thruster diameter D_t as it is preferred to use physical characteristics that are most likely quoted by the manufacturer of the bow thruster (PIANC, 2015).

$$V_0 = 1.17 \cdot \left(\frac{P_t}{\rho_w \cdot D_t^2} \right)^{0.33} \tag{2.3}$$

In Equation 2.3 P_t is the thruster power and D_t the thruster diameter which can also be specified as $D_t = f_t \cdot D_p$ with $f_t = 1.02 - 1.05$. Thrusters can be regarded as free jets with an outflow opening for which the efflux velocity can be determined with Equation 2.3that will be used throughout this thesis.

2.2.2. Flow velocity field

The basis for research on the velocity field of a propeller jet has been the work of Albertson et al. (1950). This research was based on the axial momentum theory and suggested a submerged jet could be investigated by observations from a plain water jet from an orifice. In this situation, the flow is a free jet unrestricted by any boundaries. Jets are categorized by diffusion, mixing layers and turbulence due to decreasing flow velocities (Hoffmans and Verheij, 2011). The plain water jet can be categorized in a zone of flow establishment and established flow, see Figure 2.3. In the zone of flow establishment, the maximum velocity in the potential core is constant and equals the efflux velocity of the jet. The potential core is contracting due to turbulent mixing between the core and the surrounding fluid. In the zone of established flow, the maximum velocity in the axis of the propeller starts to decay as the turbulent mixing has penetrated into the axis of the jet.
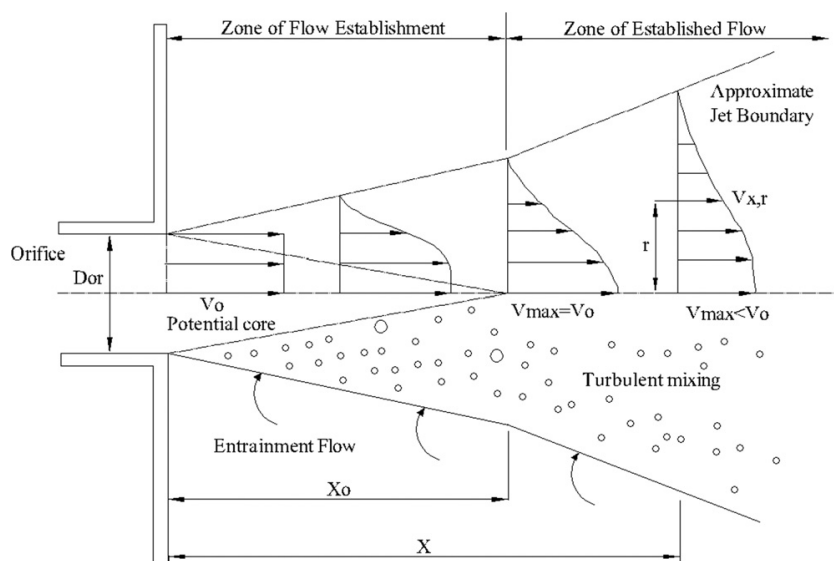
Figure 2.3: Illustration of a diffusing jet from an orifice. The zone of flow establishment is indicated with x_0 after which the zone of established flow begins (Albertson et al., 1950).

2.2.3. Comparison between a free jet and a propeller jet

Propeller jets accelerate the flow in axial radial and tangential directions. The flow field from a propeller jet can be compared to a free jet because of the diffusive character of both. However, there are also differences between the flow pattern of a propeller jet and a free jet. As the propeller jet is affected by rudders, ducts and lateral boundaries such as the bed and berthing structures. Besides this, the rotational flow velocity and the swirl at the tip of the propeller blades induce more turbulence, a shorter length of the flow establishment zone and a wider radial spread (Lam et al., 2011b). Verheij (1985) compared the free jet and the propeller jet with each other by looking at the difference in flow velocities, turbulence and divergence. As can be concluded from the left graph in Figure 2.4, the maximum velocities within the propeller jet start to reduce closer to the outflow point than the maximum velocity in the free jet, implying that the propeller jet is diverging more. When looking at the right graph in Figure 2.4 this is confirmed by the wider spread of the flow velocities in the radial direction. From Figure 2.5 can be concluded that the relative turbulence intensity (defined as the root mean square of the turbulent fluctuations divided by the mean flow velocity, Section 2.4) of approximately 30% is reached faster by the propeller jet than by the free jet, confirming that the propeller jet is diverging more and that the zone of flow establishment is shorter for the propeller jet. Verhagen (2001) also concluded from Figure 2.4 and 2.5 that the propeller jet is diverging more than a free jet.
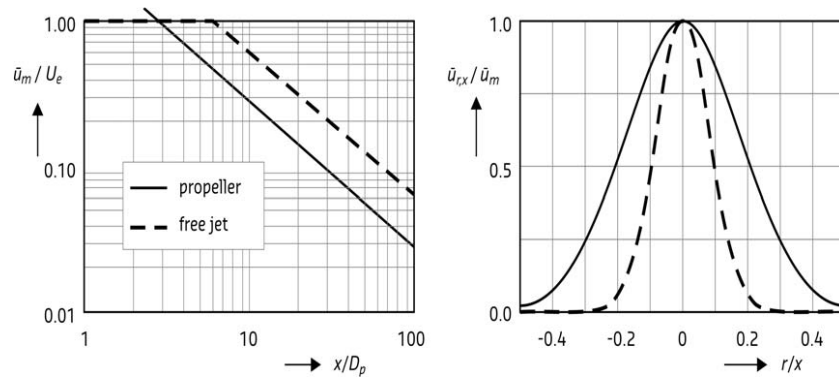
Figure 2.4: Difference in flow pattern between propeller and free jets (Verheij, 1985)
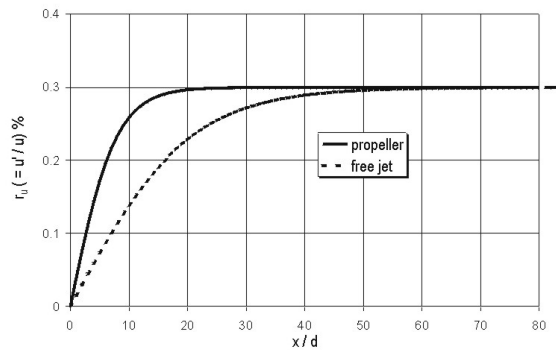
Figure 2.5: Relative turbulence intensity of a propeller and free circular jet (WL, 1985)

Based on the free jet theory from Albertson et al. (1950) other experimental research was conducted using physical scale models by among others Blaauw and van de Kaa (1978), Fuehrer et al. (1981), Berger et al. (1985), Verheij (1983) and Hamill (1987) to develop predicting equations for the velocity field of a ship's propeller jet.

2.2.4. Axial velocity distribution of a jet: Zone of flow establishment

Albertson et al. (1950) found that in the zone of flow establishment the velocities in the axis of the jet are constant and equal to the efflux velocity which can be determined with Equation 2.3. Therefore, Equation 2.4 is used in the zone of flow establishment to determine the axial velocity. An overview with the used definitions is given in Figure 2.6.

$$V_{\text{axis}} = V_0 \tag{2.4}$$

For the velocity in the jet at radial distance r from the axis Albertson et al. (1950) derived Equation 2.5. Where $V(x, r$ is the flow velocity at a distance x, in the axis direction, and radial distance r.

$$V(x, r) = V_{\text{axis}} \cdot \exp\left[-\frac{1}{2 \cdot C_2^2} \cdot \frac{r^2}{x^2}\right] \tag{2.5}$$

The length of the flow establishment zone is based on the distribution profiles of the axial component of the velocity in the jet axis direction (Bergh and Cederwall, 1981). Albertson et al. (1950) suggested that the axial velocity distribution is represented by two symmetrical halves of the probability function connected with a straight line through the central core. The limit of this zone was defined by Albertson et al. (1950) with Equation 2.6. Where x_0 is the limit of the zone of flow establishment (Figure 2.6), D_{or} the diameter of the orifice and the constant C_2 defined in Equation 2.7 with σ the standard deviation of the velocity profile in the lateral direction (Lam et al., 2011b).

$$\frac{x_0}{D_{or}} = \frac{1}{2 \cdot C_2} \tag{2.6}$$

$$C_2 = \frac{\sigma}{x_0} \tag{2.7}$$

Albertson et al. (1950) experimentally found that the limit of the zone of flow establishment occurred at $x_0/D_{or} = 6.2$ for a conventional pipe jet with a corresponding C_2 value of 0.081. Building on the research of Albertson et al. (1950), Fuehrer et al. (1987) experimentally found the zone of flow establishment to be much shorter for a propeller jet corresponding to $x_0/D_p = 2.6$ with $C_2 = 0.192$. Blaauw and van de Kaa (1978) found similar values for C_2 with $C_2 = 0.19$ for non-ducted propellers and $C_2 = 0.17$ for ducted propellers. The difference in C_2 for non-ducted and ducted propellers in the research of Blaauw and van de Kaa (1978) was assumed minimal. Therefore, calculations were carried out with $C_2 = 0.18$ resulting in $x_0/D_p = 2.8$ as the length of the flow establishment zone. Several other studies have defined a length for the zone of flow establishment, but research of Fuehrer et al. (1987) and Blaauw and van de Kaa (1978) have been mostly used and are described in the PIANC (2015) guidelines (Permanent International Commission for Navigation Congresses) as the German and Dutch method to determine the flow velocities in a propeller jet in unconfined circumstances.
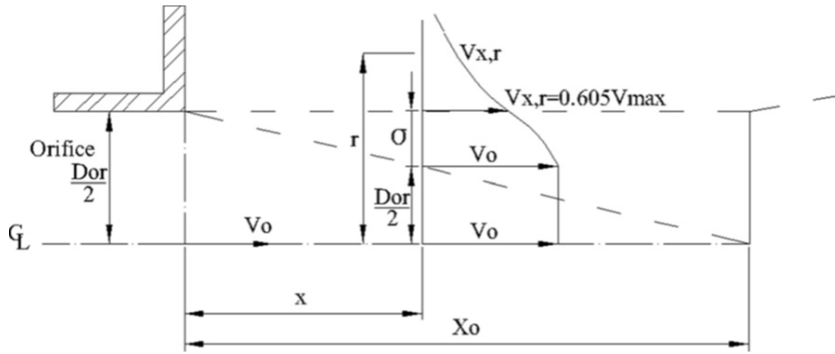
Figure 2.6: Zone of flow establishment of a free jet according to Albertson et al. (1950) (Lam et al., 2011b)

2.2.5. Axial velocity distribution of a jet: Zone of established flow
The zone of established flow as described by Albertson et al. (1950) is illustrated in Figure 2.7 with the corresponding definitions. The flow velocities in the axis of the jet of a conventional pipe jet are calculated with Equation 2.8. The radial velocity distribution at a distance x in the direction of the jet axis from the outflow point is determined with Equation 2.5 from Section 2.2.4.

$$V_{\text{axis}}(x) = \frac{1}{2 \cdot C_2} \cdot V_0 \cdot \frac{D_{or}}{x} \tag{2.8}$$

The flow velocities in the unconfined developed jet can be described in a more general form with Equation 2.9 for the velocities in the axis of the jet and Equation 2.10 for the radial velocity distribution at a distance x from the outflow point. These equations are based on the conventional pipe jet equations described by Albertson et al. (1950) but are generalized with coefficients *a*, the extent of the flow establishment region, and *b*, the radial expansion of the flow field. In Table 2.1 the coefficients are listed for the conventional pipe jet based on Albertson et al. (1950), for the Dutch method based on Blaauw and van de Kaa (1978) and for the German method based on Römisch (1975) and Fuehrer et al. (1987).

$$V_{\text{axis}}(x) = a \cdot \left[\frac{D_p}{x}\right] \cdot V_0 \tag{2.9}$$

$$V(x, r) = V_{\text{axis}}(x) \cdot exp\left[-b \cdot \frac{r^2}{x^2}\right] \tag{2.10}$$

Table 2.1: Overview of the coefficients a and b for Equation 2.9 and 2.10 to determine the flow velocities in the zone of established flow according to the theory for a conventional pipe jet, the Dutch method for a propeller jet and the German method for a propeller jet.

Jet type	a	b
Conventional pipe jet	6.2	76.2
Dutch method propeller jet	2.8	15.4
German method propeller jet	2.6	22.2

Equations 2.4-2.10 are only valid for describing the flow field during manoeuvring operations of the ship, while sailing the propeller jet behind the ship differs from the conditions described by Albertson et al. (1950) (PIANC, 2015).
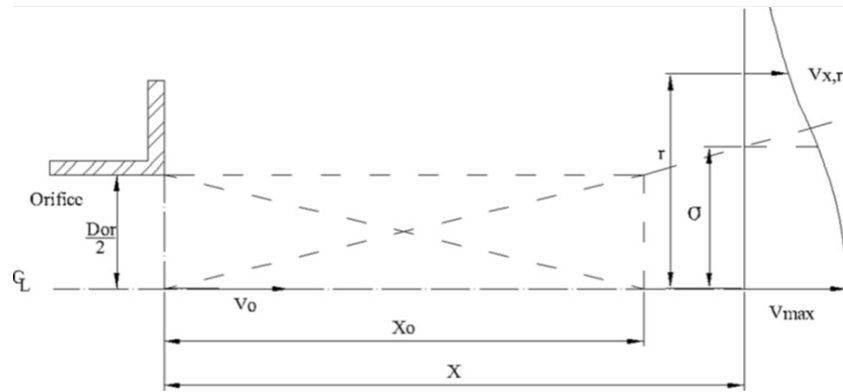
Figure 2.7: Zone of established flow of a free jet according to Albertson et al. (1950) (Lam et al., 2011b)

2.3. Flow field bow thruster jet confined by a vertical quay wall

During berthing manoeuvres, the bow thruster jet can not freely propagate into the water. The jet is confined by the bed and the quay wall which influences the flow field and flow velocities of the jet. Depending on the distance between the thruster outlet and the quay wall two different flow conditions can be observed. In Figure 2.8 the first flow condition is illustrated where the thruster outlet is in close proximity of the quay wall. The jet spreads while flowing out of the bow thruster outlet but does not reach the bed between the outlet and the quay wall. This is usually the situation when a vessel is moored to the quay wall. The second flow condition occurs when the vessel is at some distance away from the quay wall during berthing or unberthing. In this situation, two jets should be considered as illustrated in Figure 2.9. The indirect jet reflected on the quay wall and the radial flow component from the direct jet between the outlet and the bottom. For a berthing vessel, its relative position to the quay wall should be investigated to determine whether the flow velocities in the indirect and direct jet should both be considered to determine the maximum flow velocity near the bed (Verheij, 2020). Calculation methods according to PIANC (2015) for the indirect jet (Position 1,2 and 3 in Figure 2.9) are elaborated in Section 2.3.1 while the flow velocities near the bed for the direct jet (Position 4 in Figure 2.9) can be calculated with Equation 2.9 and 2.10 by substituting h_t ,the height of the bow thruster axis above the bed, for r and D_t for D_p.

For the indirect jet reflected on the quay wall, five different zones have been identified by Schmidt (1998). The first zone, the jet induction zone, is the region of flow establishment, as described in Section 2.2.4, where the velocity in the axis of the jet equals the efflux velocity. In the second zone, the jet is spreading more while the maximum flow velocity is decreasing. This is known as the zone of established flow described in Section 2.2.4. The third zone is the area where the jet reflects on the quay wall. The kinematic energy from the flow is converted to dynamic pressures at the quay wall indicated in Figure 2.8 with the max. dynamic pressure. The fourth zone is the wall jet which is directed towards the water surface and the bottom. In this area, the pressures are converted back into kinetic energy resulting in the flow along the quay wall. In the fifth zone, the wall jet directed towards the bottom is reflected on the bed resulting in an bottom jet flowing over the bed of the port.
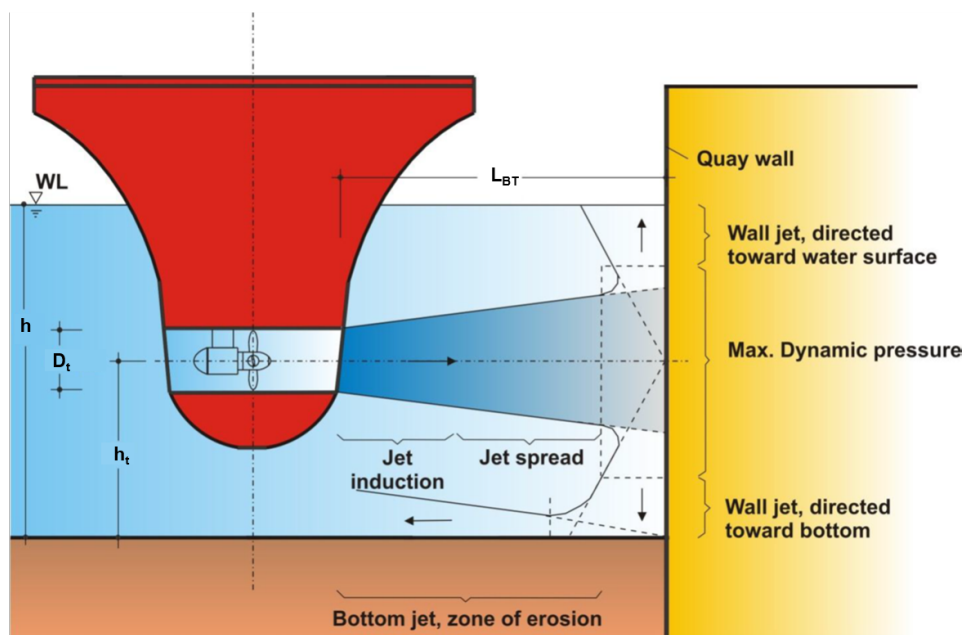
Figure 2.8: Relevant zones in the flow field of a reflected jet from a bow thruster on a vertical quay wall. Where h is the water depth, D_t the thruster diameter, h_t the height of the axis of the thruster above the bed and L_{BT} the distance between the quay wall and the outlet of bow thruster (PIANC, 2015).
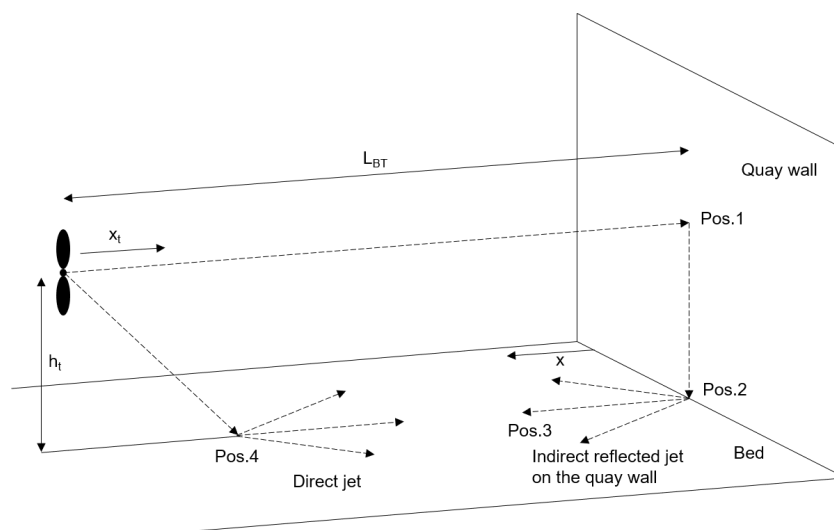
Figure 2.9: Flow situation of the bow thruster jet near the bed when the vessel is at some distance from the quay wall. L_{BT} is the distance between the bow thruster outlet and the quay wall, h_t the height of the bow thruster axis above the bed, x_t the distance from the bow thruster axis at which the velocity in the jet is calculated and x the perpendicular distance to the quay wall at which the flow velocity is measured near the bed. Illustration based on Verheij (2020).

2.3.1. Guidelines for determining the reflected flow velocities near the bed

Determining the flow velocities near the bed is the first step in estimating scour hole and bed protection dimensions. Several guidelines have been developed for protecting the bed against scour caused by jets. In Europe, the PIANC (2015) and BAW (2010) guidelines are most commonly used. German and Dutch researchers both developed methods to estimate the flow velocities in propeller jets and transverse thrusters as a function of the installed power and geometrical dimensions of the berthing area. It must be noted that these methods are developed for the final design of bed protections and not for accurately representing the physical characteristics of the propeller jet. Therefore, when designing the bed protection both the near-bed flow velocities and the bed protection dimensions must be determined with the same method (either German or Dutch) (PIANC, 2015). Secondly, both the German and Dutch method are based on measurements of the time-averaged flow velocities. The maximum flow velocities that result from the methods are the measured upper limit of the time-averaged flow velocities from the different measurement instruments used in their research.

German method

The German method as described in PIANC (2015) is based on research by Fuehrer et al. (1981) and Schmidt (1998). Schmidt (1998) empirically found that the length of the flow establishment zone x_0/D_t equals 1.9. This results in Equations 2.12 and 2.12 describing the velocity in the axis of the bow thruster for respectively the flow establishment region ($x_t/D_t < 1.9$) and the region of established flow ($x_t/D_t > 1.9$). With x_t the distance along the jet axis, L_{BT} the distance between the bow thruster outlet and the quay wall, D_t the bow thruster diameter and V_0 the efflux velocity as described in Section 2.2.1. Equations 2.11 and 2.12 are only valid between the bow thruster outlet and the quay wall, thus up to Position 1 in Figure 2.9.

$$V_{\text{axis,thruster}} = V_0 \ \text{ for } \ \frac{x_t}{D_t} < 1.9 \text{ and } \ x_t \leq L_{BT} \tag{2.11}$$

$$V_{\text{axis,thruster}} = 1.9 \cdot V_0 \cdot \left(\frac{x}{D_t} \right)^{-1.0} \ \text{ for } \ 1.9 < \frac{x_t}{D_t} \ \text{ and } \ x_t \leq L_{BT} \tag{2.12}$$

The maximum flow velocity at the bed near the intersection of the bed and the quay wall (position 2 in Figure 2.9) is computed with Equation 2.13. The maximum flow velocity near the bed is defined as the time averaged maximum measured flow velocity in x-direction. $V_{\text{wall,thruster}}$ follows from Equation 2.11 or 2.12 while $V_{\text{bed,thruster}} \leq V_{\text{wall,thruster}}$. Equation 2.13 is illustrated in Figure 2.10. It must be noted that Schmidt (1998) only conducted experiments in the range of $4.0 < L_{BT}/D_t < 7.3$. Therefore, using Equation 2.13 outside this range should be done carefully. Besides, Equation 2.13 is the formula proposed by Schmidt (1998) for the near-bed flow velocities and differs from the formula proposed in the PIANC (2015) guidelines where a power of -1 is used instead of the correct power of -1.15 proposed by Schmidt (1998).

$$\frac{V_{\text{b,thruster}}}{V_{\text{wall,thruster}}} = a_L \cdot \left(\frac{h_t}{D_t} \right)^{-1.15} \ \text{ with } a_L = 10.6 \cdot \left(\frac{L_{BT}}{D_t} \right)^{-1.0} \tag{2.13}$$
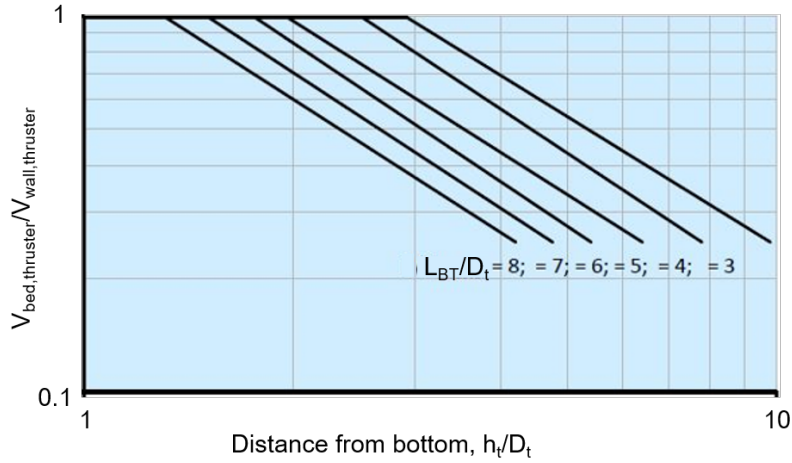
Figure 2.10: Illustration of Equation 2.13 for the flow velocity at the bottom (Position 2 in Figure 2.9) as function of the position of the bow thruster with respect to the bed and quay wall (Schmidt, 1998).

Dutch method

The Dutch method is based on research by Blaauw and van de Kaa (1978), Verheij (1983) and Blokland (1996). The maximum flow velocities in the indirect jet at Positions 1 and 2 in Figure 2.9 are assumed to be equal and are computed according to Equations 2.14 and 2.15 proposed by Blokland (1996) (Verheij, 2020). The maximum flow velocity near the bed is defined as the time-averaged maximum horizontal flow velocity consisting out of an x- and y-component.

$$V_b = 1.0 \cdot V_0 \cdot \frac{D_t}{h_t} \quad \text{for} \quad L_{BT}/h_t < 1.8 \tag{2.14}$$

$$V_b = 2.8 \cdot V_0 \cdot \frac{D_t}{L_{BT} + h_t} \quad \text{for} \quad L_{BT}/h_t > 1.8 \tag{2.15}$$

The maximum flow velocities in Position 3 of the indirect reflected jet are computed according to Equations 2.16 and 2.17.

$$V_b = 1.0 \cdot V_0 \cdot \frac{D_t}{h_t} \quad \text{for} \quad (L_{BT} + x)/h_t < 1.8 \tag{2.16}$$

$$V_b = 2.8 \cdot V_0 \cdot \frac{D_t}{L_{BT} + h_t + x} \quad \text{for} \quad (L_{BT} + x)/h_t > 1.8 \tag{2.17}$$

In Equations 2.14 - 2.17, D_t is the thruster diameter, L_{BT} represents the distance between the bow thruster outlet and the quay wall, h_t the height of the thruster above the bed and x the distance perpendicular to the quay wall over the bed.

2.3.2. Field measurements

Over the years two full scale measurements of the near-bed flow velocities have been conducted in the Port of Rotterdam. The first one by Blokland (1996) where the Dutch method in the PIANC (2015) are based on and the second one by Cantoni (2020) who measured with a similar vessel and instruments as during the measurements in Gent.

Blokland (1996)

In collaboration with the Port of Rotterdam, Blokland (1996) conducted field measurements to determine flow velocities and erosion at the bed induced by a reflected jet on a vertical quay wall in the Benelux-haven at the Port of Rotterdam. The measurement was conducted with a tugboat during bollard-pull-conditions where only one of the two main thrusters of the tugboat was activated. The main thruster has a diameter of 2.5 m which is comparable to a bow thruster from a large container vessel. During the measurements the following parameters were changed; the pitch of the thruster blades, distance from the tugboat to the quay wall (quay wall clearance) and angle between the axis of the thruster jet and the quay wall. In this thesis, the focus is at the reflected jet when the axis of the thruster jet is directed perpendicular to the quay wall (Test S.4, S.5 and S.6). Each test was conducted for 2 minutes with the maximum amount of rpm. To measure the flow velocity acoustic and electro-magnetic velocity meters (UCM and EMS) were used. The UCM measured the flow velocity in three dimensions (x, y and z) while the EMS measured the flow velocity in two dimensions in the horizontal plane (x and y). The objective of the research by Blokland (1996) was to find a stability relation for the bed material based on the time-averaged flow velocity near the bed. In the method proposed by Blokland (1996) to determine near-bed flow velocities (Dutch method Section 2.3.1), turbulent fluctuations are not taken into account. The reason for this is the large measurement volume and the low sampling frequency of the UCM. The question remains whether the main thruster of a tugboat is representative for a trans-verse thruster of a vessel as the main thruster can draw in more water and the effect of the hull of the vessel is not taken into account. Nevertheless, the method proposed by Blokland (1996) is the main theory behind the Dutch method in the PIANC (2015) guidelines for determining the velocities near the bed from a transverse thruster after reflection on a vertical quay wall (Equation 2.14 - 2.17 in Section 2.3.1). An overview of the measurement characteristics of Blokland (1996) is given in Table 2.2.

Table 2.2: Characteristics field measurements by Blokland (1996). The heights and distances are given in the diameter of the main thruster D_t. The range in height of the propeller axis above the bed is due to the tide in the Port of Rotterdam. The measurement instrument locations and quay wall clearance are in perpendicular x-direction from the quay wall measured from the middle line of the sheet pile wall.

Characteristic	Value
Max. power per main thruster	1950 kW
Max. thrust per main thruster	340 kN
Main thruster diameter (D_t)	2.5 m
Height of the main thruster axis above the bed	2.22 - 2.9 D_t
Quay wall clearance (L_{BT})	3.2 D_t (S.4), 6.2 D_t (S.5), 12 D_t (S.6)
Pitch main thruster	6°, 9°, 12°, 15°, 18°, 23°
Measurement instrument locations (x-direction)	0.49 D_t, 0.82 D_t, 1.47 D_t

Cantoni (2020)

Cantoni (2020) conducted field measurements at the Antarcticakade in the Port of Rotterdam using one of the largest inland vessels in the Netherlands, the MTS Vortsenbosch. The measurements focused on the reflection of a 4-channel bow thruster jet on the vertical quay wall. The flow velocities near the bed were measured with Acoustic Doppler Velocimeters (ADV) and Acoustic Doppler Current Profilers (ADCP). The influence of the quay wall clearance and keel clearance on the flow pattern at the bed was investigated during the measurements while also changing the used bow thruster power. Results of Cantoni (2020) showed that the mean flow velocities near the quay wall were in the order of 1 m/s with high turbulent fluctuations. This led to relative turbulence intensities (Section 2.4) higher than expected from literature, and even close to 1. The Dutch and German methods suggested by PIANC (2015) showed to be conservative when compared to the results of Cantoni (2020). Furthermore, both

methods sensitivity to wall and keel clearance was not reflected by the data of Cantoni (2020). Results showed that besides the five zones defined by Schmidt (1998) there is a sixth zone for 4-channel bow thrusters due to the inflow beneath the vessel at the bow thruster inlet. Once the return flow is dissipated due to friction and turbulence, inflow under the suction point becomes a significant load that has to be taken into account (Cantoni, 2020). Questions can be raised whether the measurement data reflect the flow field of the bow thruster well. The measurement set up had a low density of measurement points and limited redundancy. This made it difficult to determine whether the discrepancies found between the measurements of the ADV and ADCP, located near the quay wall, were due to the high spatial variability of the flow or the difference in measurement technique. An overview of the measurement characteristics of Cantoni (2020) is given in Table 2.3.

Table 2.3: Characteristics field measurements by Cantoni (2020). The heights and distances are given in the diameter of the bow thruster D_t. The range in height of the bow thruster axis above the bed is due to the tide in the Port of Rotterdam.

Characteristic	Value
Max. power bow thruster	618 kW
Diameter thruster (D_t)	1.42 m
Height of the thruster in the water column	1.21 - 2.45 D_t
Quay wall clearance (L_{BT})	2.32 D_t, 4.23 D_t
Measurement instrument locations (x-direction)	0.27 D_t, 0.39 D_t, 7.67 D_t, 9.49 D_t
Measurement instrument locations (y-direction)	1.55 D_t, 1.97 D_t and 5.14 D_t

2.3.3. Scale model

In the scale model tests the reality is simulated on a smaller scale with prototype or schematized vessels. A lot of research has been done on propeller jets and bow thrusters using scale model with several theses conducted on this topic at the TU Delft.

Bok (1996)

Bok (1996) conducted scale model tests in the fluid mechanics laboratory at the TU Delft to investigate the stability of bottom protections in front of a vertical quay under the hydraulic load of a bow thruster. In this research, the flow velocities of the reflected jet near the bed were measured and the flow field between the quay wall and the ship was analyzed. In the model, a jet was placed in a duct perpendicular to the quay wall while changing the discharge, keel clearance and wall clearance. The main conclusion from this was that Equations 2.14 and 2.15 approached the data from the scale model well.

Schmidt (1998)

Schmidt (1998) conducted scale model tests to investigate the flow field of a bow thruster jet reflecting on a vertical quay wall while varying keel clearance, quay wall clearance and rpm of the bow thruster. Schmidt (1998) distinguished five different zones of the flow field as explained in the introduction of Section 2.3 and illustrated in Figure 2.8. Schmidt (1998) measured with a two dimensional Laser Doppler Anemometer (2D-LDA) in x-direction (in the direction of the axis of the jet) and in z-direction (vertical direction towards or away from the bed). The maximum measured velocity was determined by measuring the time-averaged maximum flow velocity in x-direction. Therefore, this method differs from the measuring method of Blokland (1996) who measured the maximum time-averaged horizontal flow velocity composed out of an x- and y-component. The measured maximum time-averaged flow velocity in the jet axis (before reflection on the quay wall) was compared to a Gaussian distribution from which was concluded that the maximum velocity corresponded to a probability of exceedance of 80%. Therefore, for further analysing of the near-bed velocities also the velocity corresponding to a probability of 90% exceedance was used. The theory of Schmidt (1998) is the main theory behind the German method (Section 2.3.1) for calculating near-bed flow velocities of a reflected propeller jet on a quay wall as described in the PIANC (2015) guidelines. An overview of the measurement characteristics of Schmidt (1998) is given in Table 2.4.

Table 2.4: Characteristics scale model measurements by Schmidt (1998). The heights and distances are given in the diameter of the bow thruster D_t. The measurement instrument locations and quay wall clearance are in perpendicular x-direction from the quay wall.

Characteristic	Value
Diameter thruster (D_t)	6.8 cm
Height of the thruster in the water column	1.66 D_t, 2.18 D_t, 2.42 D_t, 2.91 D_t, 3.5 D_t, 3.93 D_t
Quay wall clearance (L)	3.97 D_t, 5.44 D_t, 7.28 D_t

Van der Laan (2005), Nielsen (2005) and Van Blaaderen (2006)

Over the years several master theses on near-bed flow velocities induced by a reflected jet on a vertical quay wall were conducted. van der Laan (2005), Nielsen (2005) and Van Blaaderen (2005) studied this topic with Computational Fluid Dynamics (CFD) models validated by physical models in the fluid mechanics laboratory at the TU Delft. van der Laan (2005) did not found a good correspondence between the physical model and CFD model, possibly due to the limited amount of measuring points and overestimation of the flow velocity of the bow thruster in the physical model. Nielsen (2005) continued on this approach, finding that the CFD and physical model showed a mildly similar flow pattern. Only in the area close to the quay wall in front of the bow thruster the velocity was alike, both in direction and size. Therefore, conclusions were made that although there are similarities the present numerical model does not yet sufficiently represent the physical situation. Building on the research by van der Laan (2005) and Nielsen (2005), Van Blaaderen (2005) focused on correctly modelling the bow thruster characteristics, geometry and induced turbulence. Although there were still discrepancies, Van Blaaderen (2005) concluded that a CFD model with a kϵ-turbulence model can be used for modelling the bow thruster induced flow. van der Laan (2005), Nielsen (2005) and Van Blaaderen (2005) questioned the assumption that a bow thruster jet can be modelled as a free jet from which the relations found by Blaauw and van de Kaa (1978) and Fuehrer et al. (1987) are derived.

For this research, the flow pattern modelled by the CFD model of Van Blaaderen (2005) is used to give an impression of the flow field after reflection of the jet on the quay wall as illustrated in Figure 2.11. The jet reflects under an angle of approximately 41°to the left and under an angle of approximately 37°to the right. The flow pattern is almost symmetric, with the highest flow velocities between the vessel and the quay over an area of approximately 5 D_t (the quay wall clearance) times 10 D_t at the left and right of the bow thruster outlet. Figure 2.11 gives valuable insight into the location on the bed where the flow velocity should be measured during the field measurements in Gent.
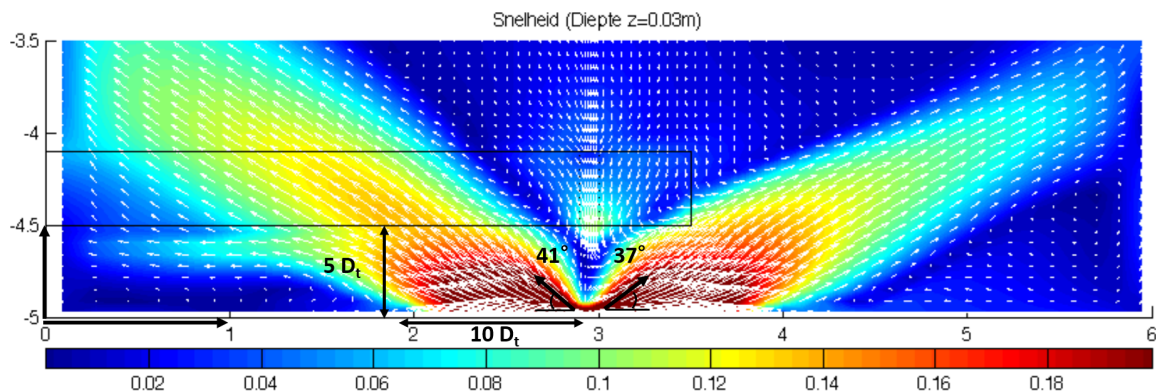
Figure 2.11: Spreading of the bow thruster jet over the bed after reflection on a vertical quay wall according to the CFD model of Van Blaaderen (2005). The rectangular shape is the schematized shape of the ships hull. The velocities are measured at 0.03 m above the bed. The bow thruster diameter D_t is 2.5 m.

Deltares (2015)

Deltares performed model tests to address the hydraulic load on the bed induced by a bow thruster jet which is reflected on a vertical quay wall. The test falls within the framework of knowledge gaps on propeller jets composed by SBRCURnet (Van der Hout, 2017). The measurements have been performed to determine the flow patterns and flow velocities caused by the bow thruster in the proximity of a vertical quay wall. In the tests, various keel clearances and wall clearances of the thruster jet were measured by doing tests in nine different vessel positions. The flow velocities were measured with Electro-Magnetic Flow sensors (EMF) that measured in two dimensions. Five EMF sensors were placed in an array at the bed measuring in the horizontal plane (x- and y-direction). This array was moved from and towards the quay wall during the test in a total of four pre-defined positions resulting in a matrix of flow velocity measurements. Two EMF sensors were placed at the quay wall to measure in x- and z-direction, where x is positive perpendicular to the quay wall and z is positive from the bed upwards (De Jong and Van Velzen, 2015). The influence of the hull of the ship was not studied as it was schematized in the test set-up. Discrepancies with the Dutch method from PIANC (2015) have been found. For most of the tests, the Dutch method was conservative but some tests with a large quay wall clearance showed flow velocities higher than predicted by the Dutch method. The maximum average flow velocities were not always found at the same location in the tests and did not always occur at the wall as current formulae suggest (De Jong and Van Velzen, 2015). These findings are of large practical relevance as the location of the maximum flow velocity is critical for designing the bottom protection and determining to what extent the bottom protection should be penetrated with colloidal concrete.

Table 2.5: Characteristics of the scale model measurements by De Jong and Van Velzen (2015). The heights and distances are given in the diameter of the bow thruster D_t. The measurement instrument locations are given in x-direction (perpendicular from the quay wall) and y-direction (along the quay wall). The quay wall clearance is is in perpendicular x-direction from the quay wall.

Characteristic	Value
Scale factor	1:15.341
Diameter thruster (D_t)	2.5 m
Height of the thruster axis in the water column	1.5 D_t, 2.5 D_t, 3.5 D_t
Quay wall clearance (L_{BT})	1.5 D_t, 5.5 D_t, 9.5 D_t
Measurement instrument locations (x-direction)	0.89 D_t, 4.76 D_t, 8.76 D_t, 12.76 D_t
Measurement instrument locations (y-direction)	-1.84 D_t,-1.23 D_t, 0 D_t, 1.23 D_t, 1.84 D_t

2.3.4. Location of the maximum flow velocity in x- and y-direction

In this section, the position on the bed where the maximum flow velocity is measured will be investigated for the research conducted by Blokland (1996), Schmidt (1998), De Jong and Van Velzen (2015) and Cantoni (2020) on the reflected jet of a bow thruster on a vertical quay wall.

Blokland (1996) measured the velocity near the bed at approximately 0.5, 0.8 and 1.5 D_t perpendicular to the quay wall (x-direction). Three different quay wall clearances were investigated for the measurements where the thruster made a $90°$ angle with the quay wall (L_{BT} = 3.2, 6.2 and 12 D_t). For every measurement, the measured flow velocities at 0.5 D_t were significantly lower than at 0.8 and 1.5 D_t. The highest flow velocities were measured at 0.8 D_t with slightly lower flow velocities measured at 1.5 D_t (Blokland, 1996).

Schmidt (1998) measured the near-bed velocities perpendicular (x-direction) to the quay wall for three different bow thruster quay wall clearances (L_{BT} = 4, 5.4 and 7.3 D_t) while h_t, the height of the bow thruster axis above the bed, was kept constant at 2.18 D_t. For L_{BT} = 4 D_t (Figure 2.12a), the flow velocities increased while moving away from the quay wall with a maximum at $x/D_t = 0.9$. After this point, the flow velocities decreased again. The same pattern can be seen for L_{BT} = 5.4 D_t (Figure 2.12b) which has a maximum flow velocity at $x/D_t = 1.47$. However, for L_{BT} = 7.3 D_t, this pattern is not recognized (Figure 2.12c). The flow velocities reach a maximum at $x/D_t = 1.77$, staying relatively constant while further moving away from the quay wall (Schmidt, 1998).
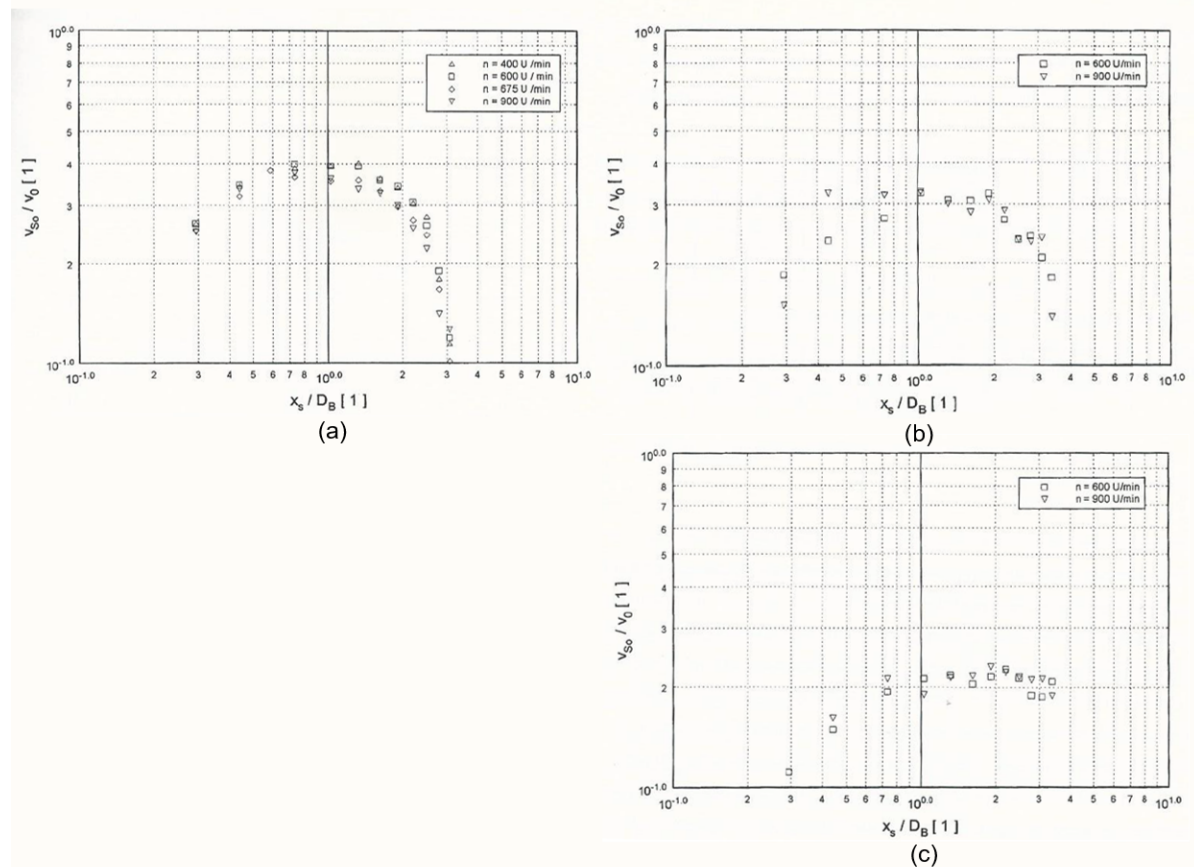
Figure 2.12: The near-bed velocities as function of the perpendicular distance (x-direction) from the quay wall. Three vessel position have been measured with a quay way clearance of 4 D_t (a), 5.5 D_t (b) and 7.3 D_t (c). The height of the axis of the bow thruster in the water column was kept constant at h_t = 2.18 D_t. $\overline{V}_x$ is the time-averaged near-bed flow velocity, x the distance from the quay wall in x-direction and D_t the diameter of the thruster (6.8 cm) (Schmidt, 1998).

Deltares conducted scale model tests with a 4x5 matrix of measurement points on the bed. Perpendicular to the quay wall (x-direction), flow velocities were measured at 0.89, 4.76, 8.76 and 12.76 D_t. Parallel to the quay (y-direction), the flow velocities were measured at 0, 1.23, 1.84 D_t from the bow thruster axis in both positive and negative y-direction. The highest flow velocities in x-direction were not always measured close to the quay at 0.89 D_t. Maximum flow velocities were measured at both 0.89 and 4.76 D_t, depending on the quay wall clearance of the bow thruster (L_{BT}) and height of the bow thruster axis above the bed (h_t). Further away from the quay, lower flow velocities were measured at 8.76 and 12.76 D_t. In y-direction, overall no significant decrease in flow velocity was noted when moving in lateral direction from the bow thruster axis to 1.23 and 1.84 D_t (De Jong and Van Velzen, 2015).

Cantoni (2020) determined the development of the near-bed flow velocities perpendicular to the quay wall (x-direction) and parallel to the quay wall (y-direction). The flow velocities parallel to the quay wall were measured by moving the vessel with respect to the fixed measurement frame. In x-direction, the flow velocity was measured at 0.27, 0.39, 7.67 and 9.49 D_t from the quay wall. In y-direction, the flow velocity was measured at 1.55, 1.97 and 5.14 D_t from the bow thruster axis. In x-direction, the highest flow velocities were measured close to the quay wall at 0.27 and 0.39 D_t. Further away from the quay wall, at 7.67 and 9.49 D_t, no significant flow velocities were measured. An exception to this was when the bow thruster inlet was nearby one of the measurement instruments. In this situation, the inflow velocity near the bow thruster inlet resulted in significant flow velocities which should be taken into account. In y-direction, the highest flow velocities were measured closest to the axis of the bow thruster at 1.55 D_t. Moving laterally to 1.97 D_t, the flow velocity started to decrease until at 5.14 D_t no significant flow velocities were measured (Cantoni, 2020).

2.4. Maximum flow velocity and relative turbulence intensity

It can be expected that not the mean flow velocity but the extremes in flow velocity are responsible for the incipient motion of the bed particles (Schiereck, G. and Verhagen, H., 2016). The flow of a bow thruster jet is highly turbulent resulting in large fluctuations around the mean flow velocity. The extremes in the flow velocity, or maximum flow velocities, can be represented by Equation 2.18. Where $\overline{V}$ is the mean flow velocity and σ the standard deviation taking into account the turbulent fluctuations. Equation 2.18 is based on the empirical rule or the three-sigma rule which states that for a normal distribution (Gaussian distribution) almost all data falls within three standard deviations from the mean ($\overline{V} \pm 3\sigma$). More precisely, stating that 99.73% of the data falls within $\pm 3\sigma$ from the mean (Wright, 2021). Using $\overline{V} + 3\sigma$ as a maximum for the flow velocity is more reliable to use instead of the actual measured maximum flow velocity since the actual measured maximum depends on the measurement duration and sampling frequency. Thus, this maximum flow velocity would be different for each measurement. The statistical maximum of $\overline{V} + 3\sigma$ is only exceeded 0.135 % of the time making it well usable alternative for the actual measured maximum flow velocity. The normal distribution, including the percentage of data that falls within each segment between the standard deviations, is visualised in Figure 2.13.

$$V_{\mathrm{max}} = \overline{V} + 3\sigma \tag{2.18}$$
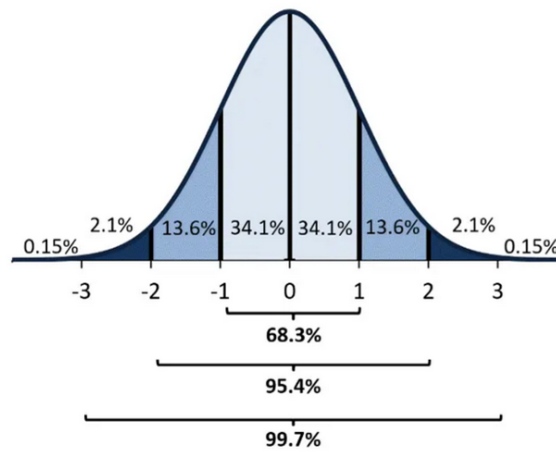
Figure 2.13: Illustration of the normal (Gaussian) distribution with the three-sigma rule. The x-axis gives the number of standard deviations from the mean with 0 as the mean. The distribution is sliced into parts coinciding with the standard deviation steps with corresponding percentage of data that falls within that slice. Within $\pm 3\sigma$, 99.73% of the data is present (Wright, 2021).

To quantify turbulence in the flow, the relative turbulence intensity r is determined. The relative turbulence intensity is defined as the root mean square of the turbulent fluctuations (V') divided by the mean ($\overline{V}$) of flow velocity component, see Equation 2.19 .

$$r = \frac{\sqrt{\overline{V'^2}}}{\overline{V}} = \frac{\sigma}{\overline{V}} \tag{2.19}$$

However, it has to be noted that the relative turbulence intensity (r) loses its meaning when the flow has a low mean flow velocity. Blaauw and van de Kaa (1978) measured turbulence intensities near the bed between 0.2-0.35 for a propeller jet while Blokland (1996) measured the relative turbulence intensity of the reflected jet on a vertical quay wall near the bed with a variety of r between 0.16-0.43 and an average of 0.3. CIRIA, CUR, CETMEF (2007) indicates that the relative turbulence intensity could reach up to 0.6 for very high turbulence levels at hydraulic structures. However, it must be noted that their is a difference in the defined r, as Blaauw and van de Kaa (1978) measured the relative turbulence intensity of a propeller jet and Blokland (1996) of a reflected jet on a vertical quay wall. Using r to define the maximum flow velocity results in Equation 2.20.

$$V_{\max} = \overline{V} + 3\sigma \approx (1 + 3r)\overline{V} \tag{2.20}$$

The Izbash and Shields stability formulae discussed in Section 2.5 can be modified with extra factors for turbulence, slope angle, vertical velocity profile and geometrical characteristics resulting in the Pilarczyk formulae for designing the stability of bed protections. In this thesis, the focus is on the turbulent flow from a bow thruster jet. Therefore, to account for the turbulence of the thruster jet in the stability formulae (Section 2.5), a turbulence factor k_t is introduced in Equation 2.21. Where r is the relative turbulence intensity as defined in Equation 2.19 (CIRIA, CUR, CETMEF, 2007).

$$k_t = \frac{1 + 3r}{1.3} \tag{2.21}$$

2.5. Stability formulae for bottom material

The flow velocities induced by the reflected bow thruster jet affect the stability of the bed material leading to scour formation when the flow velocities are higher than a certain threshold value. To prevent this from happening, bed protections are designed based on stability formulae for bottom materials. The bed protection, traditionally consisting out of loose rocks, is designed based on the ratio of the drag forces (load) in respect to the weight of the rocks (strength). Where the drag forces are proportional to the near-bed flow velocity squared. The focus of this research is on the flow velocities, however, a review of the main stability formulae is presented to understand the relation between flow velocity and the required size of the bed protection material.

Izbash

The Izbash approach considers the forces on an individual grain and determines the balance of these forces (Figure 2.14). When active forces (by flow, turbulence, etc.) become larger than the passive forces (gravity, friction between grains) the balance is lost, and the grains start to move. The active forces are referred to as the loads, while the passive forces are referred to as the strength of the grain. The Izbash approach is used especially in cases of non-uniform flow and was designed for small water depths and big stones, resulting in a high ratio of water depth/stone diameter Schiereck, G. and Verhagen, H. (2016).

$$d_{n50} \leq \beta_{Iz,cr} \frac{V_{b,\max}^2}{2g\Delta} \tag{2.22}$$

With:

- d_{n50}: nominal median stone diameter [m]
- $\beta_{Iz,cr}$: Izbash stability parameter [-]
- $V_{b,\max}$: maximum velocity near the bed [m/s]
- Δ: dimensionless relative buoyancy of rock in water [-]
- g: gravity acceleration [m^2/s]

The velocity in the Izbash formula is the velocity acting on the stone, but Izbash did not clearly define the location of the bottom velocity. Neither is it clear how the stone diameter is defined. For design purposes, the maximum flow velocity near the bed is used (Schiereck, G. and Verhagen, H., 2016).
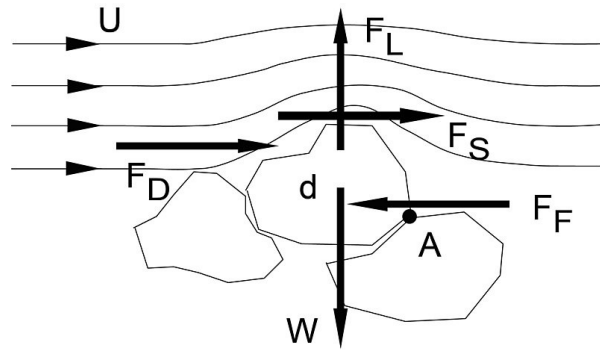
Figure 2.14: Balance of forces on an individual grain according to Izbash (Schiereck, G. and Verhagen, H., 2016)

Shields

The Shields approach considers the friction force caused by the water on the bed (i.e. on an area significantly larger than one grain). When this force exceeds a certain critical value, grains start to move and scour occurs. Shields gives the relation between the dimensionless shear stress and the so-called particle Reynolds-number. The shields approach is based on the assumption that there is an equilibrium flow. This means that the Shields approach is only valid when the Chezy-equation is applicable, which is the case for permanent uniform flow. When the flow is not uniform, the load will be higher locally. Shields is used for large water depths when the ratio water depth over stone diameter is high. The stability formula according to Shields is given in Equation 2.23 and can be modified to Equation 2.24 for design purposes.

$$\Psi_c = \frac{load}{strength} = \frac{\tau_c d^2}{(\rho_s - \rho_w) \, g d^3} = \frac{V_{*c}^2}{\Delta g d} \tag{2.23}$$

$$d_{n50} = \frac{\overline{V_c}^2}{\Psi_c \cdot \Delta \cdot C^2} \tag{2.24}$$

With:

- d_{n50}: nominal median stone diameter [m]
- Ψ_c: Shields stability parameter [-]
- τ_c: critical shear stress $[N/m^2]$
- V_{*c}: critical shear velocity [m/s]
- $\overline{V_c}$: critical, depth averaged, velocity in uniform flow [m/s]
- C: Chezy's coefficient, indicating the roughness of the bed $[m^{1/2}/s]$
- g: gravity acceleration $[m^2/s]$

Pilarczyk

The Pilarczyk formula (Equation 2.25) modified from the Izbash/Shields stability formulae for design purposes with extra factors for turbulence, slope angle of the bed, vertical velocity profile and geometrical characteristics of the protection layer. It must be noted however that the Pilarczyk formula is not validated for propeller flow (PIANC, 2015).

$$\Delta d_{n50} = \phi \frac{0.035}{\psi_{cr}} k_h k_{sl}^{-1} \frac{k_t^2 V^2}{2g} \tag{2.25}$$

With:

- d_{n50}: nominal median stone diameter [m]
- Δ: dimensionless relative buoyancy of rock in water [-]
- g: gravity acceleration [m^2/s]
- V: vertically-averaged flow velocity [m/s]
- ϕ: stability factor depending on application and placement of the bed protection layer [-]
- $\Psi_c r$: critical shields stability parameter [-]
- k_{sl}: strength reduction factor for stones on a slope [-]
- k_t: turbulence factor indicating a load deviating from uniform flow (Equation 2.21) [-]
- k_h: velocity profile factor [-]

3

Methodology

3.1. Measurement scope

The field measurements are part of the roadmap set up by the CROW joint research program as mentioned in Section 1.4. Within this research program, field measurements were proposed to contribute to the knowledge gaps on the reflection of a propeller jet on a vertical quay wall induced by a 4-channel bow thruster. In cooperation with the participating parties a measurement plan was created with three main objectives:

- *Gaining a better understanding of the flow pattern and extent of a propeller jet reflecting on a vertical quay wall (Examined in this thesis)*

- *Measuring the efflux velocity and obtaining the vertical velocity profile of a free propeller jet (Not examined in this thesis, the measurement setup can be found in Appendix E)*

- *Determine the actual transmitted power of the bow thruster (Examined by MARIN)*

The flow velocities near the bed will be measured at several positions on the bed with the aim of capturing the maximum flow velocities, decay, direction and extent of the reflected flow over the bed. From the previous chapter, it is seen that the quay wall clearance, keel clearance and used bow thruster power are key variables influencing the near-bed velocities caused by the reflection of the propeller jet on the quay wall. The influence of the quay wall clearance can be assessed by placing the vessel at various distances from the quay wall. A vessel should be chosen such that the draught of the vessel results in a keel clearance that falls in the range of keel clearances causing the highest velocities near the bed. Although this is not explicitly defined in literature assumptions based on previous studies can be made. To investigate the influence of the key variables the measurements should be executed several times with varying values for the key variables. The exception for this is the keel clearance as there is no tide at the measurement location the keel clearance can not be varied during the measurements.

3.2. Location - Moervaart quay wall, North Sea Port Gent

For the field measurements, North Sea Port Gent made the Moervaart quay wall in the Port of Gent (Belgium) available. The Moervaart quay wall is situated in the Moervaart which is a side channel of the Gent-Terneuzen channel as illustrated in Figure 3.1. The cargo company operating at the quay wall, Cargill, had a shutdown period of two weeks in which the field measurements took place from Monday the 28th of September until Thursday the 1st of October. Bollards 26 - 37 were made available for the measurements. Near bollard 31 there is a water outlet from the Cargill factory with a discharge of 700 - 1000 m^3/h during the shutdown. Between bollard 36 and 37 there is a water inlet for the factory. In Figure 3.2 the measurement location is illustrated with the measurement vessel Somtrans XXV moored with the bow at bollard 28 (Section 3.3).

Figure 3.1: Google maps illustration of the location in the North Sea Port Gent where the field measurements took place. The Moervaart is a side channel of the Gent-Terneuzen channel where in the white rectangle the Moervaart quay wall is marked where the measurements took place.
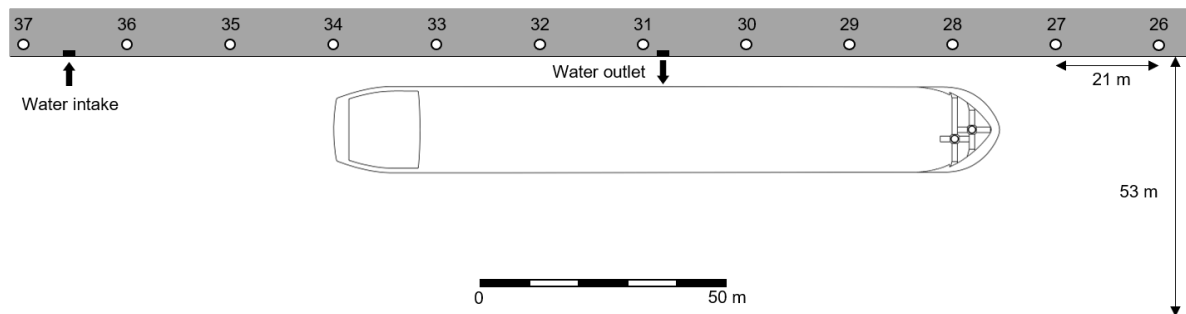
Figure 3.2: Illustration of the Moervaart quay wall from bollard 26 to bollard 37. The Somtrans XXV is moored with the bow at bollard 28. Spacing between the bollards is 21 m and the width of the Moervaart channel is 53 m. There is a water intake point from the Cargill factory between bollard 36 and 37 and a water outlet point near bollard 31.

In Figure 3.3 the cross-section of the Moervaart quay wall is illustrated. The quay wall consists out of a sheet pile wall with a concrete cap at the top. Looking from the quay wall, the bed protection consists out of 1 m colloidal concrete, 20 m of asphalt mattresses and 4 m of rip-rap all with a layer thickness of 0.3 m. Before the measurements, there was a small layer of sludge laying on top of the asphalt mattresses. This layer was approximately 5-10 cm thick in the middle of the Moervaart channel and reduces to towards the quay wall. After the measurements this layer of sludge was almost completely washed away leaving only the asphalt mattresses.
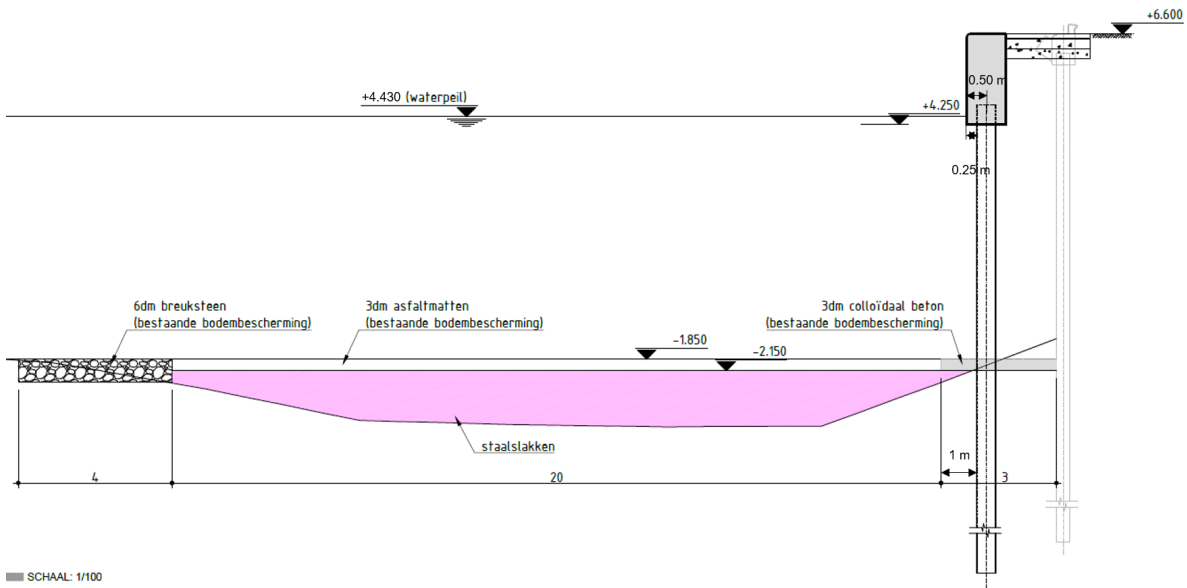
Figure 3.3: Cross-section of the Moervaart quay wall between bollard 35 and 36. This cross-section is applicable to bollard 28 but the bed level varies. The varying bed level along the bollards is illustrated in Figure 3.4. The quay wall consists out of a concrete cap with a sheet pile wall underneath that is 0.5 m wide. The shaded sheet pile wall on the outer right is the old quay wall. A new quay wall has been placed approximately 2 meters in front of the old quay wall two years ago. The bed protection consist out of 1 m colloidal concrete, 20 m of asphalt mattresses and 4 m of rubble all with a layer thickness of 0.3 m.

The configuration of the asphalt mattresses and hydrographic measurement of the bed between bollard 26 and 32 can be seen in Figure 3.4. The bed has a small slope from the shallower area close to the quay wall to the slightly deeper area in the middle of the Moervaart channel. At bollard 26 the water depth near the quay wall is shallower and unprotected. Therefore, to make sure the reflected propeller jet from the bow thruster does not reach the unprotected bed near bollard 26 the bow of the Somtrans XXV will be moored at bollard 28 with the port side towards the quay, as seen in Figure 3.2. In this position, the bow thruster outlets will be approximately 63 m (three bollards) away from the water outlet to minimize the influence on the flow velocities near the bed.
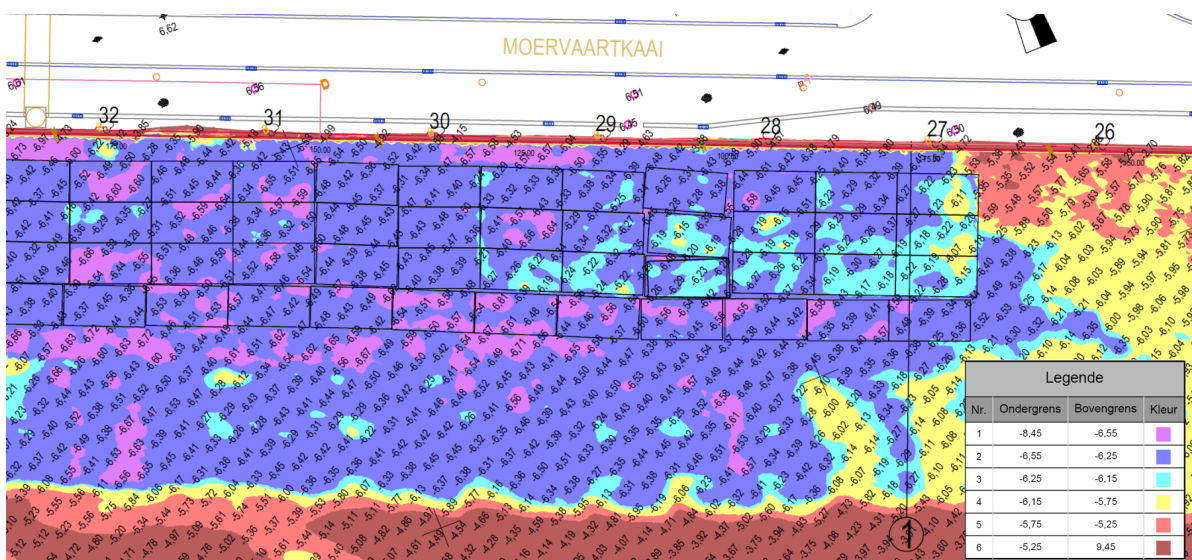
Figure 3.4: Hydrographic survey of the bed between bollard 26-32 including the locations of the asphalt mattresses (rectangular shapes). After bollard 27 no asphalt mattresses are placed leaving the bed unprotected.

3.3. Vessel - Somtrans XXV

For the measurements, the Belgian shipping company Somtrans has made the inland tanker Somtrans XXV available. The Somtrans XXV ships liquid cargo (class C) and is loaded with Nafta during the field measurements. The main dimensions of the Somtrans XXV are given in Table 3.1. The draught of the Somtrans XXV depends on the type of liquid cargo, for Nafta, the fully loaded vessel resulted in a draught of 3.88 m during the field measurements.

Table 3.1: Somtrans XXV dimensions

Dimension	Value
Length	135 m
Beam	17.5 m
Draught	3.88 m

The Somtrans XXV is equipped with two Verhaar Omega 31130-4K 4-channel bow thrusters with the characteristics given in Table 3.2. The bow thruster channel outlet has a rectangular shape. Therefore, the equivalent circular bow thruster outlet diameter is calculated according to Equation 3.1 where a is the thruster channel outlet width and b the thruster channel outlet height. The equivalent diameter is defined as a circle having the same cross-sectional area as the rectangular bow thruster outlet. The bow thruster channel diameter (D_t) is used in previous research and guidelines as input parameter to calculate the near-bed flow velocity. In addition, D_t serves as a measure to compare previous measurements with each other by comparing the characteristic (dimensionless) values for the quay wall clearance, keel clearance and measurement locations at the bed with each other as a function of D_t. As listed the tables of Section 2.3.2 and 2.3.3 for the field measurements and scale models.

$$D_t = \sqrt{\frac{4 \cdot a \cdot b}{\pi}} = 1.07m \tag{3.1}$$

Table 3.2: Somtrans XXV Verhaar Omega 31130-4K bow thruster characteristics

Characteristic	Value
Max. power	394 kW
Max. RPM	1800
Max. thrust	43.76 kN
Diameter of the water inlet suction propeller	1300 mm
Channel outlet width	1100 mm
Channel outlet height	818 mm
Equivalent circular diameter channel outlet	1070 mm

The two bow thruster are placed at different locations in the bow of the vessel resulting in two different distances between the bow thruster outlets and the quay wall (quay wall clearance L_{BT}). In Figure 3.5 a technical drawing of the bow thrusters is shown. Bow thruster 1 is the top bow thruster situated closest to the bow of the vessel, bow thruster 2 is the bottom bow thruster situated in the direction of the stern of the vessel. The technical drawing of the entire Somtrans XXV and a plot of the delivered thrust (bollard pull thrust) of the bow thruster can be found in Appendix A.
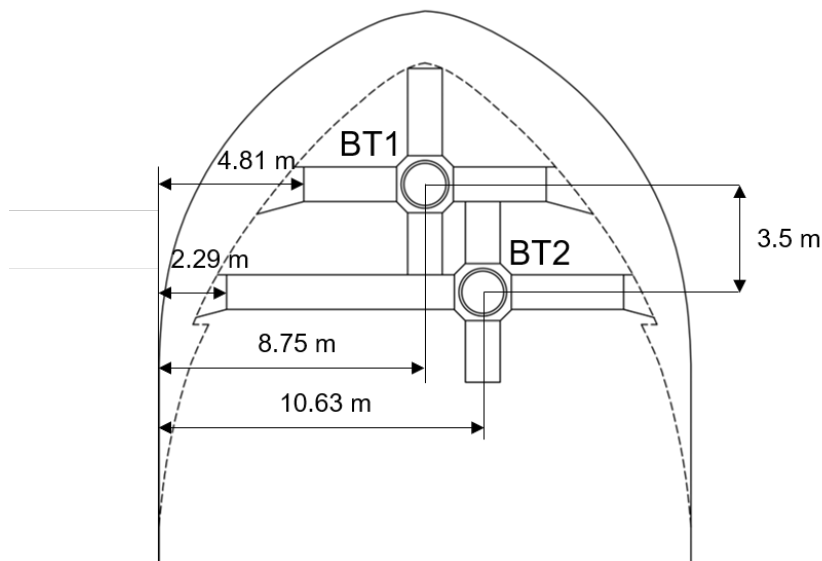
Figure 3.5: Technical drawing of the two bow thruster of the Somtrans XXV. Location of bow thruster 1 and 2 are indicated, the water inlet suction point and propeller are located in the circle where the channels join each other. The measurement for the distance between the water inlet suction points and the port side of the vessel is indicated. The distance between the bow thruster outlets and the port side of the vessel and the distance between the two channel axis is indicated.

Figure 3.6: The Somtrans XXV moored at the Moervaart quay wall during the measurements on Wednesday the 30th of September 2020. Photo by Wim van den Berg.

3.4. Instruments

In this section, the instruments and their settings used to measure the flow velocities are elaborated. For the measurements, a total of five different instruments were used. Two acoustic measurement instruments: Acoustic Doppler Velocimeter (ADV) and Acoustic Doppler Current Profiler (ADCP). They measure the velocity of water by using a principle of sound waves called the Doppler effect. Two types of pressure sensors: a programmable industrial pressure sensor provided by Boskalis and the RBRsolo pressure sensor. Lastly, an Ott current meter was used which measures the flow with an impeller.

3.4.1. The Doppler Effect - Acoustic instruments

The Doppler effect is the change in frequency of a wave when a wave source moves with respect to an observer, or when the observer itself moves relative to the wave source. A sound wave has a higher frequency, or pitch, when it moves to you than when it moves away from you (observer). You can hear the Doppler effect whenever an ambulance passes by with a characteristic building of sound

that fades when the ambulance passes (WHOI, 2020). The high pitched sound when the ambulance is approaching you is caused by the sound waves being compacted, whereas when the ambulance has passed you the low pitched sound is caused by sound waves being spread out (Figure 3.7. The change in pitch you hear tells you how fast the ambulance is moving (Nortek Manuals, 2018a). The ADV and ADCP work by transmitting sound waves with a constant frequency into the water. While travelling through the water, the sound waves scatter back on small suspended particles in the water column. Due to the Doppler effect, sound waves that scatter back from a particle moving away from the instrument have a slightly lower frequency when they return, see Figure 3.12, while sound waves scattering back on a particle that moves towards the instrument have a slightly higher frequency. The frequency stays constant for sound waves that scatter back from particles that neither move away or towards the instrument. The difference in frequency between the transmitted and reflected sound wave is called the Doppler shift (WHOI, 2020). This Doppler shift can then be used to calculate how fast the suspended particles and therefore the water is moving. It is hereby assumed that the scattering material floats passively and at the same speed as the water (Nortek Manuals, 2018c).
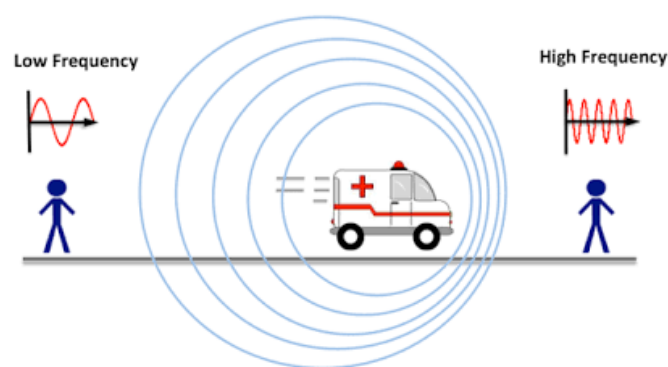
Figure 3.7: Illustration of the Doppler effect: When the ambulance is moving towards you (the person on the right) a high pitched sound can be heard, whereas when it passes (the person on the left) a low pitched sound wave can be heard (Lindner, 2021).

3.4.2. Acoustic Doppler Velocimeter (ADV)

For the measurements, the Nortek Vector (ADV) is used which can sample up to 64 Hz. It measures on a small sampling volume close to the instrument which can be seen in Figure 3.10a. The Vector is a field instrument that is designed for measurements of rapid small scale changes in 3D velocity, used for turbulence, boundary layer measurements, surf zone measurements and measurements in very low flow areas (Nortek Manuals, 2018a). The Vector consists out of a probe and a case. In the probe, the transmitter and three receivers of the acoustic signals are situated together with the temperature sensor. In the case, the pressure sensor, tilt sensor, magnetometer and compass are located. For the measurements, both fixed and flexible probe ADVs were used. An overview of the ADV with the fixed probe is given in Figure 3.8.
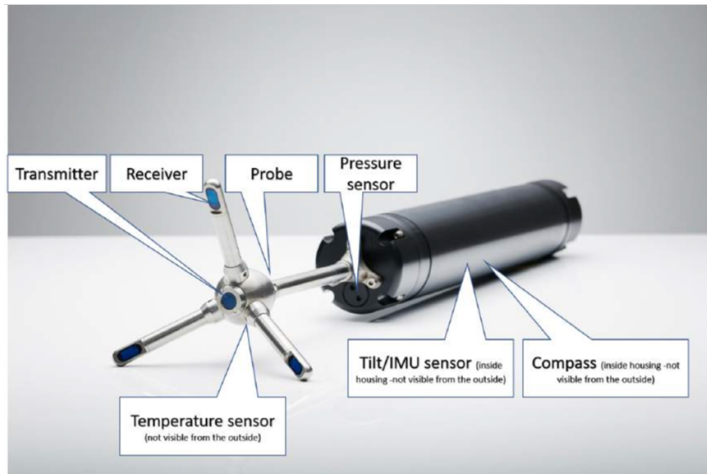
Figure 3.8: Illustration of the Nortek Vector ADV. The probe (head of the ADV) consists out of the transmitter in the centre, which sends out the sound pulses, three receiver arms, that listen to the echo of the sound pulses, and the temperature sensor. The case (housing of the ADV in black) consists out of the pressure sensor, tilt sensor, magnetometer and compass (Nortek Manuals, 2018a).

ADV working principle

The ADV measures velocity by using the Doppler effect as explained in Section 3.4.1. It sends out a short acoustic pulse pair from the transmitter element with a known time lag to determine the Doppler induced phase shift. The ADV is a pulse coherent instrument as it needs at least two pulses to measure the current velocity, opposed to the ADCP which determines the current velocity by the Doppler shift of only one emitted pulse as explained in Section 3.4.3. The advantage of the pulse coherent technique is that low noise measurements and greater accuracy are obtained compared to direct Doppler frequency shift determinations with one pulse. However, a limitation is the maximum profiling range (Nortek Manuals, 2018a). The processing technique of the ADV is illustrated in Figure 3.9. It works as follows: two pulses are sent out by the transmitter, the pulses hit a particle, part of the sound waves scatter back, the echos are recorded in the acoustic receiver arms from which the phase shift between the received echos is determined. This phase shift is then used to determine the current velocity according to Equation 3.2. Here V is the current velocity, $\Delta\phi$ the phase difference, F_{source} the transmitted frequency and Δt the time difference between two consecutive pulses.
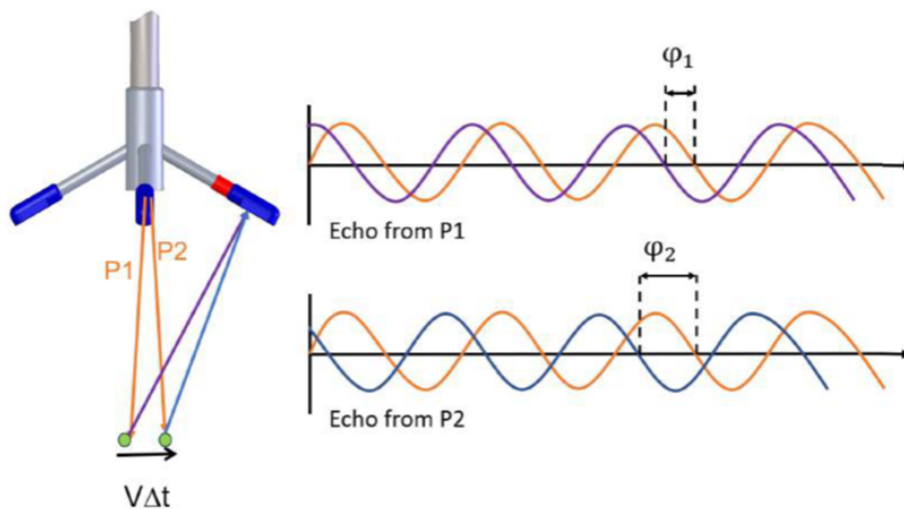
Figure 3.9: ADV flow velocity measurement technique: An acoustic pulse pair is transmitted with a known time lag from which the Doppler induced phase shift can be calculated from the received two echos. The transmitter is in blue in the center, the particles in the water where the pulse pair reflects on is illustrated in green and the receiver arms are in blue on the side of the ADV (Nortek Manuals, 2018a).

$$V = \frac{\Delta\phi \cdot C_{sound}}{4\pi \cdot F_{source} \cdot \Delta t} \qquad (3.2)$$

The Doppler shifts measured at the three receivers of the ADV provide flow velocity estimates along the three beam directions. These are then combined geometrically to obtain velocities in three dimensions (Nortek Manuals, 2018a), as seen in Figure 3.10. The ADV is a bistatic system which means that the transmitters and receivers are physically separated. The sampling volume is defined as the area where the beams intersect each other at 0.157 m from the transmitter as seen in Figure 3.10a. The ADV has a very small sampling volume and can therefore be seen as a single point measurement instrument.

(a) Illustration of the sampling volume of the Nortek Vector defined at 0.157 m from the transmitter where the beams of the receivers and transmitter intersect.

(b) Illustration of the ADV measuring velocity in three dimensions with velocity vector V in blue.
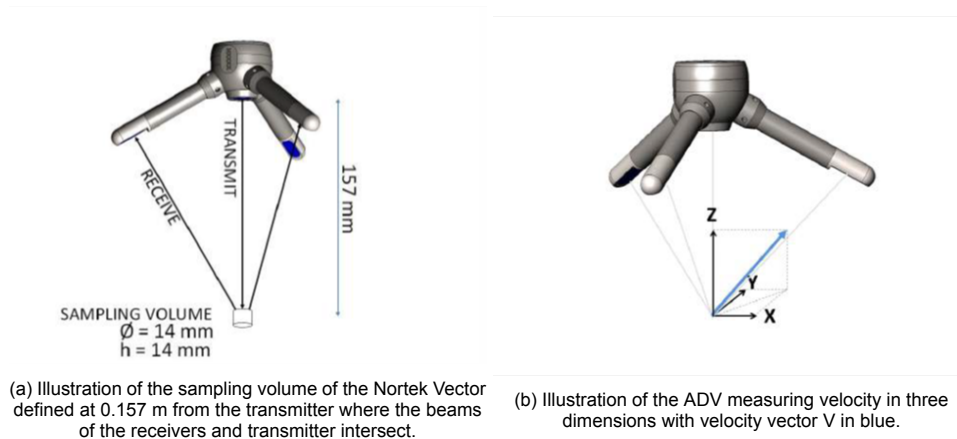
Figure 3.10: Sampling volume (a) and calculated 3D velocity vector (b) of the ADV (Nortek Manuals, 2018a)

3.4.3. Acoustic Doppler Current Profiler (ADCP)

For the measurements, the Nortek Signature 1000 Acoustic Doppler Current Profiler (ADCP) is used which can measure flow velocities up to 16 Hz. ADCPs measure the water velocity through the entire water column or over a distance set by the user prior to the measurements. ADCPs can measure turbulence profiles, current profiles, ice and waves. The Signature 1000 transmits sound pulses into the water column and listens to the return pulse. It has 5 acoustic transducers (beams), four slanted at 25° from the vertical and a fifth vertical beam (altimeter), see Figure 3.11. ADCPs measure the mean velocity over a measuring volume enclosed by the four slanted beams which increases moving further away from the instrument (See Figure 3.13b).
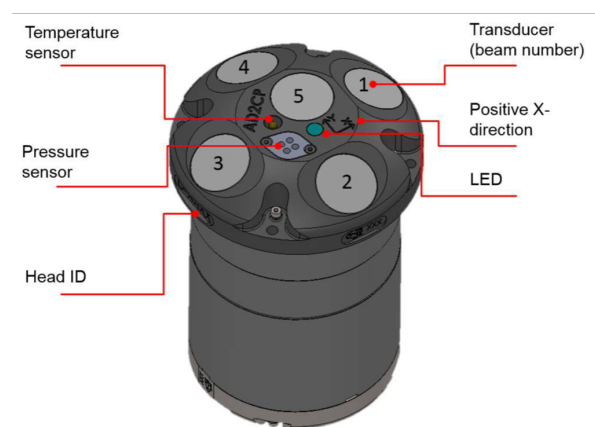
Figure 3.11: Overview of the Signature 1000 (ADCP): the 5 beams, reference system and sensors (Nortek Manuals, 2018b).

ADCP Working principle

The ADCP works by transmitting 'pings' of sound at a constant frequency into the water. The ping travels with the speed of sound through the water column and as the signal hits particles part of the acoustic energy is scattered back to the transducer, while the rest of the energy continues further into the water column and scatters back at a later point in time. By measuring the time it takes for the waves to bounce back and the Doppler shift, the ADCP can measure the current velocity at many different depths with each series of pings (WHOI, 2020). The ADCP processes the signal by comparing the transmitted wave with the received wave (Doppler frequency shift) to calculate the relative velocity (Figure 3.12). The relative velocity can be calculated using Equation 3.3, where V is the current velocity, $F_{Doppler}$ the Doppler shift, F_{source} the transmitted sound wave frequency and C the speed of sound in water (Nortek Manuals, 2018c).

$$V = \frac{F_{doppler}}{F_{source}} \cdot \frac{C_{sound}}{2} \tag{3.3}$$
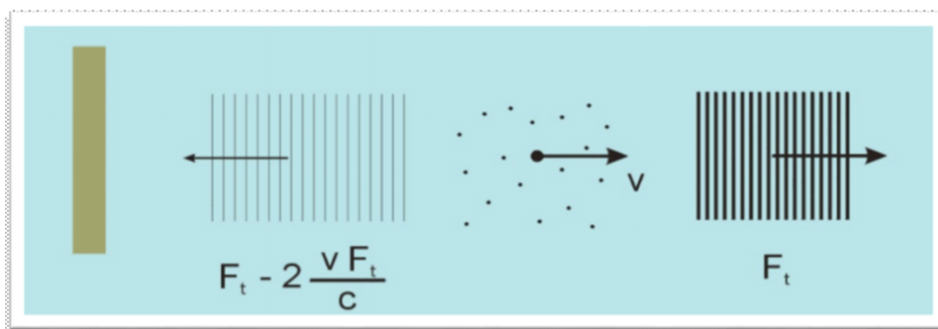
Figure 3.12: Illustration of an acoustic echo (sound wave) reflected from moving particles shifted in frequency by the Doppler shift in proportion to the particle velocity (Nortek Manuals, 2018d)

The ADCP measures the velocity profile through the water column by a sequence of depth cells (see Figure 3.13a). The cell size specifies the length of each depth cell in the profile and therefore the depth resolution. The cell size can be set prior to the measurements depending on the goal of the measurements. When a high resolution is necessary a small cell size should be chosen (Nortek Manuals, 2018c). The transducer of the ADCP works both as a transmitter and receiver. This is referred to as a monostatic instrument that has a blanking distance above the instrument in which no velocities can be measured (Figure 3.13a).

The beams measure velocities in the direction of the beam. Each pair of beams (beams 1 & 3 and 2 & 4) measure one horizontal and one vertical velocity component. To determine the three-dimensional velocity the resultant of the horizontal velocity of both beam pairs and of the vertical velocities is needed. Hereby it must be noted that particle velocities perpendicular to the ADCP beams are not measured as these do not affect the Doppler shift. The measurement method averages the velocity over the spatial area enclosed by the beams of the ADCP in one cell. While moving away from the instrument the velocities in a cell are averaged over a larger area as seen in Figure 3.13b. An assumption made hereby is horizontal homogeneity in the enclosed area. This is an accepted requirement in oceanic environments but is not in highly turbulent environments such as a propeller jet (Nortek Manuals, 2018c). In the situations where horizontal homogeneity does not hold, extra attention should be paid to the method that is used to determine the three dimensional x, y and z velocities.

(a) Definition of the velocity profile with the cell positions of the ADCP. The n-th cell is centered at a vertical distance from the transducer equal to: Center of n'th cell = blanking distance + n · cell size.

(b) Measurement area sectioned into cells of the Signature 55 (three beams). This is comparable with the Signature 1000 where the measurement area is enclosed by the four slanted beams. The velocities are spatially averaged over the area in a cell enclosed by the beams of the ADCP.

Figure 3.13: Definition of velocity profile (a) and the measurement area enclosed by the beams of an ADCP (b) (Nortek Manuals, 2018b)

3.4.4. Ott C31 current meter

The Ott C31 is a current meter that uses an impeller to measures flow velocities. They are usually used to measure discharges in rivers or channels. It is a reliable instrument that can be used under difficult conditions with high accuracy. The Ott C31 can measure flow velocities between 0.025 and 10 m/s with an accuracy of ± 2 % (OTT-HydroMet, 2021). In Figure 3.14 the C31 Ott meter is illustrated.

After a rotation of the impeller, an electrical signal is sent to a counter which registers the total amount of rotations. By determining the time span over which a certain amount of rotations take place the flow velocity can be determined with the calibration sheet for the Ott meter. For the measurements in Gent the Ott meter was programmed by Michel Ruijter to give the start time, duration and corresponding velocity of each rotation of the impeller. As a result, the amount of data output depends on the flow rate of the water. When the water is flowing rapidly, the impeller rotates fast with a large number of rotations and data point of the flow velocity. When the water is flowing slowly, the impeller rotates slowly resulting in a small number of data points. The Ott meter timestamp determined by using a GPS signal in UTC time.

Figure 3.14: Illustration of the Ott C31 current meter mounted on a rod (OTT-HydroMet, 2021).

3.4.5. Pressure sensor - Programmable Submersible Level Transmitter

To measure the pressure fluctuations at a high frequency the PTM/N programmable 4-20 mA industrial pressure sensor was used. The sensors measure absolute changes in pressure and have an analogue electrical signal output of 4-20 mA (STS-sensors, 2018). The sensors were calibrated on 0-4 bar absolute pressure. Therefore, 4 mA corresponds to 0% or 0 bar and 20 mA corresponds to 100% or 4 bar. The pressure sensors are connected by cable with a data acquisition device made by the R&D department of Boskalis. The data acquisition device uses the Gantner software and hardware to convert the analog electrical signal to a digital signal. For the measurements the pressure sensor was programmed at 100 Hz and had a fixed accuracy of ±0.25% over the 4-20 mA signal range. In Figure 3.15 the pressure sensor is illustrated.

Figure 3.15: Illustration of the Programmable Submersible Level Transmitter (STS-sensors, 2018).

3.4.6. Pressure sensor - RBR solo

The second type of pressure sensors is the RBR solo[3] which has a sampling rate of 2 Hz and an accuracy of ±0.05%. The sensor is compact, runs on batteries and stores the measured pressure changes internally. The sensors measure the absolute pressure which can be converted to pressure in meters water column when the atmospheric pressure p_{atm} and the water density ρ are known. The sensor is illustrated in Figure 3.16 where the sensing element is located at the side of the red ring.

Figure 3.16: Illustration of the RBR solo 2 Hz pressure sensor with the sensing element at the end of the red ring on the right (RBR, 2021).

3.5. Measurement set-up

In this section, the measurement set-up is elaborated used to measure the near-bed flow velocities and pressure fluctuations. The set-up consists out of two separate frames where the instruments are mounted on. A horizontal frame placed on the bed near the crossing between the sheet pile wall (quay wall) and the bed protection and a vertical frame mounted at the bottom on the horizontal frame and at the top to the stairs close to bollard 28. In Figure 3.17 the locations of the frames with respect to the bed, quay wall and Somtrans XXV are schematized.
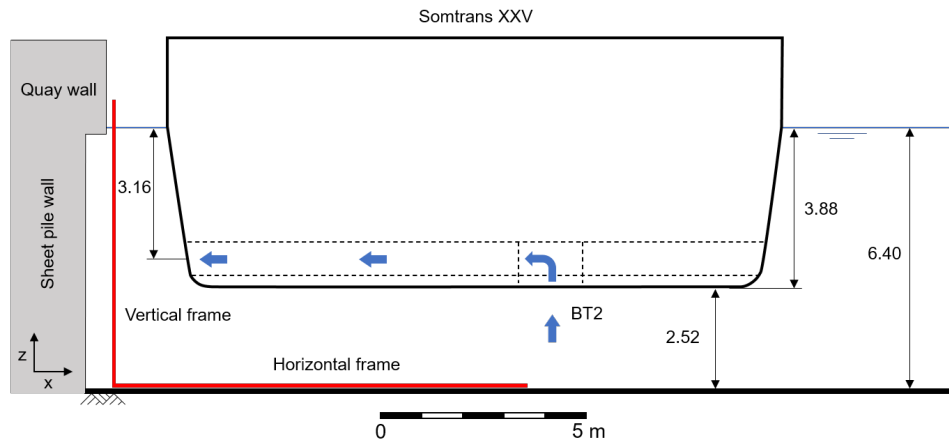
Figure 3.17: Illustration of the location of the horizontal and vertical frame (in red) with respect to the bed, quay wall and Somtrans XXV. The cross-section of the Somtrans XXV is made at the location of bow thruster 2. The shape of the hull of the Somtrans XXV is schematized to a rectangular shape. The dimensions are given in meters.

3.5.1. Reference system

As a reference point, the white stair (Figure 3.18) located 4 m away from bollard 28 is used during the measurements. During placement, the vertical and horizontal frame are aligned with the white stair. Therefore, the white stair functions as a visual point above the water to align the Somtrans XXV with the measurement frames. The middle of the white stair is the $y = 0$ reference line. The movements in y-direction of the Somtrans XXV is defined from the $y = 0$ reference line which is aligned with the axis of bow thruster 2. The positive y direction is defined towards the bow of the Somtrans XXV. The $x = 0$ reference line is defined as the heart-line of the sheet pile wall with the positive x-direction towards the open channel or directed away from the quay wall. An overview of the top view of the reference system with the Somtrans XXV is given in Figure 3.19.

Figure 3.18: The white stairs located 4 m away from bollard 28 (red box) which were used as reference point for the measurement. The top scaffolding of the vertical frame is mounted on the stairs for support. The green cables in the figure are the instrument cables from the pressure sensors, ADVs and ADCPs.
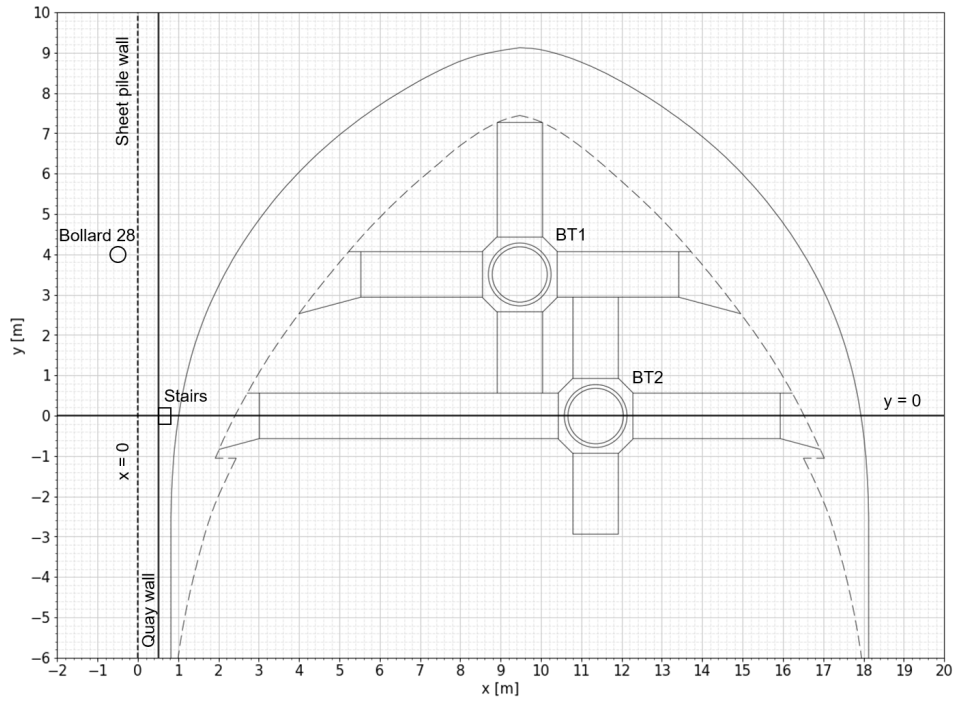
Figure 3.19: Top view of the reference system in x and y direction. The top view of the Somtrans XXV is drawn in the reference system where the dashed line is the bottom (keel) of the vessel and the solid line the top of the vessel. The axis of bow thruster 2 is aligned with the y = 0 refrence line. The sheet pile wall is located 0.5 m (in negative x direction) away from the side of the quay wall (concrete cap as illustrated in Figure 3.3).

The z = 0 reference line is the bed of the Moervaart channel defined as the top of the asphalt mattress bed protection. The positive z-direction is directed upwards towards the water surface as illustrated in Figure 3.20
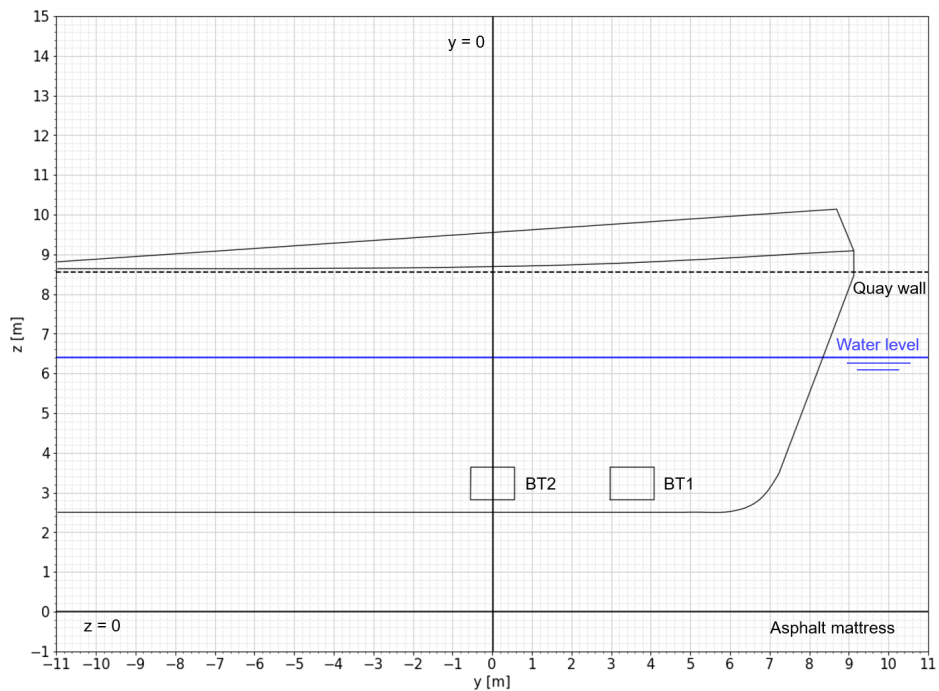
Figure 3.20: Side view of the reference system in z and y direction. The side view of the Somtranx XXV is drawn into the figure with the y = 0 reference line in the axis of the outlet channel of bow thruster 2. The blue line is the water level and the dashed black line the top of the quay wall.

3.5.2. Horizontal measurement frame

The horizontal measurement frame is made out of scaffolding with a diameter of 0.05 m. The frame has a total length of 9.92 m and is 1.35 m wide. The centerline of the frame is aligned with the centre of the white stairs which is the y = 0 reference line as discussed in Section 3.5.1. Therefore, whenever the Somtrans XXV is aligned with the white stairs it is also aligned with the horizontal measurement frame at the bed. On the measurement frame four ADVs (yellow triangles), three ADCPs (green squares), two Ott current meters (red rhombuses) and six pressure sensors (blue circles) are mounted. Their x,y and z coordinate with respect to the reference system is illustrated in Figure 3.21 and listed in Table 3.3. An overview of the measurement instrument locations with respect to the Somtrans XXV, while the measurement frame is aligned with bow thruster 2, is illustrated in Figure 3.22.
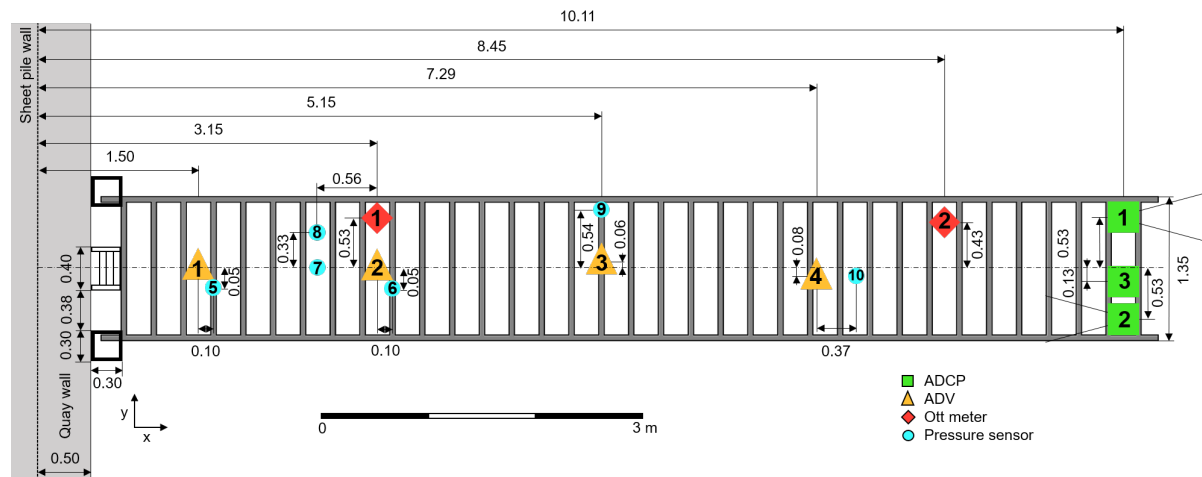
Figure 3.21: Illustration of the horizontal measurement frame with respect to the quay wall aligned with the white stairs defined as the y = 0 reference line. On the measurement frame, four ADVs (yellow triangles), three ADCPs (green squares), two Ott current meters (red rhombuses) and two RBR solo pressure sensors (blue circles) are mounted.

Table 3.3: Overview of the measurement instruments mounted on the horizontal measurement frame including their x,y,z coordinates with respect to the reference system defined in Section 3.5.1. Distance x in D_t is defined as the dimensionless distance between the sheet pile wall and the instrument calculated by dividing the x-coordinate by the equivalent circular diameter of the bow thruster (D_t = 1.07 m)

Instrument	Sampling frequency [Hz]	x [m]	x in D_t [-]	y [m]	z [m]
ADV1	64	1.50	1.40	0	0.36
ADV2	64	3.15	2.94	0	0.36
ADV3	16	5.15	4.81	0.06	0.40
ADV4	8	7.29	6.81	-0.08	0.24
ADCP1	8	10.11	9.45	0.53	0.22
ADCP2	8	10.11	9.45	-0.53	0.22
ADCP3	16	10.11	9.45	-0.13	0.24
Ott meter 1	-	3.15	2.94	0.53	0.24
Ott meter 2	-	8.45	7.90	0.43	0.24
Pressure sensor 5 (RBR1)	2	1.60	1.50	-0.05	0.06
Pressure sensor 6 (RBR2)	2	3.25	3.04	-0.05	0.06
Pressure sensor 7 (ADV1)	64	2.59	2.42	0.33	0.07
Pressure sensor 8 (ADV2)	64	2.59	2.42	0	0.07
Pressure sensor 9 (ADV3)	16	5.15	4.81	0.54	0.07
Pressure sensor 10 (ADV4)	8	7.66	7.16	0.08	0.07

Elaboration measurement instrument locations on the horizontal frame

In this section, the location of the measurement instruments in x-direction, perpendicular to the quay, of the ADVs, Ott meters, ADCPs and pressure sensors on the horizontal frame is elaborated.

The **ADVs** are placed perpendicular (x-direction) from the quay wall on the horizontal measurement frame to measure the decay of the reflected flow velocities near the bed. First, the location of ADV1, closest to the quay wall, is determined which should capture the highest flow velocities induced by the bow thruster jet. Usually, the highest flow velocities are measured near the quay wall, but not to close, as the flow needs space to develop after reflecting on the bed (Section 2.3). The location where the highest flow velocities are measured in previous research is discussed in Section 2.3.4. However, the exact location of the highest flow velocities remains uncertain as literature gives different results on this location. Schmidt (1998) most elaborately researched the location of maximum flow velocity perpendicular to the quay. Measuring maximum flow velocities at 0.9 D_t for a quay wall clearance of L = 4 D_t and 1.47 D_t for L = 5.5 D_t, while keeping the height of the bow thruster axis in the water column constant at h_t = 2.18 D_t. This corresponds well with the measurement set-up of the Somtrans XXV in Gent where the bow thruster axis height, h_t, was 2.36 D_t during all tests. For the measurements where the Somtrans XXV was moored to the quay wall, BT1 and BT2 had a quay wall clearance (L) of 5.24 and 2.89 D_t respectively. The quay wall clearance (L) of BT1 coincides well with the tests of Schmidt (1998) for which L was 5.5 D_t and the maximum flow velocity occurred at 1.47 D_t. Therefore, the first ADV (ADV1) should be placed at approximately the same distance from the quay wall, resulting in an eventual location of 1.4 D_t perpendicular to the quay wall, see Figure 3.21.

Secondly, the spatial resolution for the placement of the other three ADVs on the horizontal measurement frame is determined. The spatial resolution of the ADVs in x-direction is a trade-off between the number of ADVs available for the measurements and the distance from the quay wall where almost no significant flow velocities were measured according to literature (Section 2.3.4). As stated in the measurements of Cantoni (2020), almost no significant flow velocities were measured at 7.67 D_t from the quay wall (due to the reflected bow thruster jet). This observation is inline with scale model tests from De Jong and Van Velzen (2015) where significantly lower flow velocities were measured at 8.8 D_t from the quay wall. Keeping this in mind, a spatial step size of approximately 1.5 D_t is chosen close to the quay wall for ADV1 (1.4 D_t) and ADV2 (2.94 D_t) to capture the highest flow velocities. Moving further from the quay wall, a step size of approximately 2 D_t is chosen for ADV3 (4.81 D_t) and ADV4 (6.81 D_t). The location of ADV3 coincides well with the second measurement location in the measurements of De Jong and Van Velzen (2015) at 4.76 D_t. While ADV4 is in proximity of the second ADV location in the measurements of Cantoni (2020) at 7.67 D_t where no significant flow velocities were measured.

The first **Ott meter** has been placed at the same x-coordinate as ADV2. In this way, there is redundancy in the measurement data of the ADVs by comparing the measured flow velocities of ADV2 to those of Ott meter 1. The second Ott meter has been placed at a distance of 7.9 D_t from the quay wall to have an extra spatial point at 1 D_t from ADV4 to measure the decay in flow velocities. Besides, it could provide information on the inflow velocities near the bow thruster inlets as it is positioned close to these inflow points (Figure 3.22). Additionally, it could be used to verify flow velocities measured at ADV4. Although, the distance of 1 D_t between them should be taken into account.

The **ADCPs** are placed at the end of the measurement frame at 9.45 D_t from the quay wall. ADCP1 is mounted horizontally directed away from the quay looking in positive x-direction. It measures the reflected flow velocities until a maximum range of 10 m from the ADCP. ADCP2 is horizontally mounted directed towards the quay wall looking in negative x-direction. It measures the reflected flow velocities between the quay wall and the ADCP. ADCP3 is mounted vertically directed upwards in positive z-direction. It measures the flow velocities in positive z-direction between the ADCP and the keel of the Somtrans XXV. All ADCPs are mounted between the inflow suction points of bow thruster 1 and 2 (Figure 3.22). Therefore, the ADCPs do not only measure flow velocities due to the reflection of the propeller jet on the quay wall but also flow velocities induced by the bow thruster inlets sucking in water.

Pressure sensor 7 - 10 are the pressure sensors located in the cases of the ADVs. The ADV cases of ADV1, ADV2 and ADV3 are not positioned next to the head of the ADV. While the horizontally mounted ADV4 has a fixed stem between the case and the ADV head resulting in a distance of 0.37 m between the measurement point where the flow velocities are measured and the pressure sensor (Figure 3.24). Thus, the measurements of the pressure sensors of the ADVs do not correspond to the same location as the measurements of the velocities (Figure 3.21). The pressure sensors measure with the same

frequency as the corresponding ADV head that measures velocity.. **Pressure sensor 5 and 6** (RBR solo pressure sensors) are mounted next to ADV1 and ADV2 in order to have pressure measurements at the same location as the flow velocity measurements. PS5 is illustrated in Figure 3.23b with the sensing element indicated in red pointing towards the ADV. It has to be noted though that the RBR solo pressure sensors measure at a frequency of 2 Hz while ADV1 and ADV2 measure at 64 Hz.
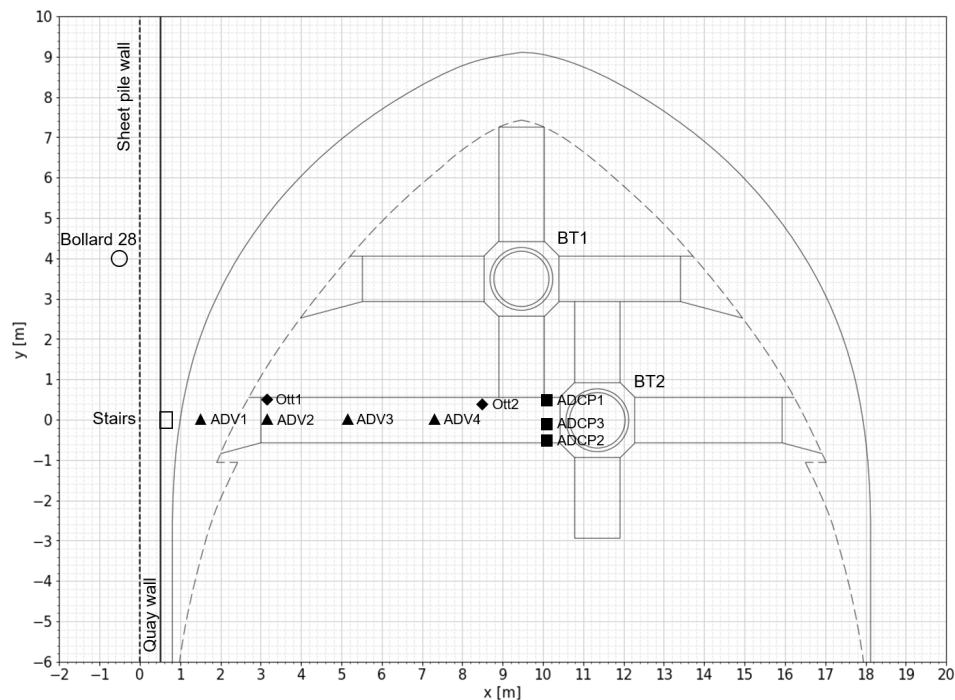
Figure 3.22: Illustration of the locations of the measurement instruments with respect to the reference system and the quay wall. The pressure sensors are left out of the overview. The outlines of the Somtrams XXV are illustrated were to bottom of the Somtrans XXV is drawn with a dashed black line (keel) and the top is drawn with a solid black line. The axis of bow thruster 2 is aligned with the instruments.

3.5.3. ADV - set-up

The set-up of the Nortek Vector ADV consists out of two parts. First, the mounting of the ADVs on the measurement frame as illustrated in Figure 3.23 for ADV 1-3, which have a flexible cable between the head and the case, and in Figure 3.24 for ADV4 with a fixed stem between the head and the case. Secondly, the ADV measurement input settings for the Vector deployment program, as listed in Table 3.4, are elaborated.

Table 3.4: ADV measurement settings

Setting	Value
Sampling mode	Continuous
Sampling frequency	64, 16, 8 Hz
Nominal velocity range	±7.00 m/s
Coordinate system	XYZ
Salinity	0 ppt

The *sampling mode* of the ADV was set to measure continuously from the moment that the ADV was turned on or from the programmed deployment time. ADV1 was directly connected with the measurement laptop while ADV2, ADV3 and ADV4 were deployed with a predefined start time from which they measured continuously until they were manually stopped at the end of the measurements. By measuring continuously the uncertainty of starting and stopping the ADV for every measurement was

(a) Illustration of the flexible head ADV (1-3) while mounted on the horizontal measurement frame. In white the wooden structure holding the ADV in place is illustrated. In red the sampling volume of the ADV is illustrated. The total height above the bed at which the ADV measures the flow velocities is 0.357 m.

(b) Photo of ADV1 and RBR solo 1 illustrating how they are mounted on the horizontal measurement frame. The black band on the ADV arm in the centre of the photo indicates the positive x-direction of the ADV. On the left the case of the ADV can be seen which is placed just behind the location of the ADV head. On the right the RBR solo is taped to the scaffolding with the sensing element (red) pointed towards ADV1.

Figure 3.23: Illustration of ADV 1-3 mounted on the horizontal measurement frame (a) and a photo of ADV1 taken before placing the frame on the bed (b).

Figure 3.24: Photo of ADV4 mounted on the horizontal measurement frame. Apposed to ADV 1-3, ADV4 has a fixed stem between the head and the case. Thus, the head could not be placed in the same manner as ADV 1-3 illustrated in Figure 3.23. The head of ADV4 is rotated 90° in anti-clockwise direction compared to ADV 1-3 with the positive x-axis (black band around ADV arm) directed upwards in positive z-direction according to the reference system.

eliminated. Besides, by measuring continuously flow velocities during zero conditions (no vessels manoeuvring at or passing by the quay wall) during various moments over the measurement period could be determined.

Since the flow induced by the reflected propeller jet is highly turbulent the highest possible *sampling frequency* of 64 Hz was set during the measurements for ADV1 and ADV2, which both had a direct power supply. The sampling frequency of ADV3 and ADV4 was set at 16 Hz and 8 Hz respectively due to limited battery power which could not be charged or changed during the measurements.

The setting for the *nominal velocity range* is a trade-off between accuracy and reliability. Uncertainty in the measured velocities by the ADVs are proportional to the velocity range. Therefore, smaller velocity ranges give a smaller measurement uncertainty. Another reason to choose a small velocity range is to reduce noise. However, if the velocities exceed the nominal velocity range the measured velocities are incorrect and the data may become unusable. With expected outflow velocities from the bow thruster

that could reach 8 m/s, the nominal velocity range was set to the maximum value of ±7 m/s (for the beam components). This corresponds with a horizontal velocity range of 8.75 m/s and a vertical velocity range of 2.5 m/s.

The *coordinate system* was set to XYZ (cartesian coordinate system) which measures the flow velocities relative to the XYZ coordinates of the probe head, see Figure 3.25. Another option would have been to measure in ENU (East-North-up) coordinates. ENU uses the compass and tilt sensor to correct for movements of the instrument. The requirement for this is that the tilt sensor in the case is orientated correctly predefined by Nortek which is either horizontal or vertical (indicated on the case). For the measurements, all cases of the ADVs could only by mounted horizontally. Therefore, not all tilt sensors could work correctly during the measurements ruling out the option for the ENU coordinate system. For the measurements, the positive x-direction of the Vector probe head was positioned to point in the direction of the positive x-direction according to the defined reference system (Section 3.5.1). This direction is also illustrated in Figure 3.23b where the ADV arm indicated with black is the positive x-direction.

The default *salinity* setting for the Vector is 35 ppt. There were no salinity measurements performed but as the Moervaart is a freshwater river removed far away from saltwater intrusion points such as the locks of Terneuzen a salinity of 0 ppt is assumed.
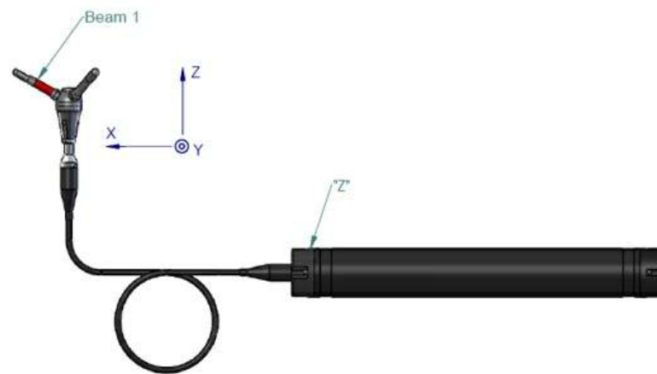
Figure 3.25: Orientation of XYZ coordinates of the Vector cable probe head (Nortek Manuals, 2018a)

3.5.4. ADCP - set-up
The set-up of the ADCPs consists out of two parts, how they are mounted on the measurement frame and the settings used for the Signature deployment programme. For the measurements, three ADCPs were used which were mounted to the horizontal measurement frame as illustrated in Figure 3.26. ADCP1 and ADCP2 are mounted horizontally looking away from the quay wall (ADCP1) and looking towards the quay wall (ADCP2). The corresponding dimensions and measurement height above the bed for the horizontally mounted ADCPs are illustrated in Figure 3.27. Beam 1 and 3 of the slanted beams can not be used as beam 1 is directed towards the bed and beam 3 is directed towards the keel of the Somtrans XXV. ADCP3 has a measurement height starting at 0.339 m including the 0.1 m blanking distance. The ADCP input settings for the Signature deployment programme are listed in Table 3.5. ADCP1 and ADCP2 are programmed to measure with the four slanted beams and the high resolution 5th beam in the middle at 8 Hz while ADCP3 only measures with the four slanted beams at 16 Hz.

Figure 3.26: Photo of ADCP1 (right), ADCP2 (left) and ADCP3 (middle). ADCP1 and ADCP2 are horizontally mounted within a wooden structure attached to the measurement frame. ADCP3 is mounted looking vertically upwards by means of a clam to the measurement frame.
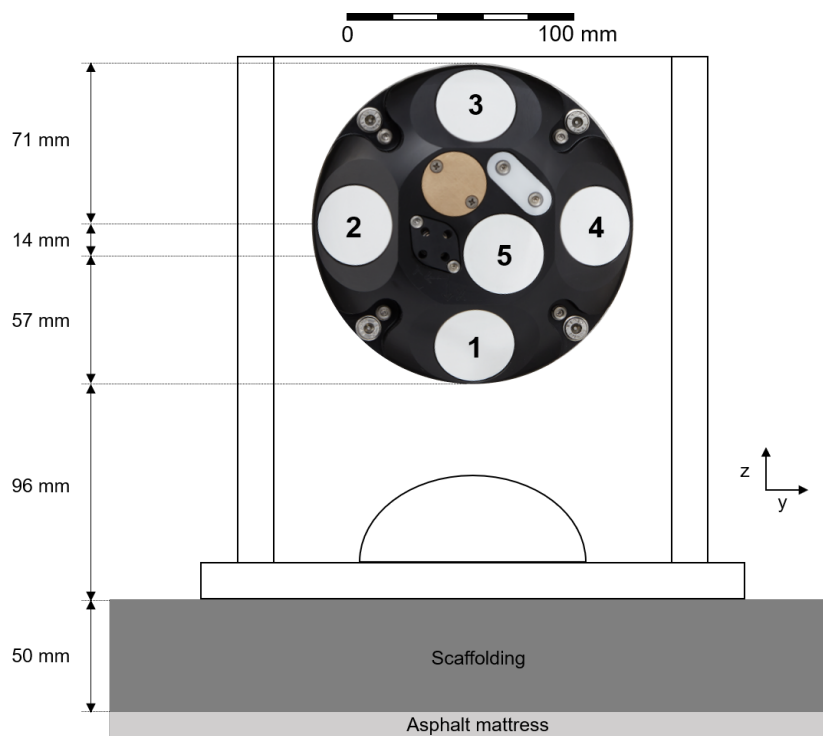
Figure 3.27: Illustration of ADCP1 horizontally directed while mounted on the horizontal measurement frame. In white the wooden structure holding the ADCP in place is illustrated. Beam 2 and 4 measure the flow velocity at 0.217 m above the bed while beam 5 measures the flow velocity at 0.203 m above the bed.

Table 3.5: Measurement settings for the four slanted ADCP beams (1-4) and the 5th beam.

Setting	Beam 1-4	5th beam
Sampling mode	Continuous	Continuous
Sampling frequency	16, 8 Hz	8 Hz
Velocity range	±2.5 m/s	±0.69 m/s
Coordinate system	Beam	Beam
Profiling range	10 m	5 m
Cell size	0.2 m	0.02 m
Blanking distance	0.1 m	0.1 m
Salinity	0 ppt	0 ppt

The three ADCPs are connected with a cable to the laptop. The *sampling mode* is set on continuous measurements which is manually started and stopped at the beginning and end of the measurement day. By measuring continuously the uncertainty of starting and stopping the ADCP for every measurement was eliminated. Besides, by measuring continuously flow velocities during zero conditions (no vessels manoeuvring at or passing by the quay wall) could be measured during the day.

The *sampling frequency* was set at its maximum value due to the highly turbulent environment which was measured in. The maximum sampling frequency is 16 Hz for the four slanted beams, but when the high-resolution 5th beam is used as well the maximum sampling frequency is 8 Hz for all 5 beams.

The *velocity range* for the four slanted beams is ±2.5 m/s while the velocity range for the high resolution 5th beam depends on the profiling range. The product of the profiling range and velocity should not exceed 3.0 m^2/s. For the profiling range 5 m was chosen which resulted in a velocity range of ±0.69 m/s. The *coordinate system* was set to measure velocities in beam direction. In this way, the velocities are not yet averaged over the cell volume which can be done later manually by using the conversion matrix. Beam velocities give a better representation of the flow velocities as when they would be averaged over the cell volume which increases with increasing distance from the instrument.

The *profiling range* for the four slanted beams was set to 10 m. This is the distance between the quay wall and the location of the ADCPs on the measurement frame. The area between the quay wall and the ADCPs is seen as the most interesting area to measure the flow velocities. ADCP1 one measures from x= 10 m until x= 20 m from the quay wall. This covers the horizontal area underneath the vessel where flow velocities are trapped between the bed and the vessel, as seen in Figure 3.22. The *cell size* is chosen as small as possible for both the four slanted beams as the 5th beam to have the highest spatial measurement resolution. This results in a cell size of 0.2 m for the four slanted beams and a cell size of 0.1 m for the 5th beam. The *blanking distance* after which the measurement profile starts is chosen as small as possible to start measuring as close as possible to the ADCP. For the four slanted beams and the 5th beam this results in a blanking distance of 0.1 m. The *salinity* was set to 0 ppt as the measurements took place in freshwater as discussed in Section 3.5.4.

3.5.5. Ott meter - set-up

The Ott current meter is mounted on a rod where it can rotate around freely following the direction of the flow velocity during the measurements. It measures the absolute horizontal flow velocity in the direction of the flow at that specific moment but it does not record the flow direction. It follows the flow direction by means of the rudder at the back of the Ott current meter as illustrated in Figure 3.28.
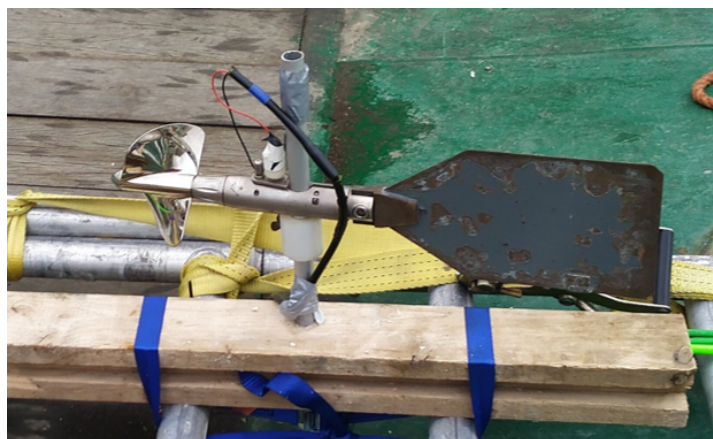
Figure 3.28: Photo of the Ott current meter mounted on a rod where it can rotate freely around following the direction of the flow by means of the rudder attached to the end of the instrument. It measures the flow velocity at a height of 0.24 m above the bed.

3.5.6. Vertical frame

The vertical frame is also made out of scaffolding with a diameter of 0.05 m. The frame consists out of a framework that is 6 m long and 1.35 m wide and three scaffolding bars attached to the top of the framework to lengthen the vertical frame such that it can be attached to the white stairs reference point. At the bottom, the vertical frame is attached to the second bar of the horizontal frame at a distance of approximately 1 m from the quay wall (x = 0 reference). An illustration of the vertical frame is given in Figure 3.29. On the vertical measurement frame, four programmable pressure sensors from Boskalis (Section 3.4.5) are attached indicated by the blue circles. The pressure sensors measure with a sampling rate of 100 Hz. Pressure sensor 2 and 3 are placed at the height of the bow thruster channel outflow point while pressure sensor 1 and 4 are placed near the bottom at the intersection of the bed protection and the quay wall.
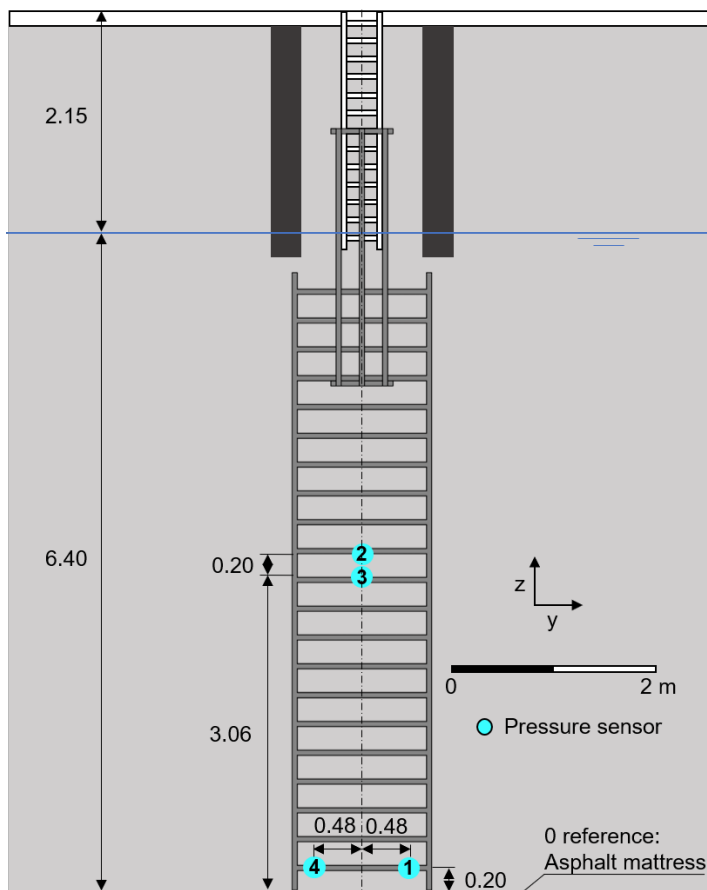
Figure 3.29: Illustration of the vertical frame attached at the top to the white stairs near bollard 28 and at the bottom to the horizontal measurement frame. The center of the frame is aligned with the center of the white stairs (y=0). The water level is illustrated in blue which is approximately 6.4 m above the bed.

Table 3.6: Overview of the programmable pressure sensors including their y and z coordinates with respect to the reference system defined in Section 3.5.1.

Instrument	Sampling frequency [Hz]	y [m]	z [m]
Pressure sensor 1	100	0.48	0.20
Pressure sensor 2	100	0	3.26
Pressure sensor 3	100	0	3.06
Pressure sensor 4	100	-0.48	0.20

In Figure 3.30 the four pressure sensors are indicated together with the Somtrans XXV. Pressure sensor

2 and 3 are at the height of the channel outlet of bow thruster 2 where the propeller jet reflects on the quay wall while pressure sensor 1 and 4 are near the bottom where the propeller jet is reflected on the bed.
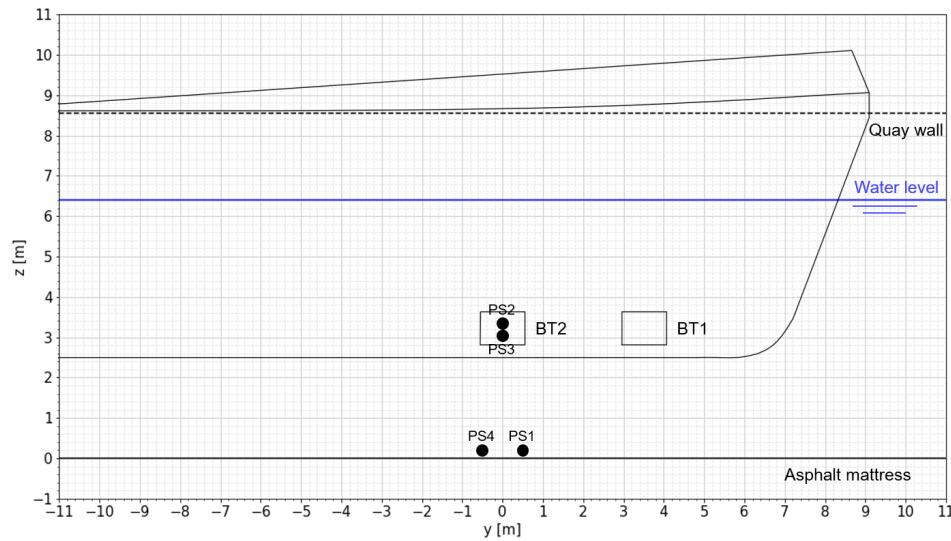
Figure 3.30: Illustration of the location of the four pressure sensors and the Somtrans XXV. For the Somtrans XXV the outer lines are drawn together with the location of bow thruster 1 and 2. Bow thruster 2 is aligned with the vertical measurement frame.

3.6. Measurement parameters

During the measurements four parameters were changed for every test: **(1)** the power load of the bow thruster, **(2)** the used bow thruster, **(3)** the distance in y-direction between the used bow thruster and the centre of the white stairs (reference point at the quay wall) and **(4)** the distance between the quay wall and the Somtrans XXV in x-direction (quay wall clearance L). The only exception on this are the two manoeuvring tests that were carried out at the last measurement day. In these tests only the applied bow thruster power and used bow thruster was changed as the vessel positions varies during the test while manoeuvring.

3.6.1. Applied bow thruster power (1)

To study the effect of the used bow thruster power on the near-bed flow velocities and their fluctuations induced by the bow thruster, three power steps are considered of 25%, 50% and 90%. The measured values for RPM and corresponding power load (%) are illustrated in Figure 3.31 for the measurement tests in Gent in red dots. In addition, the values for RPM and corresponding power load (%) provided by the bow thruster manufacturer are plotted with black dots slightly underestimating the measured values in Gent. Where for the maximum RPM of 1800 the maximum thrust is reached provided by the 394 kW installed engine of the bow thruster. However, the maximum installed power of 394 kW used at 1800 RPM does not correspond to a power load of 100% but to a power load of 90% according to the display at the bridge of the vessel during the tests. Nevertheless, as the exact reason for the display not corresponding to 100% for the maximum amount of RPM and thrust is not known, Table 3.7 is used for the RPM, power load (%) and power in kW used as input for P_t for further calculations of the theoretical efflux velocity V_0 according to Equation 2.3. Where the 90% power load corresponds to the total installed engine power of 394 kW, 50% power load with half of 394 kW equals 197 kW and 25% with a quarter of the totalled installed engine power leading to 98.5 kW.

The measured RPMs and power load (%) during the tests fluctuate around the values listed in Table 3.7 due to the fact that it is quite difficult for the captain to set the RPM on a specific exact number. According to the captain of the Somtrans XXV, both bow thrusters (BT1&2) are used simultaneously during normal manoeuvring operations while the bow thruster operates at the maximum of 1800 RPM

providing the maximum thrust. Both the RPM and corresponding power load (%) were read of from a display at the bridge during the tests.

Table 3.7: RPM of the bow thruster with corresponding power load in % and the used power for determining V_0 in kW.

RPM	Power load [%]	Used power for determining V_0 [kW]
940	25	98.5
1440	50	197
1800	90	394
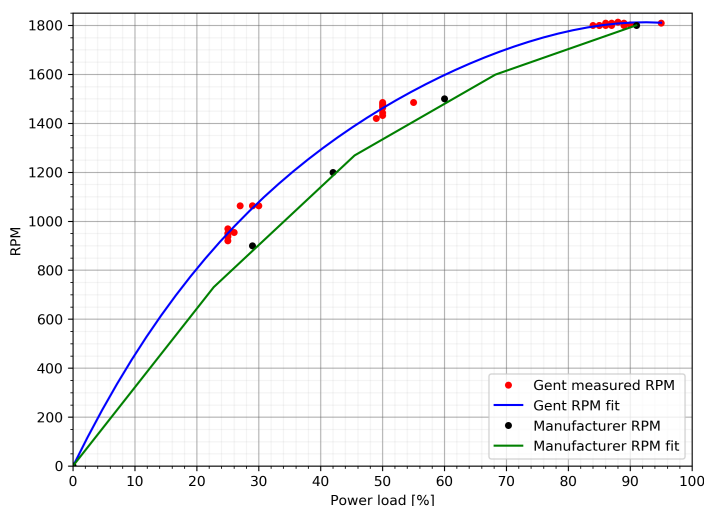
Figure 3.31: Comparison between the measured RPM and corresponding power load (%) from the bridge of the Somtrans XXV during the Gent measurements (red dots) and the values for the RPM with corresponding power load (%) provided by the manufacturer of the bow thruster (black dots).

3.6.2. Used bow thruster (2)

The Somtrans XXV has two bow thrusters, one more towards the bow (BT1) and one more towards the stern (BT2) of the vessel. Due to their different locations in the bow of the vessel they have two different channel lengths and two different quay wall clearances. Thus, the influence of the two different channel lengths and quay wall clearances can be researched by using either bow thruster 1 or bow thruster 2 during a test. To research the maximum allowable load situation the tests were also executed with both bow thruster 1 & 2 turned on at the same time. Concluding, for each position of the vessel with respect to the stairs (reference point) tests are carried out with either bow thruster 1, bow thruster 2 or bow thruster 1 & 2 at the same time.

3.6.3. Distance between BT axis and instruments (y_t): moving the vessel in y-direction (3)

By moving the vessel in y-direction with respect to the measurement frame, extra spatial measurement points are created. Moving the vessel is logistically much easier than moving the measurement frame with respect to the vessel to create extra spatial measurement points. The measurement point matrix of 3x4 for the four ADVs, which is created by moving the vessel ±2 m (1.9 D_t) in y-direction with respect to the bow thruster axis of BT1 and BT12, is schematized in the CFD flow velocity calculations of Van Blaaderen (2005) in Figure 3.32. According to the CFD model of Van Blaaderen (2005), the flow velocities reflect under an angle of approximately 40°(see Figure 2.11 in Section 2.3.3). In the CFD model of Van Blaaderen (2005), the highest flow velocities are not underneath the axis of the bow thruster jet, showing the importance of moving the vessel in y-direction. Otherwise, the maximum flow velocities near the bed could be missed by the measurement instruments.
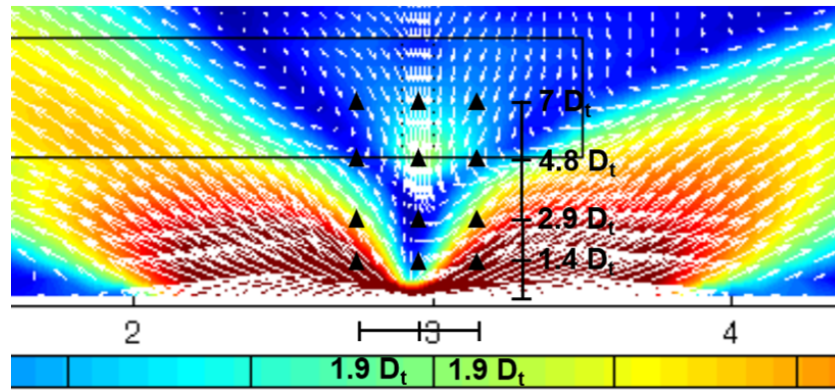
Figure 3.32: Illustration of the 3x4 ADV measurement point matrix created by moving the vessel 1.9 D_t in positive and negative y-direction. The ADV are indicated as black triangles placed at 1.4, 2.9, 4.8 and 7 D_t from the quay wall. The set-up is drawn into the CFD calculations for the flow velocity and direction by Van Blaaderen (2005) showing the reflection of the bow thruster jet on the quay wall under an angle of approximately 40 °.

When the Somtrans XXV is moored to the quay wall, there is a quay wall clearance (L) of 0.8 m in x-direction between the vessel and the sheet pile wall where the bow thruster jet reflects on. For the first six vessel positions, the quay wall clearance is kept constant while moving the vessel in y-direction with respect to the measurement instruments which are aligned with the stairs defined as the y = 0 reference line. First, the axis of BT2 is aligned with the reference line which corresponds to vessel position 1. Afterwards the Somtrans XXV is moved 2 m in negative y-direction resulting in the axis of BT2 situated 2 m below the reference line (vessel position 2). Lastly, the Somtrans XXV is moved 4 m in positive y-direction until the axis of BT2 is 2 m above the reference line (vessel position 3). An overview of vessel position 1-3 is given in Figure 3.33. In this way a spatial grid is created with a spacing of 2 m in y-direction measuring flow velocities from BT2 when the measurement instruments are located directly underneath BT2, when the measurement instruments are 2 m away from BT2 in positive y-direction and when the measurement instruments are 2 m away from BT2 in negative y-direction. The distance between the considered bow thruster axis and the reference line (measurement instruments) will from now on be defined as y_t. Where y_t is positive when the measurement instrument centre line is above the considered bow thruster axis and negative when the measurement centre line is below the considered bow thruster axis, as illustrated in Figure 3.33. For measurements with BT1&2 simultaneously, the axis is defined in the middle between BT1 and BT2.
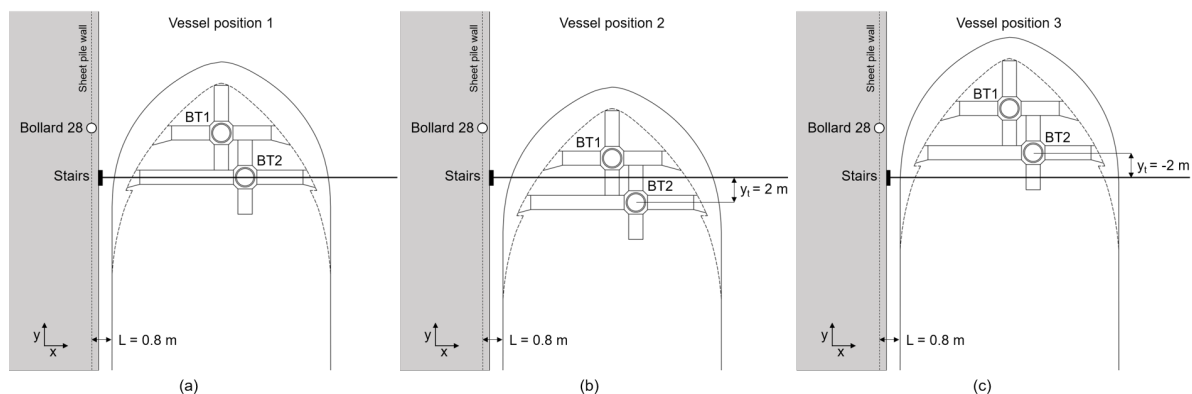
Figure 3.33: Vessel position 1-3 where BT2 is aligned with the measurement instruments (a), BT2 is 2 m below the measurement instruments in negative y-direction (b) and BT2 is 2 m above the measurement instruments in positive y-direction (c).

Vessel positions 4-6 are a repetition of vessel positions 1-3 but instead of moving the vessel in y-direction with respect to BT2 the measurements are conducted with respect to BT1. Measuring with the instruments aligned with BT1, 2 m above BT1 and 2 below BT1 as illustrated in Figure 3.34. The only difference is for vessel position 6 in which the reference line was 1.75 m below BT1 which was executed to have a measurement exactly in between BT1 and BT2 assuming the difference in 0.25 m is negligable.
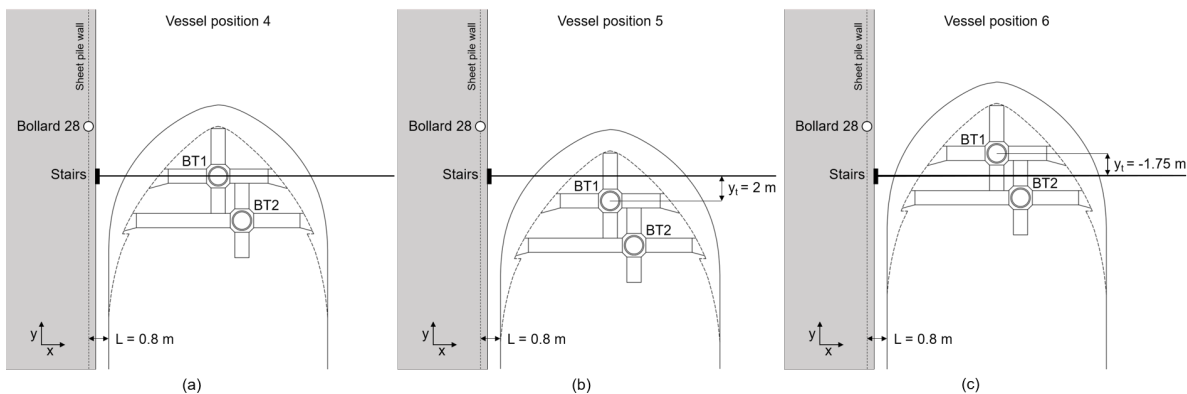
Figure 3.34: Vessel position 4-6 where the axis of BT1 is aligned with the measurement instruments (a), BT1 is 2 m below the measurement instruments in negative y-direction (b) and BT1 is 2 m above the measurement instruments in positive y-direction (c).

3.6.4. Quay wall clearance (L): moving the Vessel in x-direction (4)

By moving the vessel in x-direction the quay wall clearance is increased. From literature (Chapter 2) can be concluded that this is an important parameter influencing the near-bed flow velocities. In vessel positions 7 and 8 the Somtrans XXV is positioned with the y = 0 reference line between BT1 and BT2. From this position, the Somtrans XXV is moved away from the quay wall in positive x-direction increasing the distance between the quay wall and the vessel (L). The Somtrans XXV is moved from a quay wall clearance (L) of 0.8 m (in vessel positions 1-6) to a quay wall clearance (L) of 3 m in vessel position 7 and a quay wall clearance (L) of 5 m in vessel position 8. In Figure 3.35 the vessel positions are illustrated.
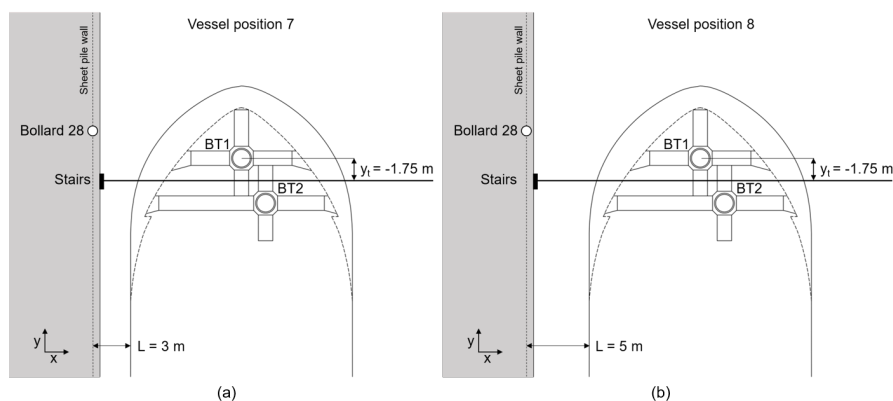
Figure 3.35: Vessel position 7 and 8 where the measurement instruments are between the axis of BT1 and BT2. The quay wall clearance is increased to 3 m (a) and 5 m (b).

While moving the vessel in positive x-direction the lines attached to the bow are loosened to let the bow of the vessel move away from the quay to the desired location. The stern of the vessel is held in place to make sure the vessel does not move unsafely when the bow thrusters are activated. This results in a small angle between the Somtrans XXV and the quay wall. In this situation, the axis of the bow thruster channel will not intersect the quay wall under an angle of 90° as when the Somtrans XXV was moored

parallel to the quay wall, as illustrated in Figure 3.36. The angle α at which the propeller jet from the bow thruster hits the quay wall is 1.15° for vessel position 7 and 2.2° for vessel position 8. This results in the axis of the propeller jet intersecting with the quay wall 0.04 m and 0.16 m in positive y-direction from the location where the propeller jet intersected with the quay wall while directed perpendicular to the quay wall. These distances are small compared to the width of the propeller jet when it intersects with the quay wall and therefore the influence on the near-bed velocities is assumed neglectable.
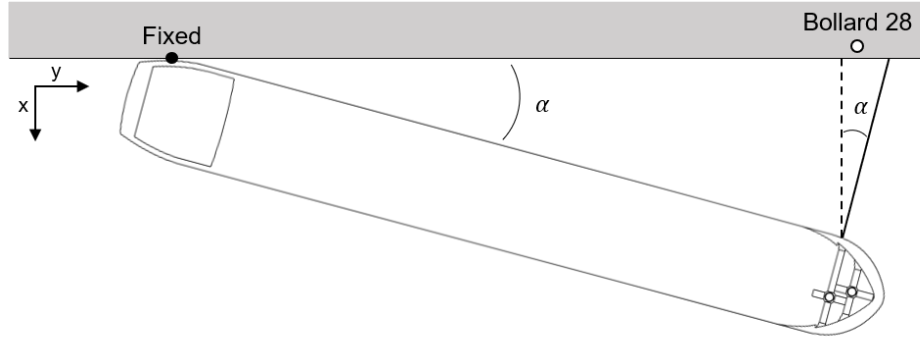
Figure 3.36: Illustration of the angle between the Somtrans XXV and the quay wall due to the stern being fixed with mooring lines to the quay while the bow is loosened to increase the quay wall clearance. As a result the propeller jet from BT1 and BT2 will intersect with the quay wall under the same angle α. The illustration is not to scale and exaggerated to illustrate the effect.

Overview of quay wall clearances
In vessel positions 1-8 the Somtrans XXV was moored at three different distances in x-direction from the quay wall. BT1 and BT2 have a different quay wall clearance resulting in six varying quay wall clearances during the measurements. An overview of the quay wall clearances is given in Table 3.8. The distance between the outlet of the bow thrusters and the port side of the Somtrans XXV are 4.81 m for BT1 and 2.29 m for BT2 (Figure 3.5).

Table 3.8: Overview of the six different quay wall clearances (L) of the bow thrusters during the measurements. In vessel position 1-6 the distance between the vessel and quay wall (L) equals 0.8 m, for vessel position 7 L equals 3 m and for vessel position 8 L equals 5 m. The distance between the port side of the vessel and the bow thruster outlet equals 4.81 m for BT1 and 2.29 m for BT2 as illustrated in Figure 3.5. The resulting total quay wall clearances for BT1 and BT2 are given below for every vessel position in m and D_t.

Bow thruster	Vessel position	Quay wall clearance [m]	Quay wall clearance [D_t]
1	1-6	5.61	5.24
2	1-6	3.09	2.89
1	7	7.81	7.30
2	7	5.29	4.94
1	8	9.81	9.17
2	8	7.29	6.81

3.7. Measurement programme

The measurements consist out of 24 test spread over two days of measuring (Wednesday 30th of September 2020 and Thursday 1st of October 2020). Two types of measurements were carried out: moored measurements were the Somtrans XXV lays with the port side towards the quay wall in a specific position (Test 1-21) and two manoeuvring measurements (Test 22-24). Every test is divided into one, two or three subtests where each subtest corresponds to a power load step.

Measurement duration per subtest:
To select the measurement duration per subtest the characteristic time scale of the turbulent motion should be determined (Equation 3.4). However, as this is quite complicated, engineering choices are made based on the maximum length scale of the turbulent fluctuations at the bottom and the advective velocity of the turbulent motion. The maximum length scale of the turbulent fluctuations at the bottom is equal to the distance between the thruster and the bed while the advective velocity is set equal to the maximum flow velocity at the bed (De Jong and Van Velzen, 2015). The maximum flow velocity differs per test due the different vessel configuration. By means of the Dutch method for calculating the maximum near-bed flow velocity, according to Equation 2.14 and 2.15, a maximum flow velocity of 2.65 m/s is computed. The height of the bow thruster in the water column (h_t) equals 3.24 m for all tests, resulting in a characteristic time scale T_c of 1.22 seconds. For the duration of a subtest, 100 times the characteristic time scale T_c is chosen, corresponding to a duration of 122 seconds which is approximately 2 min.

$$T_c = \frac{h_t}{V_{b,max}} \tag{3.4}$$

A point of attention is that this characteristic time scale is determined by the maximum near-bed flow velocity. If the minimum near-bed flow velocity of 1.17 m/s, according to the Dutch method, was used this would result in T_c = 2.77 seconds corresponding to a subtest duration of 277 seconds (4 min and 37 sec). Nevertheless, as the focus of the near-bed velocities is on the maximum flow velocities and measuring for a longer period would results in a longer test program (which was no option due to the limited time the Somtrans XXV was available), a subtest duration of 2 min is chosen.

The general measurement protocol for test 1-21 is as follows:
First bow thruster 2 is activated for the first power step of 25%. When the bow thruster is stable at 25% the measurement time starts for a duration of 2 min. After the two minutes the time measurement of the subtest stops and the process is repeated for the other power steps of 50% and 90%. The subtests together form one test. For the next test, the previously explained protocol is repeated for bow thruster 1 and bow thruster 1 & 2 together. The three tests are carried out for every vessel position (1-6).

There are a few exceptions on this protocol:

- Test 1 is a long measurement test where the bow thruster was activated for a duration of 10 min only for 25% and 50% power load.

- From test 6 onward, BT2 could not stay stable at 50% power load. Therefore, for BT2 only the power loads 25% and 90% are measured. An exception to this is Test 19 for which BT2 managed to stay stable.

- For vessel position 5 only BT1 was measured (test 11) as the distance along the quay wall in y-direction between the measurement instruments and BT2 is 5.14 D_t. According to (Cantoni, 2020), no significant flow velocities are measured at a distance of 5 D_t in y-direction from the bow thruster outlet.

- For vessel position 3 the distance between BT1 and the measurement frame is also 5.14 D_t in y-direction. Therefore, no test for BT1 in vessel position 3 is executed. On the contrary to vessel position 5, BT1&2 are measured for this vessel position in test 16 to research the difference in flow velocities compared to test 15 (BT2).

- In test 17-21 the power load step of 25% was not included in the tests anymore as from the real-time velocity monitoring 25% did not have the highest flow velocities near the bed.

- For vessel position 6 only BT1&2 are measured in test 17 due to time restrictions. Vessel position 6 and 2 are very similar (difference of 0.25 m).

- For vessel position 8 only BT1&2 (test 21) is measured.

An overview of the tests is given in Table 3.9. The manoeuvring tests are explained in Section 3.7.1

Table 3.9: Overview of the measurement programme were a total of 24 tests were measured.

Test	Bow thruster	Vessel position	Power load steps (subtests) [%]	Duration of subtest [min]	Total duration test [min]
1	2	1	25, 50	10	20
2	2	1	25, 50, 90	2	6
3	1	1	25, 50, 90	2	6
4	1 & 2	1	25, 50, 90	2	6
5	2	2	25, 50, 90	2	6
6	2	2	25, 90	2	4
7	1	2	25, 50, 90	2	6
8	2	2	25, 90	2	4
9	1	2	25, 50, 90	2	6
10	1 & 2	2	25 ,50	2	4
11	1	5	25, 50, 90	2	6
12	1	4	25, 50, 90	2	6
13	2	4	25, 90	2	4
14	1 & 2	4	25, 50, 90	2	6
15	2	3	25, 90	2	4
16	1 & 2	3	25, 50, 90	2	6
17	1 & 2	6	50, 90	2	4
18	1 & 2	7	50, 90	2	4
19	2	7	50, 90	2	4
20	1	7	50, 90	2	4
21	1 & 2	8	50, 90	2	4
22	1 & 2	Berthing	25, 50, 90	3	9
23	1 & 2	Sailing	80	3	3
24	1	Sailing	90	3	3

3.7.1. Manoeuvring measurements

The manoeuvring measurements consist out of a berthing manoeuvre (Figure 3.37) and a sailing manoeuvre where the Somtrans XXV uses its bow thrusters as main propulsion to sail forward (Figure 3.38).

Berthing manoeuvre

In the berthing manoeuvre measurement the Somtrans XXV will first use its bow thrusters in port direction to move the bow away from the quay wall as if the Somtrans XXV is deberthing. When the bow has reached the middle of the Moervaart channel the bow thruster is used in starboard direction to move the bow back to the quay wall as it would do while berthing. During the berthing manoeuvre test, both BT1 & BT2 were used together at power load steps of 25%, 50% and 90%.
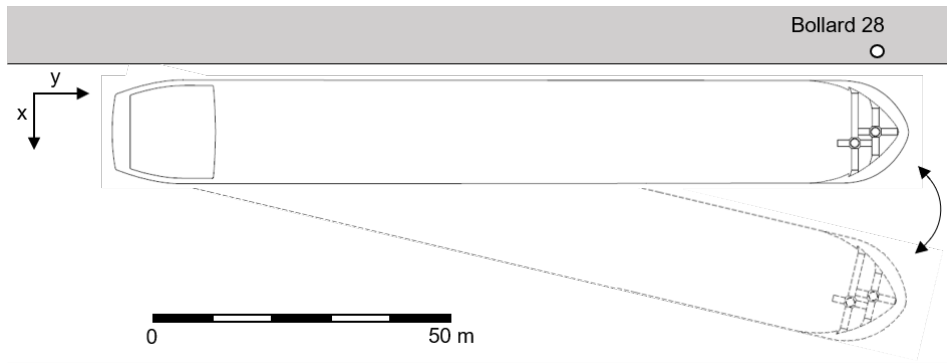
Figure 3.37: Manoeuvring test illustration

Sailing manoeuvre

In the sailing manoeuvre test the Somtrans XXV slowly sails past the quay wall at a distance of approximately 4 m while using the stern directed channel of the bow thrusters to sail forward. The stern directed channel of the bow thrusters is directed under a small angle towards the bed. Therefore, when slowly sailing over the measurement instruments the bow thrusters induce a propeller jet which impacts directly on the measurement instruments. To let the Somtrans XXV move very slowly over the measurement instruments the main propellers are turned on backwards. In the first test both BT1 & BT2 are used at 80% power load while in the second test only BT1 is used as this bow thruster is closest to the quay wall (Figure 3.5) and therefore more likely to cause flow velocities measurable by the instruments.
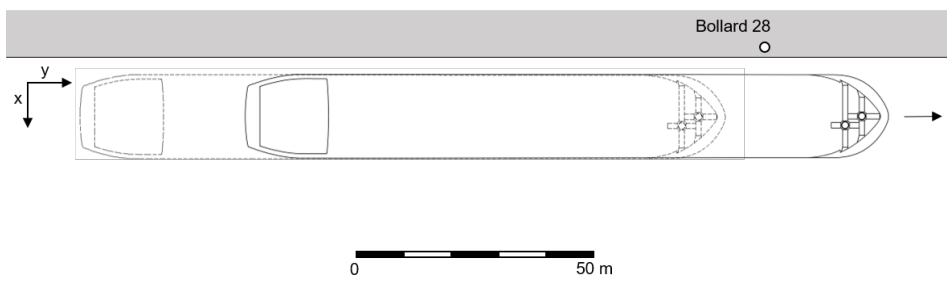
Figure 3.38: Sailing test illustration

3.8. Test overview

In Table 3.10 an overview is presented of the tests where the Somtrans XXV was moored at the quay wall for different vessel positions. The parameters used in Table 3.10 are elaborated by means of Figure 3.39. In Table 3.11 an overview is listed of the manoeuvring tests. The measurement tests will be post-processed by means of the methods explained in Chapter 4 after which the results will be compared in 5. However, a few tests from the measurement programme in Table 3.9 are not further analysed and therefore excluded from Table 3.10 and 3.11. These tests are listed below:

- Test 6 and 7 are excluded from the test overview as these tests researched the actual transmitted power by measuring the loads in the mooring lines which will be determined by Marin.

- Test 5 50% power did not stay stable at 50% power, therefore, it will not be further analysed.

- Test 15 25% power did not stay stable at 25% power, thus, it will not be further analysed.
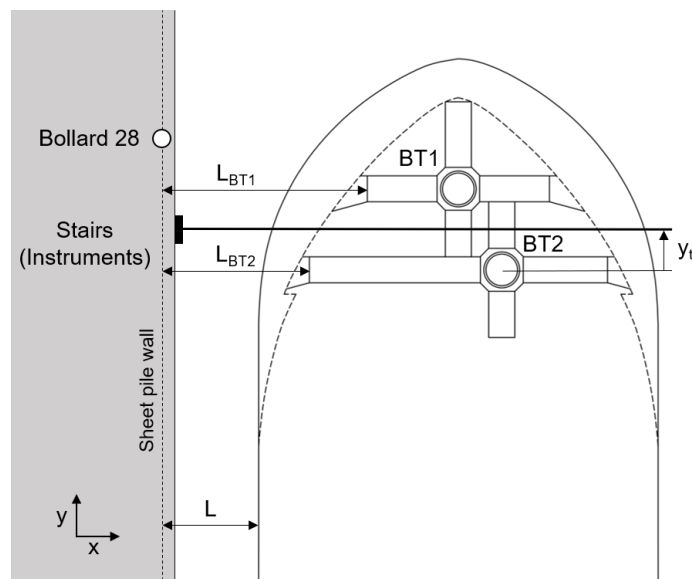
Figure 3.39: Illustration of the defined parameters listed in Table 3.10 and 3.11. Where L is the quay wall clearance between the port side of the vessel and the sheet pile wall, L_{BT1} and L_{BT2} the quay wall clearance of BT1 and BT2 and y_t the distance in y-direction between the center line of the horizontal measurement frame (the stairs used as reference line for the instruments) and the considered bow thruster axis. y_t is positive when the instruments are above the considered bow thruster axis. $L_{BT1\&2}$ is defined as the average L_{BT} of BT1 and BT2.

Table 3.10: Test data overview of the measurements where the Somtrans XXV was moored to the quay wall. Where L is the quay wall clearance between the port side of the vessel and the sheet pile wall, L_{BT} the quay wall clearance of BT1, BT2 or BT1&2 and y_t the distance in y-direction between the bow thruster axis and the instruments. The bow thruster axis of BT1&2 together is defined as the middle between BT1 and BT2.

Test	BT	Vessel position	L [m]	L_{BT} [m]	y_t [m]	Power step [%]
Test 1	2	1	0.8	3.09	0	25,50
Test 2	2	1	0.8	3.09	0	25,50,90
Test 3	1	1	0.8	5.61	-3.5	25,50,90
Test 4	1&2	1	0.8	4.35	-1.75	25,50,90
Test 5	2	2	0.8	3.09	2	25,90
Test 8	2	2	0.8	3.09	2	25,90
Test 9	1	2	0.8	5.61	-1.5	25,50,90
Test 10	1&2	2	0.8	4.35	0.25	25,50
Test 11	1	5	0.8	5.61	2	25,50,90
Test 12	1	4	0.8	5.61	0	25,50,90
Test 13	2	4	0.8	3.09	3.5	25,90
Test 14	1&2	4	0.8	4.35	1.75	25,50,90
Test 15	2	3	0.8	3.09	-2	90
Test 16	1&2	3	0.8	4.35	-3.75	25,50,90
Test 17	1&2	6	0.8	4.35	0	50,90
Test 18	1&2	7	3	6.55	0	50,90
Test 19	2	7	3	5.29	1.75	50,90
Test 20	1	7	3	7.81	-1.75	50,90
Test 21	1&2	8	5	8.55	0	50,90

Table 3.11: Test data overview of the manoeuvring measurements with the Somtrans XXV. Where L is the quay wall clearance between the port side of the vessel and the quay wall and type is the kind of manoeuvring test that is conducted.

Test	BT	L [m]	Power step [%]	Type
Test 22	1&2	Max. 15 m	25,50,90	Berthing
Test 23	1&2	4.25 m	90	Sailing
Test 24	1	4.25 m	90	Sailing

4

Pre-processing

The collected data of the field measurements in Gent is post-processed to check the correct functioning of the instruments and filter out any noise or errors in the data that are not related to the measured flow velocities or pressures. The pre-processing methods are discussed for every measurement instrument separately due to their distinctive measuring techniques. The pre-processing steps for the ADV are elaborated in Section 4.1, the Ott meter is discussed in Section 4.2 and in Section 4.3 the pre-processing steps for the pressure sensors are elaborated. The ADCP measurement data will not be further analysed in this thesis.

The pre-processing methods in this chapter are applied to Test 14 as example after which the methods are applied to the other tests as listed in Table 3.10 and 3.11. For Test 14, BT1&2 were activated simultaneously, the vessel was placed in position 4 (Figure 3.34) with a quay wall clearance (L) of 0.8 m (moored at the quay) while the measurement frame was aligned with BT1. The vessel configuration with respect to the quay wall and measurement instruments is illustrated in Figure 4.1.
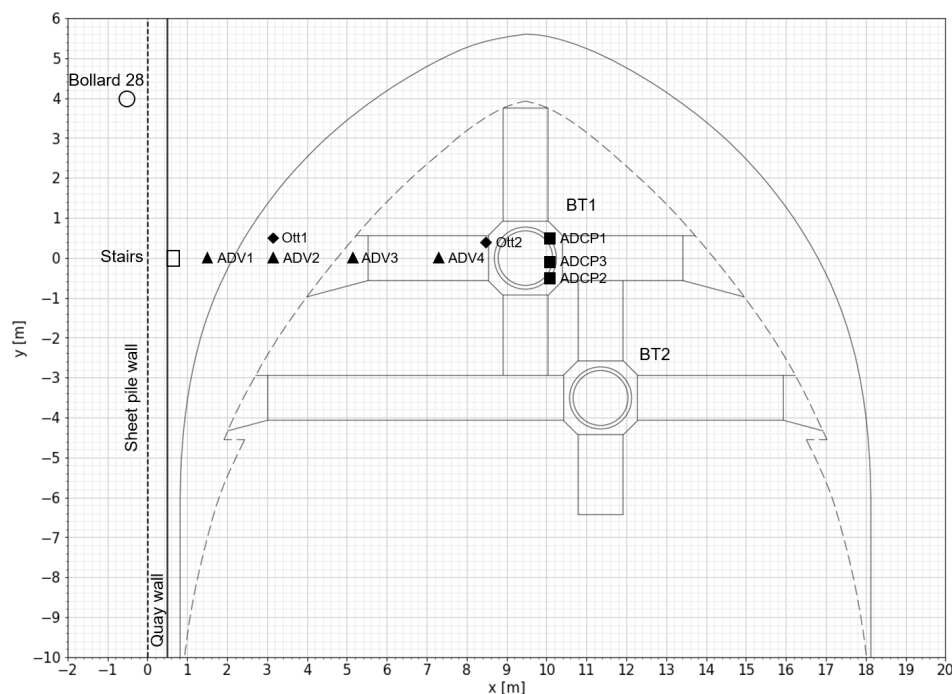
Figure 4.1: Instrument locations during Test 14 for which the Somtrans XXV is placed in vessel position 4 while the instruments are aligned with BT1.

4.1. Acoustic Doppler Velocimeter (ADV)

In this section the pre-processing steps for the flow velocity measurements of the ADVs are discussed. Before any data is filtered, some general corrections are applied to the ADV in Section 4.1.1 after which data is filtered on signal strength (Section 4.1.2), correlation (Section 4.1.3) and outliers (Section 4.1.4). Afterwards, the zero measurements are analyzed in Section 4.1.6 and finally a spectral analyses is examined in Section 4.1.7.

4.1.1. ADV general corrections

During the measurements some settings of the ADV were not set correctly, therefore, corrections are applied to the ADV data in this section before the measured flow velocities are further post-processed.

Correcting for the ADV orientation

During the measurements in Gent, the orientation of the x,y and z axis of ADV3 and ADV4 was not in line with the defined reference system elaborated in Section 3.5.1. Thus, the orientation of ADV3 and ADV4 is corrected to conform to the reference system.

During the measurements, the positive x-direction of ADV3 was towards the quay wall. Opposed to ADV1 and ADV2, it was turned with $180°$. The orientation of the positive xy-plane for ADV3 is opposite to that of the defined reference system. Thus, the velocity measurements in x- and y-direction of ADV3 are multiplied with a factor of -1 to confirm with the defined reference system in Section 3.5.1.

ADV4 is the only ADV with a fixed stem as illustrated in Figure 3.24. During the tests, the tilt sensor of ADV4 did not record the orientation of the ADV. Consequently, the x,y and z velocities should be corrected manually to comply with the reference system defined in Section 3.5.1. The original x-direction of ADV4 is pointing upwards illustrated with the red band around the ADV arm in Figure 4.2. The original z-direction is towards the ADV transmitter in the middle between the ADV arms while the original y-direction is aimed out of the paper. The x,y and z velocities corresponding to the original orientation are corrected to conform with the reference system as illustrated in Figure 4.2. The measured z velocity becomes the x velocity, the measured x velocity becomes the z velocity and the measured y velocity is multiplied with a factor of -1.
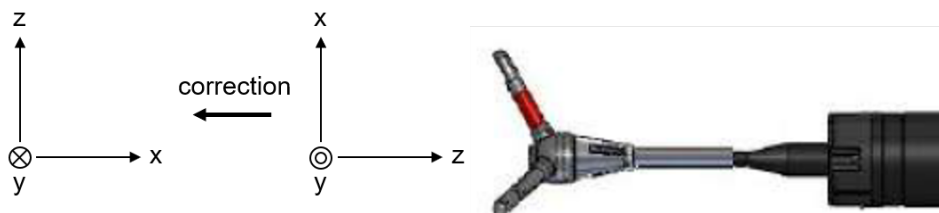
Figure 4.2: Illustration of the orientation correction for ADV4. The originally measured x velocities are converted to z velocities, the original z velocities become the x-velocities and the original y velocities are multiplied with a factor of -1 to comply with the defined reference system.

Correcting for the speed of sound

The speed of sound in water influences the calculation of the velocity data (see Equation 3.2). The ADVs compute the speed of sound based on the measured temperature and a user defined salinity, as the sound speed is more sensitive to temperature variation than it is to salinity variation (Nortek Manuals, 2018a). The water is assumed to be fresh (0 ppt) at the Moervaart quay wall in Gent (as explained in Section 3.5.3). This corresponds with an average calculated speed of sound of 1477.7 m/s ($C_{sound,new}$). However, in the set-up of ADV1 and ADV4 the standard setting for the salinity of 35 ppt was used resulting in an average speed of sound of 1517.2 m/s ($C_{sound,old}$). Thus, a correction for the sound speed in water must be applied for the measured velocities of ADV1 and ADV4. The applied correction factor is calculated with Equation 4.1 corresponding to 0.974.

$$V_{corrected} = V_{old} \frac{C_{sound,new}}{C_{sound,old}} \tag{4.1}$$

4.1.2. Signal strength

To be confident about the data quality and allow for correct calculations of the flow velocities, the received echo after reflection on the water particles must be over a certain threshold level (Nortek Manuals, 2018a). The signal strength is a measure for the magnitude of the acoustic reflection from the water. To quantify the data quality, the signal to noise ratio is used which represents the level of the signal strength with reference to the background noise level. When collecting raw data, the Signal to Noise Ratio (SNR) should be consistently above 15 dB (Nortek Manuals, 2018a). The SNR is calculated according to Equation 4.1.2 and can be found in the output files per ADV beam. Therefore, if the SNR is below 15 dB for either one of the beams this data point is removed from the data set.

$$SNR = 20 \log_{10} \frac{Amplitude_{signal}}{Amplitude_{noise}} \tag{4.2}$$

In Figure 4.3 the SNR is plotted against time for ADV1 test 14 25% power. Some of the SNR fall below the 15 dB threshold, however, most of the data points are well above this threshold ensuring satisfactory data quality. For ADV 2-4 the SNR was well above the 15 dB threshold resulting in no discarding of the data. The same applies for ADV 1-4 for the power steps 50% and 90%, having SNR well above the threshold value of 15 dB.
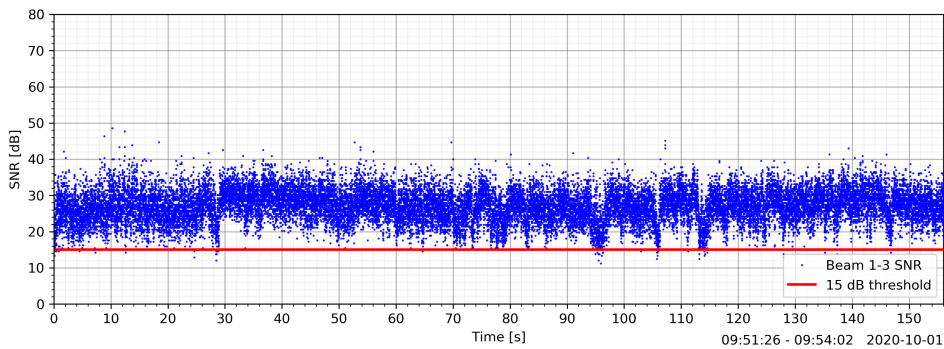
Figure 4.3: The SNR of ADV1 plotted against time of test 14 for 25% power. Some of the data points SNR falls below the threshold of 15 dB. Overall, the data points are well above this threshold ensuring satisfactory data quality.

4.1.3. Correlation

The ADV sends out a short acoustic pulse pair from the transmitter element and listens to the echo of this pulse pair to determine the flow velocity by means of the Doppler Effect. The correlation is an indication of the similarity between the two pulse echoes being measured (Nortek Manuals, 2018a). The correlation of the ADVs is a normalized correlation value ranging between 0-100%. Where at 0% the two echoes are not similar at all and at 100% the two echoes are identical. Ideally, high correlation values are measured during the tests as this gives confidence the receivers measured the two pulses that were originally sent out by the transmitter. Low correlations should be discarded from the data set as correlation is a strong indicator of data quality in the sense of a valid Doppler phase shift determination. Therefore, data with correlations below 70% are removed from the data set (Nortek Manuals, 2018a). Hereby it must be noted that the correlation is bound to a specific beam (1-3) and not to the x,y or z coordinate of the velocities. To filter on correlation, a data point is discarded when the correlation of either beam 1,2 or 3 is below 70%. To investigate the effect of the correlation threshold, the percentage of data points that is filtered out per power step (25%, 50% and 90%) for ADV 1-4 is determined and listed in Table 4.1.

Table 4.1: Overview of the percentage of data points that falls underneath the 70% threshold for Test 14 ADV 1-4 and power steps 25%,50% and 90%.

Power step [%]	ADV1 [%]	ADV2 [%]	ADV3 [%]	ADV4 [%]
25	48.25	59.07	12.49	3.20
50	47.56	55.33	16.03	3.29
90	58.56	64.49	11.20	5.65

From Table 4.1 can be concluded that the percentage of removed data for ADV1 and ADV2 is roughly around 50% for the three different power steps. The highest percentage of removed data is found for ADV2 at 90% power which is illustrated as example of the correlation plots in Figure 4.4. These percentages of removed data are quite high as approximately half of the data is removed for ADV1 and ADV2. Nevertheless, the data can still be considered reliable as the number of data points for ADV1 and ADV2 after filtering on correlation is around 3000 data points due to the high sampling frequency of 64 Hz. Whereas after filtering on correlation the number of data points for ADV3 (16 Hz) and ADV4 (8 Hz) is around 1800 and 1000 data points. A reason for the large amount of data points that falls below the 70% correlation threshold could be the highly turbulent flow situation close to the quay wall were ADV1 and ADV2 are positioned. ADV3 and ADV4 have a significantly lower percentage of discarded data. Ranging between 10-16 % for ADV3 and between 3-6% for ADV4. This could be either due to less turbulence further away from the quay wall or the lower output sampling frequency for ADV3 (16 Hz) and ADV4 (8 Hz) which results in more internal sampling of the data points. Further elaboration on the difference in output sampling frequency is given in Section 4.1.4.

A clear relation between the power load and correlation values for the ADVs can not be found based on Table 4.1. For ADV1 and ADV2, increasing from 25% to 50 % power results in less discarded data while increasing to 90% power results in the highest percentage of removed data. Considering ADV3, increasing from 25% to 50% gives an increase in the percentage of removed data while 90% power results in the lowest percentage of discarded data for ADV3. For ADV4, a small increase in percentage is seen while increasing in power load.

In Table 4.2, the mean correlations of the ADVs are listed after discarding the data points with a correlation below 70%. The mean values do not show a large variation for different power steps. For ADV1 and ADV2 the mean correlations are between 74.35 and 79.65 while ADV3 and ADV4 have higher mean correlations ranging from 83.36 to 90.64.

Table 4.2: Overview of the mean correlation of the data points for Test 14 ADV 1-4 and power steps 25%,50% and 90%.

Power step	ADV1 [%]	ADV2 [%]	ADV3 [%]	ADV4 [%]
25%	79.65	75.88	87.12	90.64
50%	79.12	76.95	83.36	88.39
90%	76.06	74.35	85.27	89.04
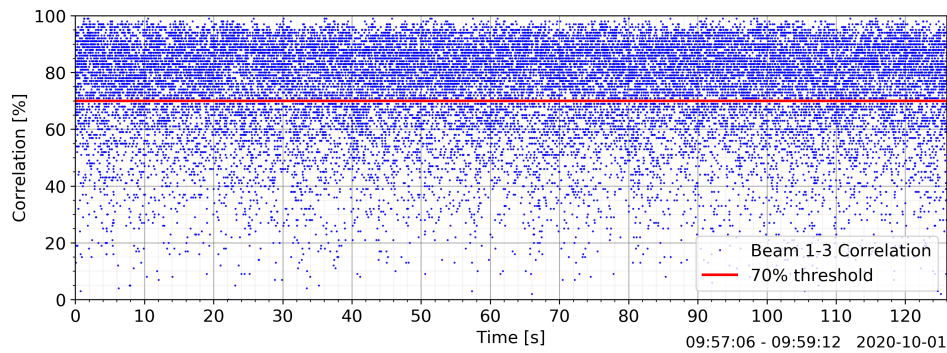
Figure 4.4: Test 14 90% power ADV2, time series of the correlation. In red the 70% threshold line.

4.1.4. Filtering on outliers

The third step in pre-processing the ADV data is filtering on outliers. Outliers are data points that lie at a significantly larger distance from the others. These random outliers are called spikes which are caused by aliasing of the Doppler signal. This occurs when the phase shift between the outgoing and incoming pulse lies outside the range between -180° and +180° and there is ambiguity (Goring and Nikora, 2002). The cause of these spikes (outliers) is due to interference of previous pulses reflected from the flow boundaries or due to the presence of bubbles, sediments or other particles in the flow where the ADV pulses can reflect on (Durgesh et al., 2014). To investigate outliers in the flow velocity measurements, the data is plotted against time during Test 14 at 25% power for the x,y and z velocity component in Figure 4.5. The other plots for ADV2-4 can be found in Appendix C.1. In Figure 4.6a, for the velocity in x-direction, two bands of outliers can be observed around ±3 m/s and ±6 m/s. Some flow velocities even reach values up to 8 m/s, nearly as high as the maximum horizontal velocity range of 8.75 m/s that the ADV can measure. It is unlikely that these measurement points are actual measured flow velocities near the bed. Both their magnitude and pattern is not inline with expectations for the flow velocities. For example, the efflux velocity of one bow thruster of the Somtrans XXV, for 25% power, equals 5.08 m/s according to Equation 2.1 with ρ_w = 1000 kg/m^3. Therefore, these measurement points are not actual measured flow velocities but spikes caused by aliasing and should be removed from the data set. For the velocity in y-direction, a similar pattern of outliers around ±6 m/s is observed. Whereas for the velocity in z-direction, this pattern is not recognized. Nevertheless, when zooming in on the measurement signal some outliers can be observed although the values or more similar to the the other data points in z-direction.

According to Nortek, the company that develops and produces the ADVs, using high velocity ranges and a high sampling frequency generally introduces more noise (the outliers found in the data sets in Figure 4.5). With a horizontal velocity range of 8.75 m/s opposed to the vertical velocity range of 2.5 m/s, this could provide an explanation for the difference in outlier patterns observed for the x and y velocity components and the z velocity component. Although, according to Huang et al. (2020) a large velocity range and high sampling frequency leads to high Doppler noise energy levels, which is noise induced by the instrument similar to white noise (Durgesh et al., 2014). This will be further elaborated in Section 4.1.7 as Doppler noise (white noise) is better observed in a spectral domain. Nevertheless, for future measurements the velocity range and sampling frequency should be set as low as possible to minimize the effect of outliers and Doppler noise in the data.
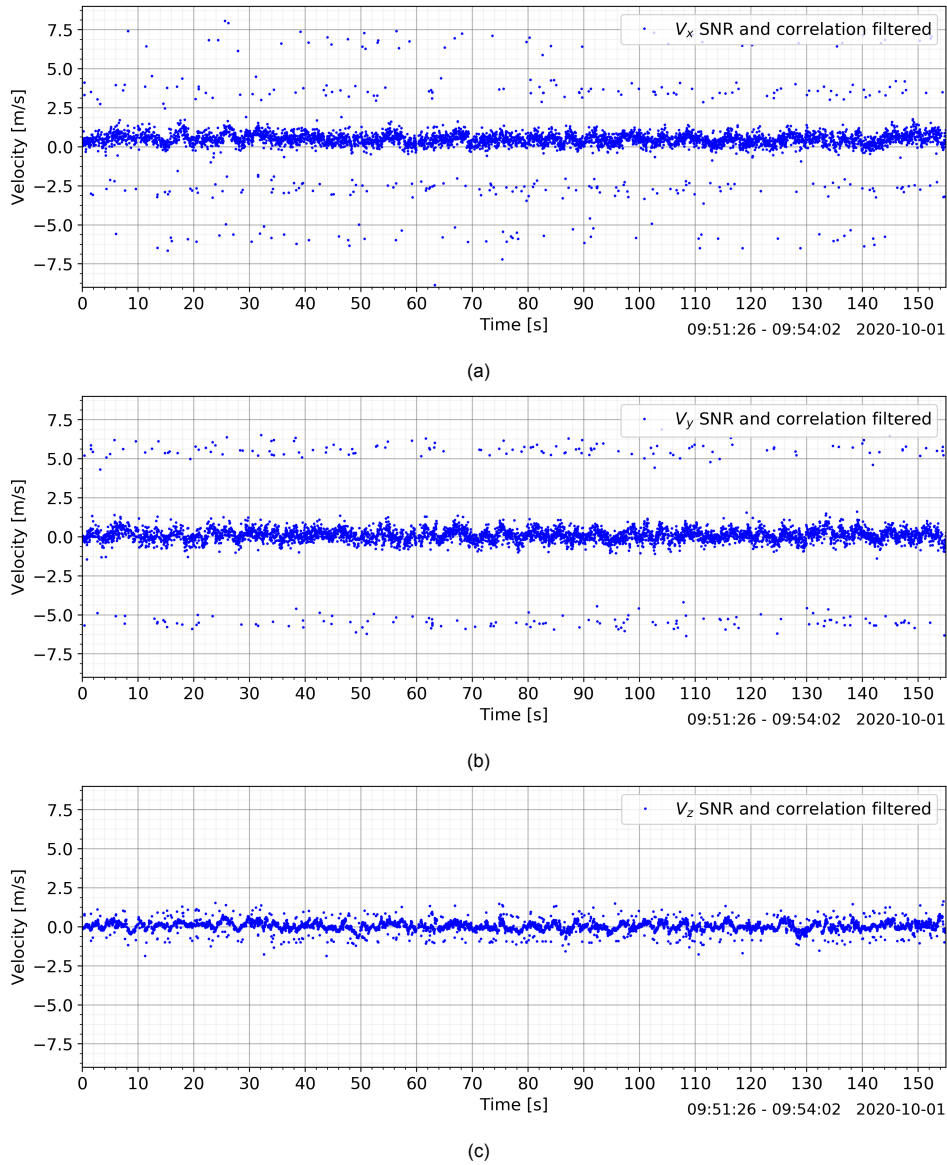
Figure 4.5: Test 14 25% power ADV1. V_x (a), V_y (b) and V_z (c) velocity components after filtering on SNR and correlation.

In Figure 4.6, the pattern in outliers is investigated for ADV 1-4 at 25% power in x-direction. ADV2 shows the same pattern of outliers as observed for ADV1. However, for ADV3 and ADV4 this phenomenon is not observed. Only some random outliers are recognized for ADV3 in Figure 4.6c. The fact that ADV3 and ADV4 do not show bands of outliers at a certain value can be explained by the internal sampling rate and the output sampling rate of the ADVs. The internal sampling rate of the ADVs is constant for a predefined nominal velocity range. For a velocity range of 7 m/s (used throughout the measurements in Gent), the internal sampling rate is 125 Hz for all four ADVs. The output sampling rate for the ADVs can be defined in the Nortek software. This was set at 64 Hz for ADV1 and ADV2, at 16 Hz for ADV3 and at 8 Hz for ADV4, see Section 3.5.3. Thus, for ADV1 and ADV2 most of the output data points are averaged over two samples (125 Hz / 64 Hz = 1.95), but a few will only be based on one sample. The output data points for ADV3 will be averaged over eight or seven samples (125 Hz / 16 Hz = 7.8) while the data from ADV4 will be averaged over 16 or 15 samples (125 Hz / 16 Hz = 15.6). Concluding, the output data will have less outliers when the output sampling rate is lower. A lower output sampling rate means the output data is internally averaged over more samples.
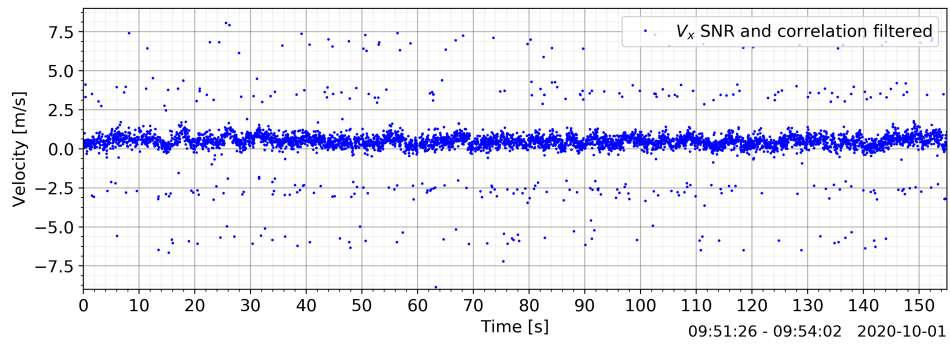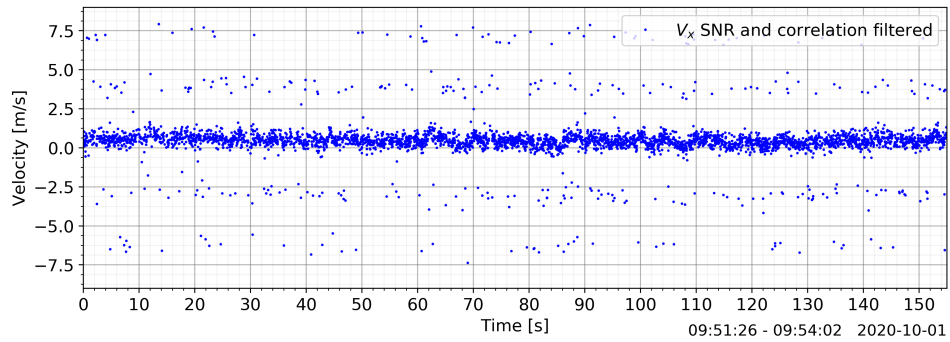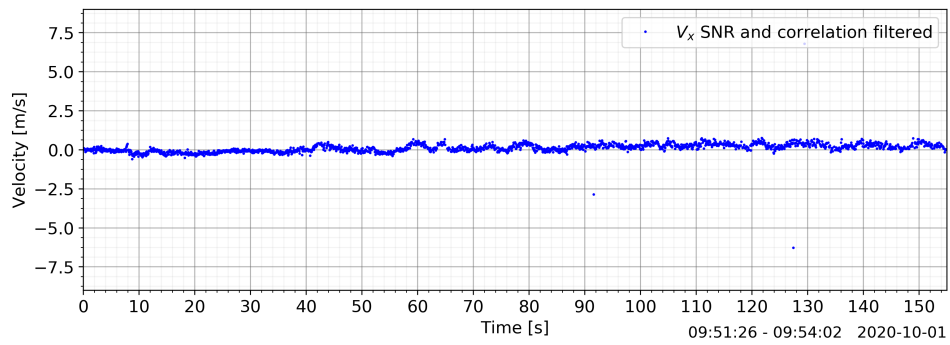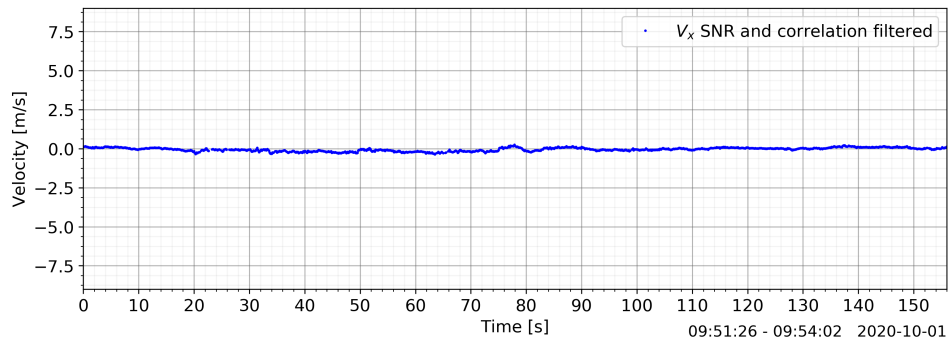
Figure 4.6: Test 14 25% power data filtered on SNR and correlation for ADV1 (a), ADV2 (b), ADV3 (c) and ADV4 (d) for V_x.

Filtering technique

To filter the data on outliers, a standard deviation filter and a median filter are compared with each other to find the most suitable filtering technique. A standard deviation filter eliminates data by applying an upper and low limit based on the mean and standard deviation of the data set. The upper and lower limit is set on two times the standard deviation above and below the mean, see Equation 4.3. If a data point falls outside these limits for either the x,y or z velocity, the data point is discarded. After researching several values for the factor that should be multiplied with the standard deviation, a factor of two gave the best fit for eliminating the outliers (Equation 4.3).

$$\overline{V} - 2\sigma < V_{data} < \overline{V} + 2\sigma \tag{4.3}$$

The median filter slides through the data set point by point replacing each point by the median of the neighbouring data points. The window size of the neighbouring points over which the median is determined can be altered in the filter. For the flow velocity data, a window size of three and five were investigated as the window size must be an odd number. A window size of three did not filter out all the outliers from the data set, therefore, a window size of five was applied to filter the flow velocity data.

The standard deviation and median filter are illustrated in Figure 4.7 for a time segment between 80 and 90 seconds of Test 14 ADV2 at 25% power in x-direction. The standard deviation filter accurately removes the outliers while following the peaks in the measurement data (Figure 4.7a). The median filter also eliminates the outliers adequately, however, it also smooths out the data decreasing the variance (Figure 4.7b) of the data set. Thus, the standard deviation filter is selected to discard the outliers from the measurement data.
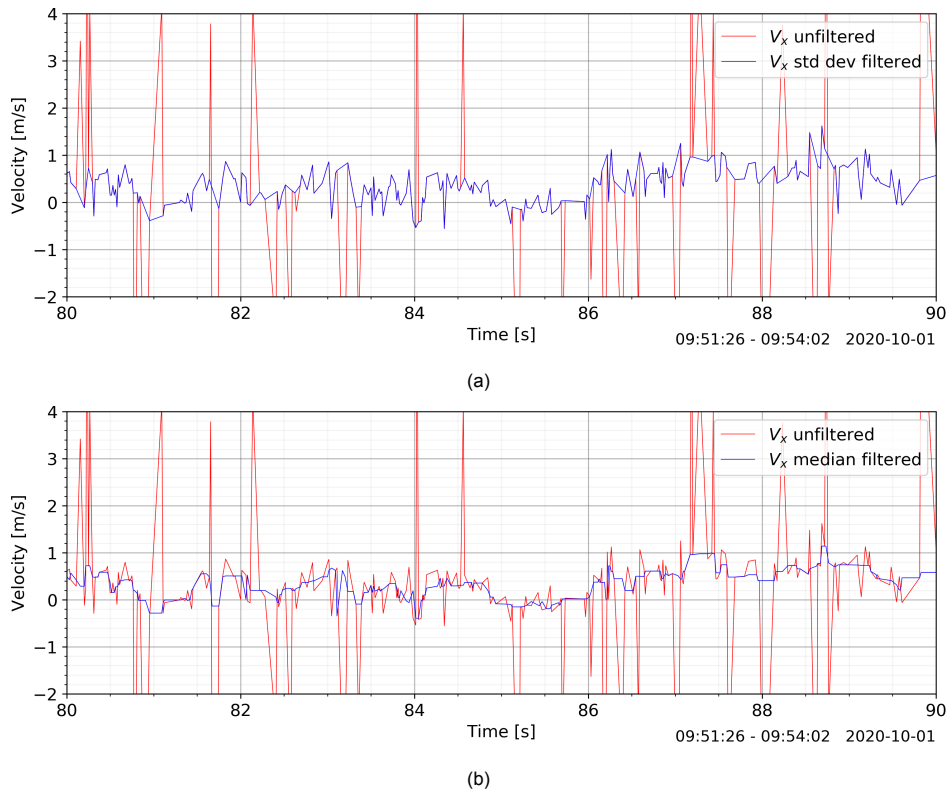
Figure 4.7: Standard deviation filter (a) and median filter with a window size of five (b) for Test 14 25% power ADV2 in x-direction.

In conclusion, to filter the outliers from the measurement data of ADV1 and ADV2 the standard deviation filter defined in Equation 4.3 is used. Overview of the mean horizontal flow velocity ($\overline{V}_{hor}$) and standard deviation (σ_{hor}) before and after applying the standard deviation filter of 2σ for every measurement

test is given in Appendix C.2. In addition, a comparison is made between applying the 2σ standard deviation filter and a 4σ standard deviation twice on the measurement tests for which a very similar result (difference below 2%) is observed. For the data of ADV3 and ADV4, the random outliers (Figure 4.6c) are filtered by a simple upper and lower limit for the flow velocity of ±4 m/s. The value of 4 m/s is based on the SNR and correlation filtered data sets for ADV3 and AVD4 from which was observed that the flow velocity trend is well below 4 m/s during all the tests. Therefore, only filtering the random outliers. An example of the eliminated data by the standard deviation filter is illustrated in Figure 4.8 for V_x of Test 14 25% power ADV2.
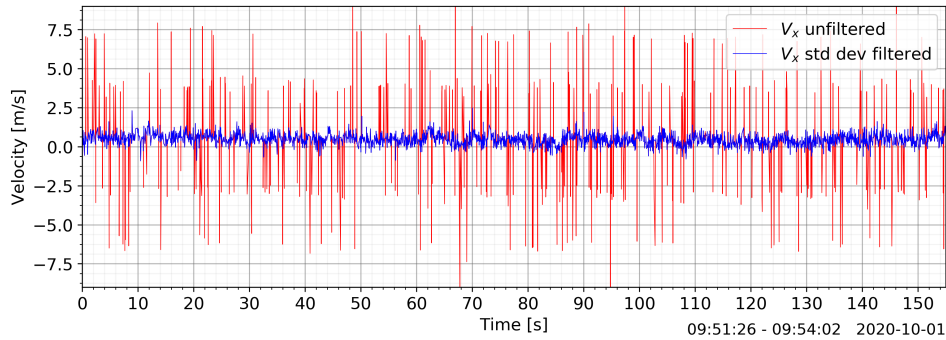
Figure 4.8: Test 14 25% power V_x standard deviation filtered. In red the unfiltered data and in blue the filtered data.

4.1.5. Statistical analyses flow velocities

In Section 2.4 the calculation value for the maximum flow velocity is defined as the mean flow velocity plus three times the standard deviation ($\overline{V} + 3\sigma$). This definition for the maximum flow velocity is more reliable to use instead of the actual measured maximum flow velocity since the actual measured maximum depends on the measurement duration and sampling frequency. Thus, this maximum flow velocity would be different for each measurement. The statistical maximum of $\overline{V} + 3\sigma$ is only exceeded 0.135 % of the time making it well usable alternative for the actual measured maximum flow velocity.

To evaluate the validity of the statistical parameters of the normal distribution for the flow velocities measured by the ADVs, histograms of the x- and y-component of the flow velocity for Test 14 at 50% power are plotted in Figure 4.9 for ADV1. The histograms have a uniform bin width of 0.05 m/s and have been normalized meaning that the area underneath the histogram integrates to 1. Although the velocity components have been filtered on signal strength, correlation and outliers according to the previous sections, they still confirm to the normal distribution plotted in orange in the figures. This conclusion can also be drawn for ADV2-4 plotted in Figure C.8, C.9 and C.10 respectively.
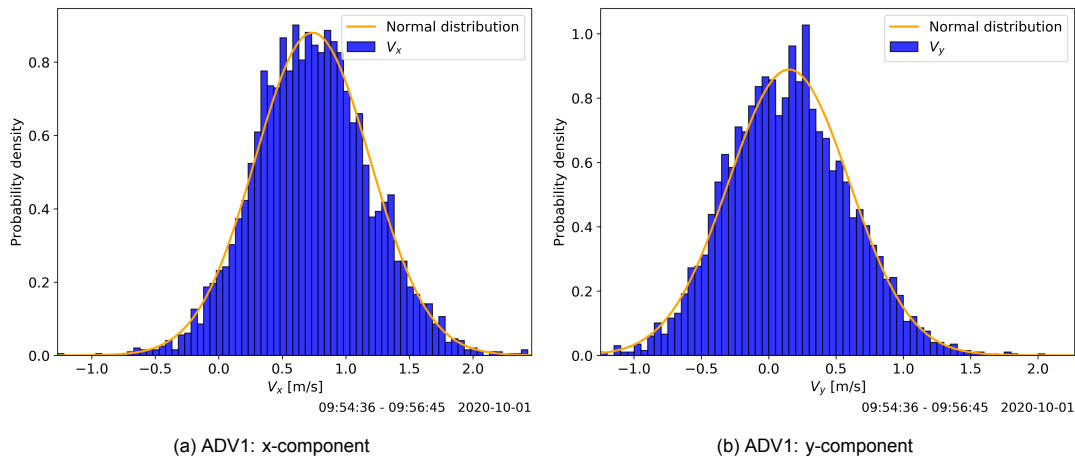
(a) ADV1: x-component   (b) ADV1: y-component

Figure 4.9: Histograms for the x- and y-component of the flow velocity for Test 14 50% power ADV1 including the corresponding normal distribution in orange.

From Figure 2.14 can be concluded that the drag force according to Izbash (Section 2.5), defined as the load on the stones (or bed), is parallel to the bed. This is also adopted in the Dutch method for determining the near-bed flow velocity (load) who defined the mean flow velocity in horizontal (x- and y-component parallel to the bed) direction. Therefore, the horizontal velocity is defined as the resultant flow velocity from the x- and y- component measured by the ADVs, computed with Equation 4.4. This will be used throughout this thesis as a measure for the hydraulic load on the bed to compare the flow velocity measurement results in the next chapter. The corresponding histograms of the horizontal flow velocity for ADV1-4 are plotted in Figure 4.10. Similar to the previous histograms, a uniform bin width of 0.05 m/s is used and the histogram has been normalized meaning that the area underneath the histogram integrates to 1. However, the formulation of the horizontal flow velocity in Equation 4.4 results in the absolute horizontal flow velocity without any negative values. Therefore, the measurement results correspond with a skewed normal distribution as illustrated with the orange line in Figure 4.10.

$$V_{hor} = \sqrt{V_x^2 + V_y^2} \tag{4.4}$$

(a) ADV1: horizontal

(b) ADV2: horizontal

(c) ADV3: horizontal

(d) ADV4: horizontal
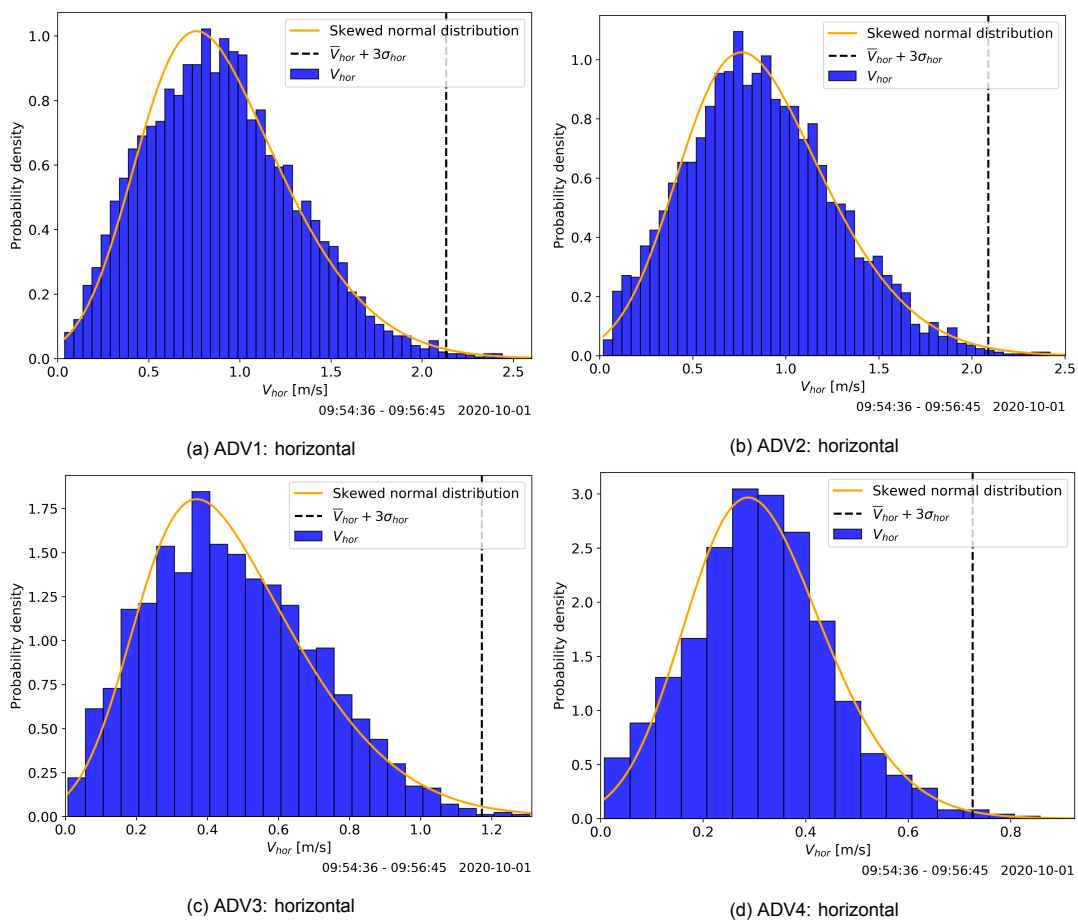
Figure 4.10: Histograms including the normal distribution of the horizontal flow velocity (V_{hor}) for Test 14 50% power ADV 1-4. In orange the normal distribution based on $\overline{V}$ and σ_{hor} is plotted. The black dashed line gives the calculation value for the maximum flow velocity defined as $\overline{V}_{hor} + 3\sigma_{hor}$.

From Figure 4.10 can be concluded that the statistical histograms from ADV 1-4 follow the skewed normal distribution sufficiently supporting the calculation value for the maximum load $\overline{V}_{hor} + 3\sigma_{hor}$ as illustrated with the dashed black line. In Table 4.3 the values for the maximum measured instantaneous horizontal flow velocity $V_{max,in}$ and the calculation value of the maximum load $V_{max} = \overline{V}_{hor} + 3\sigma_{hor}$ are given for ADV 1-4. As expected based on the statistical definition of V_{max}, the measured maximum

instantaneous flow velocity ($V_{max,in}$) is higher than the calculation value for V_{max} for every ADV. Therefore, the calculation value for $V_{max} = \overline{V}_{hor} + 3\sigma_{hor}$ provides a good estimation to base the maximum load.

Table 4.3: Overview of the measured maximum instantaneous flow velocities ($V_{max,in}$) and the calculation value for the maximum load V_{max} ($\overline{V}_{hor} + 3\sigma_{hor}$) for the horizontal velocity of Test 14 50% power ADV 1-4.

	$V_{\mathbf{max,in}}$ [m/s]	$V_{\mathbf{max}} = \overline{V}_{\mathbf{hor}} + 3\sigma_{\mathbf{hor}}$ [m/s]
ADV1	2.60	2.13
ADV2	2.50	2.09
ADV3	1.31	1.17
ADV4	0.92	0.73

In Figure 4.11 the horizontal flow velocity V_{hor} of ADV1-4 is statistically illustrated by means of a boxplot (Matplotlib, 2021) showing the overal decay pattern of the horizontal flow velocity in perpendicular x-direction from the quay wall. ADV1 and ADV2 show similar results both in velocity range as mean flow velocity (orange line), although ADV2 has a slightly lower mean velocity. Moving further away from the quay, to ADV3 and ADV4, the range in measured flow velocities decreases while also the mean flow velocity reduces significantly.
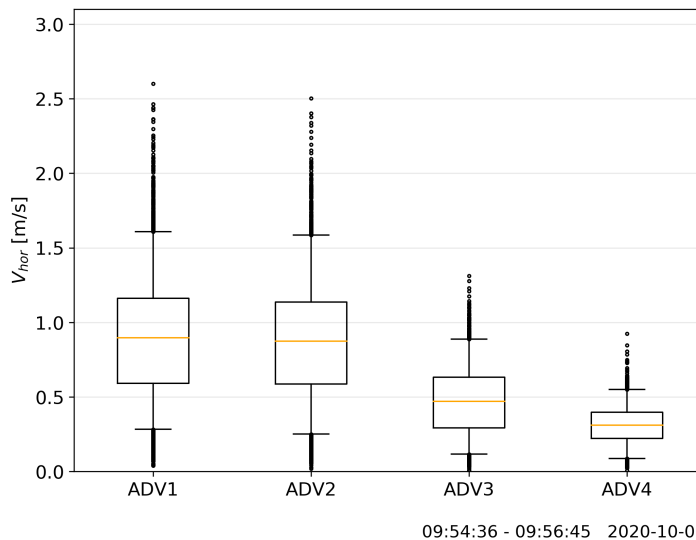
Figure 4.11: Test 14 50% power V_{hor} boxplot for ADV1-4. The orange line in the middle of the box is the mean velocity, the black box illustrates the region of data points that falls between the 25th and 75th percentile while the black caps mark the range between the 5th and 95th percentile of the data points. Outside this region, the data is illustrated by black dots.

4.1.6. Zero measurement

When the bow thrusters of the Somtrans XXV are not activated, it is expected that the ADVs and Ott meters (zero measurements discussed in Section 4.2.1) do not measure any flow velocities near the bed. To check whether there are background velocities present at the Moervaart quay wall, three zero measurements are investigated. During the field measurements in Gent the ADVs have been measuring continuously from Tuesday afternoon, when the frame was placed on the bed, until Thursday afternoon, when the frame was retrieved. An exception to this is ADV2 which was activated manually everyday in the morning and deactivated at the end of the measurement day. For the zero measurements three moments are picked when the bow thrusters of the Somtrans XXV were not activated. The first zero measurement is at Wednesday the 30th of September from 12:15-12:45 (30 min), the second at Thursday the 1st of October from 02:00-03:00 (60 min) and the third at Thursday the 1st of October from 08:40-09:10 (30 min).

Table 4.4: Overview of the standard deviations from the mean flow velocity in x,y and z direction for the three zero measurements.

ADV	Velocity component	Wednesday 12:15 - 12:45 [m/s]	Thursday 02:00 - 03:00 [m/s]	Thursday 08:40 - 09:10 [m/s]
ADV1	x	0.14	0.18	0.23
	y	0.15	0.18	0.25
	z	0.03	0.03	0.05
ADV2	x	0.18	-	0.24
	y	0.18	-	0.24
	z	0.03	-	0.04
ADV3	x	0.10	0.13	0.12
	y	0.10	0.12	0.11
	z	0.02	0.02	0.02
ADV4	x	0.06	0.01	0.07
	y	0.06	0.07	0.07
	z	0.01	0.08	0.01

For every zero measurement the mean flow velocity and its standard deviation is determined for ADV 1-4 and their x,y and z velocity components. The resulting mean flow velocities of the zero measurements were all zero or very close to zero. However, the standard deviations were not zero and varied between 0.01 m/s and 0.25 m/s as listed in Table 4.4. In Figure 4.12 the velocities in x-direction are plotted against time for the zero measurement of Wednesday from 12:15 to 12:45. Two main conclusions can be drawn from the standard deviations. First of all, the standard deviations for the x and y velocity component are significantly higher than for the z velocity component, with the exception of ADV4 for Thursday night between 02:00 and 03:00. This difference in standard deviation could be due to actual higher measured deviations in the horizontal plane over the bed than in the vertical plane. An other explanation could be the difference between the horizontal velocity range of 8.75 m/s and vertical velocity range of 2.5 m/s. A higher velocity range induces more noise to the signal (As described in Section 4.1.4). The second conclusion is that the standard deviations of ADV1 (64 Hz) and ADV2 (64 Hz) are significantly higher than the standard deviations of ADV3 (16 Hz) and ADV4 (8 Hz). A clear relation between lower output sampling rates and smaller standard deviations can be observed in Figure 4.12. This is due to the internal averaging of the ADVs, as discussed in Section 4.1.4, where for ADV3 and ADV4 more internal data points are averaged to construct one output data point resulting in lower deviations. In Section 4.1.7 the zero measurements are analysed in the spectral domain to further elaborate on the effect of the background standard deviations measured during the zero measurements.
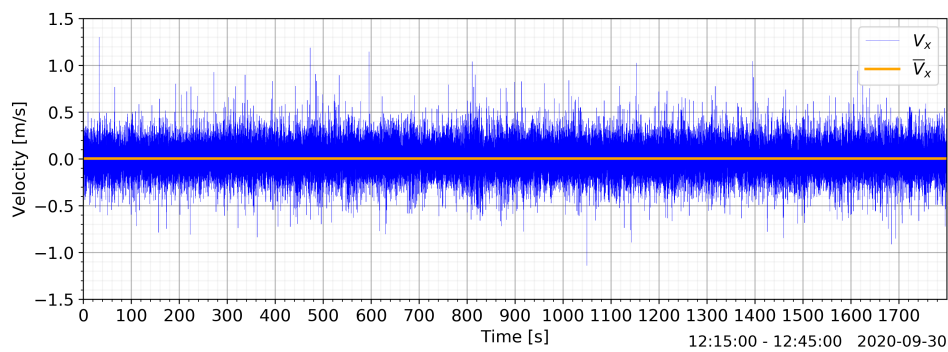
(a) ADV1
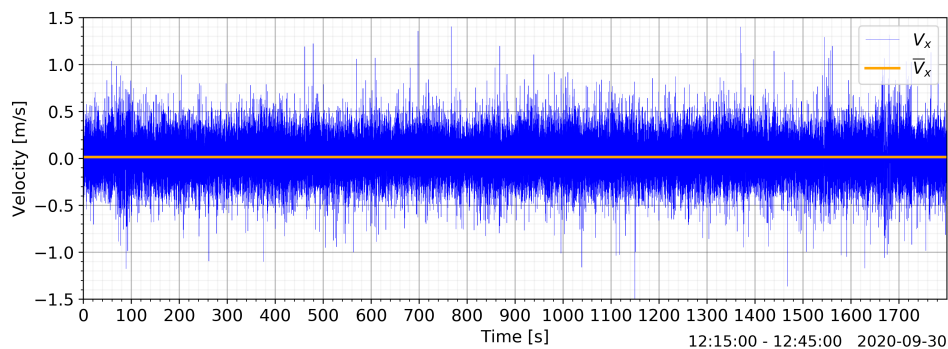
(b) ADV2
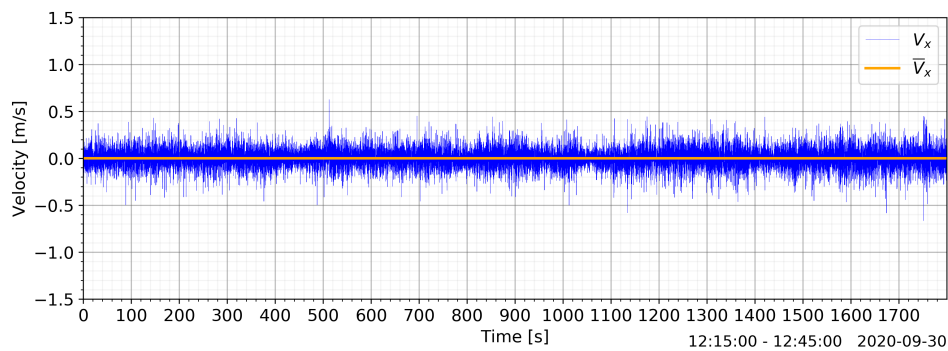
(c) ADV3
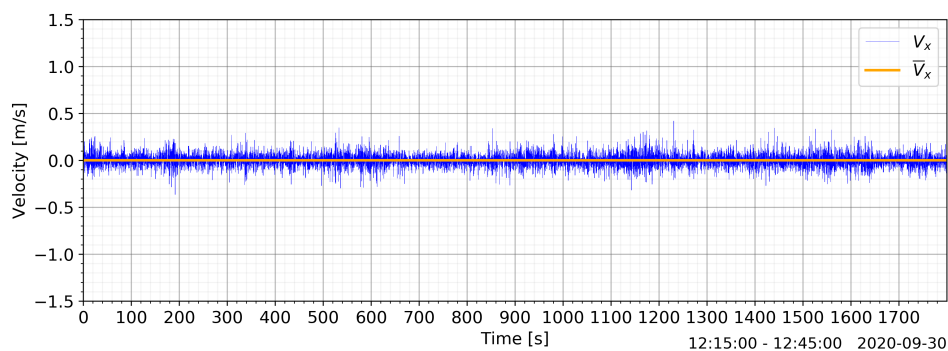
(d) ADV4

Figure 4.12: Zero measurement Wednesday 30th of September 12:15-12:45 ADV1-4 V_x. In blue the velocity measurements in x-direction and in orange the mean velocity is visualized.

4.1.7. Spectral analyses

The research the flow velocities in the spectral domain a spectral analyses is carried, giving insight on the energy distribution over the frequencies present in the flow velocity signal. The spectral analyses in this section consists out of four parts. First the method used for determining the variance density spectra is discussed. Secondly, this method is applied to the flow velocity measurements of ADV1-4 for Test 14. Thirdly the variance density spectrum for the zero measurement of Wednesday the 30th of September is examined and finally the influence of the background standard deviation/noise from the Wednesday zero measurement on Test 14 is discussed.

Welch's method

A signal can be converted from the time domain to the frequency domain by a Fourier transformation. This decomposes the time signal into a sum of simple sinusoids of different frequencies, amplitudes, and phases (Bevel, 2010). The Fast Fourier Transform (FFT) (Maklin, 2019) is applied to the signal to obtain the power density spectrum which is also referred to as the variance density spectrum for statistical processes, formally defined in Equation 4.5 (Holthuijsen, L.H., 2007). Where $\underline{a}$ is the amplitude of a harmonic component (sinusoid), $E\{\frac{1}{2}\underline{a}^2\}$ the expected variance and Δf the frequency resolution. The frequency resolution is defined as the lowest frequency that can be measured in the spectrum. This is dependent on the total duration D of the signal. Thus, the signal should have a sufficient duration to capture the desired range of low frequencies in the spectrum. The variance density spectrum can be interpreted as the distribution of the total variance of the signal over frequencies.

$$E(f) = \lim_{\Delta f \to 0} \frac{1}{\Delta f} E\{\frac{1}{2}\underline{a}^2\} \quad \text{with } \Delta f = \frac{1}{D} \tag{4.5}$$

For the spectral analyses of the measurement data, the *Welch's power spectral density estimate* is carried out. This is a FFT method that splits the signal into multiple segments, applies the Fourier transform to each segment individually and averages the results of all the segments for each frequency separately to compute the variance density spectrum of the signal (Welch, P., 1967). The signal is broken down into multiple segments to reduce the error in the variance density spectrum, increasing the reliability. The error is defined according to Equation 4.6 (Holthuijsen, L.H., 2007). Where p is the number of segments over which the time record is divided. However, the improved reliability comes at the expense of the spectral resolution Δf. As the duration (D) of each segment decreases when the number of segments (p) increases. Therefore, a balance must be found between the spectral resolution (Δf) and the number of segments (p) of the variance density spectrum (Holthuijsen, L.H., 2007).

$$error \approx \frac{100\%}{\sqrt{p}} \tag{4.6}$$

The FFT is based on an periodic input signal. If the signal is not periodic, the signal jumps back to its beginning value at the end of the signal. Assuming that the signal continues as the dashed line of stead of the solid line in Figure 4.13 (O'Reilly, 2021). This introduces a discontinuity at the edge resulting in spectral leakage (NI, 2021). To minimize this effect, windows are applied to the signal reducing the amplitude of the discontinuities at the boundaries. For the measurement data, the *Hann window* is used which reduces the amplitude at the sides to zero by means of a weighted cosine (SciPy, 2021b).
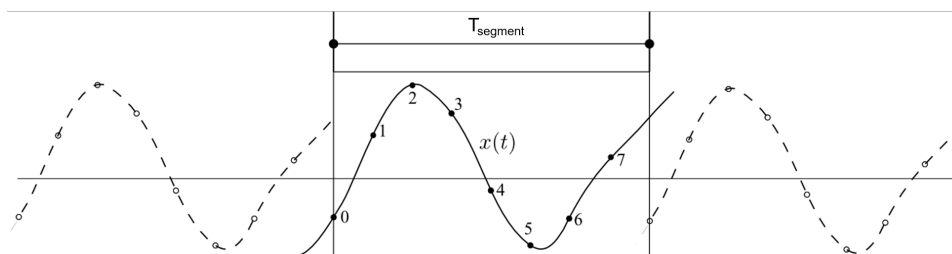
Figure 4.13: Illustration of the discontinuities at the edge of a signal segment due to a non-periodic signal. Where the solid line is a segment of the signal with a period $T_{segment}$ and the dashed line the periodic assumption of the signal by the FFT (O'Reilly, 2021).

Due to the *Hann window*, the information at the edges of the signal have less influence on the FFT results than in the middle of the signal (Figure 4.14). This may result in important information being lost when located at the sides of the segment. Hence, a correction is made for the windowing affect by overlapping the segments of the signal by 50%. In this way, information of the signal that is on the side in one segment appears in the middle of the next segment (Figure 4.15).
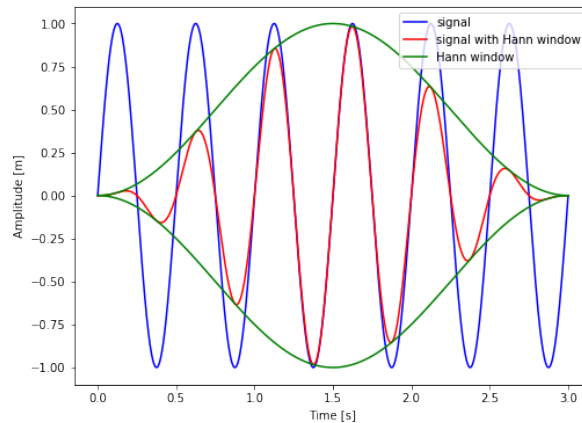
Figure 4.14: Illustration of the effect of the Hann window on the amplitude of the signal.
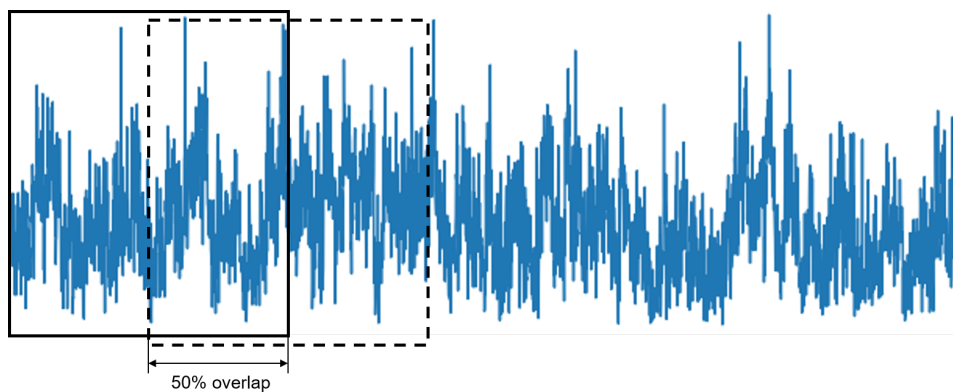
Figure 4.15: Example of a signal which is cut into segments with a 50% overlap.

Variance density spectrum: ADV 1-4
To determine the variance density spectrum, the Welch's method is applied to the measurement signal. However, before the spectral analyses can be executed, the data must first be interpolated to confirm to the original sampling frequency of the ADVs. Due to filtering on signal strength (Section 4.1.2), correlation (Section 4.1.3) and outliers (Section 4.1.4) the data of each test does not have an equidistant time step anymore between consecutive data points. By interpolating the data the equidistant time steps are resolved which is necessary to execute a FFT such as the Welch's method. The variance density spectrum for the horizontal flow velocity of Test 14 at 90% power measured by ADV 1-4 is illustrated in Figure 4.16. For the computation of the variance density spectrum a fixed spectral resolution $\Delta f = 0.1$ is used. Leading to a lowest measurable frequency of 0.1 Hz corresponding to a maximum period of 10 seconds. Resulting in each test of 2 min being split into 12 segments. However, as the segments have an overlap of 50% a each test is split into a total of 23 segments (p) leading to an error in the spectral densities of approximately 21%. To filter out frequencies below the cutoff frequency of 0.1 Hz a Butterworth filter (SciPy, 2021a) is applied as described in Appendix C.4.1. The maximum frequency measured by the ADVs is called the Nyquist frequency, calculated by dividing the sample frequency (fs) by two ($f_{nyq} = fs/2$) (Holthuijsen, L.H., 2007). The Nyquist frequency for ADV1 (fs = 64 Hz) and ADV2 (fs = 64 Hz) equals 32 Hz, while for ADV3 (fs = 16 Hz) and ADV4 (fs = 8 Hz) it equals 8 and 4 Hz

respectively. From Figure 4.16 can be observed that most of the energy is within the lower frequencies of the spectrum. Almost all the energy is within 0-10 Hz with the highest peaks close to 0 Hz at the left side of the spectrum. For the other power steps of 25% and 50% a similar shape but lower peak near 0 Hz is observed (Figure C.13).
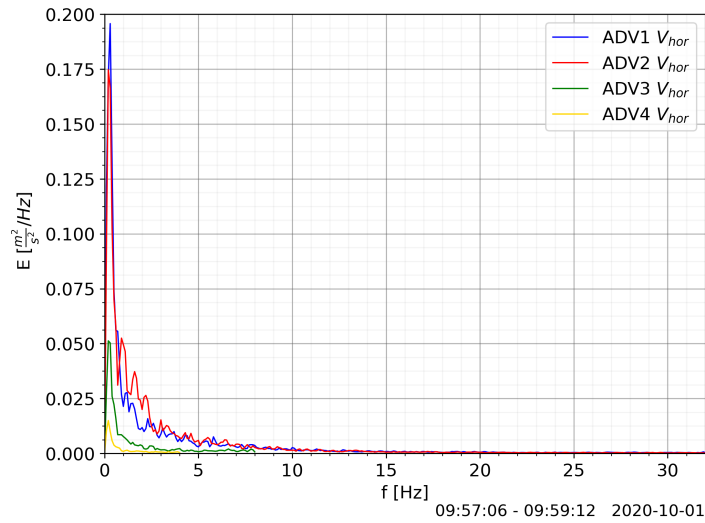
Figure 4.16: Variance density spectrum of Test 14 at 90% power for V_{hor} ADV 1-4. Δf = 0.1, BT 1 & 2, Vessel position 4 (L$_{BT}$ = 4.35 and y$_t$ = 1.75 m).

In Figure 4.17 the variance density spectrum is plotted with a logarithmic x-axis while on the y-axis the energy (E) is multiplied by the frequency (f). With a logarithmic x-axis, the lower frequencies are visualised more clearly. While multiplying E with f preserves that the area under the graph is still equivalent to the energy of the signal. From Figure 4.17 the influence of the lower frequencies on the total energy in the signal is observed. After approximately 7 Hz the variance decreases rapidly for ADV1 and ADV2 until it reaches a constant level of approximately 0.1 $E \cdot f$ at the higher frequencies. The 25% power spectrum shows different results with the peak moved more to the right around 3.5 Hz. For 50% power the energy stays rather constant from 0.1 to 10 Hz at 0.025 $E \cdot f$ after which it decreases to approximately 0.1 $E \cdot f$ (Figure C.14).
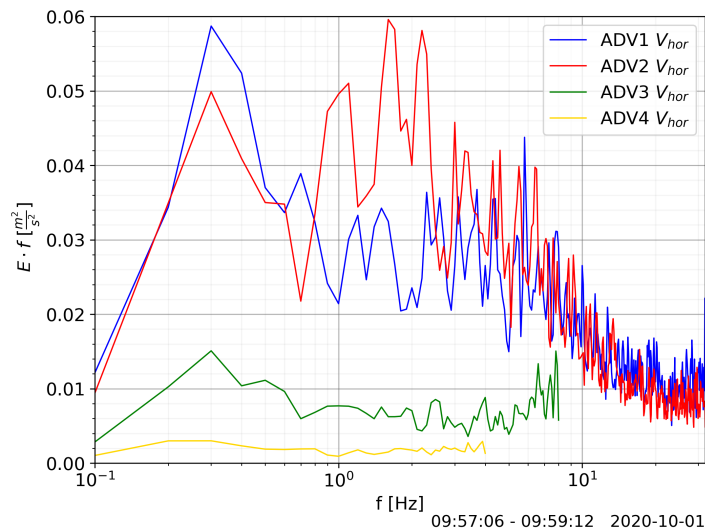
Figure 4.17: Logarithmic x-axis plot of the variance density spectrum of Test 14 at 90% power for V_{hor} ADV 1-4. Δf = 0.1, BT 1 & 2, Vessel position 4 (L$_{BT}$ = 4.35 and y$_t$ = 1.75 m).

Kolmogorov (1941) derived the -5/3 law for the universal scaling in turbulence velocity spectra for very large Reynolds numbers in the inertial subrange. The intertial subrange is the turbulent scale between the energy containing eddies and the viscous eddies. In this inertial subrange zone the net energy coming from the energy containing larger eddies is in equilibrium with the net energy cascading to the viscous eddies where it is dissipated. This theory of unidirectional transfer of turbulent energy from large to small scales is known as the energy cascade Katopodes (2019). Kolmogorov (1941) law can be used as an indication whether actual turbulence was measured with the ADVs during the tests. In Figure 4.18 the variance density spectrum is plotted logarithmic at both the x- and y-axis together with a black line at a slope of -5/3. Between approximately 0.3 Hz and 10 Hz the signal of ADV 1-4 follows the 5/3 law. After 10 Hz, the slope becomes steeper for ADV1 and ADV2. Nevertheless, it can be concluded that actual turbulence was measured during Test 14 for 90% power. By means of Figure C.15 this can also be concluded for the power steps of 25% and 50%.
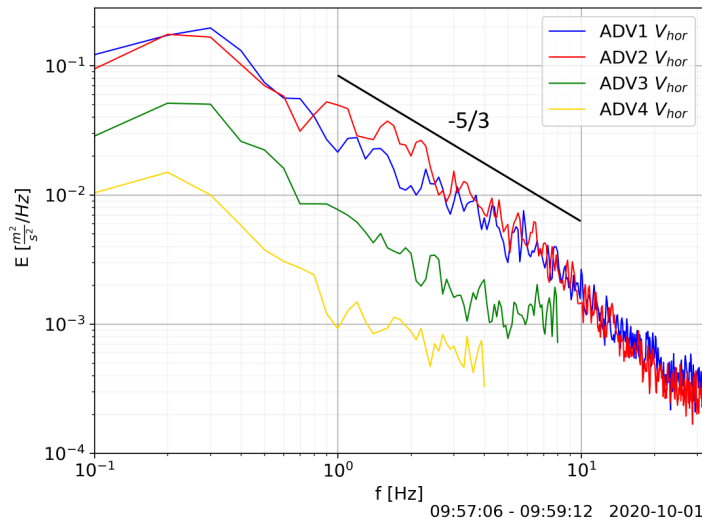
Figure 4.18: Logarithmic plot of the variance density spectrum of Test 14 at 90% power for V_{hor} ADV 1-4. Δf = 0.1, BT 1 & 2, Vessel position 4 (L_{BT} = 4.35 and y_t = 1.75 m).

Variance density spectrum: zero measurement

In Figure 4.19 the variance density spectra of the zero measurement at Wednesday the 30th of September for the horizontal flow velocity (V_{hor}) of ADV1-4 are plotted. To better distinguish between the four ADVs the individual spectra are plotted in Figure 4.20. Similar to the observations in section 4.1.6, there can be concluded that during the zero measurements the variance is not equal to zero. It appears that there is noise on the signal which reaches a constant value at the higher frequencies (right part of the spectrum) while having a peak close to 0 Hz. This type of noise is known as Doppler noise which is caused by the instrument showing the intrinsic limit to the accuracy of the Doppler processing (Durgesh et al., 2014). This type of noise is similar to white noise and is characterized by flattening of the velocity spectra at the higher frequencies. In Figure 4.19 the peak is higher for ADV1 and ADV2 while for ADV3 and ADV4 a more constant noise level is observed. Thus, the actual measured variance is a summation of the bow thruster induced flow velocities and the noise. The investigate the influence of the resulting noise level on the variance for Test 14, a noise correction method is proposed in the next section by eliminating the constant noise level from the measurement signal to determine the actual variance of the flow velocity near the bed.
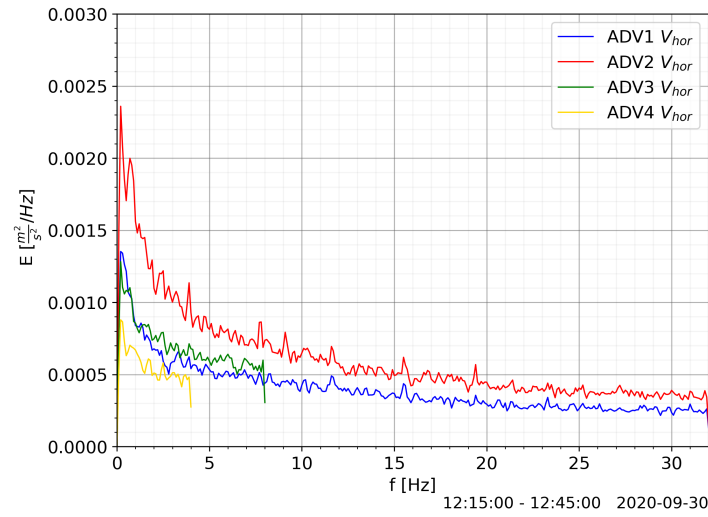
Figure 4.19: Variance density spectrum of the zero measurement at Wednesday 30th of September for V_{hor} ADV 1-4.
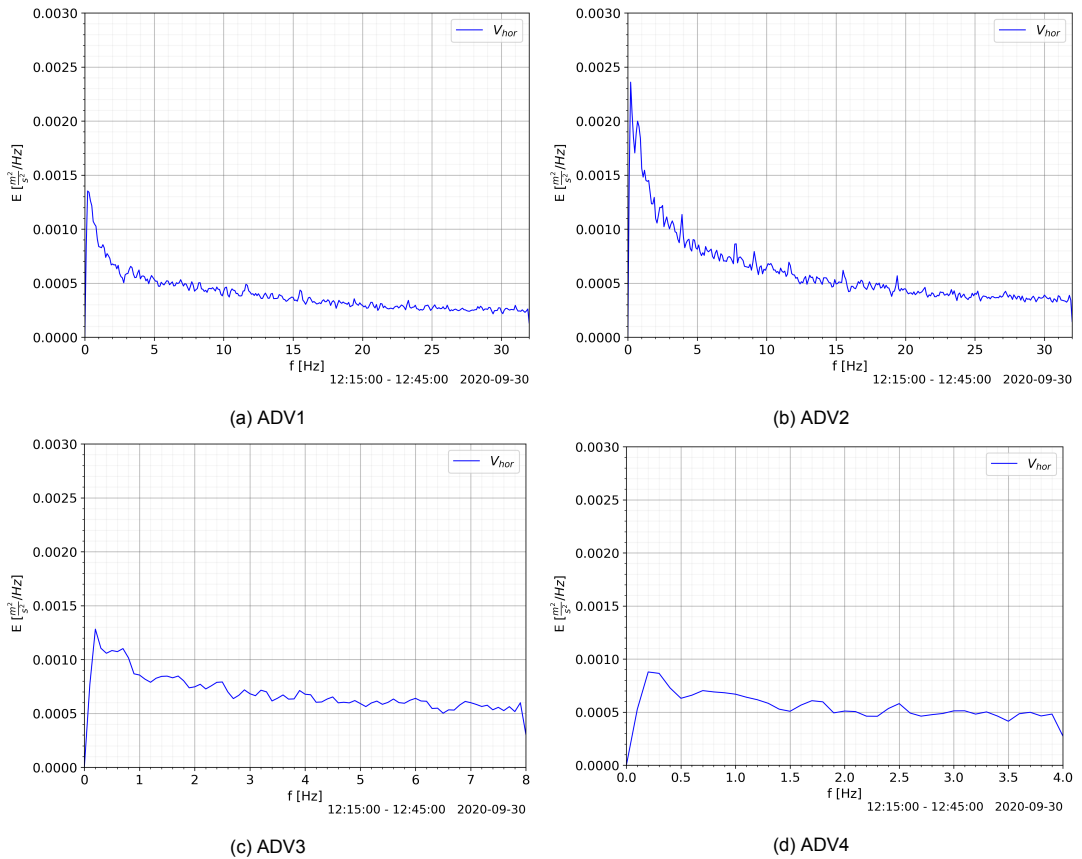
Figure 4.20: Variance density spectrum of the zero measurement at Wednesday 30th of September for V_{hor} ADV 1-4 plotted separately.

Noise correction method

The velocity signal is corrected for the noise by subtracting the variance induced by the noise from the variance of the measurement signal according to Equation 4.7. The variance is calculated by integrating the area underneath the graph with the Simpson's rule (SciPy, 2021c). This method is illustrated in Figure 4.21, where the resulting noise level is determined by fitting a horizontal line through

the variance level at the higher frequencies indicated in red. The corrected variance is indicated in blue as the area between V_{hor} and the noise level (red). However, this method induces a small error as the peak in the variance density spectrum from the zero measurement, observed in Figure 4.20, can not be corrected for in the measurements while the bow thruster is activated. The correction method is applied to every ADV and power step of Test 14 to determine the actual variance of the bow thruster induced flow velocities. An overview of the variance and resulting standard deviations of V_{hor} for ADV 1-4 Test 14 25%, 50% and 90% power is given in Table 4.5, 4.6 and 4.7 respectively. Where Var_{cor} is the corrected variance and σ_{cor} the corrected standard deviation. By correcting for the constant noise level the standard deviation (σ) is reduced by approximately 2-14% depending on the power step and ADV. Overall, the smallest corrections are applied for ADV1 and ADV2 while most of the corrections for ADV3 and ADV4 stay within a correction of 10% with the exception of ADV3 for 25% power. Therefore, it can be concluded that the background noise, as observed during the zero measurements in Section 4.1.6, is only responsible for a small portion of the total standard deviation (σ) measured during the flow velocity measurements. An overview of the corrections for the standard deviation (σ) per measurement test is listed in Appendix C.5.

$$\sigma_{corrected} = \sqrt{\sigma^2 - \sigma_{noise}^2} \tag{4.7}$$
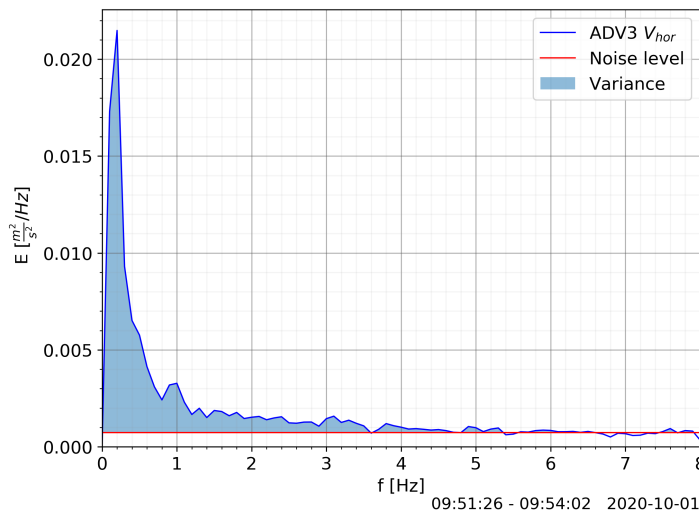
Figure 4.21: Correction for the constant noise level (red) of the variance (blue) for Test 14 at 25% power V_{hor} ADV3. $\Delta f = 0.1$, BT 1& 2, Vessel position 4 (L_{BT} = 4.35 and y_t = 1.75 m).

Table 4.5: Overview of the variance and standard deviation corrections based on the constant noise level for V_{hor} Test 14 at 25% power ADV 1-4. Where Var_{noise} is the variance due to the constant noise level illustrated in red in Figure 4.21, Var_{cor} the corrected variance and σ_{cor} the corrected standard deviation. The variance is rounded of to three decimal places while the standard deviation (σ) is rounded of to two decimal places.

	Var [m²/s²]	Var$_{noise}$ [m²/s²]	Var$_{cor}$ [m²/s²]	σ [m/s]	σ_{cor} [m/s]	σ_{cor} / σ [%]
ADV1	0.096	0.012	0.084	0.31	0.29	93.80
ADV2	0.094	0.010	0.083	0.31	0.29	94.37
ADV3	0.023	0.006	0.017	0.15	0.13	86.34
ADV4	0.008	0.001	0.007	0.09	0.08	91.28

Table 4.6: Overview of the variance and standard deviation correction based on the constant noise level for V_{hor} Test 14 at 50% power ADV 1-4. Where Var$_{noise}$ is the variance due to the constant noise level illustrated in red in Figure 4.21, Var$_{cor}$ the corrected variance and σ_{cor} the corrected standard deviation. The variance is rounded of to three decimal places while the standard deviation (σ) is rounded of to two decimal places.

	Var [m²/s²]	Var$_{noise}$ [m²/s²]	Var$_{cor}$ [m²/s²]	σ [m/s]	σ_{cor} [m/s]	σ_{cor} / σ [%]
ADV1	0.170	0.016	0.154	0.41	0.39	95.17
ADV2	0.164	0.013	0.150	0.40	0.39	95.85
ADV3	0.055	0.008	0.046	0.23	0.22	91.98
ADV4	0.019	0.004	0.016	0.14	0.12	90.31

Table 4.7: Overview of the variance and standard deviation corrections based on the constant noise level for V_{hor} Test 14 at 90% power ADV 1-4. Where Var$_{noise}$ is the variance due to the constant noise level illustrated in red in Figure 4.21, Var$_{cor}$ the corrected variance and σ_{cor} the corrected standard deviation. The variance is rounded of to three decimal places while the standard deviation (σ) is rounded of to two decimal places.

	Var [m²/s²]	Var$_{noise}$ [m²/s²]	Var$_{cor}$ [m²/s²]	σ [m/s]	σ_{cor} [m/s]	σ_{cor} / σ [%]
ADV1	0.238	0.122	0.226	0.49	0.48	97.40
ADV2	0.232	0.009	0.223	0.48	0.47	97.98
ADV3	0.066	0.011	0.055	0.26	0.24	91.45
ADV4	0.016	0.002	0.014	0.13	0.12	92.61

4.2. Ott meter

For the Ott meter no filtering techniques are applied to its regarded accuracy and reliability for measuring flow velocities (Section 3.4.4). In addition, the irregular sampling frequency makes filtering and a spectral analyses not straightforward. In this section, the zero measurement of Wednesday the 30th of September is analyzed for Ott meter 2 (Section 4.2.1) after which the flow velocity data of ADV 1-4 is resampled to the irregular sampling frequency of the Ott meters. In this way the flow velocity results of ADV2 and ADV4 (located close to Ott meter 1 and 2) can be compared with the results of Ott meter 1 and 2.

4.2.1. Zero measurement

From the three zero measurements that were analysed in Section 4.1.6 only Ott meter 2 was measuring during the zero measurement at Wednesday the 30th of September. During the other zero measurements the Ott meters were either not activated or there were no flow velocities recorded by the Ott meter due to the lack of flow velocity at the bed. As explained in Section 3.4.4, the Ott meter measures flow velocity when the impeller makes one rotation. If there are no significant flow velocities near the bed the impeller will not rotate. In Figure 4.22 the flow velocity measurement of Ott meter 2 at Wednesday the 30th of September is illustrated. The flow velocities range between 0.03 and 0.07 m/s in which each rotation of the impeller is illustrated by a red dot. The gaps in the measurement at 400-500 seconds and 740-920 seconds indicate that the flow velocities near the bed were not significant enough for the impeller to rotate. The results are inline with the expectations that during the zero measurements the flow velocities are zero or close to zero.
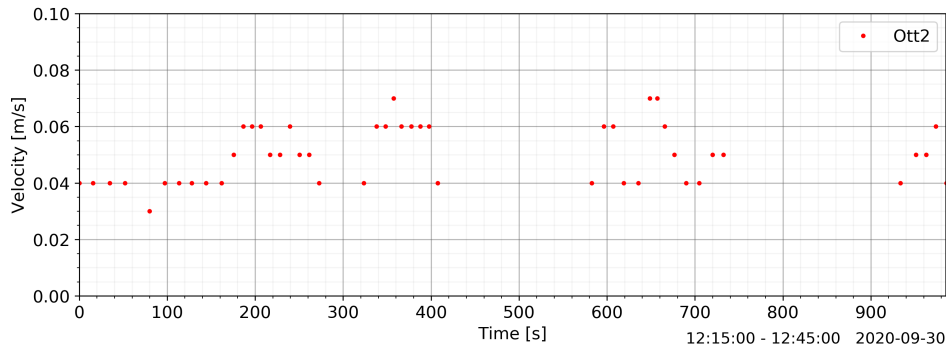
Figure 4.22: Zero measurement of Ott meter 2 at Wednesday the 30th of September (12:15-12:45).

4.2.2. ADV resampling to irregular Ott meter sampling frequency

Ott meter 1 is placed at the same distance from the quay wall as ADV2 (3.15 m, 2.94 D_t) while Ott meter 2 (8.45 m, 7.90 D_t) is located approximately one meter further away from the quay wall than ADV4 (7.29 m, 6.81 D_t). Thus, ADV2 and ADV4 are resampled to the sampling frequency of Ott meter 1 and 2 respectively to compare the measured flow velocities of the two different measurement instruments. The Ott meters do not have a regular sampling frequency, this is depended on the flow velocity as discussed in Section 3.4.4. In the output file of the Ott meters the duration of every rotation is given in seconds. After every rotation the Ott meter calculates the flow velocity corresponding to that specific rotation time. Therefore, the ADVs can be resampled to the Ott meters by averaging all the data points of the ADV that occurred within the duration of one rotation of the Ott meter. By repeating this for every rotation of the Ott meter the ADV data is averaged to the same amount of data points as the Ott meter. The results of this method are illustrated in Figure 4.23 as a boxplot (Matplotlib, 2021) for Test 14 at 90% power. The boxplot is used to statistically represent the data. The results for 25% and 50% power are illustrated in Figure C.16 in Appendix C.
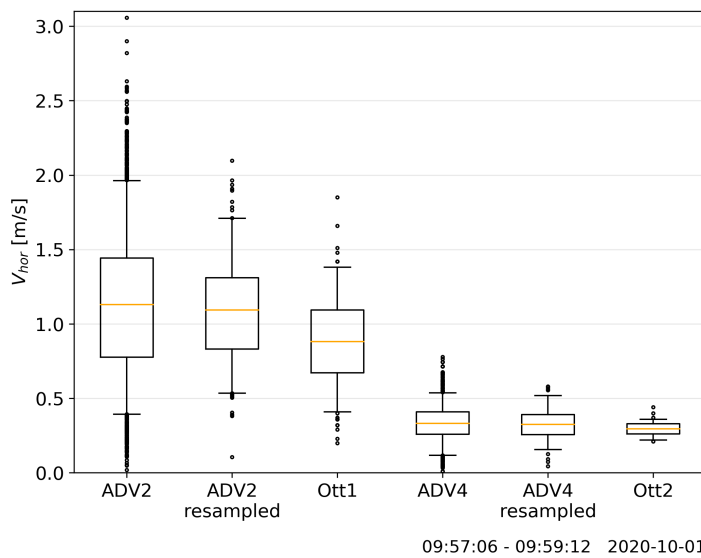
Figure 4.23: Boxplot of Test 14 90% power for ADV2 and ADV4 resampled to Ott meter 1 and 2 sampling frequency and the original ADV2 and ADV4 measurement data. The black box of the boxplot indicates the range of data that falls between the 25th and 75th percentile of the data while the orange line represents the mean flow velocity.

By resampling the ADV data to the sampling frequency of the Ott meter, the ADV measurements resemble the Ott meter measurements reasonably well. Especially for ADV2 the velocity range is significantly reduced complying with Ott meter 1. Although for every power step the mean velocity and box resembling the 25th and 75th percentile of ADV2 are slightly higher than those of Ott meter 1. By resampling

ADV4 the velocity range is somewhat reduced while the average velocity stays similar to the original boxplot of ADV4. The boxplot of ADV4 and Ott meter 2 have very similar average velocities while the flow velocity range of ADV4 is larger than Ott meter 2. Similar observations are found for 25% and 50% power in Figure C.16. Overall the Ott meter measures lower flow velocities with a smaller range.

4.3. Pressure sensors

Three types of pressure sensors are used during the measurements. Four high frequency pressure sensors (100 Hz), labeled PS1-4 in Figure 3.29, two RBR solo pressure sensors (2 HZ) labeled PS5 and PS6 and four pressure sensors located in the ADV cases (64 Hz, 16 Hz and 8 Hz), labeled PS7-10. First the pressure sensor measurements are transformed to surface elevation in meter water column, secondly the pressure sensors are plotted to determine any outliers or noise that must be filtered out and lastly the pressure sensor measurements are transformed to corresponding flow velocity data according to Bernoulli to compare with the ADV flow velocity measurements.

4.3.1. Transformation to surface elevation

The RBR solo pressure sensors (PS5 and PS6) measure absolute pressure in dbar, the ADV pressure sensors (PS 7-10) measure pressure in dbar with a predefined offset for the atmospheric pressure while the high frequency pressure sensors (PS1-4) have an analog electrical signal output of 4-20 mA which is calibrated on 0-4 bar absolute pressure. The pressure measured by the ADV and RBR solo is converted to pressure in meter water column (p_{depth}) by means of Equation 4.8 (without p_{atm} for the ADV pressure sensors) whilst the high frequency pressure sensors are first converted to dbar. The atmospheric pressure (p_{atm}) is determined by the RBR solo which started measuring before the horizontal measurement frame was placed on the bed in the Moervaart. This resulted in an atmospheric pressure (p_{atm}) of 10.153 dbar just before the frame went into the water. A similar value of 10.112 dbar was reported by a nearby weather station in Westdorpe (The Netherlands). During the tests the atmospheric pressure was not measured, therefore, this starting value of 10.112 dbar for the atmospheric pressure is used for all conversion calculations to meter water column. The water density (ρ_w) is resolved with the average water temperature, measured by the ADVs during the measurements, and the assumed 0 ppt salinity in the Moervaart corresponding to a water density (ρ_w) of 998.5 kg/m^3. An overview of the data used to convert the pressure to meter is given in Table 4.8.

$$p_{depth} = \frac{(p_{measured} - p_{atm}) \cdot 10^4}{\rho_w \cdot g} \tag{4.8}$$

Table 4.8: Moervaartkaai Gent atmospheric and water characteristics

Characteristic	Value
ρ_w	998.5 kg/m^3
p_{atm}	10.153 dbar
g	9.813 m/s^2

4.3.2. Zero measurement

In Figure 4.24 the time series of PS1, PS3, PS5 and PS7 are plotted for the zero measurement at Wednesday the 30th of September to compare their pressure measurements when there was no bow thruster activated. From every pressure sensor type one sensor is illustrated in Figure 4.24 as example for the zero measurement with the exception of PS3 for which a noticeably different signal is observed than for the other high frequency pressure sensors (PS1, PS2 and PS4). The sensors were placed at different depths underneath the water surface, therefore, the signals are first detrended by subtracting their mean values to compare their pressure fluctuations. For the pressure signal of PS3, PS5 and PS7 the same pattern can be observed with a varying water level in the range of ±0.04 m. These small fluctuations are inline with expectations and most likely caused by maritime activities and locks in the port area. PS1 however, has a very noise signal ranging between ±0.20 m. It seems that there is some kind of disturbance/noise on the PS1 signal that has to be filtered out to get a signal similar

to PS3, PS5 and PS7. The same noisy signal can be observed for the other high frequency pressure sensors (PS2 and PS4) plotted in Figure C.17. In Section 4.3.3 a spectral analyses is carried out for the pressure sensors with the exception of the RBR pressure sensors (PS5 and PS6). In the variance density spectrum of PS1-4 a peak is observed at 48 Hz for PS1,PS2 and PS4 (Figure 4.25). To filter out the noise at 48 Hz, a low-pass Butterworth filter (Section C.4.1) is applied to the pressure signal. The cutoff frequency is chosen at 64 Hz to correspond to the sampling frequency of PS7 (ADV1) and PS8 (ADV2) resulting in a Nyquist frequency of 32 Hz as highest measurable frequency. In Figure 4.24a and 4.24b the original 100 Hz and low-pass filtered 64 Hz pressure signal are plotted for PS1 and PS3. After filtering out the noise, the pressure signals of PS1, PS2 and PS4 are similar to the zero measurements of PS3 and PS5-10. In addition, the PS3 signal is likewise filtered to 64 Hz to match the sampling frequency of PS1,PS2 and PS4. As a result, the PS3 signal bandwidth is slightly decreased as illustrated in Figure 4.24b. An overview of all the pressure sensors zero measurements for Wednesday the 30th of September can be found in Appendix C.7.1.
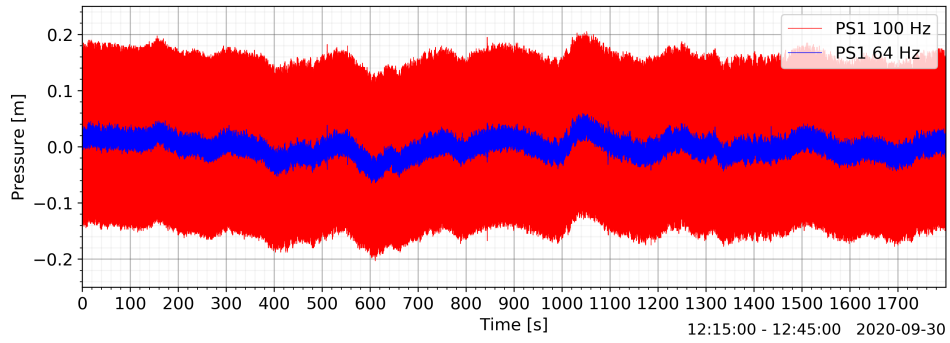
(a) High frequency pressure sensor 1 (PS1)
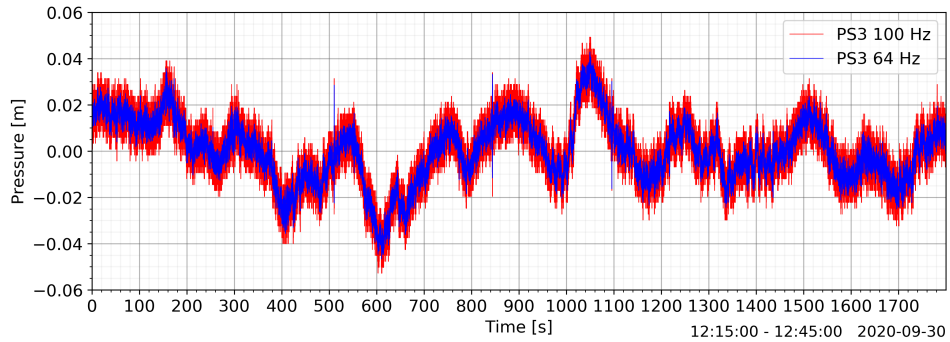
(b) High frequency pressure sensor 3 (PS3)
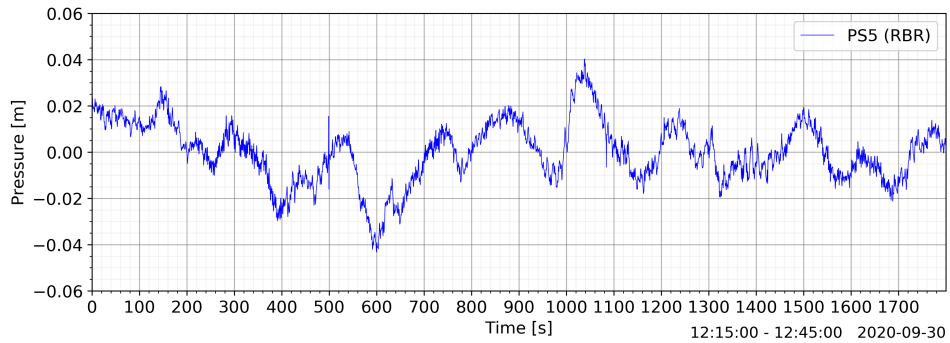
(c) RBR solo pressure sensor (PS5)
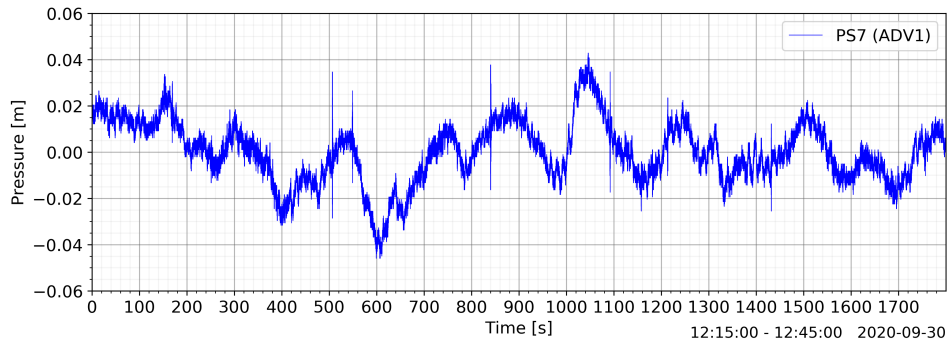
(d) Pressure sensor corresponding to ADV1 (PS7)

Figure 4.24: Zero measurement Wednesday 30th of September 12:15-12:45 for PS1 (a), PS3 (b), PS5 (c) and PS7 (d). Note the different scale for the y-axis of PS1 (a) ranging between ±0.25 due to the signal noise.

4.3.3. Spectral analyses

To investigate the frequency domain of the pressure sensor signals the Welch's method , as described in Section 4.1.7, is used to determine the variance density spectrum. Just as for the ADV velocity spectra, a value for Δf of 0.1 is selected resulting in a lowest measurable frequency of 0.1 Hz. Below this frequency, the pressure signal is filtered with a high-pass Butterworth filter (Section C.4.1). First the variance density spectrum of the high frequency pressure sensors (PS1-4) is elaborated after which the variance density spectrum of pressure sensors PS7-10 (ADV1-4) is discussed. The spectrum of PS5 and PS6 is not determined as these pressure sensors (RBR) measured with 2 Hz resulting in limited information on the energy levels throughout the frequency domain.

High frequency pressure sensor (PS1-4)

For the zero measurement on Wednesday the 30th of September and Test 14 at 90% power the variance density spectra are visualized in Figure 4.25. PS1 and PS4 are located at the intersection of the quay wall and the bed while PS2 and PS3 are placed at the quay wall around the same height as the axis of the bow thrusters (Section 3.5.6). At 48 Hz a clear peak is observed for PS1, PS2 and PS4 which is not present in the signal of PS3. Inline with the findings of Section 4.3.2 for the noise on the signal of PS1, PS2 and PS4 during the zero measurements. The noise might be due to an error in the pressure sensors as a high frequency disorder caused by an external factor would result in the noise being present in the signal of every sensor (PS1-4). For further analysing of PS1-4 the signal is filtered with a Butterworth low-pass filter to a sampling frequency of 64 Hz (f_{nyq}= 32 Hz) as explained in Section 4.3.2.

(a) Wednesday 30th of September zero measurement.   (b) Test 14 90% power.
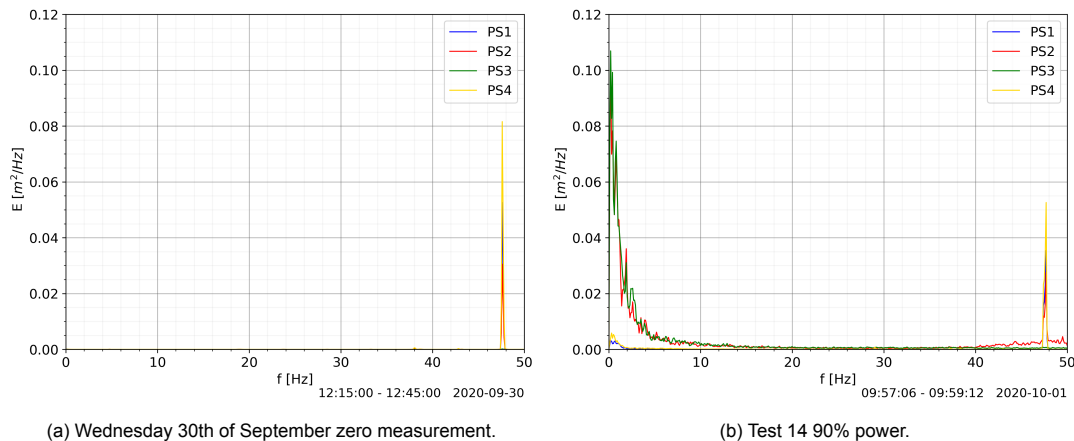
Figure 4.25: Variance density spectrum for the high frequency pressure sensors PS1-4 (100 Hz) during the zero measurement of Wednesday the 30th of September (a) and Test 14 90% power (b).

In Figure 4.26 the variance density spectrum of PS1-4 for Test 14 at 90% power is plotted with a logarithmic x-axis and the energy (E) multiplied by the frequencies (f) on the y-axis. This results in a better visualization of the lower frequencies which have the most energy in the spectrum. While moving from PS2 and PS3 (at the axis height of the bow thruster) to PS1 and PS4 (at the intersection between the bed and the quay wall) a lot of energy has been dissipated as observed by the difference in height and area. Similarly to the velocity measurements of the ADVs, most of the energy is located within the lower frequencies. Figure 4.26b is zoomed in on PS1 and PS4 which show similar results as PS2 and PS3 with most energy located in the lower frequencies. Although a second peak can be observed for PS4 around 5 Hz.

(a) PS1-4

(b) Zoomed in at PS1 and PS4
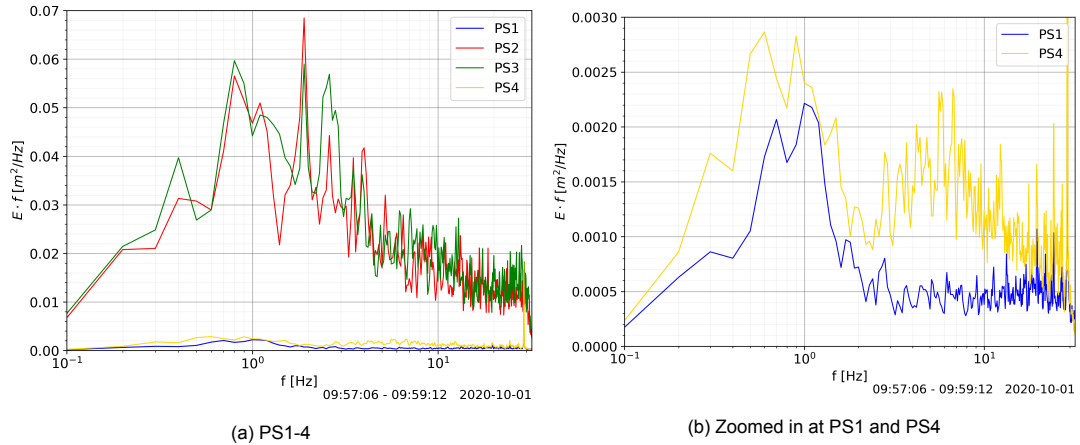
Figure 4.26: Logarithmic x-axis plot of the variance density spectrum of Test 14 at 90% power for PS1-4. $\Delta f = 0.1$, BT 1 & 2, Vessel position 4 (L_{BT} = 4.35 and y_t = 1.75 m). Note the difference in scale on the y-axis.

Similar to the -5/3 power law for the energy distribution in turbulent velocity spectra, Kolmogorov (1941) derived the -7/3 power law for the pressure spectra in the inertial subrange (Patwardhan and Ramesh, 2014). Therefore, the -7/3 power is plotted together with the pressure spectra on a logarithmic scale in Figure 4.27 as check whether the pressure sensors measured turbulence. Between approximately 1-20 Hz the signal of PS1-4 follows the -7/3 power law confirming the right functioning and turbulence measurements of the pressure sensors.
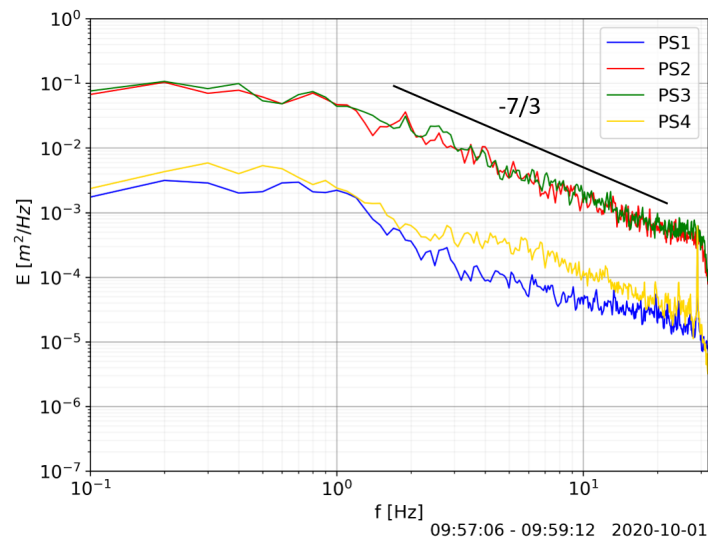
Figure 4.27: Logarithmic plot of the variance density spectrum of Test 14 at 90% power for the pressure signal of PS1-4. $\Delta f = 0.1$, BT 1 & 2, Vessel position 4 (L = 0.8 and y = -3.5 m).

ADV pressure sensors (PS7-10)
The ADV pressure sensors (PS7-10) measure with the same sampling frequency as for the velocity measurements. ADV1 (PS7) and ADV2 (PS8) measure at 64 Hz while ADV3 (PS9) measures at 16 Hz and ADV4 (PS10) measures at 8 Hz. In Figure 4.28 the variance density spectrum is visualised for PS7-10 during Test 14 at 50% and 90% power. A similar trend as for PS1-4 and the flow velocity spectra for V_{hor} is observed with high peaks close to 0 Hz decreasing exponentially while moving towards the higher frequencies. After approximately 10 Hz almost no energy is within the spectrum. Contrary to the other variance density spectra, a peak is observed for PS9 and PS10 around 3 Hz in Figure 4.28b. The peak of PS10 is the highest peak measured in the spectrum and only observed during the 90% power step. A similar peak is measured for other Tests during 90% power in which the peak of PS10

is always higher than the peak of PS9.

(a) Test 14 50% power   (b) Test 14 90% power.
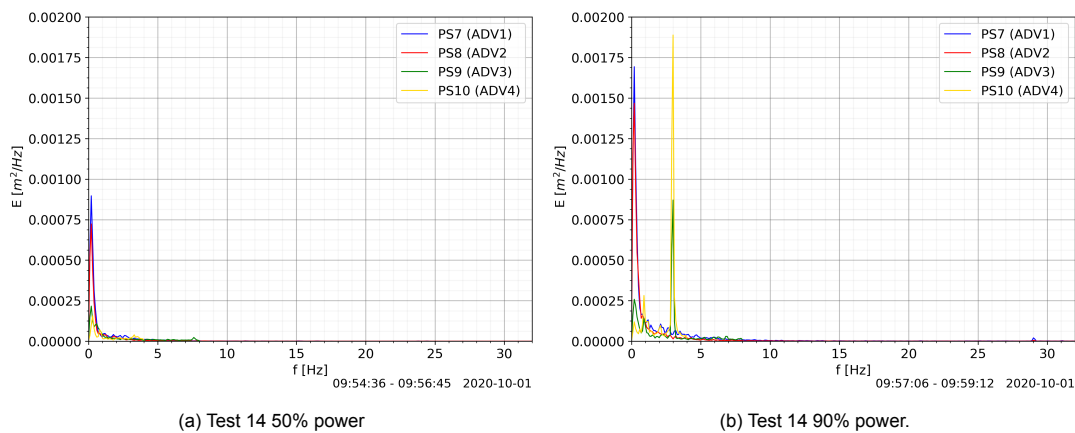
Figure 4.28: Variance density spectrum for the ADV pressure sensors (PS7-10) for Test 14 at 50 % (a) and 90% power (b). Δf = 0.1, BT 1 & 2, Vessel position 4 (L_{BT} = 4.35 and y_t = 1.75 m).

In Figure 4.29 the variance density spectrum of PS7-10 for Test 14 at 50% and 90% power is plotted with a logarithmic x-axis and the energy (E) multiplied by the frequencies (f) on the y-axis. At 50% power (Figure 4.29a), PS7-PS10 show similar results as PS1-4 (Figure 4.26) and the velocity measurements of ADV1-4 (Figure 4.17) with most energy located in the lower frequencies. However, PS9 and PS10 also show high narrow peaks at 3 Hz and 7 Hz which are not observed for the other pressure sensors or ADV velocity measurements. For 90% power (Figure 4.29b) the spectrum is dominated by the high and narrow peak at 3 Hz for PS9 and PS10 as also observed in Figure 4.28b leading to the reasoning that the signal of PS9 and PS10 is influenced by an external disturbance not associated with the bow thruster induced flow velocities. For instance, the engine sound from the bow thrusters.

(a) Test 14 50% power   (b) Test 14 90% power.
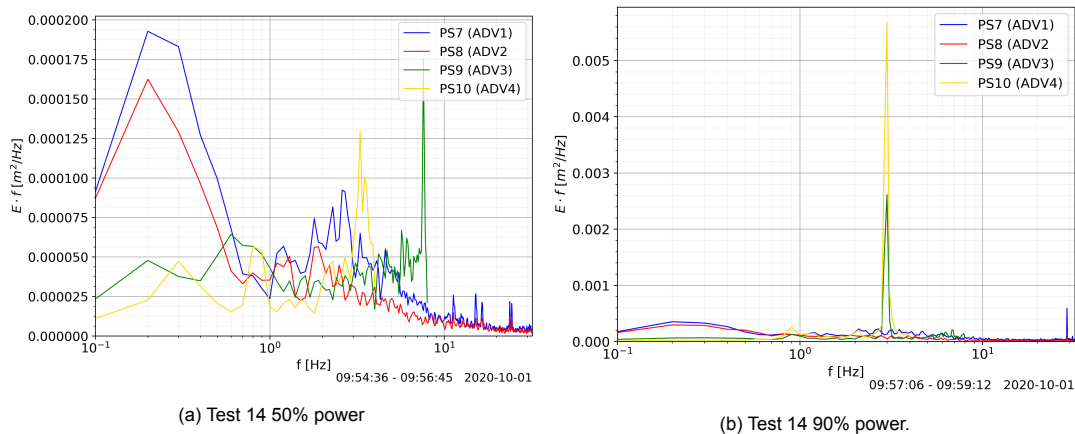
Figure 4.29: Logarithmic x-axis plot of the variance density spectrum of Test 14 at 50% (a) and 90% power (b) for PS7-10 (ADV pressure sensors). Δf = 0.1, BT 1 & 2, Vessel position 4 (L_{BT} = 4.35 and y_t = 1.75 m).

Similar to the the pressure spectra of PS1-4 a slope of -7/3 is observed in Figure 4.30 for Test 14 at 50% and 90% power in the inertial subrange as derived by (Patwardhan and Ramesh, 2014). Although, PS9 (green) and PS10 (yellow) slightly deviate from the -7/3 law.

(a) Test 14 50% power   (b) Test 14 90% power.
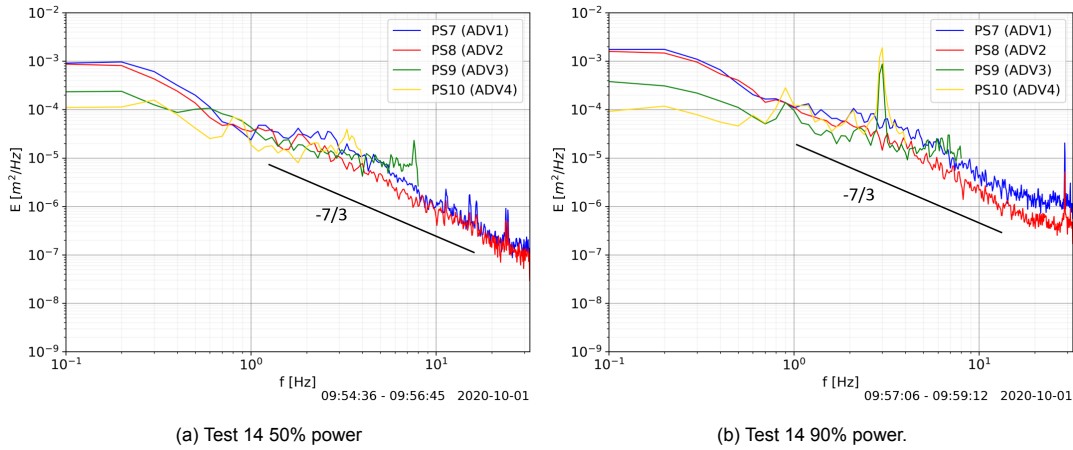
Figure 4.30: Logarithmic plot of the pressure variance density spectrum of Test 14 at 50% (a) and 90% (b) power for the pressure signal of PS7-10 (ADV pressure sensors). $\Delta f = 0.1$, BT 1 & 2, Vessel position 4 (L_{BT} = 4.35 and y_t = 1.75 m).

4.3.4. Statistical analyses of the pressure sensor signals

The pressure sensors PS1-4 and PS7-10 are illustrated in Figure 4.31 by means of a boxplot for Test 14 at 90% power. In Figure 4.31a, for the high frequency pressure sensors, a clear distinction in pressure range between PS2 and PS3, placed at the bow thruster outlet height at the quay wall, and PS1 and PS4, placed at the intersection between the quay and the bed, can be observed. PS2 and PS3 range in pressure fluctuations between roughly 2 m and -1.5 m while PS1 and PS4 range between 0.4 m and -0.6 m. PS2 and PS3 measure higher positive than negative pressures due to the fact that they are positioned in the direction of the flow velocity while PS1 and PS4 are positioned perpendicular to the flow velocity resulting in higher negative than positive pressures. In Figure 4.31b the pressure sensors attached the the ADV cases (PS7-10) are plotted. PS7 (ADV1) and PS8 (AVD2) are both placed at the same x-distance from the quay wall (Figure 3.21) and have similar pressure fluctuations with PS7 ranging between 0.10 m and -0.15 m and for PS8 ranging between 0.08 m and -0.12 m. PS9 (ADV3) and PS10 (ADV4) are located significantly further away from the quay wall but still have pressure fluctuations ranging between 0.08 and -0.07 with similar box shapes (25th to 75th percentile) as PS7 and PS8. Thus, not showing the same reduction in pressure fluctuations as decrease in flow velocities observed for ADV1-4 in Figure 4.23. In Addition, PS7-9 are positioned at the back of the ADV case not directly inline with the flow velocity in x-direction while PS10 is located directly behind the fixed ADV head mounted to the case (Figure 3.24), inline with the flow in x-direction.

(a) PS1-4   (b) PS7-10 (ADV pressure sensors)
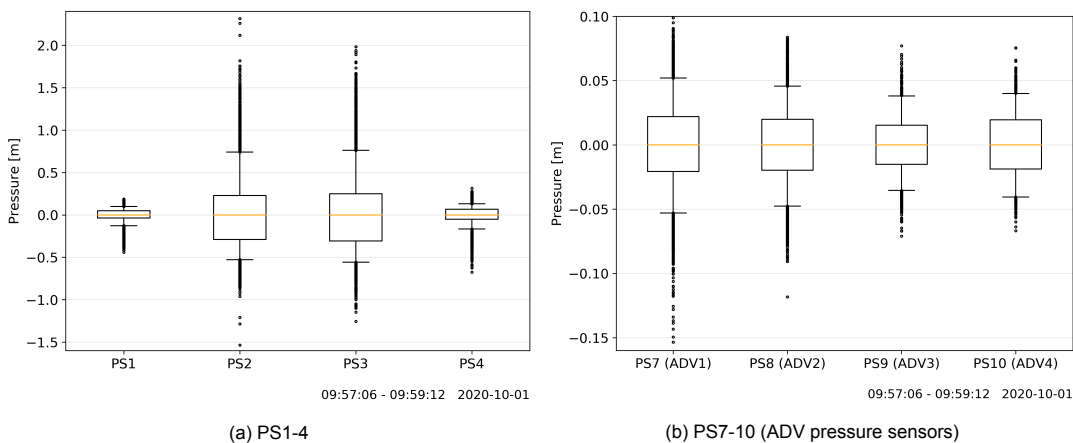
Figure 4.31: Boxplot for PS1-4 (a) and PS7-10 (b) for Test 14 at 90% power. $\Delta f = 0.1$, BT 1 & 2, Vessel position 4 (L_{BT} = 4.35 and y_t = 1.75 m). Note the difference in scale for the y-axis.

In Figure 4.32a PS1-4 are plotted together with PS7-10. The difference in pressure fluctuations be-

tween the pressure sensors mounted at the bow thruster outlet height (PS2 and PS3) and the pressure sensors at the bed (PS1, PS4 and PS7-10) is significant. Therefore, the pressure sensors near the bed (PS1, PS4 and PS7-10) are compared with each other in Figure 4.32b. PS1 and PS4 are mounted on the vertical frame which is attached to the horizontal frame at 1 m from the quay wall (Section 3.5.6). PS7 and PS8 are located at 2.6 m from the quay wall (Figure 3.21) resulting in a distance in x-direction from PS1 and PS4 of 1.6 m. Nevertheless, the pressure fluctuations of PS1 and PS4 are significantly higher than the fluctuations of PS7 and PS8.

(a) PS1-4 and PS7-10 (ADV pressure sensors)   (b) PS1, PS4 and PS7-10 (ADV pressure sensors)
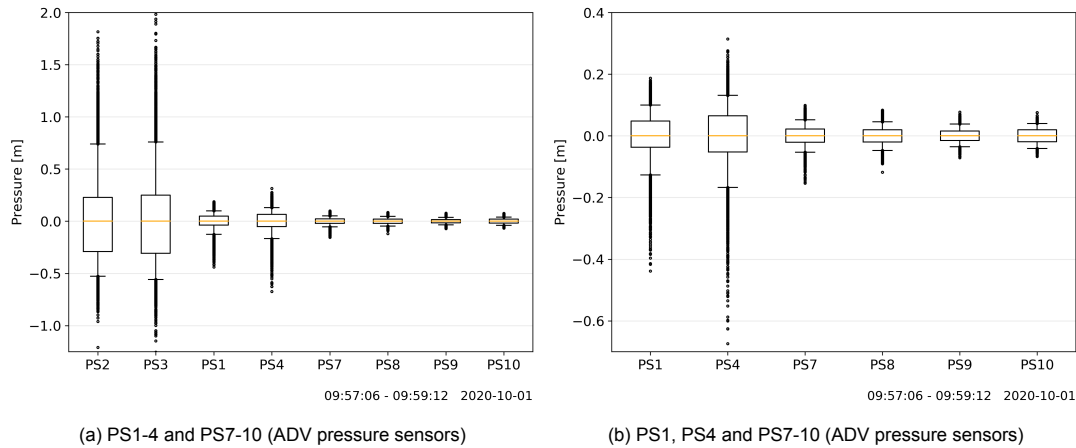
Figure 4.32: Logarithmic plot of the variance density spectrum of Test 14 at 50% (a) and 90% (b) power for the pressure signal of PS7-10 (ADV pressure sensors). $\Delta f = 0.1$, BT 1 & 2, Vessel position 4 (L_{BT} = 4.35 and y_t = 1.75 m).

In Table 4.9 the standard deviations of the high frequency pressure sensors (PS1-4) and the ADV pressure sensors (PS7-10) are listed. The standard deviations for all pressure sensors rise while increasing the power step of the bow thruster. Focusing on the highest standard deviations for 90% power, PS2 and PS4 are approximately 4-5.5 times larger than the standard deviations of PS1 and PS4. While moving away from the quay wall the standard deviations decrease further as the σ of PS1 and PS4 is approximately 2-3 times larger than the σ of PS7 and PS8. Moving towards PS9 and PS10 however does not show significant reduction in the standard deviation as the σ of PS7 and PS8 is approximately 1.1-1.5 times larger than the σ of PS9 and PS10.

Table 4.9: Standard deviation (σ) for PS1-4 (high frequency pressure sensors and PS7-10 (ADV pressure sensors) during Test 14 at 25%, 50% and 90% power.

	$\sigma_{25\%}$ [m]	$\sigma_{50\%}$ [m]	$\sigma_{90\%}$ [m]
PS1	0.0224	0.0521	0.0706
PS2	0.1186	0.2898	0.3944
PS3	0.1288	0.2885	0.4134
PS4	0.0272	0.0624	0.0977
PS7 (ADV1)	0.0093	0.0259	0.0339
PS8 (ADV2)	0.0085	0.0229	0.0296
PS9 (ADV3)	0.0108	0.0176	0.0225
PS10 (ADV4)	0.0079	0.0156	0.0254

$$\Large 5$$

Results

In this chapter the results of the near-bed flow velocity measurements are presented while the Somtrans XXV is moored to the quay wall and during the manoeuvring tests. Throughput this chapter, every test has a particular color where it can be recognized by in the measurement plots. Before analyzing the results, the definition and value(s) for the theoretical efflux velocity (V_0) and the thruster diameter (D_t) are elaborated in Section 5.1. The tests are generally discussed by comparing the horizontal mean flow velocity ($\overline{V}_{hor}$), standard deviation (σ_{hor}), maximum horizontal flow velocity load ($V_{max} = \overline{V}_{hor} + 3\sigma_{hor}$) and relative turbulence intensity (r_{hor}) for the moored tests (Section 5.2). Then the influence of y_t, the distance between the bow thruster axis and the measurement instruments, is analyzed in Section 5.3. Afterwards, the effect of using different bow thrusters (Section 5.4) is studied and the influence of the quay wall clearance on the maximum horizontal flow velocity load ($V_{max} = \overline{V}_{hor} + 3\sigma_{hor}$) is analysed in Section 5.5. Thereafter, the manoeuvring tests are compared to the measurements where the Somtrans XXV was moored to the quay wall in Section 5.6. Lastly, the pressure fluctuations measured by the pressure sensors are elaborated in Section 5.7. An overview of the moored tests is presented in Table 5.1 while the manoeuvring tests are listed in Table 5.2. The definitions for L, L_{BT} and y_t are illustrated in Figure 5.1.

Table 5.1: Test data overview of the measurements analysed in the results were the Somtrans XXV was moored to the quay wall. Where L is the quay wall clearance between the port side of the vessel and the quay wall and L_{BT} the quay wall clearance of BT1 and BT2 while for BT1&2 the average of BT1 and BT2 is used. The distance in y-direction alongside the quay wall between the bow thruster axis (in between BT1 and BT2 for BT1&2) and the instruments is defined as y_t.

Test	BT	Vessel position	L [m]	L_{BT} [m]	y_t [m]	Power step [%]
Test 2	2	1	0.8	3.09	0	25,50,90
Test 3	1	1	0.8	5.61	-3.5	25,50,90
Test 4	1&2	1	0.8	4.35	-1.75	25,50,90
Test 8	2	2	0.8	3.09	2	25,90
Test 9	1	2	0.8	5.61	-1.5	25,50,90
Test 10	1&2	2	0.8	4.35	0.25	25,50
Test 11	1	5	0.8	5.61	2	25,50,90
Test 12	1	4	0.8	5.61	0	25,50,90
Test 13	2	4	0.8	3.09	3.5	25,90
Test 14	1&2	4	0.8	4.35	1.75	25,50,90
Test 15	2	3	0.8	3.09	-2	90
Test 16	1&2	3	0.8	4.35	-3.75	25,50,90
Test 17	1&2	6	0.8	4.35	0	50,90
Test 18	1&2	7	3	6.55	0	50,90
Test 19	2	7	3	5.29	1.75	50,90
Test 20	1	7	3	7.81	-1.75	50,90
Test 21	1&2	8	5	8.55	0	50,90

Table 5.2: Test data overview of the manoeuvring measurements with the Somtrans XXV. Where L is the quay wall clearance between the port side of the vessel and the quay wall and the type is the kind of manoeuvring test that is conducted.

Test	BT	L [m]	Power step [%]	Type
Test 22	1&2	Max. 15 m	25,50,90	Berthing
Test 23	1&2	4.25 m	90	Sailing
Test 24	1	4.25 m	90	Sailing
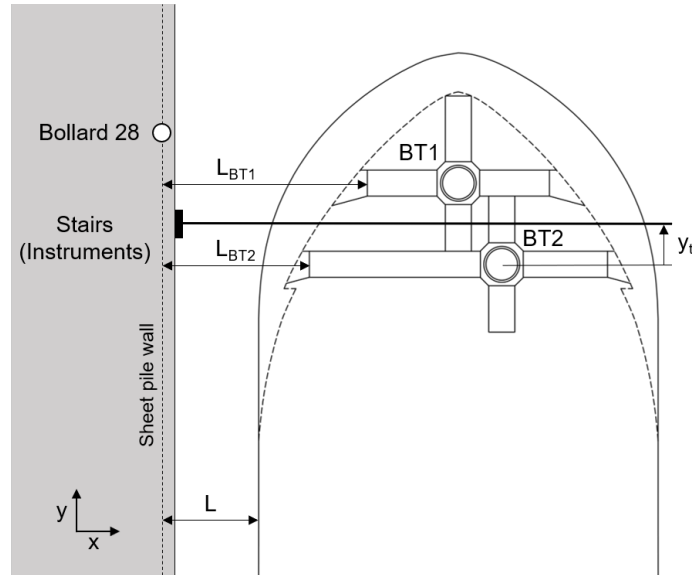
Figure 5.1: Illustration of the defined parameters listed in Table 5.1 and 5.2. Where L is the quay wall clearance between the port side of the vessel and the quay wall, L_{BT1} and L_{BT2} the quay wall clearance of BT1 and BT2 and y_t the distance in y-direction between the center line of the horizontal measurement frame (the stairs used as reference line for the instruments) and the considered bow thruster axis. y_t is positive when the instruments are above the considered bow thruster axis. $L_{BT1\&2}$ is defined as the average value for L_{BT} of BT1 and BT2

5.1. Theoretical efflux velocity and bow thruster diameter

To compare the flow velocities measured during the different power steps of 25%, 50% and 90%, the near-bed flow velocities are divided by the theoretical efflux velocity V_0 corresponding to the used power step and bow thruster. Giving insight in the decay of the flow velocities from the bow thruster outlet towards the measurement points as ratio of V_0. By means of Equation 5.1, the theoretical value for V_0 is calculated for BT1 (= V_0 for BT2) at 25%, 50% and 90% power for which the power inputs in kW (P_t) are listed in Table 5.3. The total installed power for each bow thruster is 394 kW (P_t) which is fully applied when the engine reaches 1800 RPM corresponding with the 90% power step (See Section 3.6.1).

The bow thruster channel outlet has a rectangular shape. Therefore, the equivalent circular bow thruster outlet diameter (D_t) is calculated as Equation 5.1 is defined for circular bow thruster outlets. The equivalent diameter (D_t) is determined with Equation 3.1 where a = 1.1 m is the thruster channel outlet width and b = 0.82 m the thruster channel outlet height. The equivalent diameter is defined as a circle having the same cross sectional area as the rectangular bow thruster outlet. This results in D_t = 1.07 m which is used to determine the theoretical efflux velocity (V_0) and make the distance x, where the sensors measure the flow, dimensionless (x/D_t) to compare the measurement positions to previous research and guidelines. Although, for the specific case of the Somtrans XXV, x/D_t results in a similar values as x due to D_t (= 1.07) being close to 1.

$$V_0 = 1.17 \cdot \left(\frac{P_t}{\rho_w \cdot D_t^2} \right)^{0.33} \tag{5.1}$$

$$D_t = \sqrt{\frac{4 \cdot a \cdot b}{\pi}} = 1.07m \tag{5.2}$$

Table 5.3: Bow thruster power step [%] and corresponding power [kW] used for determining V_0.

Power load [%]	P_t [kW]
25	98.5
50	197
90	394

When BT1&2 are activated simultaneously, V_0 is determined according to Equation 5.3 by assuming quadratic superposition of the theoretical efflux flow velocities (V_0) of the individual jets from BT1 and BT2. Equation 5.3 is modified from the PIANC (2015) guidelines in which the method of quadratic superposition is applied to the Dutch or German method (Section 2.3.1) to determine the maximum bed velocities caused by two jets together. Therefore, this step differs from the usual design practice by applying quadratic superposition directly to the efflux velocity V_0 instead of at the end on the determined near-bed flow velocity. Where $V_{0,BT1\&2}$ is the efflux velocity for BT1&2 activated simultaneously, $V_{0,BT}$ the efflux velocity of one single bow thruster, h_t the height of the bow thruster axis above the bed and a_t the distance between the axis of BT1 and BT2 (See Figure 3.5). During the measurements $h_t = 3.24$ m and $a_t = 3.5$ m were constant resulting in $h_t/(a_t/2) = 1.85$ satisfying the condition for applicability of Equation 5.3. An overview of the theoretical efflux flow velocities (V_0) used throughout this chapter is listed in Table 5.4

$$V_{0,BT1\&2} = V_{0,BT} \cdot \sqrt{2} \quad \text{for} \ \ h_t/(a_t/2) > 1 \tag{5.3}$$

Table 5.4: Theoretical value for the efflux velocity V_0 of a single bow thruster, BT1 and BT2, as well as V_0 for BT1&2 (activated simultaneously) at 25%, 50% and 90% power.

	V_0 25% [m/s]	V_0 50% [m/s]	V_0 90% [m/s]
BT1 / BT2	5.08	6.39	8.03
BT1&2	7.19	9.03	11.35

5.2. General results for the moored measurement tests

The general results of the moored tests (Table 5.1) are elaborated for the mean flow velocity ($\overline{V}_{hor}$), standard deviation (σ_{hor}), maximum horizontal flow velocity ($V_{max} = \overline{V}_{hor} + 3\sigma_{hor}$) and relative turbulence intensity (r_{hor}). For each power setting, the results are plotted against the distance x from the quay wall to study the velocity decay profile perpendicular to the quay. In the figures, the circles represent the measurement points of ADV1-4 while the squares illustrate the measurement points of Ott meter 1 and 2 (Ott1 and Ott2). Ott1 measured at the same location as ADV2 to check whether the order of magnitude measured by both instruments are similar. In Appendix D the values for $\overline{V}_{hor}$, σ_{hor}, $V_{max} = \overline{V}_{hor} + 3\sigma_{hor}$ and r_{hor} are listed for every ADV and Ott meter for the moored tests.

5.2.1. Mean flow velocity

In Figure 5.2, 5.3 and 5.4 the mean flow velocities are plotted for 25%, 50% and 90% power respectively. For every power step, at the first two measurement points (ADV1 and ADV2) the highest mean flow velocities are measured (with the exception of Test 15 and 16) with ADV1 and ADV2 measuring similar velocities although for most tests the mean flow velocity increases from ADV1 towards ADV2 showing that the highest values are not necessarily measured closest to the quay wall. Increasing in power step

results in a broader range in measured mean flow velocities for every measurement point. Focusing on the highest flow velocities measured at ADV1 and ADV2, a flow velocity range of 0.3 - 1.05 m/s is observed for 25% power, at 50% power it varies between 0.45 - 1.55 m/s while for 90% power it falls between 0.45 - 1.70 m/s. Between ADV2 and ADV3 the mean flow velocity decays quite rapidly for almost every test (with the exception of Test 9, 15 and 16) which is most pronounced for the 90% power step. Moving from ADV3 to ADV4 the mean flow velocities continue to dissipate, although at a considerably lower rate than between ADV2 and ADV3. The last measurement point, at 8.5 m from the quay wall, is Ott2 which measures a variety of lower, similar or even higher mean flow velocities than ADV4. Therefore, Ott2 gives some uncertainty in the general observed mean flow velocity pattern. It is expected that the mean flow velocities continue to dissipate moving further away from the quay. However, as Ott2 is positioned very close to the bow thruster inlet it could measure higher mean flow velocities than expected due to the suction of the inlet. Two exceptions to this general flow velocity pattern described above are observed for Test 15 and 16 which have a rather large value for y_t. Both show a slightly increasing or constant flow velocity between ADV1-3, after which at ADV4 the flow velocity declines while rising again at Ott2. Overall showing a rather constant level in flow velocities with respect to the velocity decay profile observed for the other tests. However, for Test 15 at 90% power the increase in mean flow velocity is even extremely high between ADV4 and Ott2. An explanation for this will be further discussed in Section 5.3. The measured mean flow velocities at ADV4 and Ott2 for all the tests vary between 0.05 - 0.65 m/s at 25% power and 0.05 - 1.00 m/s for both 50% and 90% power. An overview of the mean flow velocity values is listed in Table D.4 in Appendix D.
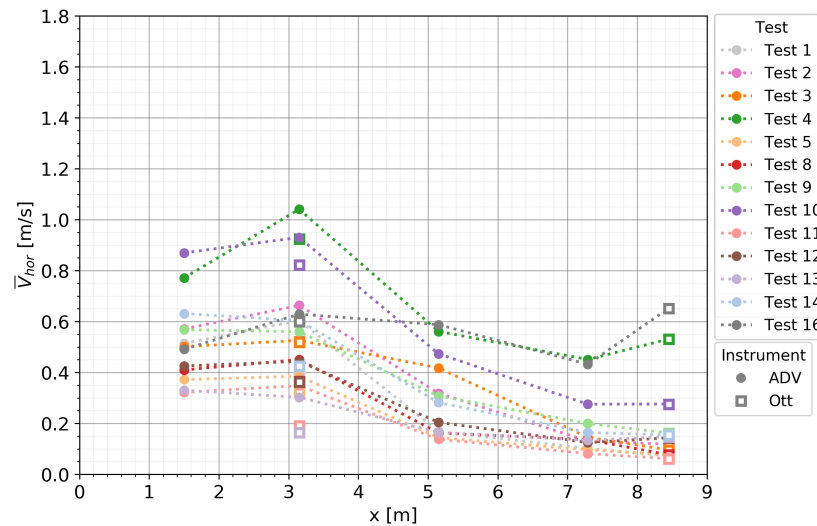
Figure 5.2: Mean horizontal flow velocity for the moored measurement tests plotted together at 25% power. With on the x-axis the x-coordinate of ADV1-4 along with Ott1 and Ott2 relative to the quay wall.
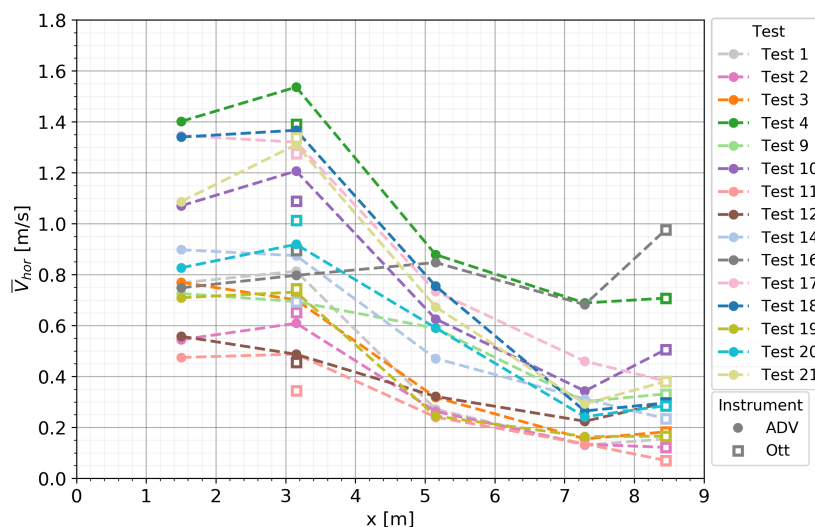
Figure 5.3: Mean horizontal flow velocity for the moored measurement tests plotted together at 50% power. With on the x-axis the x-coordinate of ADV1-4 along with Ott1 and Ott2 relative to the quay wall.
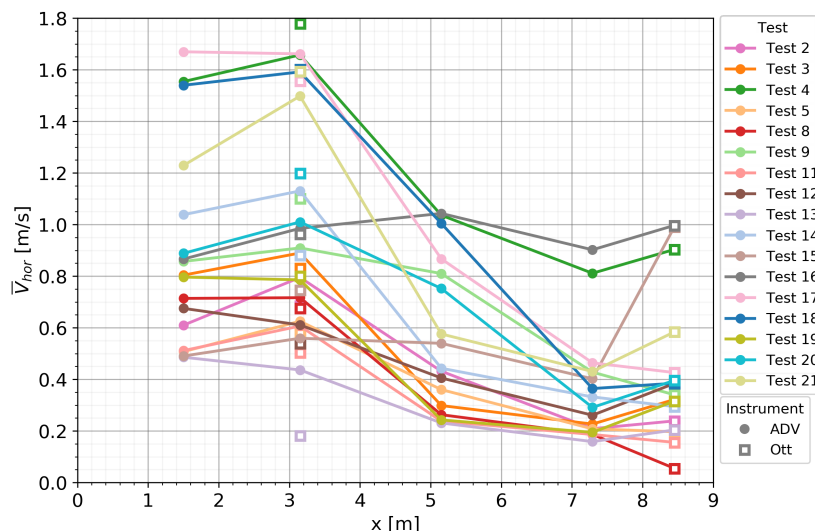
Figure 5.4: Mean horizontal flow velocity for the moored measurement tests plotted together at 90% power. With on the x-axis the x-coordinate of ADV1-4 along with Ott1 and Ott2 relative to the quay wall.

In Figure 5.5 $\overline{V}_{hor}$ is plotted for ADV2 against Ott1 which both measured at x = 3.15 m from the quay wall. Similar values are observed for all the moored tests during the three different power steps. Although, on average $\overline{V}_{hor}$ for ADV2 is 0.04 m/s (5%) higher than for Ott2. Concluding that ADV2 and Ott1 measure similar magnitudes for the mean horizontal flow velocity. In Figure 5.6 the same plot is illustrated for ADV4 and Ott2 which are positioned at x = 7.29 m and 8.45 m respectively. Despite not being placed at the same location comparable values for $\overline{V}_{hor}$ are measured. On average $\overline{V}_{hor}$ for Ott2 is 0.04 m/s (12%) higher than for ADV4 due to the influence of the bow thruster inlet drawing in water.
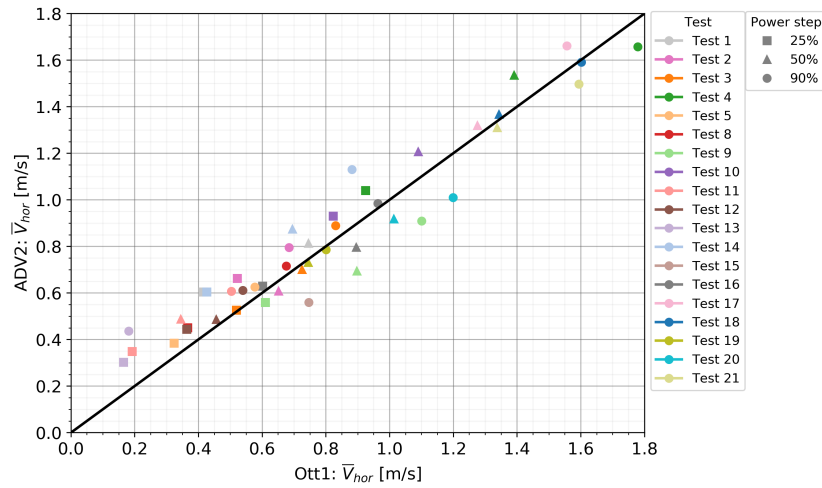
Figure 5.5: Mean horizontal flow velocity ($\overline{V}_{hor}$) of ADV2 compared to Ott1 for 25%, 50% and 90% power. Both ADV2 and Ott1 are located at 3.15 m from the quay wall. In black, the line x=y is plotted.
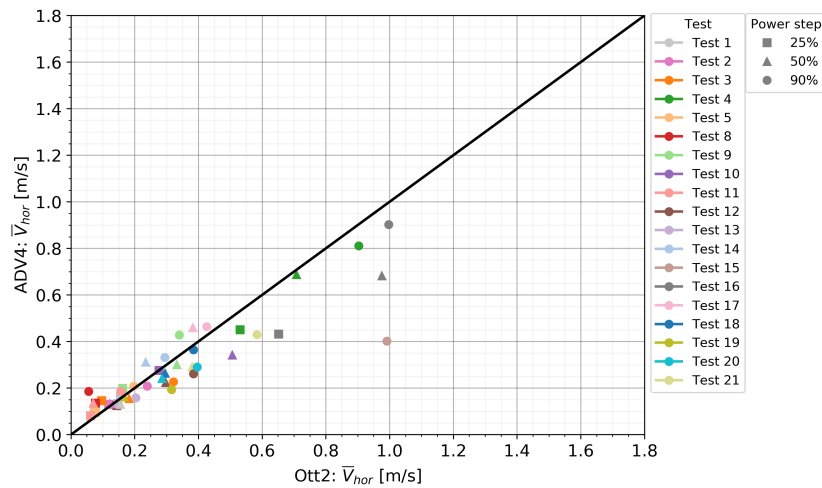
Figure 5.6: Mean horizontal flow velocity ($\overline{V}_{hor}$) of ADV4 compared to Ott2 for 25%, 50% and 90% power. ADV4 is located at x = 7.29 m while Ott2 is positioned at x = 8.45 from the quay wall. In black, the line x=y is plotted.

In Table 5.5 the average over all the measurement tests is presented for $\overline{V}_{hor}$ per power step and measurement location while in Table 5.6 the dimensionless values are listed as $\overline{V}_{hor}/V_0$. Where V_0 depends on the power step and whether one or two bow thruster are activated as listed in Table 5.4. The x-coordinates of the measurement instruments are made dimensionless by dividing over D_t = 1.07 m which is the diameter of a single bow thruster. In this way the distance from the quay wall is presented as function of D_t making the results more comparable to previous research. For both 50% and 90% power the average of all the mean horizontal flow velocities ($\overline{V}_{hor}$) is close to 1 m/s for the measurement instruments close to the quay at 1.5 m and 3.15 m. Near the end of the measurement frame at ADV4 and Ott2 the average of $\overline{V}_{hor}$ reduces to 0.30 - 0.42 m/s for 50% and 90% power showing a smaller increase in $\overline{V}_{hor}$ between 50% power and 90% power than from 25% to 50% power. For every power step $\overline{V}_{hor}$ increases from ADV4 to Ott2 displaying the effect of the bow thruster inlet on the flow velocities measured by Ott2. $\overline{V}_{hor}$ reduces from an average of measured by ADV2 Focusing on the relative mean horizontal flow velocity ($\overline{V}_{hor}/V_0$) near the quay wall, average values between 0.08-0.12 V_0 are observed while decreasing towards 0.03-0.04 V_0 furthest from the quay wall at ADV4 and Ott2.

Table 5.5: Overview of the average value for the mean horizontal flow velocity determined over all the measurement tests $(\overline{\overline{V}}_{hor})$ for every measurement instrument per power step.

	ADV1 [m/s] x = 1.50 m	ADV2 [m/s] x = 3.15 m	Ott1 [m/s] x = 3.15 m	ADV3 [m/s] x = 5.15 m	ADV4 [m/s] x = 7.29 m	Ott2 [m/s] x = 8.45 m
$\overline{V}_{hor}$ 25%	0.52	0.58	0.48	0.3	0.19	0.2
$\overline{V}_{hor}$ 50%	0.88	0.92	0.91	0.52	0.3	0.34
$\overline{V}_{hor}$ 90%	0.9	0.97	0.95	0.56	0.36	0.42

Table 5.6: Overview of the average value for the relative mean horizontal flow velocity determined over all the moored measurement tests $(\overline{V}_{hor}/V_0)$ for every measurement instrument per power step.

	ADV1 [-] x/D_t = 1.40	ADV2 [-] x/D_t = 2.94	Ott1 [-] x/D_t = 2.94	ADV3 [-] x/D_t = 4.81	ADV4 [-] x/D_t = 6.81	Ott2 [-] x/D_t = 7.90
$\overline{V}_{hor}/V_0$ 25%	0.09	0.1	0.08	0.05	0.03	0.03
$\overline{V}_{hor}/V_0$ 50%	0.11	0.12	0.12	0.07	0.04	0.04
$\overline{V}_{hor}/V_0$ 90%	0.09	0.1	0.1	0.06	0.04	0.04

5.2.2. Standard deviation

The standard deviation ($\sigma_{hor} = \sqrt{\sigma_x^2 + \sigma_y^2}$) or absolute turbulence intensity of the moored measurement tests are illustrated in Figure 5.7, Figure 5.8 and Figure 5.9 for 25%, 50% and 90% power respectively. The standard deviations show a similar decay pattern as the mean flow velocities where at the first two measurement points, ADV1 and ADV2, the highest values for σ_{hor} are measured. Afterwards, σ_{hor} decreases rapidly to ADV3, although for several tests at 25% power (Test 10, 16 and 4) σ_{hor} declines gradually while moving further from the quay wall. During 90% power, Test 15 and 16 are exceptions to the general decay pattern observed for the other tests which was also observed for the mean flow velocity. For 25% power the highest measured values for σ_{hor} ranges between 0.14-0.32 m/s, for 50% power it is bounded by 0.22-0.48 m/s while for 90% power it varies between 0.24-0.58 m/s. Further away from the quay at ADV4 and Ott2 σ_{hor} decreases to 0.01 - 0.09 m/s for 25% power, 0.02 - 0.30 m/s for 50% power and 0.01 - 0.33 m/s for 90% power. Similar as for the mean flow velocities, the standard deviations increase the most from 25% towards 50% power while the spreading between the highest and lowest values advances from 25% towards 90% power.
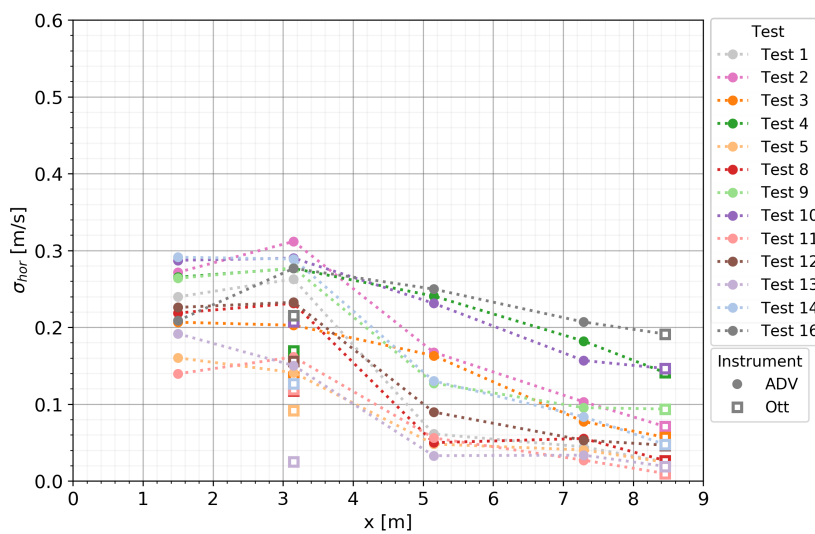
Figure 5.7: Standard deviation of V_{hor} for the moored measurement tests plotted together at 25% power. With on the x-axis the x-coordinate of ADV1-4 along with Ott1 and Ott2 relative to the quay wall.
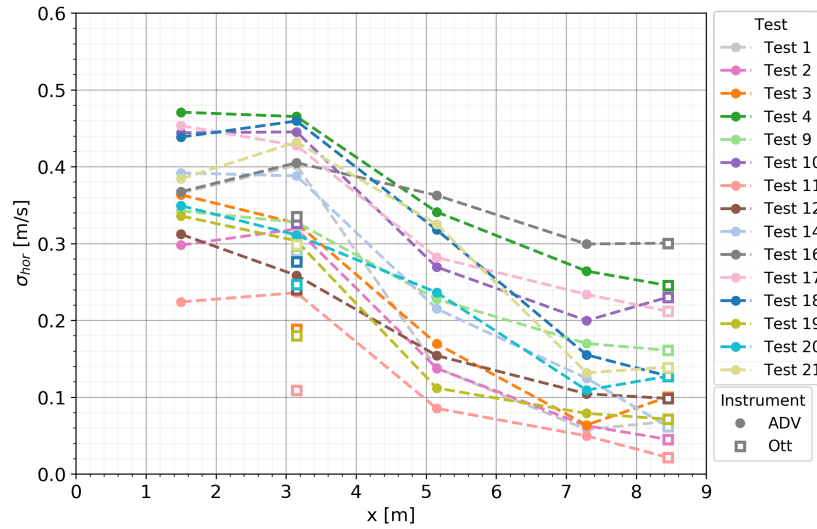
Figure 5.8: Standard deviation of V_{hor} for the moored measurement tests plotted together at 50% power. With on the x-axis the x-coordinate of ADV1-4 along with Ott1 and Ott2 relative to the quay wall.
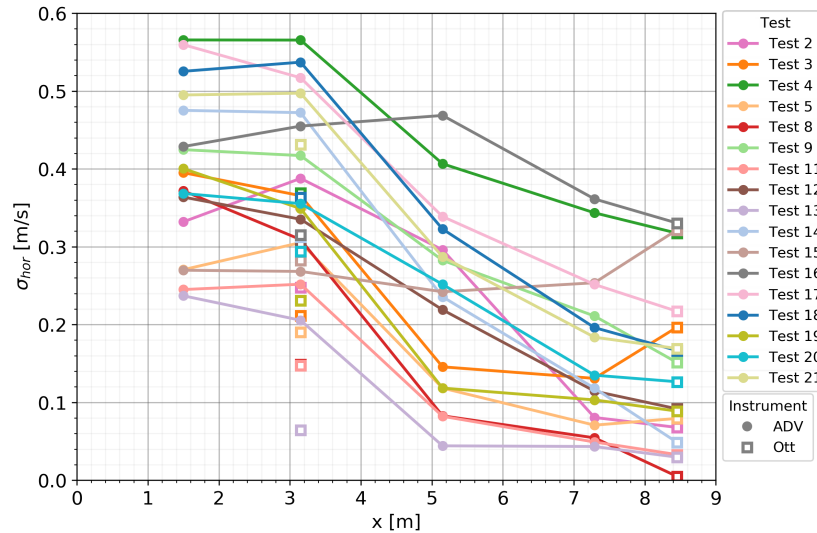
Figure 5.9: Standard deviation (σ_{hor}) of the horizontal flow velocity (V_{hor} for the moored measurement tests plotted together at 90% power. With on the x-axis the x-coordinate of ADV1-4 along with Ott1 and Ott2 relative to the quay wall.

In Figure 5.10 σ_{hor} is plotted for ADV2 against Ott1 which both measured at x = 3.15 m from the quay wall. For every test and power step (with the exception of Test 15 at 90% power) higher standard deviations are measured by ADV2 than for Ott1. Showing that the ADV can more accurately measure the high turbulent fluctuations close to the quay wall than the Ott meter. On average, σ_{hor} is 0.10 m/s (45%) higher for ADV2 than for Ott1. This is inline with the measuring technique of the ADV being able to measure high turbulent fluctuations. In Figure 5.11 the same plot is illustrated for ADV4 and Ott2 which are positioned at x = 7.29 m and 8.45 m respectively. Despite not being placed at the same location, comparable values for σ_{hor} are measured. On average, σ_{hor} is 0.014 m/s (11.5%) higher for ADV4 than for Ott2. Showing that between x = 7.29 m and 8.45 m the standard deviations decreased slightly and overall lower turbulent fluctuations were measured than close to the quay wall resulting in Ott2 being able to measure values for σ_{hor} comparable to ADV4. In addition, the bow thruster inlet drawing in water results in less turbulent flow conditions near the inlet. Therefore, the Ott2 measuring lower values for σ_{hor} can be ascribed to the larger distance from the quay wall, the lower sampling frequency and the influence of the bow thruster inlet. Concluding that the values for σ_{hor} measured by

ADV1-4 are most trustworthy.
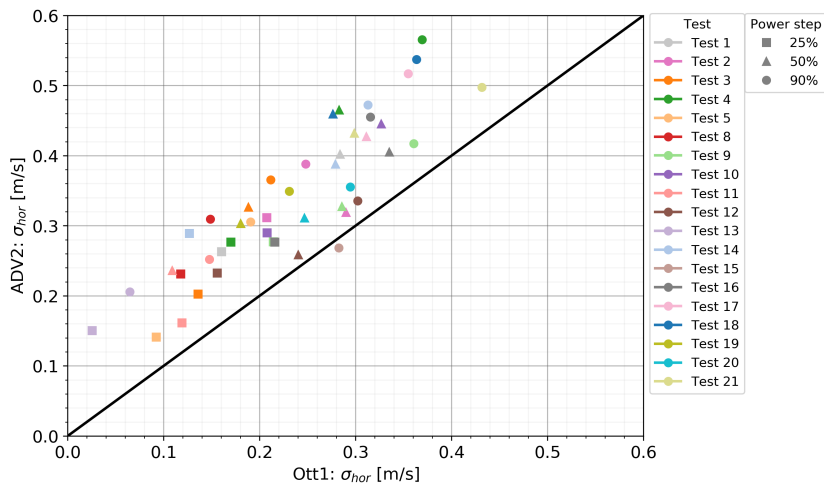
Figure 5.10: Standard deviation (σ_{hor}) of the horizontal flow velocity (V_{hor}) for ADV2 compared to Ott1 for 25%, 50% and 90% power. Both ADV2 and Ott1 are located at 3.15 m from the quay wall. In black, the line x=y is plotted.
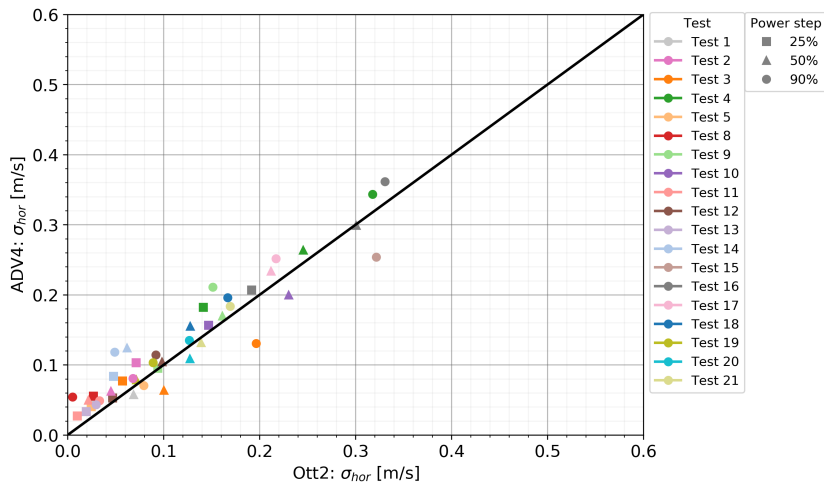
Figure 5.11: Standard deviation (σ_{hor}) of the horizontal flow velocity (V_{hor}) of ADV4 compared to Ott2 for 25%, 50% and 90% power. ADV4 is located at x = 7.29 m while Ott2 is positioned at x = 8.45 from the quay wall. In black, the line x=y is plotted.

In Table 5.7 the average standard deviation (σ_{hor}) for the horizontal flow velocity (V_{hor}) of all the moored tests per power step and measurement instrument are listed. Increasing in power shows an advance in average standard deviation while moving further away from the quay wall the standard deviations decrease rapidly from an average of 0.40 m/s at ADV2 (highest measured value) for 90% power towards 0.16 m/s at ADV4 resulting in a reduction of 60%.

Table 5.7: Overview of the average standard deviation (σ_{hor}) for the horizontal flow velocity (V_{hor}) for every measurement instrument per power step.

		ADV1 [m/s] x = 1.50 m	ADV2 [m/s] x = 3.15 m	Ott1 [m/s] x = 3.15 m	ADV3 [m/s] x = 5.15 m	ADV4 [m/s] x = 7.29 m	Ott2 [m/s] x = 8.45 m
σ_{hor}	25%	0.23	0.24	0.15	0.13	0.09	0.07
σ_{hor}	50%	0.37	0.37	0.26	0.22	0.14	0.13
σ_{hor}	90%	0.4	0.39	0.27	0.23	0.16	0.14

5.2.3. Maximum horizontal flow velocity

In Figure 5.12, 5.13 and 5.14 the maximum horizontal flow velocities defined as $V_{max} = \overline{V}_{hor} + 3\sigma_{hor}$ (Section 2.4) are plotted for 25% , 50% and 90% power respectively. For the maximum horizontal flow velocity plots Ott1 has been left out as σ_{hor} is not accurately measured by Ott1 (Figure 5.10). The decay pattern for every power step is quite similar to the previous described mean flow velocity and standard deviation as the maximum horizontal flow velocity is a combination of these two. The highest values for the maximum horizontal flow velocity are measured at ADV1 and ADV2 ranging between 0.7-1.9 m/s at 25% power, for 50% power it varies between 1.1-2.9 m/s while for 90% power it falls between 1.0-3.4 m/s. Moving in x-direction from the quay wall to ADV4 and Ott2 the maximum horizontal flow velocities decline to 0.1-1.2 m/s for 25% power, 0.1-1.9 m/s for 50% power and 0.1-2.0 m/s for 90% power. Showing still a broad variety in measured maximum horizontal flow velocities at 7.5-8.5 m from the quay wall. However, the high flow velocities are mainly caused by Test 4, 10, 15, 16 and 17 for which BT1&2 were activated simultaneously with the exception of Test 15 were BT2 was used.
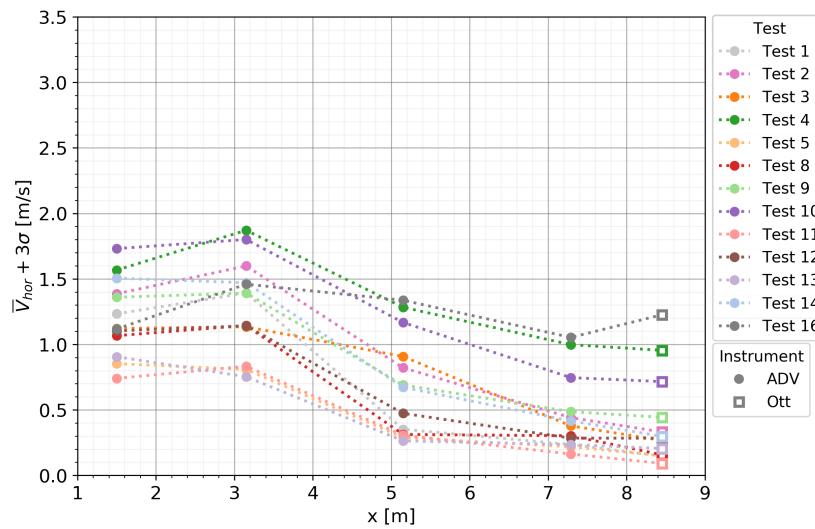
Figure 5.12: Maximum horizontal flow velocity ($V_{max} = \overline{V}_{hor} + 3\sigma_{hor}$) for the moored measurement tests at 25% power. With on the x-axis the x-coordinate of ADV1-4 and Ott2 relative to the quay wall.
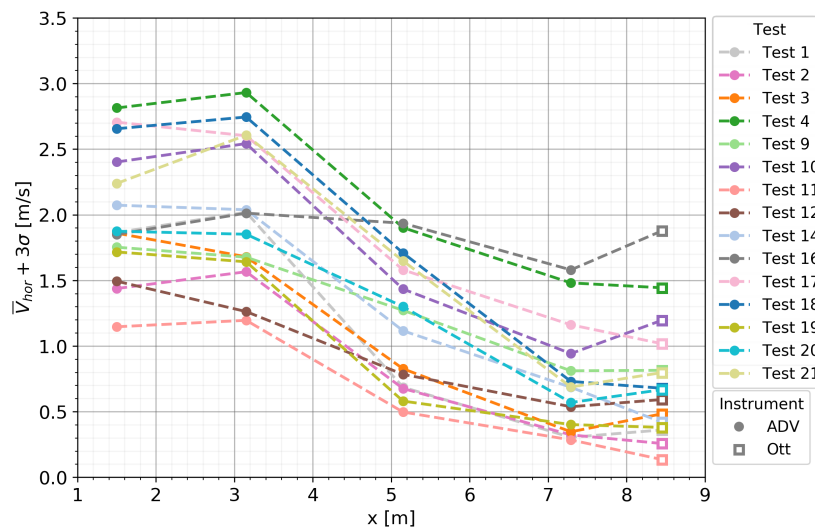
Figure 5.13: Maximum horizontal flow velocity ($V_{max} = \overline{V}_{hor} + 3\sigma_{hor}$) for the moored measurement tests at 50% power. With on the x-axis the x-coordinate of ADV1-4 and Ott2 relative to the quay wall.
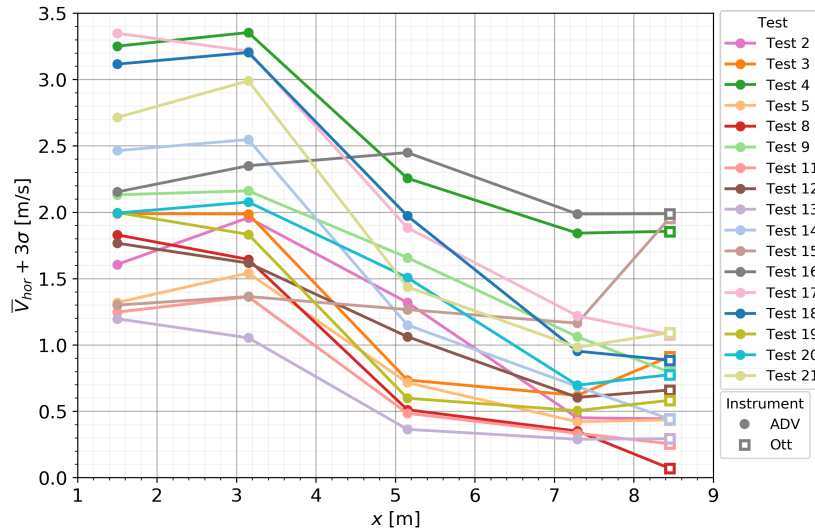
Figure 5.14: Maximum horizontal flow velocity ($V_{max} = \overline{V}_{hor} + 3\sigma_{hor}$) for the moored measurement tests at 90% power. With on the x-axis the x-coordinate of ADV1-4 and Ott2 relative to the quay wall.

In Figure 5.15 $V_{max} = \overline{V}_{hor} + 3\sigma_{hor}$ is plotted for ADV4 against Ott2 which measured at x = 7.29 m and 8.45 m respectively. Very similar values for V_{max} are measured by ADV4 and Ott2. On average, V_{max} is 0.001 m/s (0.2%) higher for ADV4 than for Ott2. This can be explained by the fact that Ott2 measured higher values for $\overline{V}_{hor}$ while ADV2 measured greater values for σ_{hor} resulting in quite similar average values for V_{max}.
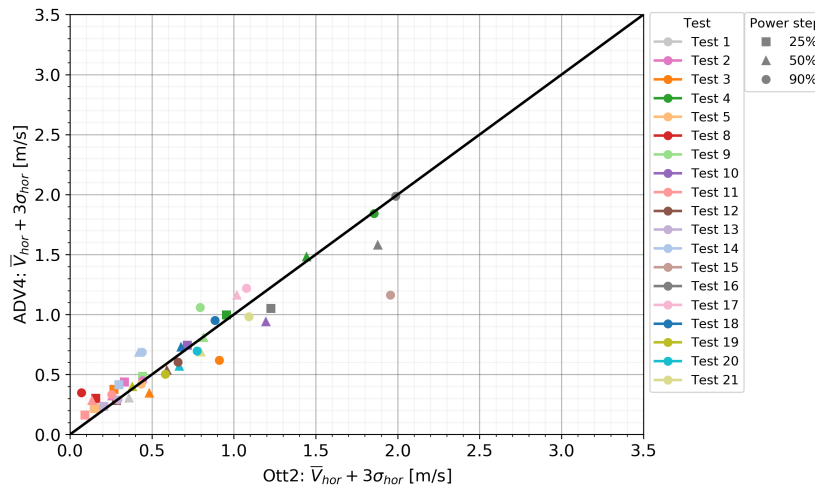
Figure 5.15: Maximum horizontal flow velocity ($V_{max} = \overline{V}_{hor} + 3\sigma_{hor}$) of ADV4 compared to Ott2 for 25%, 50% and 90% power. ADV4 is located at x = 7.29 m while Ott2 is positioned at x = 8.45 from the quay wall. In black, the line x=y is plotted.

In Table 5.8 an overview for the maximum horizontal flow velocity (V_{max}) averaged over all the measurement tests per measurement point and power step is given. In Table 5.9 this is determined for the relative maximum horizontal flow velocity (V_{max}/V_0). On average the flow velocity reduces from 0.21 - 0.26 V_0 near the quay wall at 1.40 and 2.94 D_t to 0.07 - 0.09 V_0 at ADV4 and Ott2 (6.81 and 7.90 D_t respectively) reducing on average between 57-73% in maximum horizontal flow velocity while moving from the quay wall towards the last measurement points.

Table 5.8: Overview of the maximum horizontal flow velocity ($V_{max} = \overline{V}_{hor} + 3\sigma$) averaged over all the measurement tests per measurement point and power step.

	ADV1 [m/s] x = 1.50 m	ADV2 [m/s] x = 3.15 m	ADV3 [m/s] x = 5.15 m	ADV4 [m/s] x = 7.29 m	Ott2 [m/s] x = 8.45 m
V_{max} 25%	1.21	1.29	0.68	0.46	0.41
V_{max} 50%	1.99	2.02	1.2	0.72	0.74
V_{max} 90%	2.08	2.13	1.26	0.83	0.85

Table 5.9: Overview of the relative maximum horizontal flow velocity ($V_{max}(= \overline{V}_{hor} + 3\sigma)/V_0$) averaged over all the measurement tests per measurement point and power step.

	ADV1 [-] x/D_t = 1.40	ADV2 [-] x/D_t = 2.94	ADV3 [-] x/D_t = 4.81	ADV4 [-] x/D_t = 6.81	Ott2 [-] x/D_t = 7.90
V_{max}/V_0 25%	0.21	0.23	0.11	0.08	0.07
V_{max}/V_0 50%	0.26	0.26	0.15	0.09	0.09
V_{max}/V_0 90%	0.22	0.23	0.13	0.09	0.09

5.2.4. Relative turbulence intensity

The relative horizontal turbulence intensity is defined as the standard deviation (σ_{hor}) divided by the mean horizontal near-bed flow velocity ($\overline{V}_{hor}$) measured at the same location as σ_{hor} by the measurement instruments as explained in Section 2.4 and calculated according to Equation 5.4. In Figure 5.16, Figure 5.17 and Figure 5.17 the relative turbulence intensity (r_{hor}) is plotted for ADV1-4 at 25%, 50% and 90% power respectively. The Ott meters measure with an irregular and much lower sampling frequency than the ADVs. As observed in Figure 5.10, σ_{hor} is not measured accurately by Ott1 in the highly turbulent region close to the quay wall. Ott2 measures on average 11.5% lower values for σ_{hor} than ADV2 while measuring on average 12% higher values for $\overline{V}_{hor}$ than ADV4. Due to Ott2 being influenced by the bow thruster inlets drawing in water. Therefore, the values for r_{hor} are not considered trustworthy for the Ott meters leaving them out of the comparison of r_{hor}. The most constant representation for r_{hor} is observed for 50% power where for ADV1-4 r_{hor} ranges between 0.3 and 0.6 while most of the tests have constant values for r_{hor} moving further from the quay wall in x-direction. For 25% power, a similar pattern is observed although the spreading of r_{hor} is increased and there are a few tests for ADV1-4 (Test 2, 4, 13 and 11) that fall outside the 0.3 - 0.6 range for r_{hor}. The most deviating and non constant values for r_{hor} are found at 90% power. Especially between ADV3 and ADV4 where several tests show a rapid increase in r_{hor}. Overall, the range of r_{hor} between 0.3 - 0.6 gives a good representation of the relative turbulence intensities measured for the horizontal near-bed flow velocity for ADV1-4. Complying well with literature (Section 2.4) indicating relative turbulence intensities ranging between 0.25 - 0.6. The measured average relative turbulence intensities from Table 5.10 result in a calculation value for the maximum horizontal near-bed flow velocities (maximum hydraulic load) between 2.2 - 2.41 times the mean horizontal flow velocity according to Equation 5.5. Looking from a design perspective, the highest measured value for r_{hor} measured at the highest power step of 90% is approximately 0.7 resulting in a calculation value for the maximum horizontal flow velocities of 3.1 times the mean flow velocity respectively.

$$r = \frac{\sqrt{V'^2}}{\overline{V}} = \frac{\sigma}{\overline{V}} \tag{5.4}$$

$$V_{\max} = \overline{V} + 3\sigma \approx (1 + 3r)\overline{V} \tag{5.5}$$
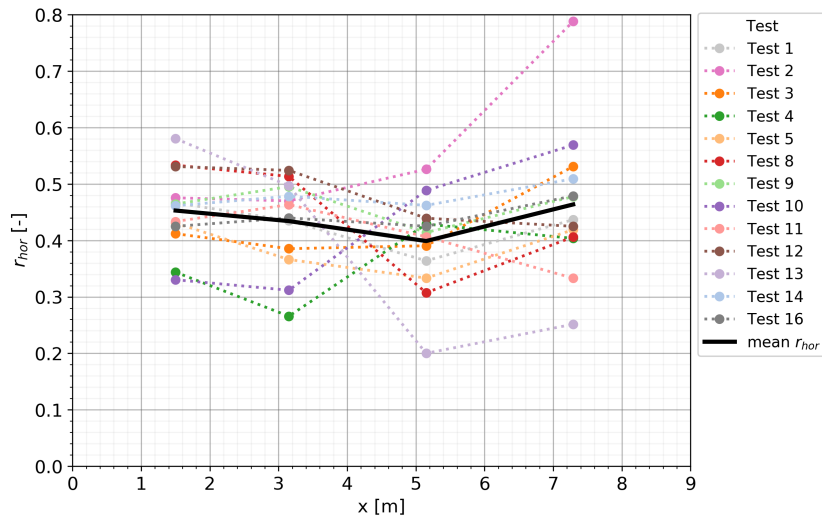
Figure 5.16: Relative turbulence intensity (r_{hor}) of the horizontal flow velocity for the moored measurement tests at 25% power. With on the x-axis the x-coordinate of ADV1-4 with respect to the quay wall. In black, the mean value for r_{hor} is plotted.
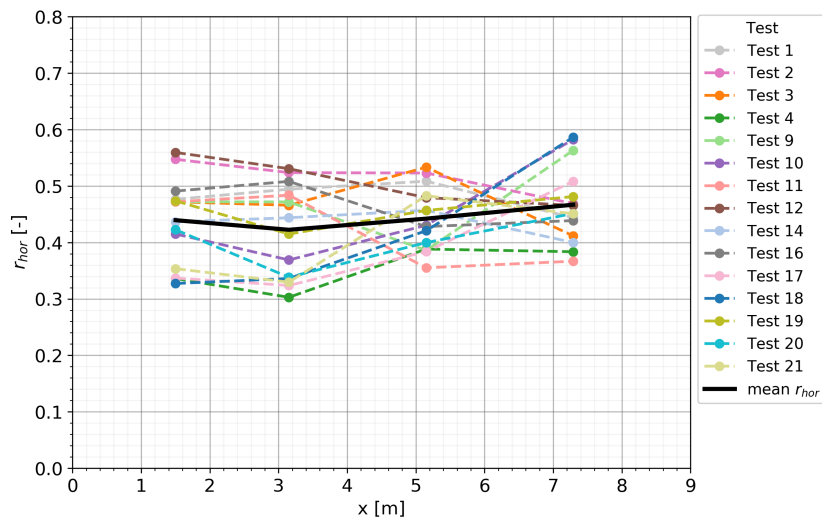

Figure 5.17: Relative turbulence intensity (r_{hor}) of the horizontal flow velocity for the moored measurement tests at 50% power. With on the x-axis the x-coordinate of ADV1-4 with respect to the quay wall. In black, the mean value for r_{hor} is plotted.
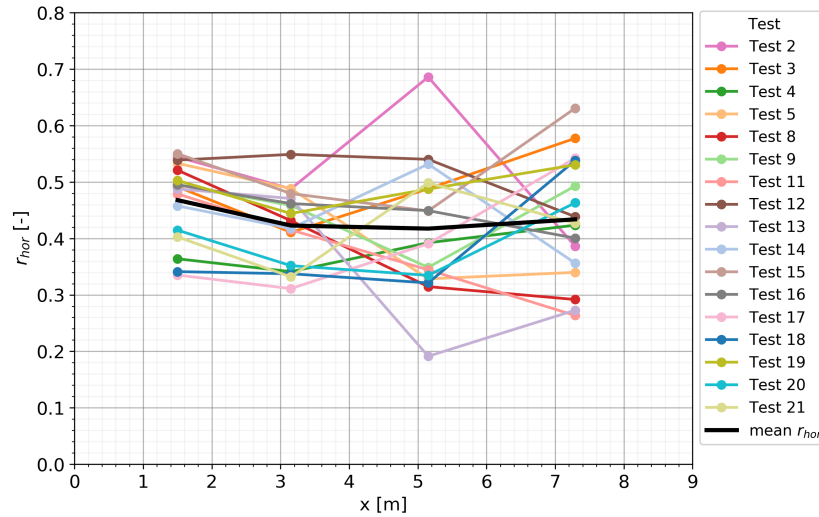
Figure 5.18: Relative turbulence intensity (r_{hor}) of the horizontal flow velocity for the moored measurement tests at 90% power. With on the x-axis the x-coordinate of ADV1-4 with respect to the quay wall. In black, the mean value for r_{hor} is plotted.

In Table 5.10 the average values for the relative horizontal turbulence intensity (r_{hor}) are listed per measurement instrument and power step. The ADVs show constant values for r_{hor} ranging between 0.42 - 0.47 for every power step falling in the middle of the observed range for r_{hor} of 0.3-0.6 resulting in a an average calculation value for the maximum flow velocity of 2.3 times the mean horizontal flow velocity according to Equation 5.5.

Table 5.10: Overview of the average relative turbulence intensity (r_{hor}) for the horizontal flow velocity determined over all the tests per measurement point and power step.

	ADV1 [m/s] x = 1.50 m	ADV2 [m/s] x = 3.15 m	ADV3 [m/s] x = 5.15 m	ADV4 [m/s] x = 7.29 m
r_{hor} 25%	0.45	0.43	0.4	0.46
r_{hor} 50%	0.44	0.42	0.44	0.47
r_{hor} 90%	0.47	0.42	0.42	0.43

5.3. Distance y_t between bow thruster axis and instruments

The Somtrans XXV is moved during the tests along the quay wall with respect to the measurement frame in positive and negative y-direction creating extra spatial measurement points together forming a larger measurement grid (Section 3.6.3) to analyse the decay in flow velocities in both x- and y-direction. In this way, the maximum flow velocities of the reflected jet that occur further away from the bow thruster axis are captured that could have been missed when only measuring at one position underneath the bow thruster axis in x-direction. In addition, the distance between the bow thruster axis and the instruments (y_t) where the highest values for the maximum horizontal flow velocity load (V_{max}) is measured can be determined which is not necessarily directly underneath the bow thruster axis. Where y_t (illustrated in Figure 5.1) is defined as the distance between the considered bow thruster axis and the center line of the horizontal measurement frame. The matrix of measurement points created by moving the vessel in y-direction with respect to the measurement frame is illustrated in Figure 5.19, 5.22 and 5.25 for BT1, BT2 and BT1&2 respectively. The impact of y_t is elaborated in this Section for BT1, BT2 and when BT1&2 are activated simultaneously. In the last situation, for BT1&2, the axis of the bow thruster is defined as the center line between BT1 and BT2. During the tests for y_t the Somtrans XXV was moored to the quay wall with L = 0.8 m resulting in a quay wall clearance in L_{BT1} = 5.61 m, L_{BT2} = 3.09 m and $L_{BT1\&2}$ = 4.35 m.

5.3.1. Bow thruster 1 (BT1)

For BT1 the flow velocities are measured at y_t = 2 m, y_t = 0 m, y_t = -1.5 m and y_t = -3.5 m between the center line of the measurement instruments and the axis of BT1 as illustrated in Figure 5.19. The results for the maximum flow velocity (V_{max}) are illustrated in Figure 5.20 for the three power steps of 25%, 50% and 90%. Focusing on the general decay in x-direction, the lowest flow velocities are measured for y_t = 2 m increasing in flow velocities for y_t = 0 m when the instruments were directly underneath the bow thruster axis. For y_t = -3.5 m, overall higher flow velocities are measured than for y_t = 0, however, at ADV3 y_t = -3.5 shows lower values than for y_t = 0. The highest flow velocities are measured for y_t = -1.5 m (Test 9) at every measurement point except Ott2, which shows a similar but slightly lower value for V_{max} than observed for y_t = -3.5 (Test 3). For y_t = -1.5 m (Test 9) a constant decrease in flow velocity while moving in x-direction from the quay wall is observed. When considering the highest values per measurement instrument in y-direction, ADV1-4 measured the highest velocities for y_t = -1.5 m (Test 9) while for Ott2 the highest value is measured for y_t = -3.5 m (Test 3). Therefore, it can be concluded that for BT1 the highest flow velocities have the tendency to be located towards the stern of the vessel in negative y-direction.
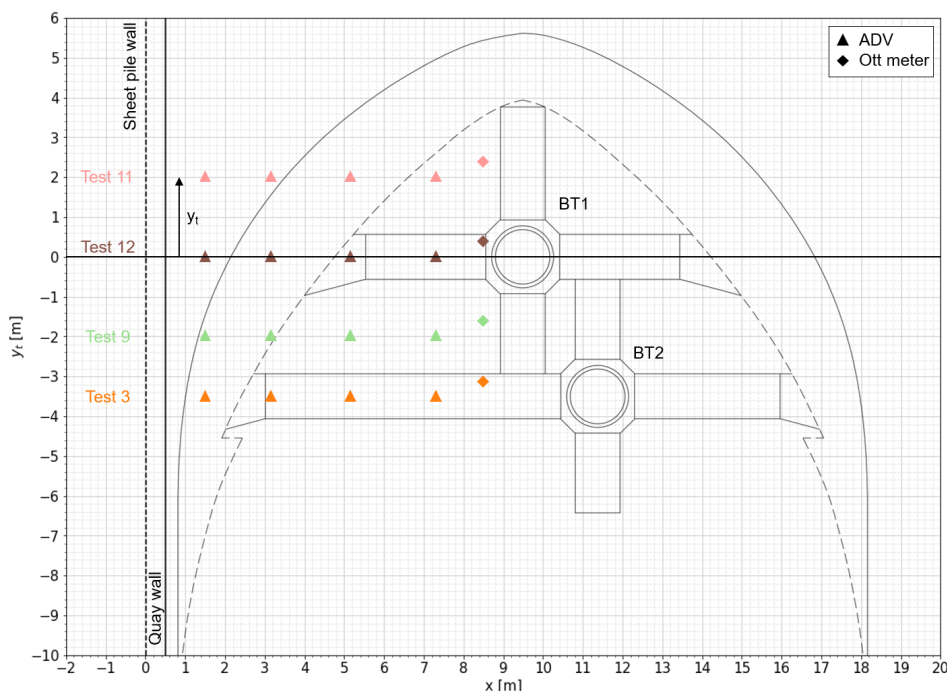
Figure 5.19: Measurement point matrix for ADV1-4 and Ott2 created by moving the vessel in y-direction along the quay wall with respect to the measurement frame. The vessel was moved to y_t = 2 m (Test 11), y_t = 0 m (Test 12), y_t = -1.5 m (Test 9) and y_t = -3.5 m (Test 3) in respect to the axis of BT1.
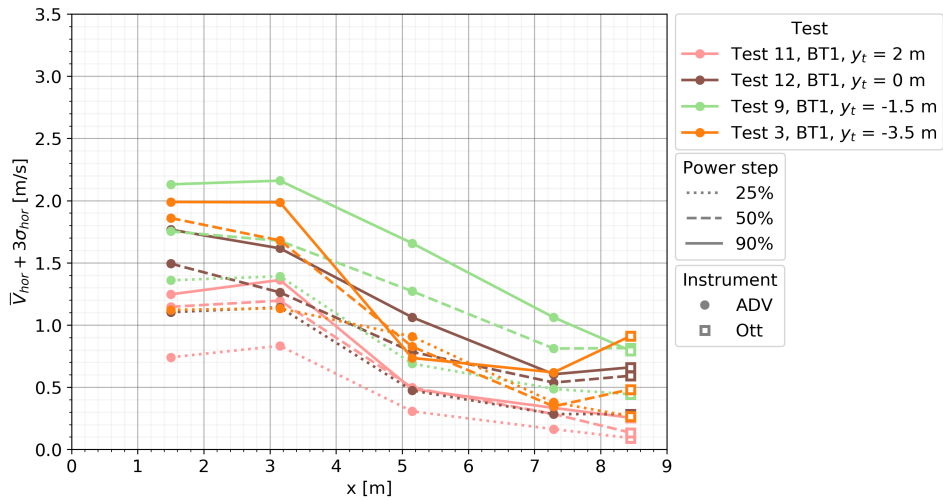
Figure 5.20: Maximum horizontal flow velocity ($V_{max} = \overline{V}_{hor} + 3\sigma$) illustrated for y_t = 2 m, y_t = 0 m, y_t = -2 m and y_t = -3.5 m at 25%, 50% and 90% power. During the tests the Somtrans XXV was moored to the quay wall with L = 0.8 m.

In Figure 5.21 the results for BT1 are visualised by dividing the maximum horizontal flow velocity (V_{max}) by the theoretical efflux velocity (V_0) corresponding to BT1 for 25%, 50% and 90% power as listed in Table 5.4. The x-coordinates of the measurement instruments are divided by the bow thruster diameter (D_t = 1.07 m) of a single bow thruster resulting in a dimensionless y- and x-axis. In this way, the relative near-bed velocities are presented as proportion of the theoretical efflux velocity V_0, giving a measure for the decay in flow velocity between the moment the jet exits the bow thruster outlet to the point when the jet is measured near the bed. In addition, the power steps can be compared with each other based on the relative decrease in flow velocity instead of the absolute value for the flow velocity near the bed. For BT1, the relative flow velocities of the different power steps correspond well with each other for y_t = -1.5 m (Test 9) and y_t = 0 m (Test 12) at 50% and 90% power while for y_t = 2 m (Test 11) the 25% and 90% power step correspond well. The highest measured flow velocities range between 0.15 - 0.30 V_0 decreasing to 0.02 - 0.13 V_0 around 7-8 D_t from the quay wall at ADV4 and Ott2. The highest relative flow velocities at every measurement point are measured for y_t = -1.5 m (Test 9) with the exception of ADV1 at which for y_t = -3.5 m (Test 3), during 50% power, slightly higher values for V_{max}/V_0 are observed. Therefore, for BT1 no indications are observed that the highest relative flow velocities at the bed are located under an a large angle with the quay wall as in that situation higher values for V_{max} are expected at ADV3, ADV4 or Ott2 for greater values of y_t than the current observed maximum at y_t = 1.5 m.
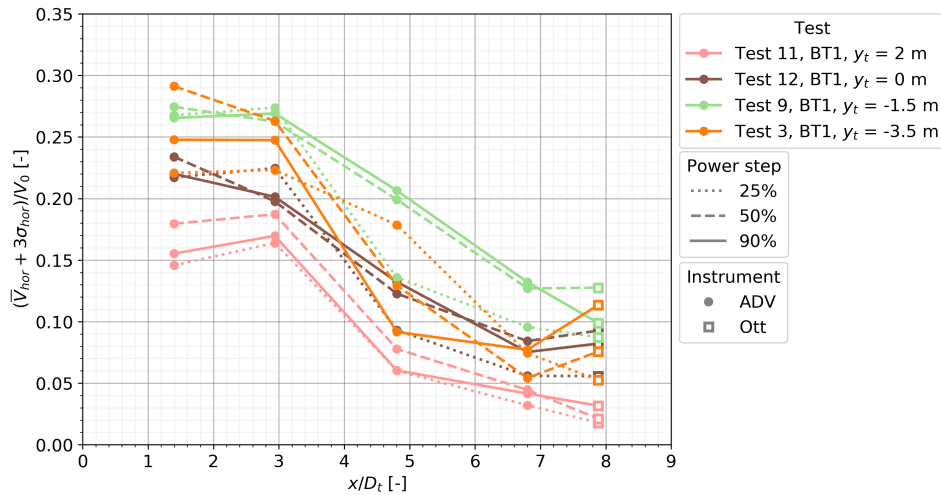
Figure 5.21: Dimensionless plot of the maximum horizontal flow velocity ($V_{max}(= \overline{V}_{hor} + 3\sigma)/V_0$) for y_t = 2 m, y_t = 0 m, y_t = -2 m and y_t = -3.5 m at 25%, 50% and 90% power. During the tests the Somtrans XXV was moored to the quay wall with L = 0.8 m resulting in a quay wall clearance for BT1 of L_{BT1} = 5.61 m.

5.3.2. Bow thruster 2 (BT2)

For BT2 the flow velocities are measured at y_t = 3.5 m, y_t = 2 m, y_t = 0 m and y_t = -2 m with respect to the axis of BT2 as illustrated in Figure 5.25. The resulting maximum horizontal flow velocities are plotted in Figure 5.23 for 25%, 50% and 90% power. Focusing on the general decay in x-direction, overall the lowest velocities are measured for y_t = 3.5 m followed by y_t = 2 m while the highest flow velocities are measured for y_t = 0. During the measurements of y_t = -2 m (Test 15) a rather constant flow velocity level is observed for ADV1-4 while increasing to the highest measured flow velocity at Ott2. The flow decay pattern for y_t = -2 m is completely different from the other tests with relatively low measured flow velocities at ADV1 and ADV2 while measuring relatively high flow velocities at ADV3, ADV4 and Ott2 compared with the other tests. Analyzing the highest values observed per measurement instrument in y-direction not a clear pattern is observed. At ADV1 the absolute highest flow velocities are measured for y_t = 2 m (Test 8) while for ADV2 and ADV3 the highest values are observed for y_t = 0 m (Test 2) after which at ADV4 and Ott2 the highest values are measured for y_t = -2 m (Test 15). Therefore, close to the quay the highest flow velocities are located in the direction of the bow (positive y-direction) while moving further from the quay in x-direction the highest flow velocities are located in the direction of the stern (negative y-direction).
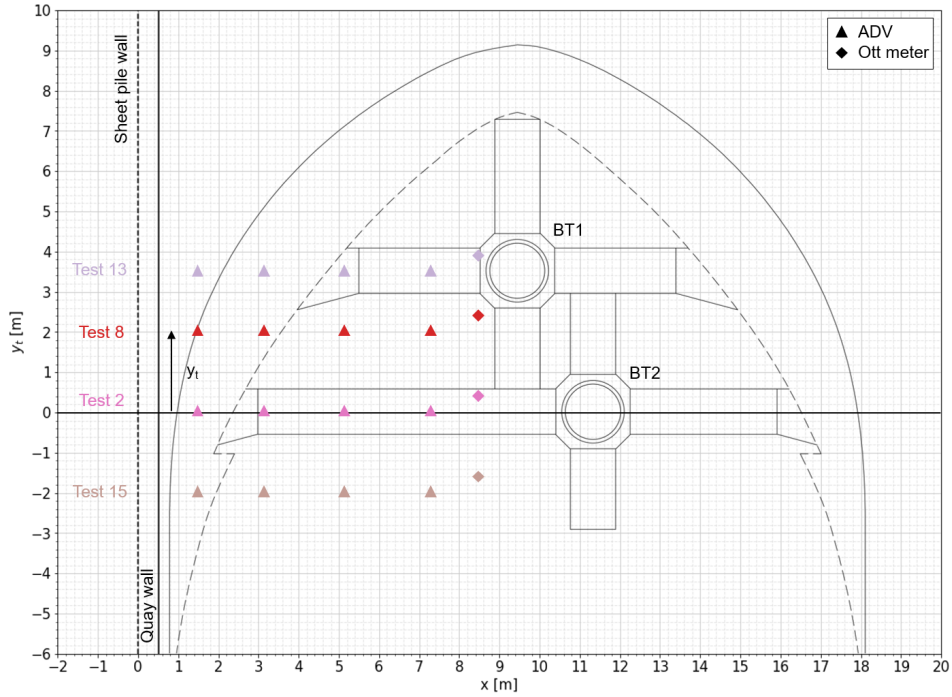
Figure 5.22: Measurement point matrix for ADV1-4 and Ott2 created by moving the vessel in y-direction along the quay wall with respect to the measurement frame. The vessel was moved to y_t = 3.5 m (Test 13), y_t = 2 m (Test 8), y_t = 0 m (Test 2) and y_t = -2 m (Test 15) in respect to the axis of BT2.
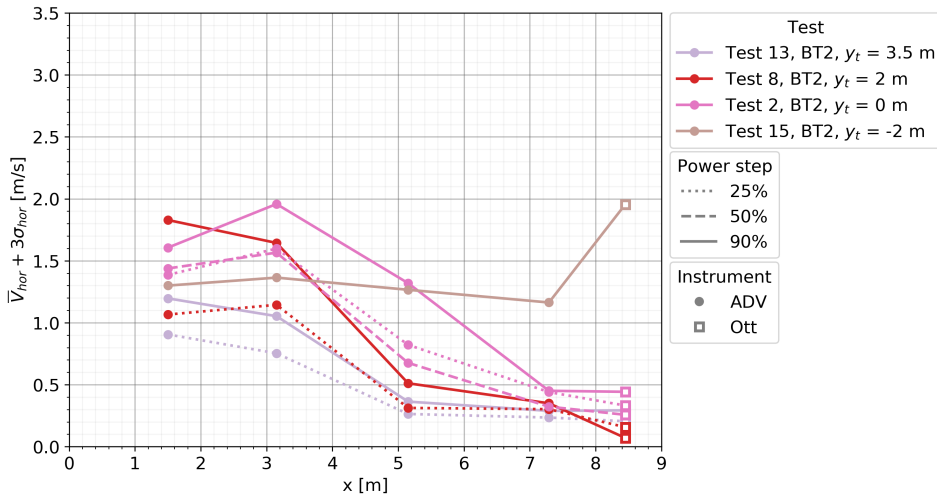
Figure 5.23: Maximum horizontal flow velocity ($V_{max} = \overline{V}_{hor} + 3\sigma$) for y_t = 3.5 m, y_t = 2 m, y_t = 0 m and y_t = -2 m at 25%, 50% and 90% power. During the tests the Somtrans XXV was moored to the quay wall with L = 0.8 m resulting in a quay wall clearance for BT2 of L_{BT2} = 3.09 m.

In Figure 5.24 the maximum relative horizontal flow velocity (V_{max}/V_0) plotted against x/D_t where D_t(=1.07 m) is the diameter of a single bow thruster. For y_t = 3.5 m and y_t = 2 m the 25% and 90% power step approach each other well while for y_t = 0 the 25% power step reaches values of 0.32 V_0, much higher than the other power steps and tests with different values for y_t. No comparison can be made for y_t = -2 m between the power steps as only the 90% power step had trustworthy data according to the pre-processing steps from Chapter 4. The highest measured flow velocities range between 0.15 - 0.25 V_0 for most tests with the exception of y_t = 0 at 25% power reaching values of 0.32 V_0. Moving in x-direction from the quay, velocities decrease to 0.01 - 0.07 V_0 with the exception of y_t = -2 m (Test 15)

showing rather high flow velocities at ADV4 and Ott2 of approximately 0.15 and 0.25 V_0 respectively.
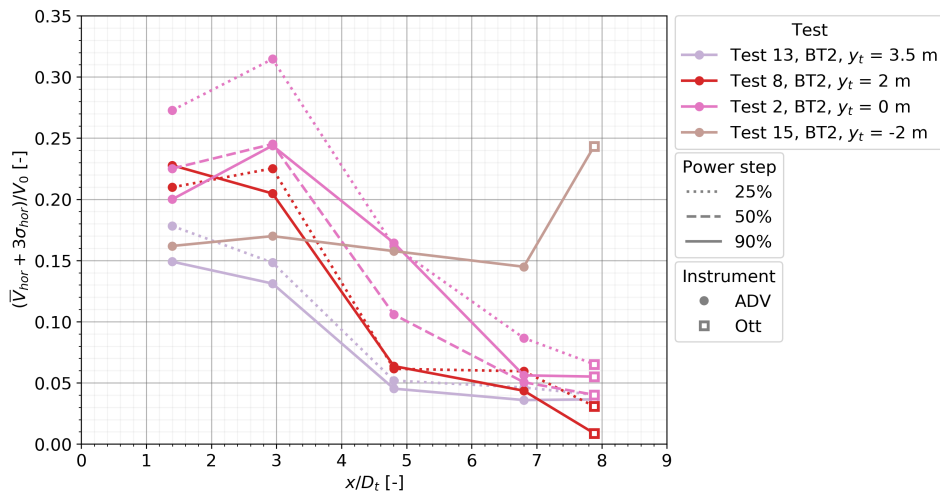
Figure 5.24: Relative maximum horizontal flow velocity ($V_{max}(= \overline{V}_{hor} + 3\sigma)/V_0$) plotted against x/D_t for y_t = 3.5 m, y_t = 2 m, y_t = 0 m and y_t = -2 m at 25%, 50% and 90% power. During the tests the Somtrans XXV was moored to the quay wall with L = 0.8 m.

5.3.3. Bow thruster 1&2 (BT1&2)

For BT1&2 activated simultaneously, the flow velocities are measured at y_t = 1.75 m, y_t = 0 m, y_t = -1.75 m and y_t = -3.75 m with respect to the axis of BT1&2 as illustrated in Figure 5.25. The axis of the bow thruster for BT1&2 from which y_t is measured is defined in the center between BT1 and BT2. The resulting maximum horizontal flow velocities are plotted in Figure 5.23 for 25%, 50% and 90% power. Overall, the lowest flow velocities are measured for y_t = 1.75 m followed by y_t = 0 m while the highest flow velocities are measured for y_t = -1.75 m. Test 16 at y_t = -3.75 m shows a different decay pattern than the other tests with the lowest measured values of all the tests at ADV1 and ADV2 while moving in x-direction from the quay the flow velocities increase towards ADV3 leading to the highest measured flow velocities of all the tests at ADV3, ADV4 and Ott2. Altough, for these position the values are comparable to he results of y_t = -1.75 m (Test 4). This decay pattern or rather constant looking flow pattern for increasing values of x is similar to the observations of Test 15 y_t = -2 m for BT2. Concentrating on the highest measured values for V_{max} in y-direction per measurement instrument, at ADV1 the highest values are measured for y_t = 0 m (Test 17) just above the values for y_t = -1.75 m (Test 4). At ADV2 for y_t = -1.75 m (Test 4) the highest flow velocities are measured while moving in x-direction from the quay towards ADV3, ADV4 and Ott2 at y_t = -3.75 m (Test 16) the highest flow velocities are measured closely follow by y_t = -1.75 m (Test 4). Therefore, the highest flow velocities induced by BT1&2 are also located towards the stern in negative y-direction.
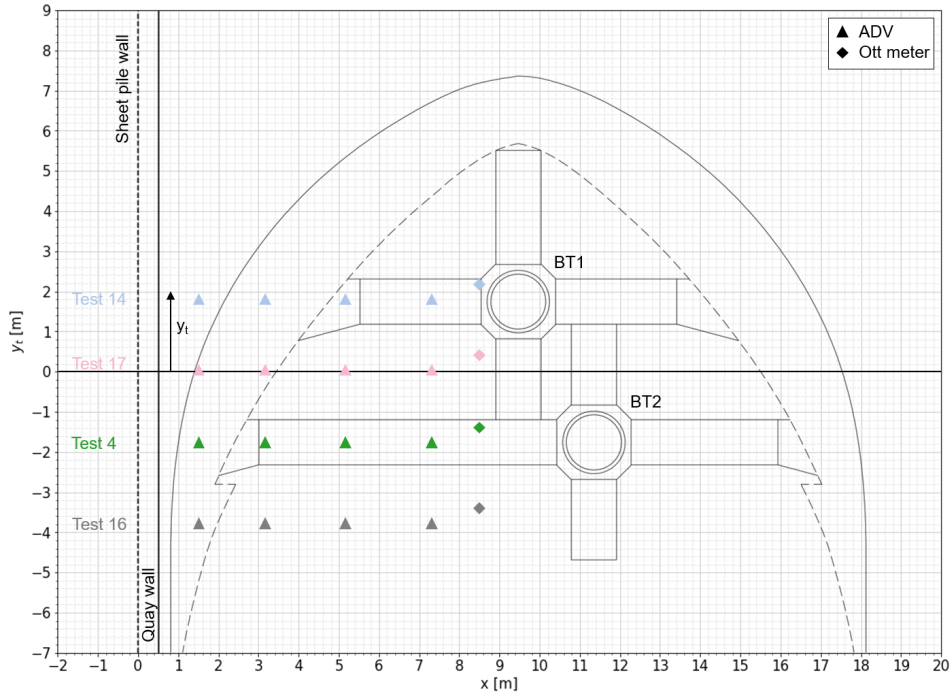
Figure 5.25: Measurement point matrix for ADV1-4 and Ott2 created by moving the vessel in y-direction along the quay wall with respect to the measurement frame. The vessel was moved to y_t = 1.75 m (Test 14), y_t = 0 m (Test 17), y_t = -1.75 m (Test 4) and y_t = -3.75 m (Test 16) in respect to the axis of BT1&2 defined in between BT1 and BT2.
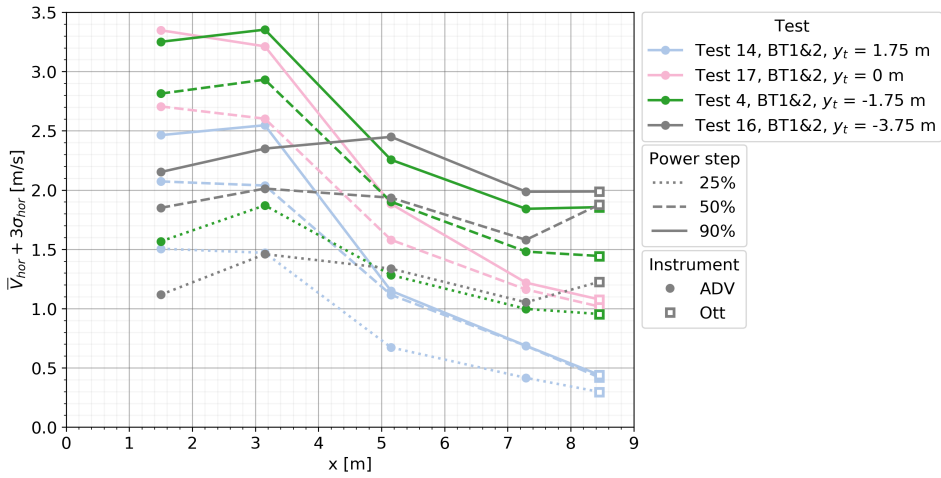
Figure 5.26: Maximum horizontal flow velocity ($V_{max} = \overline{V}_{hor} + 3\sigma$) for y_t = 1.75 m, y_t = 0 m, y_t = -1.75 m and y_t = -3.75 m at 25%, 50% and 90% power. During the tests the Somtrans XXV was moored to the quay wall with L = 0.8 m resulting in a quay wall clearance for BT1&2 of $L_{BT1\&2}$ = 4.35 m.

In Figure 5.27 the maximum relative horizontal flow velocity is plotted against x/D_t. For y_t = 1.75 m, the 25%, 50% and 90% power step comply well with each other along with y_t = 0, y_t = -1.75 and y_t = -3.75 for 50% and 90% power. The highest measured flow velocities close to the quay range between 0.15 - 0.33 V_0 decreasing to 0.04 - 0.21 V_0 further away from the quay at Ott2. Overall, the flow velocities induced by BT1&2 result in higher flow velocities close to the quay wall and further away from the quay at Ott2 compared to BT1 and BT2. This is expected for the absolute values for the flow velocities but is surprisingly also observed in Figure 5.27 for the relative values of the maximum horizontal flow velocity.
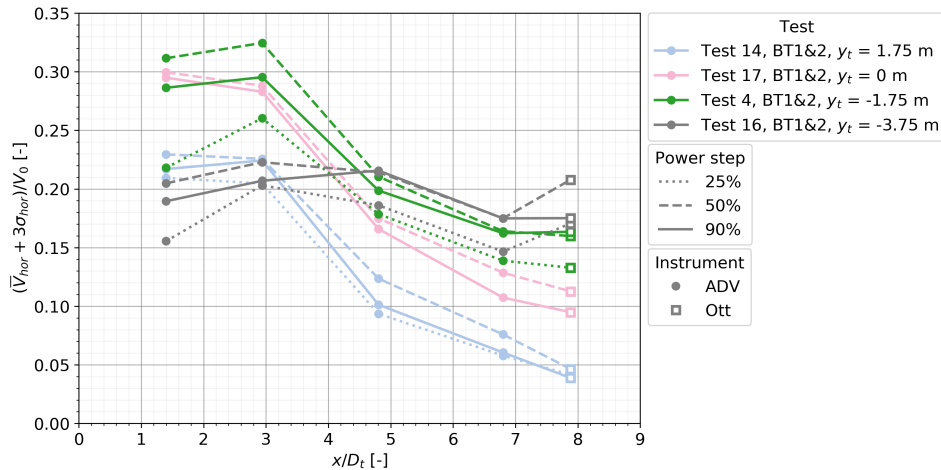
Figure 5.27: Relative maximum horizontal flow velocity ($V_{max}(= \overline{V}_{hor} + 3\sigma)/V_0$) for y_t = 1.75 m, y_t = 0 m, y_t = -1.75 m and y_t = -3.75 m at 25%, 50% and 90% power. During the tests the Somtrans XXV was moored to the quay wall with L = 0.8 m.

5.4. Use of different bow thrusters

The influence of using either BT1 or BT2 is researched in this section by plotting the maximum horizontal flow velocity (V_{max}) for the different tests were the quay wall clearance of the Somtrans XXV (L) equals 0.8 m. Similar to the previous section, the measurements of Ott1 are left out of the visualizations. For BT1, the tests were y_t = 2 m, y_t = 0 m and y_t = -1.5 m are illustrated and compared with BT2 for the tests were y_t = 2 m, y_t = 0 m and y_t = -2 m (Figure 5.28). BT1 and BT2 differ from each other in two ways, first of all the quay wall clearance of BT1 (L_{BT1} = 5.61 m) is larger than of BT2 (L_{BT2} = 3.09 m) for the moored position at the quay with L = 0.8 m. The second difference is the shorter channel length of BT1 (3.94 m) compared to BT2 (8.34 m) as illustrated in Figure 3.5. For both y_t = 2 m and y_t = 0 m, BT2 induces higher flow velocities than BT1. However, comparing y_t = -1.5 m (BT1) and y_t = -2 m (BT2) the flow velocities measured by ADV1-3 are much larger for BT1 than for BT2, this changes around ADV4 when the flow velocities for BT2 become much larger at Ott2. Although it has to be noted that this comparison between BT1 and BT2 is not completely correct as y_t differs with 0.5 m. The relative maximum horizontal flow velocities for the power steps correspond well with each other with the exception of Test 2 BT2 with y_t = 0 m and Test 8 BT2 with y_t = 2 m (Figure Figure 5.29). For 25% power, Test 2 shows a much higher relative flow velocity at ADV2 in comparison to the other tests. The highest measured relative flow velocities close to the quay range between 0.14 - 0.25 V_0 with the exception of Test 2 (BT2 y_t= 0 m) at 50% power with a flow velocity of 0.32 V_0. The lowest relative flow velocities are measured at ADV4 and Ott2 around 7-8 D_t from the quay varying between 0.01 - 0.10 V_0. An exception to this is Test 15 (BT2 y_t= -2 m) for which a value of 0.24 V_0 is observed. To conclude, based on these measurement tests discussed in this section neither BT1 or BT2 consistently induces higher flow velocities than the other bow thruster. Therefore, in the next section the effect of the quay wall clearance of the bow thrusters L_{BT} on V_{max} is analyzed.
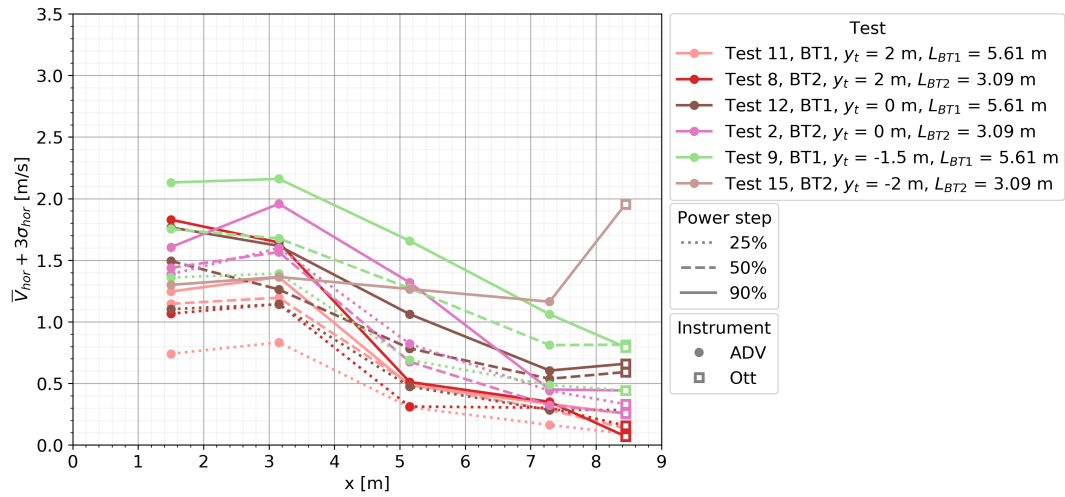
Figure 5.28: Maximum horizontal flow velocity ($V_{max} = \overline{V}_{hor} + 3\sigma$) for BT1 and BT2 with y_t = 0 m and y_t = 2 m at 25%, 50% and 90% power. During the tests the Somtrans XXV was moored to the quay wall with L = 0.8 m.
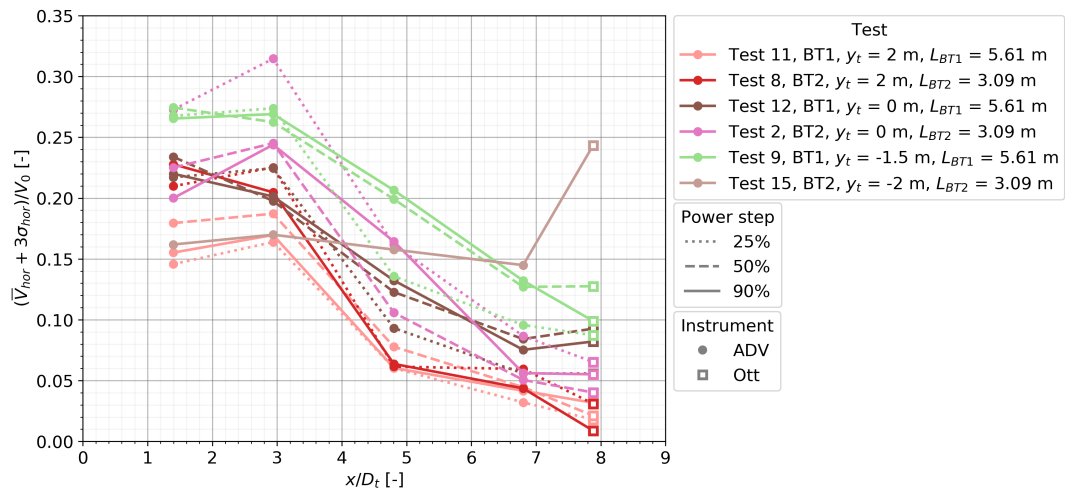
Figure 5.29: Relative maximum horizontal flow velocity ($V_{max}(= \overline{V}_{hor} + 3\sigma)/V_0$) for BT1 and BT2 with y_t = 0 m and y_t = 2 m at 25%, 50% and 90% power. During the tests the Somtrans XXV was moored to the quay wall with L = 0.8 m.

5.5. Quay wall clearance

The influence of the quay wall clearances on $V_{max} = \overline{V}_{hor} + 3\sigma_{hor}$ is studied by increasing the quay wall clearance of the Somtrans XXV from L = 0.8 m to L = 3 m for BT1, BT2 and BT1&2. In addition, the quay wall clearance of the Somtrans XXV (L) is increased from L = 3 m to L = 5 m for BT1&2. During the tests with an increased quay wall clearance of L = 3 m and L = 5 m the instruments were aligned between BT1 and BT2 resulting in a small discrepancy in y_t of 0.25 m for the measurements of BT1 and BT2 compared to the tests with a quay wall clearance of L = 0.8 m. For the visualizations in this section the measurement results of Ott1 are excluded from the plots as Ott1 did not measure σ_{hor} accurately. However, they can be observed in the general results in Section 5.2 for each of the moored tests.

5.5.1. Quay wall clearance L = 0.8 m and L = 3 m
In Figure 5.30 the maximum horizontal flow velocity (V_{max}) is plotted for BT1, BT2 and BT1&2 at L = 0.8 m and L = 3 m. For BT1 the measured flow velocities for the two quay wall clearances are very similar both in value as in decay profile. At 50% power the flow velocities measured by ADV1 and ADV2 for L

= 3 m are higher than for L = 0.8 m turning around after ADV3 when the flow velocities for L = 0.8 m are larger than those for L = 3 m. For 90% power the measured flow velocities for L = 0.8 m are higher for every distance x from the quay wall. For BT2, the flow velocities for L = 0.8 and L = 3 m closely resemble each other as well, although slightly higher flow velocities are measured at L = 3 m than at L = 0.8 m. At 50% power, L = 3 m corresponds well with the 90% power step of L = 0.8 m. Activating BT1&2 simultaneously results in almost indistinguishable flow velocity measurements for L = 0.8 and L = 3 m at both 50% and 90% power.
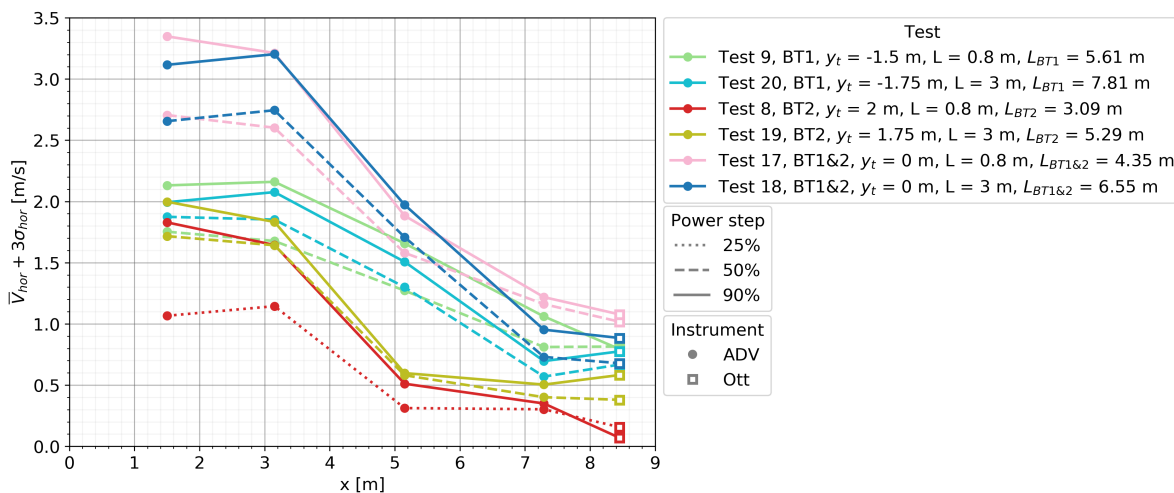
Figure 5.30: Maximum horizontal flow velocity ($V_{max} = \overline{V}_{hor} + 3\sigma$) for BT1, BT2 and BT1&2 at a quay wall clearance of L = 0.8 m (Test 9, 8 and 17) and L = 3 m (Test 20, 19, and 18) at 25%, 50% and 90% power.

In Figure 5.31 the relative maximum horizontal flow velocities are presented by dividing by V_0 corresponding to the use of either one bow thruster (BT1 or BT2) or two bow thruster (BT1&2). The relative maximum horizontal flow velocities of BT1 and BT1&2 comply well together for the power steps of 50% and 90% with a comparable slope from ADV2 to ADV4. For BT2 lower relative flow velocities are observed. The shape of the decay profile for BT2 is corresponding to the general observations in Section 5.2 for the maximum horizontal flow velocity with a steep decline between ADV2 and ADV3 whereas BT1 and BT1&2 show a more constant decline between ADV2 and ADV4. To conclude, increasing the quay wall clearance of the Somtrans XXV from L = 0.8 m to L = 3 m results in slightly lower flow velocities for 90% power for BT1. Focusing on BT2, increasing the quay wall clearance leads to slightly higher flow velocities while for BT1&2 increasing the quay wall clearance has no significant effect.
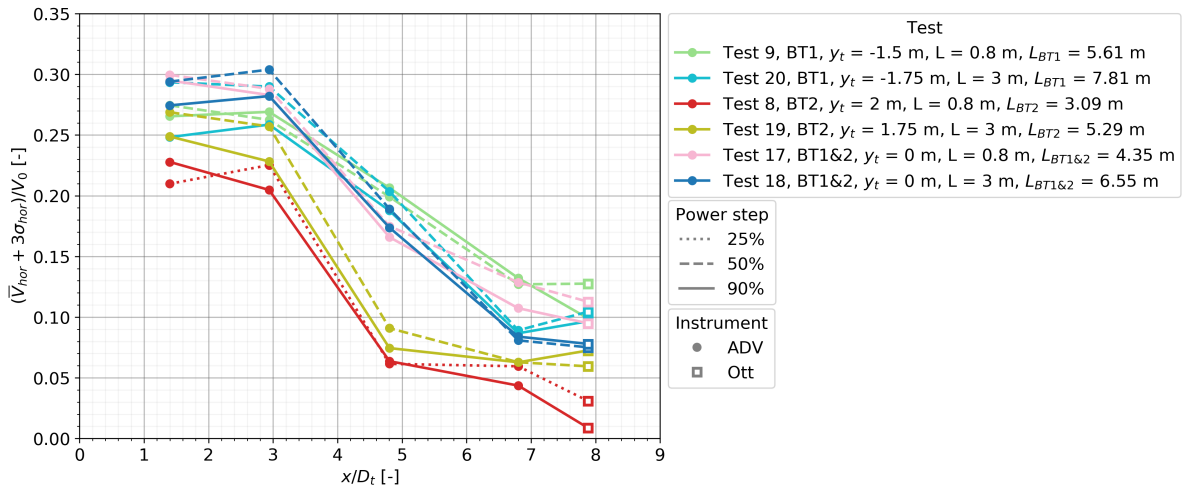
Figure 5.31: Relative maximum horizontal flow velocity ($V_{max}(= \overline{V}_{hor} + 3\sigma)/V_0$) for BT1, BT2 and BT1&2 at a quay wall clearance of L = 0.8 m (Test 9, 8 and 17) and L = 3 m (Test 20, 19, and 18) at 25%, 50% and 90% power.

5.5.2. Quay wall clearance BT1&2: L = 0.8 m, L = 3 m and L = 5 m

In Figure 5.32 the maximum horizontal flow velocity for BT1&2 are plotted for a quay wall clearance of L = 0.8 m, L = 3 m and L = 5 m. Only for BT1&2 simultaneously, the additional quay wall clearance of L = 5 m is measured. As concluded from the previous section, the measurements for L = 0.8 and L = 3 m comply very well with each other between ADV1-3 after which the flow velocities are slightly smaller for ADV4 and Ott2 at L = 3 m. At L = 5 m, the flow velocities are lower for ADV1-3 while at ADV4 similar values are measured for L = 3 m and L = 5 m.
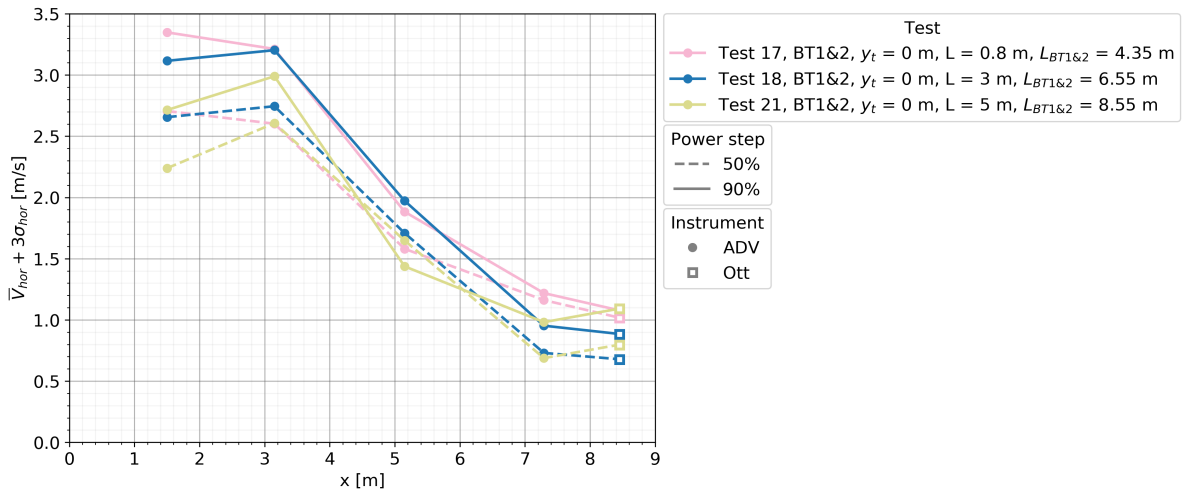
Figure 5.32: Maximum horizontal flow velocity ($V_{max} = \overline{V}_{hor} + 3\sigma$) for BT1&2 at a quay wall clearance of L = 0.8 m (Test 17), L = 3 m (Test 18) and L = 5 m (Test 21) at 50% and 90% power.

In Figure 5.33 the relative maximum horizontal flow velocities are compared for BT1&2. The decay is similar for every power step and quay wall clearance L with the exception of L = 5 m at 90% power which decays faster than the other tests. In Addition, for L = 0.8 m V_{max} at ADV4 is higher than for L = 3 m and L = 5 m while at 50% power V_{max} for Ott2 is larger than during the other quay wall clearances. Therefore, from both Figure 5.32 5.33 can be concluded that increasing the quay wall clearance for BT1&2 from L = 0.8 m to L = 3 m results in slightly lower values for V_{max} at ADV4 and Ott2 while increasing the quay wall clearance to L = 5 m leads to smaller maximum horizontal (V_{max}) flow velocities for the 90% power step.
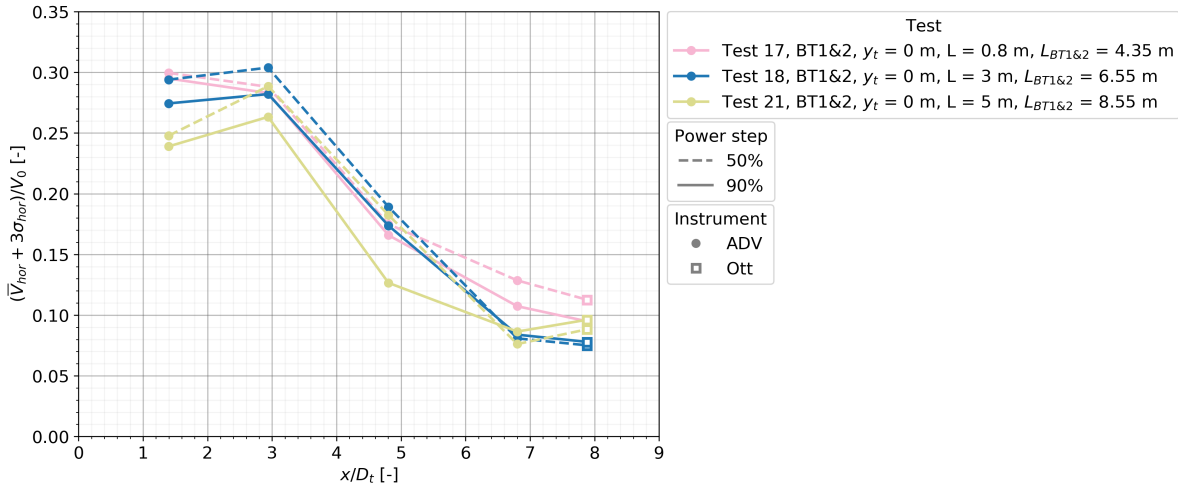
Figure 5.33: Relative maximum horizontal flow velocity ($V_{max}(= \overline{V}_{hor} + 3\sigma)/V_0$) for BT1&2 at a quay wall clearance of L = 0.8 m (Test 17), L = 3 m (Test 18) and L = 5 m (Test 21) at 50% and 90% power.

5.6. Dynamic manoeuvring tests

In this section the dynamic measurements are compared to the moored measurements to analyze the difference between an actual berthing manoeuvre and the simplified setup where the vessel is moored at a fixed position to the quay wall. For the dynamic measurements the maximum horizontal flow velocity ($V_{max,in}$) is defined as the highest instantaneous measured horizontal flow velocity in comparison to $V_{max} = \overline{V}_{hor} + 3\sigma_{hor}$ for the moored tests. This difference is due to the non constant measured flow velocities when the vessel is moving over the measurement instruments. Therefore, using the mean and standard deviation of the dynamic measurements is not possible. For Test 22, when the vessel was performing a berthing manoeuvring test with BT1&2, the results are compared in Figure 5.34 to the moored tests when BT1&2 were activated for L = 0.8 , L = 3 m and L = 5 m. For the berthing test, lower flow velocities are observed for both 50% and 90% power in comparison to the moored tests. However, at 50% power the berthing test (Test 22) shows higher flow velocities at ADV4 and Ott2 than the moored test for L = 3 m (Test 18) at 50% power. In Figure 5.35 the relative flow velocities are presented from which can be observed that the power steps for the berthing test (Test 22) do not comply well both in values as in velocity decay profile. However, the 50% and 90% power steps for Test 22 do correspond well with the moored tests between ADV3 and Ott2 showing a similar decay in flow velocity. Concluding, the moored tests induce higher maximum flow velocities near the bed than the berthing test. Showing that the results for the moored tests are conservative with respect to actual berthing operations.
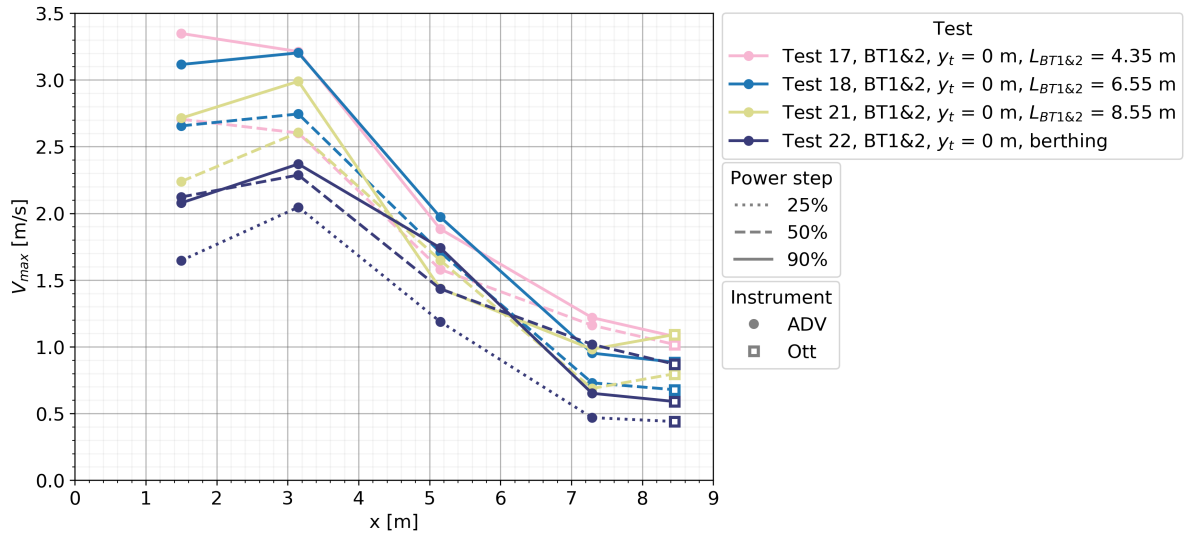
Figure 5.34: Comparison of the berthing manoeuvring test (Test 22) with the corresponding moored tests (Test 17, 18 and 21). The maximum horizontal flow velocity for the moored tests is defined as $V_{max} = \overline{V}_{hor} + 3\sigma$ while for the dynamic tests this is defined as the maximum instantaneous measured horizontal velocity ($V_{max,in}$). The dynamic manoeuvring test with BT1&2 consists out of the 25% 50% and 90% power steps while the moored tests are measured for 50% and 90% power.
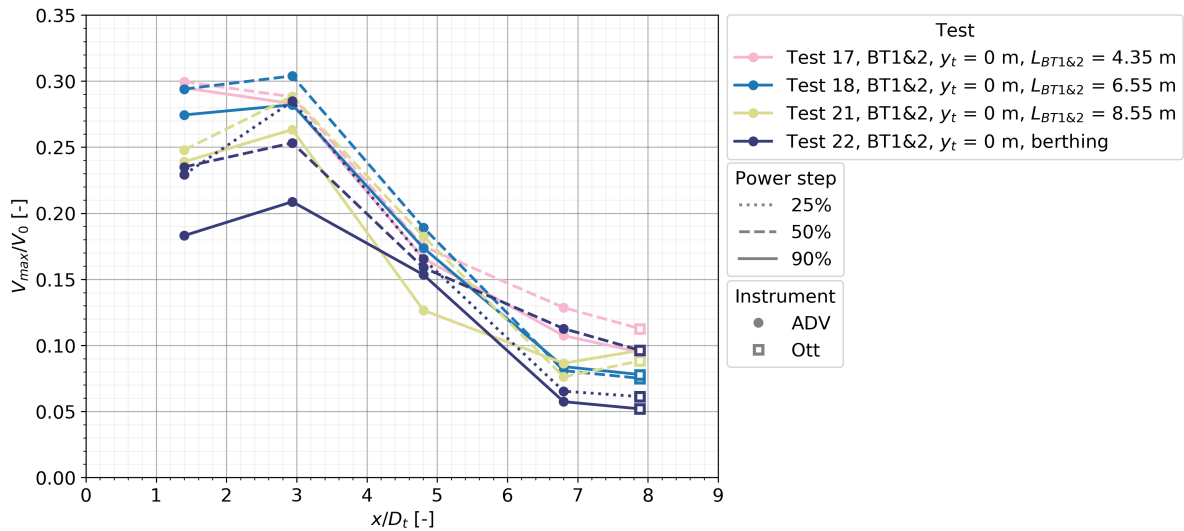
Figure 5.35: Comparison of the relative maximum flow velocities for the berthing maneuvering test (Test 22) with the corresponding moored tests (Test 17, 18 and 21). The maximum horizontal flow velocity for the moored tests is defined as $V_{max}(= \overline{V}_{hor} + 3\sigma)/V_0$ while for the dynamic tests this is defined as the maximum instantaneous measured horizontal velocity ($V_{max,in}/V_0$). The dynamic manoeuvring test with BT1&2 consists out of the 25% 50% and 90% power steps while the moored tests are measured for 50% and 90% power.

In Figure 5.36 the sailing tests, as explained in Section 3.7.1, are plotted for BT1&2 (Test 23) and BT1 (Test 24) for 90% power. While sailing over the instruments a constant flow velocity level is observed for BT1&2 while for BT1 only at ADV2 high flow velocities are measured. The area of the jet that hits the bed is much larger for BT1&2 than for BT1. The maximum flow velocities induced by sailing Test 23 are lower than the berthing and moored tests from Figure 5.34 for BT1&2. However, at ADV4 and Ott2 the measured flow velocities are higher for sailing Test 23. Compared to other moored tests from Figure 5.14, Test 23 has one of the highest measured maximum horizontal flow velocities (V_{max})for ADV4 and Ott2.
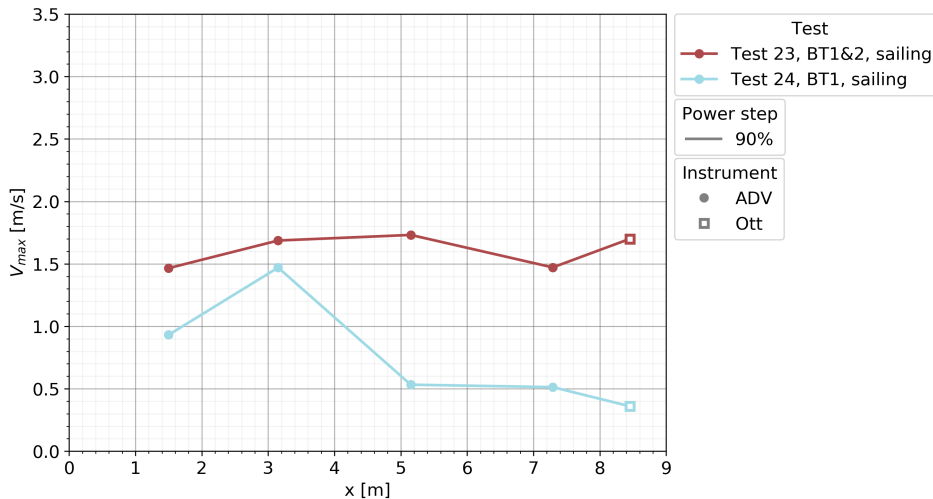
Figure 5.36: Comparison of the sailing tests with BT1&2 simultaneously activated (Test 23) and BT1 (Test 24). The maximum horizontal flow velocity is defined as the maximum instantaneous measured horizontal velocity ($V_{max,in}$). Both tests are performed at 90% power.

5.7. Pressure sensors

For the pressure sensors a comparison between the measured absolute turbulence intensities (standard deviations σ_{pres}) is made for the high frequency pressure sensors (PS1-4) and the ADV pressure sensors (PS7-10). The high frequency pressure sensors are positioned at the vertical measurement frame (Figure 3.29) against the quay wall to measure the pressure fluctuations at the same height as the bow thruster outlet directly in the jet (PS2 and PS3) and at the intersection of the quay wall and the bed (PS1 and PS4). PS2 is located at 3.26 m above the bed while PS3 is positioned at 3.06 m above the bed both at a similar height as the bow thruster outlet measuring the pressure fluctuations of the jet just before it hits the quay wall. PS1 and PS4 are both positioned at 0.2 m above the bed and approximately 1 m from the quay wall in x-direction measuring the pressure fluctuations close to the reflection point of the jet on the bed. PS7-10 (ADV1-4 pressure sensors) are positioned on the horizontal measurement frame placed on the bed. The pressure sensors are positioned at x = 2.59, 5,15 and 7.66 m from the quay wall as illustrated in Figure 3.21. With this setup, the pressure fluctuations of the jet are measured over the vertical quay wall (PS1-4) and over the bed (PS7-10), visualising the total decay in standard deviation σ_{pres} over the distance travelled by the jet. In Section 5.7.1 the standard deviations of all the pressure sensors are plotted together after which in Section 5.7.2 the focus is on the pressure sensors positioned near the bed (PS1, PS4 and PS7-10). The exact values for the standard deviations of all the pressure sensors are listed in Appendix D.6. In addition, it must be noted that during the measurements PS1-4 did not record the pressure fluctuations for Test 3-10 due to a malfunction in the data retrieving system.

5.7.1. Standard deviations of the pressure sensors (PS1-4 and PS7-10)

In Figure 5.37, 5.38 and 5.39 the standard deviations σ_{pres} are plotted for the high frequency pressure sensors (PS1-4) and the ADV pressure sensors (PS7-10) for 25%, 50% and 90% power respectively. On the x-axis, the distance travelled by the jet in meter over the quay wall down towards to bed after which it reflects and continues over the bed is used (x_p) to represent the locations of the pressure sensors over the quay wall and the bed. Starting at PS2, positioned the highest above the bed at z = 3.26 m, which measurement point is defined as x_p = 0 after which the jet moves down over the quay wall (PS3 at x_p = 0.2 m) towards the bed (PS1 and PS4 at x_p = 3.06 m). Continuing over the bed towards PS7 and PS8 positioned at x_p = 4.85 m on the horizontal measurement frame towards PS9 at x_p = 7.41 m and PS10 at x_p = 9.92 m. Therefore, x_p is a measure for the total traveled distance of the jet over the quay wall and bed with the 0 starting point at PS2. At 25% power, PS2 and PS3 measure values for σ_{pres} reaching up to 0.28 m increasing in value for higher power steps towards a maximum of 0.54 m at 50% power and 0.78 m at 90% power. During every power step, the highest

σ_{pres} is measured for Test 2 during which BT2 was activated and the measurement instruments were aligned with BT2 (y_t = 0 m) resulting in a direct impact of the jet on PS2 and PS3. Moving down along the quay wall towards PS1 and PS4 significantly lower values for σ_{pres} are measured decreasing even further while moving in x-direction from the quay over the bed towards PS7-10. Making a comparison between these pressure sensors for σ_{pres} based on Figure 5.37, 5.38 and 5.39 is difficult due to the large difference in σ_{pres}. Therefore, in the next section the pressure sensors positioned near the bed (PS1, PS4 and PS7-10) are considered to further analyse the decay in σ_{pres} over the bed.
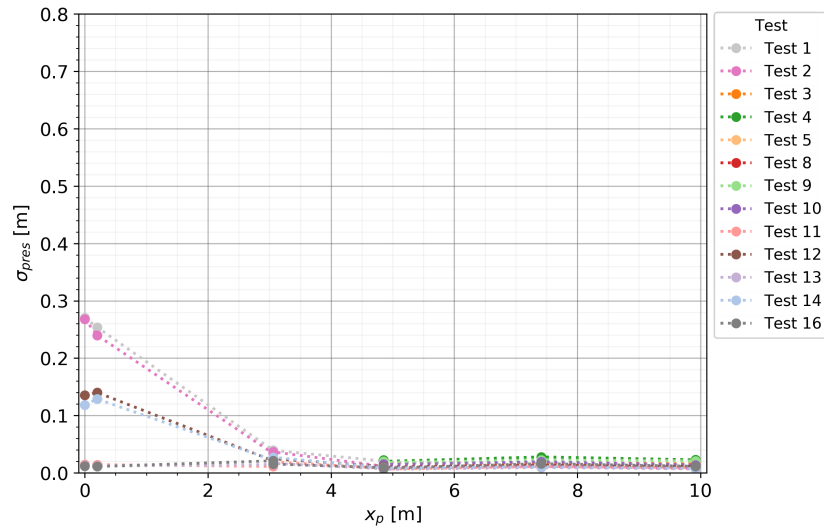
Figure 5.37: Standard deviation (σ_{pres}) plot of the high frequency pressure sensors PS1-4 together with the ADV pressure sensors (PS7-10) for 25% power.
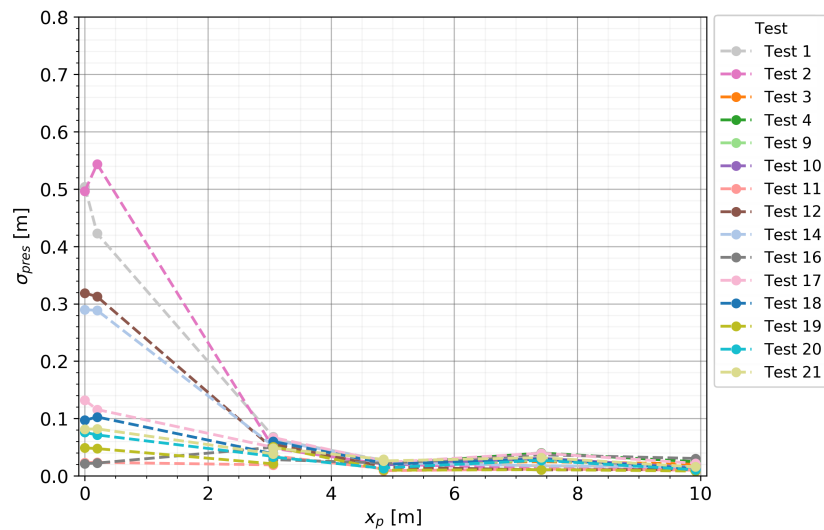
Figure 5.38: Standard deviation (σ_{pres}) plot of the high frequency pressure sensors PS1-4 together with the ADV pressure sensors (PS7-10) for 50% power.
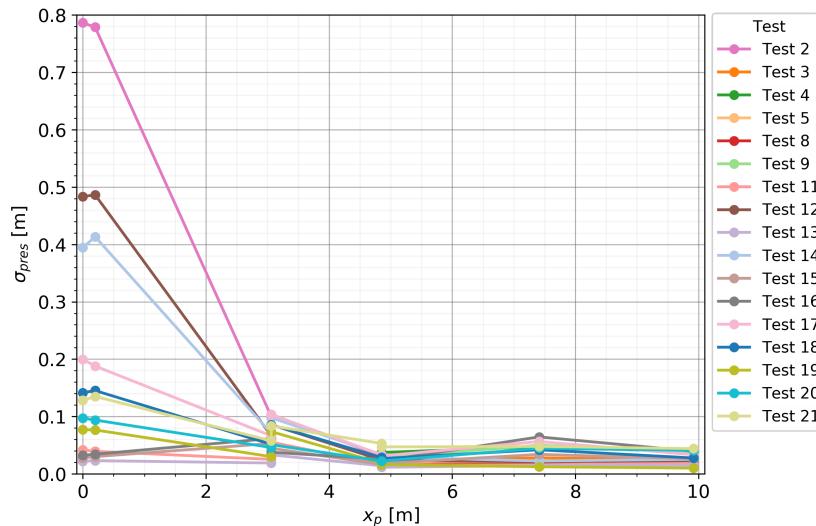
Figure 5.39: Standard deviation (σ_{pres}) plot of the high frequency pressure sensors PS1-4 together with the ADV pressure sensors (PS7-10) for 90% power.

5.7.2. Pressure sensors near the bed (PS1, PS4 and PS7-10)

The results of the decay in pressure fluctuations expressed in σ_{pres} over the bed in x-direction from the quay wall are plotted for 25% power (Figure 5.40), 50% power (Figure 5.41) and 90% power (Figure 5.42). PS1 and PS4 are both positioned at x = 1 m from the quay wall just as PS7 and PS8 are both positioned at x = 2.59 m from the quay wall. Therefore, PS1 and PS7 are plotted separately as a dot in the same color as the corresponding measurement test. An overview of the locations of PS7-10 with respect to the quay wall in x-direction is given in Figure 3.21.

For every power step the highest σ_{pres} is measured by PS1 and PS4 after which σ_{pres} rapidly decreases to PS7 and PS8 (x = 2.59 m). Moving in x-direction from the quay wall to PS9 (x = 5.15 m), σ_{pres} increases again for most tests followed by a decline towards PS10 (x = 7.66 m). The tests that do not follow this pattern stay rather constant or slightly decrease in σ_{pres} moving from PS7 to PS10. Increasing in power results in higher values for σ_{pres} with PS1, PS4 and PS9 advancing the most. The increase in σ_{pres} for PS9 can be explained by the position of the pressure sensor with respect to the flow direction. For PS7 (ADV1) and PS8 (ADV2) the pressure sensors were not positioned directly in the flow direction, contrary to PS9 (ADV3) and PS10 (ADV4). Also giving an explanation why during some tests PS10 measured higher values for σ_{pres} than PS7 and PS8. For 25% power the highest measured values for σ_{pres} at x = 1 m from the quay wall range between 0.01 - 0.04 m while at approximately 8 m from the quay σ_{pres} is between 0.01 - 0.025 m. At 50% power σ_{pres} varies between 0.02 - 0.07 m close to the quay and around 0.01 - 0.03 at x = 7.66 m from the quay wall. The highest power step of 90% results in σ_{pres} varying between 0.02 - 0.105 at x = 1 m and 0.01 - 0.045 at x = 7.66 m.
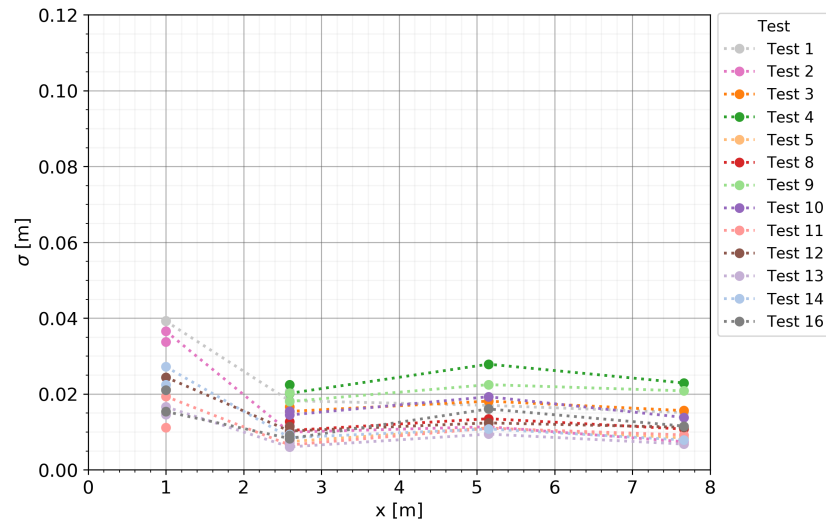
Figure 5.40: Standard deviation (σ_{pres}) plots of the high frequency pressure sensors PS1 and PS4 together with the ADV pressure sensors (PS7-10) for 25% power.
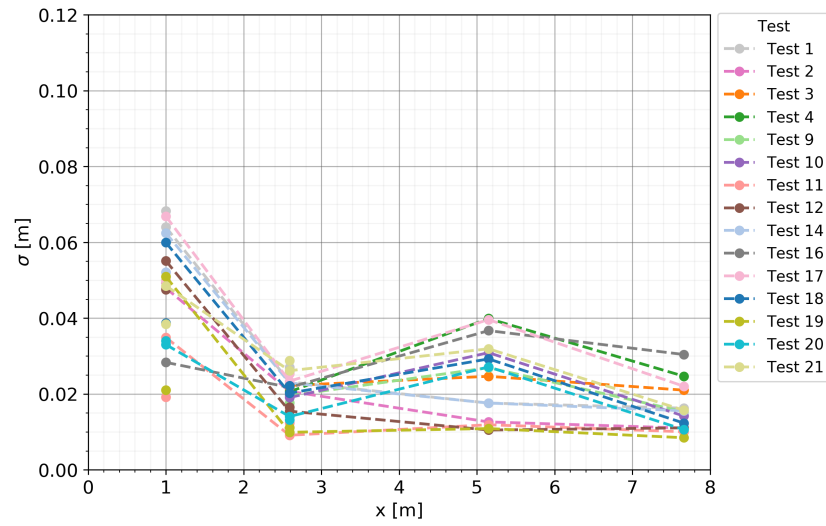
Figure 5.41: Standard deviation (σ_{pres}) plots of the high frequency pressure sensors PS1 and PS4 together with the ADV pressure sensors (PS7-10) for 50% power.
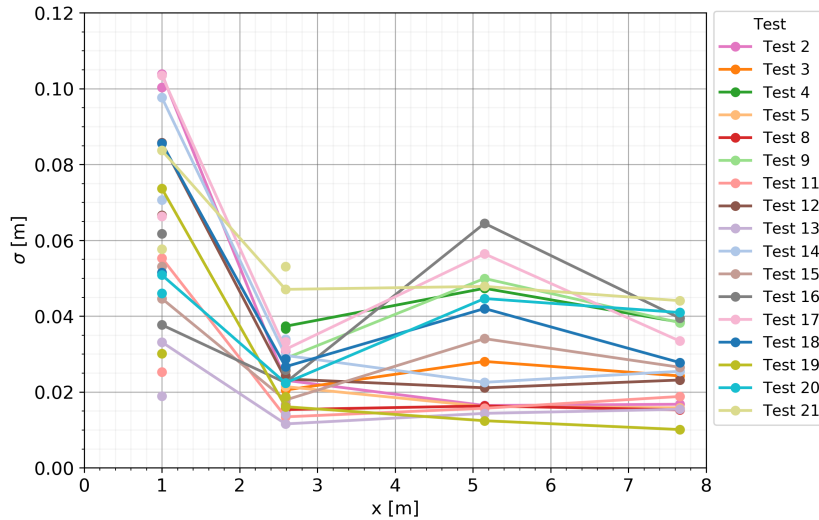
Figure 5.42: Standard deviation (σ_{pres}) plots of the high frequency pressure sensors PS1 and PS4 together with the ADV pressure sensors (PS7-10) for 90% power.

5.8. Conclusions

General observations for all the measurement tests plotted together

The mean flow velocity ($\overline{V}_{hor}$), standard deviation (σ_{hor}) and maximum horizontal flow velocity ($V_{max} = \overline{V}_{hor} + 3\sigma$) show a similar decay profile with the highest values measured near the quay wall at ADV1 (x = 1.50) and ADV2 (x = 3.15 m) after which a strong decline in these statistical parameters is observed towards ADV3 (x = 5.15 m). Further away from the quay wall, the flow velocity either stabilizes or declines on a smaller rate. At Ott2 there is no clear pattern observed with mean flow velocities increasing, decreasing or stabilizing. The standard deviation (σ_{hor}) of Ott2 shows a similar behaviour but the accuracy is questionable due to the low sampling frequency. An explanation for this can be found by the influence of the bow thruster inlets of BT1 and BT2 which are in close proximity of Ott2 drawing in the water from underneath the vessel resulting in higher flow velocities in the area around the bow thruster inlets but reduce the turbulent character of the flow. Dependent on the position of Ott2 with respect to the inlet this can influence the measured flow velocities. Comparing the Ott meters with the ADVs results in similar values for $\overline{V}_{hor}$ measured by ADV2 and Ott1 at every power step while Ott2 measures slightly higher values for $\overline{V}_{hor}$ than ADV4 due to the influence of the bow thruster inlet. The turbulence intensities for Ott1 are significantly lower than for ADV2 while Ott2 measures on average 11.5% lower values for σ_{hor} than ADV4. Whether this is due to the difference in distance x from the quay, the inflow at the bow thruster inlets or the low sampling frequency of the Ott meters is open for discussion.

The highest values for the mean ($\overline{V}_{hor}$) and maximum horizontal flow velocities (V_{max}) at x = 1.50 and 3.15 m (ADV1 and ADV2) are measured during 90% power with BT1&2 activated simultaneously (Test 14, Test 21, Test 18, Test 17 and Test 4). For these tests the mean flow velocities at ADV1 and ADV2 are between 1.25 and 1.7 m/s while the maximum horizontal flow velocities (V_{max}) varies between 2.7 and 3.4 m/s. When only one bow thruster is used, Test 9 (BT1) and Test 20 (BT1) show the largest values for the mean (0.85 and 1.0 m/s) and maximum horizontal (2.0 and 2.2 m/s) flow velocities. Further away from the quay wall at ADV4 and Ott2, the highest flow velocities are measured by Test 4 and Test 16 with BT1&2 activated simultaneously. For these two tests, significantly larger mean (0.8 and 1.0 m/s) and maximum horizontal flow velocities (1.8 and 2.0 m/s) are observed than for the other tests. The standard deviation (σ_{hor}) per test shows similar values for ADV1 and ADV2 while the values increase for higher power steps comparable to the mean and maximum horizontal flow velocity measurements. The largest standard deviations (σ_{hor}) are measured at 90% power for ADV1 and ADV2 ranging between 0.20 and 0.56 m/s. The relative turbulence intensity (r_{hor}) generally varies between 0.3 and 0.6 for ADV1-4. Especially for ADV1, ADV2 and during the 50% power step for every ADV r_{hor} falls between 0.3 and 0.6. This results in an average calculation value for the maximum

horizontal flow velocity near the bed of 2.3 times the mean horizontal flow velocity for the ADVs with a maximum of 3.1 observed for one measurement instrument (ADV3) during 90% power.

Influence distance y_t between bow thruster axis and instruments
The highest flow velocities for BT1 are not measured directly underneath the bow thruster axis but at y_t = -1.5 m reaching values for V_{max} of 2.2 m/s. Showing that the highest flow velocities are located towards the stern of the vessel for BT1. Using BT2, the flow velocities show a more complex pattern. At y_t = 2 m the highest values for V_{max} are measured at ADV1. However, for ADV2 and ADV3, the highest values are measured directly underneath the bow thruster axis at y_t = 0 m with V_{max} equals 2.0 m/s (highest measured value). While at y_t = -2 m, the highest values at ADV4 and Ott2 are measured with a flow velocity (V_{max}) of 2.0 m/s measured by Ott2 at x = 8.45 m, unusually high compared to the other measurements of Ott2. For BT1&2 overall overall the highest flow velocities are measured at y_t = -1.75 m measuring the highest value for V_{max} of all the measurement tests of 3.4 m/s. Moving in x-direction from the quay slightly higher flow velocities are observed for ADV3-Ott2 at y_t = -3.75 m. To conclude, generally higher maximum flow velocities are located towards the stern in negative y-direction. In addition, for increasing distance in x-direction from the quay higher maximum flow velocities are located further away from the bow thruster axis in negative y-direction (negative values of y_t).

Influence use of different bow thrusters
Comparing BT1 and BT2 for the same (or almost equal) distances y_t and L = 0.8 m results in higher measured flow velocities for BT2 at y_t = 2m and y_t = 0 while for y_t = -1.5 m (BT1) and y_t = -2 m (BT2) higher flow velocities are measured for BT1. Therefore, a clear relation between flow velocities measured by BT1 and BT2 at equal (or similar) distances y_t is not recognized. Nonetheless, based on the general observations of Section 5.2 the highest flow velocities for a single bow thruster are observed for BT1.

Quay wall clearance
Increasing the quay wall clearance of the Somtrans XXV from L = 0.8 m to L = 3 m generally leads to comparable but slightly lower flow velocities for BT1. Analyzing BT2, at every power step greater flow velocities are measured for L = 3 m than at L = 0.8 m. Leading to the conclusion that for L = 0.8 m the jet of BT2 has not fully developed jet. Therefore, increasing the quay wall clearance (L$_{BT2}$) leads to higher flow velocities. While BT1, which already has a larger quay wall clearance (L$_{BT1}$) than BT2, the jet is fully developed leading to lower flow velocities near the bed for an increased quay wall clearance. Examining BT1&2, a larger quay wall clearance of L = 3 m induces similar flow velocities near the bed while further increasing to L = 5 m leads to an overall decline in flow velocities.

Dynamic maneuvering and moored tests
The highest instantaneous velocities measured for the dynamic berthing test are generally smaller than the maximum horizontal flow velocities from the moored tests at different quay wall clearances (L). Nevertheless, the flow velocity decay pattern is very similar and during 50% and 90% power the dynamic berthing test shows similar flow velocities measured at ADV3, ADV4 and Ott2. The sailing tests do not lead to comparable flow velocities and decay patterns as observed for the moored tests. Nevertheless, using BT1&2 simultaneously induces a very constant flow velocity level of 1.5 m/s measured by all the instruments due to the two jets spreading broadly over the bed.

Pressure sensors
PS2 and PS3 are positioned directly in the flow direction of the bow thruster jet at the outlet height resulting in standard deviations (σ_{pres}) as high as 0.8 m. The other pressure sensors, located near the bed, measure significantly lower standard deviations (σ_{pres}) of maximally 0.1 m close to the quay (PS1 and PS4) declining while moving in x-direction from the quay to PS7 (ADV1) and PS8 (ADV2) with a maximum value for σ_{pres} of 0.055 m. Remarkably, σ_{pres} increases again for PS9 (ADV3) with a peak value of 0.065 m after which σ_{pres} declines again at PS10 (ADV4) with a maximum value of 0.045 m. In Addition, most of the standard deviations for PS10 are either higher or equal to the measured values of σ_{pres} for PS7 and PS8. This unusual pattern can be explained by the orientation of the pressure sensors, for which PS7 and PS8 are not in the direction of the flow contrary to PS9 and PS10.

6

Comparison to previous research and guidelines

In this chapter the upper limits for the near-bed flow velocities determined in Chapter 5 are compared to previous research and guidelines in order to place the measurements into perspective with the literature framework elaborated in Chapter 2. For each bow thruster the test with the highest measured near-bed flow velocities for a quay wall clearance of the Somtrans XXV of L = 0.8 m is selected. In Addition, Test 18-21 are analyzed to determine the quay wall clearance dependency of the near-bed flow velocities compared to previous research and guidelines. An overview of all the tests that will be considered in this chapter is given in Table 6.1 including their characteristic (dimensionless) parameters.

Table 6.1: Characteristic (dimensionless) parameters of the tests that will be compared to previous research and guidelines sorted by increasing values for L_{BT}. Where L_{BT} is the quay wall clearance between the considered bow thruster outlet and the quay wall (for BT1&2 the average of BT1 and BT2 is taken), y_t the distance in y-direction between the bow thruster axis and the measurement instruments (see Figure 3.39 for the illustration of L, L_{BT} and y_t), D_t = 1.07 m the bow thruster diameter and h_t = 3.24 m the height of the bow thruster axis above the bed. The illustrations of the vessel positions can be found in Section 3.6.3 and 3.6.4.

Test	BT	Vessel position	L_{BT} [m]	y_t [m]	L_{BT}/D_t [-]	h_t/D_t [-]
Test 2	2	1	3.09	0	2.89	3.03
Test 4	1&2	1	4.35	-1.75	4.07	3.03
Test 19	2	7	5.29	1.75	4.94	3.03
Test 9	1	2	5.61	-1.5	5.24	3.03
Test 18	1&2	7	6.55	0	6.12	3.03
Test 20	1	7	7.81	-1.75	7.30	3.03
Test 21	1&2	8	8.55	0	7.99	3.03

6.1. German and Dutch method application range

In Section 2.3.1 the German and Dutch method are elaborated for determining the flow velocities at the bed after reflection on a vertical quay wall. The German method is mainly based on scale model tests by Schmidt (1998) whereas the Dutch method is primarily based on full scale measurements by Blokland (1996). The definitions used for the near-bed flow velocities and application range of the measurements were the methods are based on are discussed in this section.

6.1.1. Difference in definition for the near-bed flow velocity

Besides the difference in methodology of the measurements were the German and Dutch method are based on (scale model test and full scale measurement), they vary in definition for the near-bed flow velocity. Schmidt (1998) measured the near-bed flow velocities in x- and z- direction (German method) while Blokland (1996) measured the flow in three dimensions (x, y and z) complying with

the defined reference system in Section 3.5.1 used throughout this thesis. Schmidt (1998) defined the mean near-bed flow velocity in his guidelines based on the flow velocity in x-direction ($\overline{V}_x$) while Blokland (1996) used the x and y component to define the mean horizontal near-bed flow velocity ($\overline{V}_{hor}$) for his guidelines. Resulting in two different definitions for the mean near-bed flow velocity. In addition, the German and Dutch method are based on the upper limit of the mean near-bed flow velocities measured during the measurement tests in their research. The velocity resulting from the methods is therefore based on the upper limit of the measured mean flow velocity $\overline{V}_x$ (German) or $\overline{V}_{hor}$ (Dutch). Thus, to analyse the results from the Gent measurements with the German and Dutch method the tests with the highest flow velocities from Chapter 5 are selected and compared to the German and Ducth method based on their measured values for $\overline{V}_x$ and $\overline{V}_{hor}$. An overview of the selected measurement tests is listed in Table 6.1 and compared to the German and Dutch method in Section 6.3.

6.1.2. Characteristic parameter range

The range of characteristic parameters of the measurements were the German and Dutch method are based on are listed in Table 6.2 together with the range of locations in x-direction were the instruments measured the flow velocity near the bed. The characteristic parameters are divided by the bow thruster diameter D_t = 1.07 m to compare the research by Schmidt (1998), Blokland (1996) and the measurements in Gent with each other. The quay wall clearance for the bow thruster outlet (L_{BT}/D_t) of the measurements with the Somtrans XXV varies between 2.89 - 7.99 L_{BT}/D_t. Test 2 for BT2 with L_{BT}/D_t = 2.89 does not correspond to the range in L_{BT}/D_t for both the Dutch and the German method while Test 21 for BT1&2 with L_{BT}/D_t = 7.99 falls outside of the applicability range for the German method. Therefore, comparing these test to the methods should be done with care while keeping in mind that they fall outside of the measurement range for the methods. During the tests in Gent with the Somtrans XXV the height of the bow thruster axis above the bed was constant at h_t/D_t = 3.03. Comparing to the Dutch method, this falls just above the upper limit of h_t/D_t = 2.9. Considering the German method, h_t/D_t = 3.03 falls in the range of 1.66 - 3.93 h_t/D_t. The Dutch method measured flow velocities at three different locations in x-direction from the quay wall in the reach of 0.49 - 1.47 x/D_t. For the German method, the flow velocities were measured at 12 different locations ranging between 0.29 - 3.38 x/D_t. In Gent the flow velocities were measured from 1.40 to 7.90 x/D_t perpendicular to the quay wall in x-direction. Consequently, this results in more information of the flow velocity decay profile further away from the quay but less spatial resolution near the quay wall as for the German and Dutch method.

Table 6.2: Characteristic parameters of the measurements were the German and Dutch method are based on for determining the near-bed flow velocities. In Addition, the location of the measurement points in x-direction are listed in x/D_t.

Method	L_{BT}/D_t [-]	h_t/D_t [-]	Measurement locations x/D_t [-]
German (and Schmidt (1998))	3.97, 5.44, 7.28	1.66 - 3.93	0.29 - 3.38
Dutch	3.2, 6.2, 12	2.22 - 2.9	0.49, 0.82, 1.47
Gent measurements	2.89 - 7.99	3.03	1.40, 2.94, 4.81, 6.81, 7.90

6.1.3. Resulting Dutch and German method formulae

From Section 2.3.1 the German and Dutch method formulae are presented in this section for the application range of the measurements in Gent including the definition for the near-bed flow velocities were the methods are based on. Equation 6.1 represents the total formula as combination of Equation 2.12 and 2.13 to determine the near-bed flow velocities for values of L_{BT}/D_t larger than 1.9 according to the German method. It must be noted that the German method in this thesis is the correct formulae for the near-bed flow velocities as presented by PIANC (2015) guidelines. During the Gent measurements the smallest value for L_{BT}/D_t equals 2.89. Therefore, only the formulae for the German method where the jet is fully developed with L_{BT}/D_t larger than 1.9 is considered. In Addition, the German method is based on the highest measured values for the mean flow velocity in x-direction ($\overline{V}_x$) at the intersection between the quay wall and the bed for a specific quay wall clearance and keel clearance. Thus, the German method does not include a relation for the decay in flow velocity moving in x-direction from the quay wall.

$$\overline{V}_{x,\text{German}} = 1.9 \cdot V_0 \cdot \left(\frac{L_{BT}}{D_t}\right)^{-1.0} \cdot 10.6 \cdot \left(\frac{L_{BT}}{D_t}\right)^{-1.0} \cdot \left(\frac{h_t}{D_t}\right)^{-1.15} \quad \text{for} \ \ 1.9 < \frac{L_{BT}}{D_t} \tag{6.1}$$

The Dutch method is based on the highest measured values for the mean horizontal near-bed flow velocity ($\overline{V}_{hor}$) measured by Blokland (1996) at a certain distance x from the quay wall dependent on the total distance travelled by the jet (x_s). Where x_s is the sum of the quay wall clearance of the bow thruster (L_{BT}), the height of the bow thruster axis above the bed (h_t) and the distance x from the quay wall. Equation 6.2 gives the relation for $\overline{V}_{hor}$ in the region where the jet is developing (($L_{BT}+x)/h_t < 1.8$) and Equation 6.3 for the region where the jet is fully developed (($L_{BT}+x)/h_t > 1.8$).

$$\overline{V}_{\text{hor,Dutch}} = 1.0 \cdot V_0 \cdot \frac{D_t}{h_t} \quad \text{for} \ \ (L_{BT}+x)/h_t < 1.8 \tag{6.2}$$

$$\overline{V}_{\text{hor,Dutch}} = 2.8 \cdot V_0 \cdot \frac{D_t}{L_{BT}+h_t+x} \quad \text{for} \ \ (L_{BT}+x)/h_t > 1.8 \tag{6.3}$$

6.2. Near-bed flow velocity measurements by Schmidt (1998)

The German method is primarily based on measurements by Schmidt (1998) of the bow thruster jet up to position 2 in Figure 6.1 at the transition of the the quay wall and the bed (x/D_t = 0). However, Schmidt (1998) also measured the flow velocity development and decay in x-direction to the quay wall between x/D_t = 0.3 and 3.4 in position 3 of Figure 6.1. The measurements with the characteristics that comply with the measurements in Gent are R5, S4 and T1 which parameters are listed in Table 6.3. For the near-bed measurements in x-direction from the quay wall, Schmidt (1998) did not derive a formulae and therefore these measurements are not included in the German method in the PIANC (2015) guidelines. The reason for this is that Schmidt (1998) observed very turbulent and unstable flow conditions during these measurements. Schmidt (1998) allocated this to the superposition of the direct jet in position 4 of Figure 6.1 towards the quay and the near-bed flow velocities directed away from the quay wall. Therefore, the near-bed flow velocities in position 3 were not further analysed by Schmidt (1998). Instead, erosion measurements were conducted near the quay wall to further analyse the jet impact at the transition between the quay wand the bed. For the measurements in Gent, the direct jet on the bed plays no significant role as for an angle of 12-13°(Schmidt, 1998) the jet does not hit the bed before it reflects on the quay wall. In addition, the angle of 12-13°is not based on measurements for a channel bow thruster. The jet from a channel bow thruster is more similar to a free jet meaning that less spreading of the jet is expected after it leaves the bow thruster outlet. Besides, the results for the mean flow velocities measured in Gent showed a flow velocity direction in positive x-direction away from the quay wall.

Even tough Schmidt (1998) did not further analyse the near-bed flow velocity measurements, comparing them to the Gent measurements could contribute to new provide new conclusions on the decay of the bow thruster jet. Therefore, the measurements by Schmidt (1998) are compared to measurement tests from Gent that have similar values for L_{BT}/D_t and h_t/D_t as listed in Table 6.3.

Table 6.3: Overview of the near-bed flow velocity measurements by Schmidt (1998) that are compared to measurements in Gent with corresponding values for L_{BT}/D_t and h_t/D_t.

Schmidt (1998) test:	L_{BT}/D_t [-]	h_t/D_t [-]	Compared to Gent test:
R5	3.97	2.91	Test 4
S4	5.44	2.42	Test 9
T1	7.28	2.18	Test 20
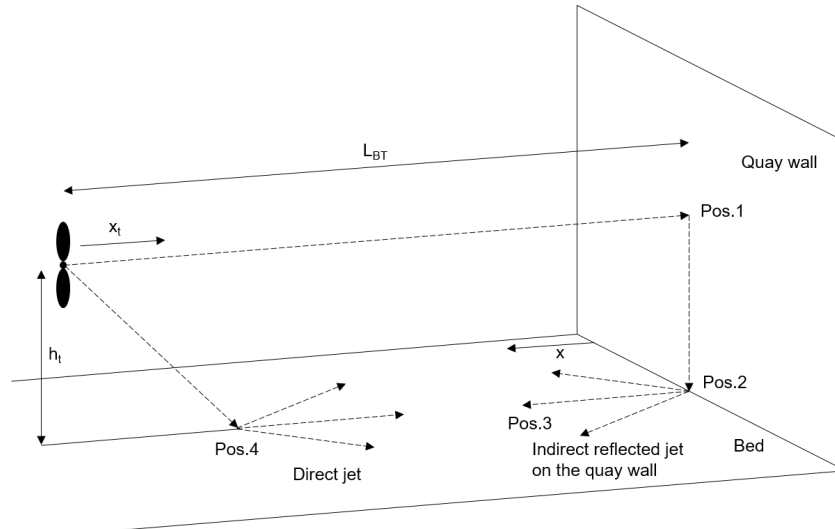
Figure 6.1: Flow situation of the bow thruster jet near the bed when the vessel is at some distance from the quay wall. L_{BT} is the distance between the bow thruster outlet and the quay wall, h_t the height of the bow thruster axis above the bed, x_t the distance from the bow thruster axis at which the velocity in the jet is calculated and x the perpendicular distance to the quay wall at which the flow velocity is measured near the bed. Illustration based on Verheij (2020).

6.3. Comparison to guidelines per test

For each test listed in Table 6.1 the near-bed mean flow velocity in x-direction ($\overline{V}_x$) and horizontal direction ($\overline{V}_{hor}$) from the measurements in Gent are compared with the Dutch ($\overline{V}_{hor,Dutch}$) and German method ($\overline{V}_{x,German}$). In addition, the results for $\overline{V}_x$ are compared with the near-bed flow velocity measurements by Schmidt (1998) as listed in Table 6.3. The Gent measurements are analyzed in the order of increasing values for L_{BT}/D_t as listed in Table 6.1 as this is the main variable where the results are compared on to previous research and guidelines due to h_t/D_t being constant throughout the Gent measurements.

The measured near-bed flow velocities are presented as their relative value to the theoretical efflux velocity V_0 (See Chapter 5 and Table 5.2). In addition, on the horizontal axis the distance x from the quay is divided by $D_t = 1.07$ m to compare the different measurements and guidelines with each other based on D_t. However, as D_t is close to 1, x/D_t is almost equivalent to the distance from the quay wall in x-direction. The results for $\overline{V}_x$ and $\overline{V}_{hor}$ are presented in a table per test rounded of to two decimal numbers. The ratio of $\overline{V}_{hor}/\overline{V}_x$ and $\overline{V}_{hor,Dutch}/\overline{V}_{hor}$ are presented in a separate table for each test which is also rounded of to two decimal numbers after the ratio is calculated. Therefore, due to the rounded off numbers calculating the ratio by hand from the results table per test could lead to slightly different outcomes.

Test 2, BT2, L_{BT}/D_t = 2.89, h_t/D_t = 3.03
Test 2 has the smallest distance between the bow thruster outlet and the quay of L_{BT}/D_t = 2.89 falling outside the range of applicability of the German and method. Therefore, extra attention should be payed to the validity of this comparison. In Figure 6.2 the flow velocities for Test 2 are plotted together with the corresponding value of $\overline{V}_{x,German}$ determined with the German method (x/D_t = 0) and the corresponding values for $\overline{V}_{hor,Dutch}$ determined with the Dutch method between 0 and 8 x/D_t. Noteworthy is the extremely high flow velocity determined with the German method of 0.66 V_0 which is not reflected by the measurements of Test 2 and the Dutch method. Leading to the conclusion that outside the range of L_{BT}/D_t the German methods leads to extremely high values for the near-bed flow velocity. The Gent measurements of $\overline{V}_{hor}$ show significantly lower near-bed flow velocities at every measurement point and power step compared to the Dutch method ($\overline{V}_{hor,Dutch}$). An overview of the relative near-bed flow velocities per measurement point and power step is presented in Table 6.4.
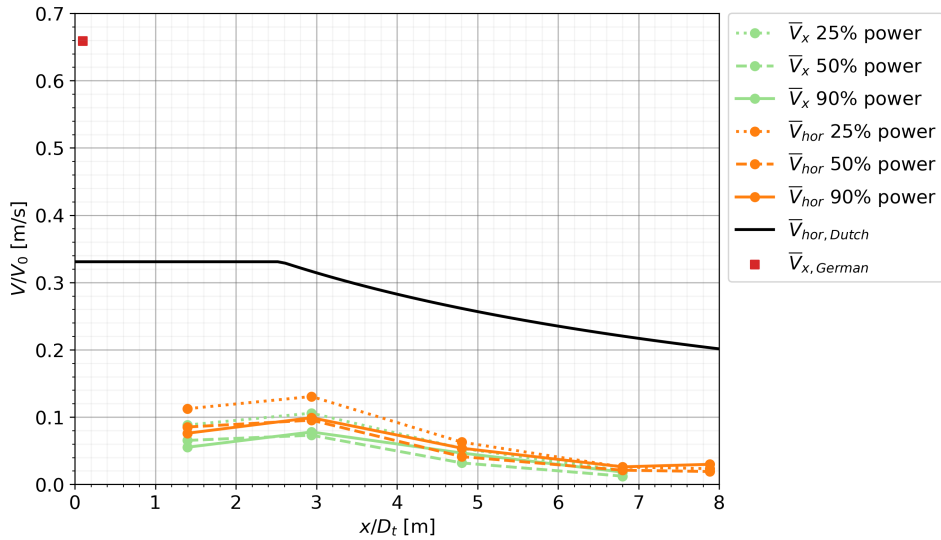
Figure 6.2: Decay of the relative near-bed flow velocities in x-direction from the quay wall for Test 2, BT2 L_{BT}/D_t = 2.89. $\overline{V}_x$ and $\overline{V}_{hor}$ at 25%, 50% and 90% power are compared with $\overline{V}_{hor,Dutch}$ and $\overline{V}_{x,German}$ respectively.

Table 6.4: Overview of the relative near-bed flow velocities ($\overline{V}_x/V_0$ and $\overline{V}_{hor}/V_0$) for Test 2 (BT2, L_{BT}/D_t = 2.89) measured by ADV1-4 and Ott2 at 25%, 50% and 90% power compared with $\overline{V}_{hor,Dutch}/V_0$ and $\overline{V}_{x,German}/V_0$.

	$x/D_t = 0$ [-]	ADV1 $x/D_t = 1.40$ [-]	ADV2 $x/D_t = 2.94$ [-]	ADV3 $x/D_t = 4.81$ [-]	ADV4 $x/D_t = 6.81$ [-]	Ott2 $x/D_t = 7.90$ [-]
$\overline{V}_x/V_0$ 25% [-]	-	0.09	0.11	0.05	0.02	-
$\overline{V}_x/V_0$ 50% [-]	-	0.07	0.07	0.03	0.01	-
$\overline{V}_x/V_0$ 90% [-]	-	0.06	0.08	0.05	0.02	-
$\overline{V}_{hor}/V_0$ 25% [-]	-	0.11	0.13	0.06	0.03	0.02
$\overline{V}_{hor}/V_0$ 50% [-]	-	0.09	0.1	0.04	0.02	0.02
$\overline{V}_{hor}/V_0$ 90% [-]	-	0.08	0.1	0.05	0.03	0.03
$\overline{V}_{hor,Dutch}/V_0$ [-]	0.33	0.33	0.32	0.26	0.22	0.2
$\overline{V}_{x,German}/V_0$ [-]	0.66	-	-	-	-	-

In Table 6.5 the ratio of the relative near-bed flow velocity per power step for the mean horizontal flow velocity over the mean flow velocity in x-direction ($\overline{V}_{hor}/\overline{V}_x$) are presented. In addition, the ratio between the calculated mean horizontal flow velocity by the Dutch method and the measured mean horizontal flow velocity ($\overline{V}_{hor,Dutch}$ / $\overline{V}_{hor}$) is determined. From Table 6.5 can be concluded that $\overline{V}_{hor}$ results in 17-72% higher flow velocities compared to $\overline{V}_x$. Comparing the Dutch method ($\overline{V}_{hor,Dutch}$) to the measured values for $\overline{V}_{hor}$ during Test 2 results in an overestimation of $\overline{V}_{hor}$ with a factor ranging between 2.43-10.65. Whereas the German method ($\overline{V}_{x,German}$) overestimates the highest measured value for $\overline{V}_x$ at ADV2 (x/D_t = 2.94) during the 25% power step with a factor of 6 (Table 6.4).

Table 6.5: Overview of the ratio for the relative near-bed flow velocity $\overline{V}_{hor}/\overline{V}_x$ and $\overline{V}_{hor,Dutch}/\overline{V}_{hor}$ for Test 2 (BT2, L_{BT}/D_t = 2.89) measured by ADV1-4 and Ott2 at 25%, 50% and 90% power.

	ADV1 $x/D_t = 1.40$ [-]	ADV2 $x/D_t = 2.94$ [-]	ADV3 $x/D_t = 4.81$ [-]	ADV4 $x/D_t = 6.81$ [-]	Ott2 $x/D_t = 7.90$ [-]	Average [-]
$\overline{V}_{hor}$ / $\overline{V}_x$ 25% [-]	1.27	1.23	1.17	1.27	-	1.24
$\overline{V}_{hor}$ / $\overline{V}_x$ 50% [-]	1.31	1.31	1.29	1.72	-	1.41
$\overline{V}_{hor}$ / $\overline{V}_x$ 90% [-]	1.38	1.27	1.16	1.43	-	1.31
$\overline{V}_{hor,Dutch}$ / $\overline{V}_{hor}$ 25% [-]	2.94	2.43	4.17	8.56	8.72	5.36
$\overline{V}_{hor,Dutch}$ / $\overline{V}_{hor}$ 50% [-]	3.88	3.32	6.35	10.5	10.65	6.94
$\overline{V}_{hor,Dutch}$ / $\overline{V}_{hor}$ 90% [-]	4.35	3.2	4.86	8.48	6.82	5.54

Test 4, BT1&2, L_{BT}/D_t = 4.07, h_t/D_t = 3.03

For Test 4 the flow velocities are illustrated in Figure 6.3 and listed in Table 6.6. Close to the quay the German method ($\overline{V}_{x,German}$) leads to the highest flow velocity value of 0.34 V_0 slightly above the Dutch method ($\overline{V}_{hor,Dutch}$). Test R5 of Schmidt (1998) is plotted as well in Figure 6.3 representing the measured values for $\overline{V}_{x,Schmidt}$ at L_{BT}/D_t = 3.97 and h_t/D_t = 2.91. For R5, $\overline{V}_{x,Schmidt}$ first increases towards a maximum around x/D_t = 1 after which a decline is observed falling below the measured values for $\overline{V}_x$ from Gent near x/D_t = 3. Showing significantly higher values for $\overline{V}_{x,Schmidt}$ measured by Schmidt (1998) compared to the $\overline{V}_x$ measured in Gent until x/D_t = 2.5. Close to the quay wall around x/D_t = 1 $\overline{V}_{x,Schmidt}$ corresponds well with the $\overline{V}_{x,German}$. Comparing $\overline{V}_{hor,Dutch}$ with the measurements for $\overline{V}_{hor}$ from Gent results in an overestimation of $\overline{V}_{hor}$ for every measurement point and power step by the Dutch method although the decay pattern is similar between ADV2 and ADV4.
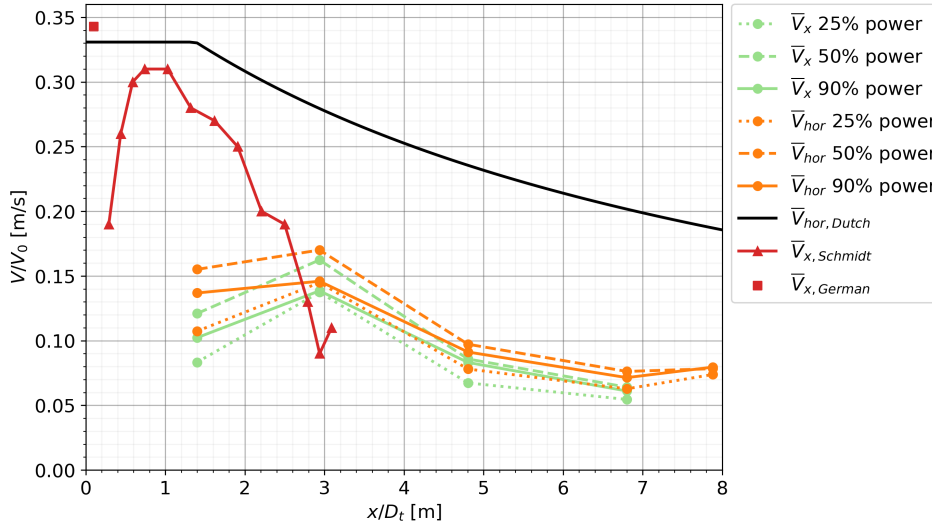
Figure 6.3: Decay of the relative near-bed flow velocities in x-direction from the quay wall for Test 4, BT1&2 L_{BT}/D_t = 4.07, h_t/D_t = 3.03. $\overline{V}_x$ and $\overline{V}_{hor}$ at 25%, 50% and 90% power are compared with $\overline{V}_{x,German}$ and $\overline{V}_{hor,Dutch}$. In addition, $\overline{V}_x$ is compared to measurement R5 by Schmidt (1998) ($\overline{V}_{x,Schmidt}$) with L_{BT}/D_t = 3.97 and h_t/D_t = 2.91.

Table 6.6: Overview of the relative near-bed flow velocities ($\overline{V}_x/V_0$ and $\overline{V}_{hor}/V_0$) for Test 4 (BT1&2, L_{BT}/D_t = 4.07, h_t/D_t = 3.03) measured by ADV1-4 and Ott2 at 25%, 50% and 90% power compared with $\overline{V}_{hor,Dutch}/V_0$,$\overline{V}_{x,German}/V_0$ and $\overline{V}_{x,Schmidt}/V_0$ for measurement R5 (L_{BT}/D_t = 3.97, h_t/D_t = 2.91).

	$x/D_t = 0$ [-]	ADV1 $x/D_t = 1.40$ [-]	ADV2 $x/D_t = 2.94$ [-]	ADV3 $x/D_t = 4.81$ [-]	ADV4 $x/D_t = 6.81$ [-]	Ott2 $x/D_t = 7.90$ [-]
$\overline{V}_x/V_0$ 25% [-]	-	0.08	0.14	0.07	0.05	-
$\overline{V}_x/V_0$ 50% [-]	-	0.12	0.16	0.09	0.06	-
$\overline{V}_x/V_0$ 90% [-]	-	0.1	0.14	0.08	0.06	-
$\overline{V}_{hor}/V_0$ 25% [-]	-	0.11	0.14	0.08	0.06	0.07
$\overline{V}_{hor}/V_0$ 50% [-]	-	0.16	0.17	0.1	0.08	0.08
$\overline{V}_{hor}/V_0$ 90% [-]	-	0.14	0.15	0.09	0.07	0.08
$\overline{V}_{hor,Dutch}/V_0$ [-]	0.33	0.33	0.28	0.24	0.2	0.19
$\overline{V}_{x,German}/V_0$ [-]	0.34	-	-	-	-	-
$\overline{V}_{x,Schmidt}/V_0$ [-]	0.19	0.27	0.11	-	-	-

In Table 6.7 $\overline{V}_{hor}/\overline{V}_x$ and $\overline{V}_{hor,Dutch}/\overline{V}_{hor}$ are presented for the 25%, 50% and 90% power step showing the ratio between the mean flow velocities in horizontal and x-direction as well as the ratio of the determined mean horizontal flow velocities by the Dutch method and the measurements in Gent. From Table 6.5 can be concluded that $\overline{V}_{hor}$ results in 5-34% higher flow velocities compared to $\overline{V}_x$. Comparing the Dutch method ($\overline{V}_{hor,Dutch}$) to the measured values for $\overline{V}_{hor}$ during Test 4 results in an overestimation of

$\overline{V}_{hor}$ with a factor ranging between 1.64-3.21. Whereas the German method ($\overline{V}_{x,\text{German}}$) overestimates the highest measured value for $\overline{V}_x$ at ADV2 (x/D_t = 2.94) during the 50% power step with a factor of 2.13 (Table 6.6).

Table 6.7: Overview of the ratio for the relative near-bed flow velocity $\overline{V}_{hor}/\overline{V}_x$ and $\overline{V}_{hor,\text{Dutch}}/\overline{V}_{hor}$ for Test 4 (BT1&2, L_{BT}/D_t = 4.07, h_t/D_t = 3.03) measured by ADV1-4 and Ott2 at 25%, 50% and 90% power.

	ADV1 $x/D_t = 1.40$ [-]	ADV2 $x/D_t = 2.94$ [-]	ADV3 $x/D_t = 4.81$ [-]	ADV4 $x/D_t = 6.81$ [-]	Ott2 $x/D_t = 7.90$ [-]	Average [-]
$\overline{V}_{hor}$ / $\overline{V}_x$ 25% [-]	1.29	1.05	1.16	1.15	-	1.16
$\overline{V}_{hor}$ / $\overline{V}_x$ 50% [-]	1.28	1.05	1.13	1.19	-	1.16
$\overline{V}_{hor}$ / $\overline{V}_x$ 90% [-]	1.34	1.05	1.1	1.17	-	1.16
$\overline{V}_{hor,\text{Dutch}}$ / $\overline{V}_{hor}$ 25% [-]	3.08	1.93	3.02	3.21	2.53	2.75
$\overline{V}_{hor,\text{Dutch}}$ / $\overline{V}_{hor}$ 50% [-]	2.13	1.64	2.42	2.65	2.39	2.25
$\overline{V}_{hor,\text{Dutch}}$ / $\overline{V}_{hor}$ 90% [-]	2.41	1.91	2.58	2.82	2.35	2.42

Test 19, BT2, L_{BT}/D_t = 4.94, h_t/D_t = 3.03

For Test 19 the flow velocities are illustrated in Figure 6.4 and listed in Table 6.8. The flow velocity point determined with the German method ($\overline{V}_{x,\text{German}}$) at x/$D_t$ = 0 falls below the Dutch method ($\overline{V}_{hor,\text{Dutch}}$) for the first time showing a greater dependency on L_{BT}/D_t. However, a significant discrepancy between the German method to the measured values for $\overline{V}_x$ is still observed with the German method overestimating $\overline{V}_x$ for every measurement point. The same observation applies for the comparison of the Dutch method ($\overline{V}_{hor,\text{Dutch}}$) with the measured values for $\overline{V}_{hor}$ for Test 19.
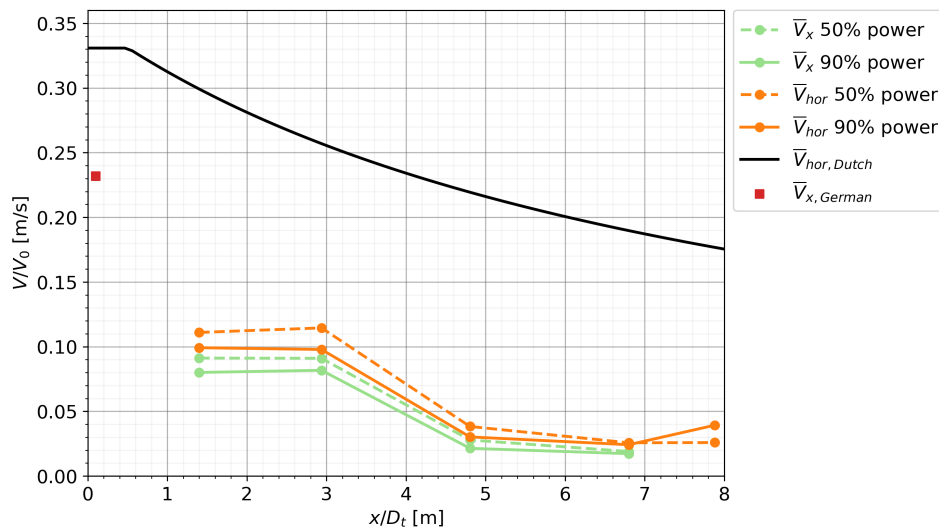
Figure 6.4: Decay of the relative near-bed flow velocities in x-direction from the quay wall for Test 19, BT2 L_{BT}/D_t = 4.94. $\overline{V}_x$ and $\overline{V}_{hor}$ at 25%, 50% and 90% power are compared with $\overline{V}_{hor,\text{Dutch}}$ and $\overline{V}_{x,\text{German}}$ respectively.

Table 6.8: Overview of the relative near-bed flow velocities ($\overline{V}_x/V_0$ and $\overline{V}_{hor}/V_0$) for Test 19 (BT2, L_{BT}/D_t = 4.94) measured by ADV1-4 and Ott2 at 50% and 90% power compared with $\overline{V}_{hor,Dutch}/V_0$ and $\overline{V}_{x,German}/V_0$.

	$x/D_t = 0$ [-]	ADV1 $x/D_t = 1.40$ [-]	ADV2 $x/D_t = 2.94$ [-]	ADV3 $x/D_t = 4.81$ [-]	ADV4 $x/D_t = 6.81$ [-]	Ott2 $x/D_t = 7.90$ [-]
$\overline{V}_x/V_0$ 50% [-]	-	0.09	0.09	0.03	0.02	-
$\overline{V}_x/V_0$ 90% [-]	-	0.08	0.08	0.02	0.02	-
$\overline{V}_{hor}/V_0$ 50% [-]	-	0.11	0.11	0.04	0.03	0.03
$\overline{V}_{hor}/V_0$ 90% [-]	-	0.1	0.1	0.03	0.02	0.04
$\overline{V}_{hor,Dutch}/V_0$ [-]	0.33	0.3	0.26	0.22	0.19	0.18
$\overline{V}_{x,German}/V_0$ [-]	0.23	-	-	-	-	-

In Table 6.9 the ratio of $\overline{V}_{hor}$ over $\overline{V}_x$ is determined for 50% and 90% power in addition to the ratio of $\overline{V}_{hor,Dutch}$ over $\overline{V}_{hor}$ measured in Gent. $\overline{V}_{hor}$ is between 20-41% larger than $\overline{V}_x$ with an average difference of 30%. The Dutch method results in a factor of 2.24-7.83 times higher values for $\overline{V}_{hor,Dutch}$ than $\overline{V}_{hor}$. Especially further away from the quay wall at ADV3, ADV4 and Ott2 this factor is significantly larger than for ADV1 and ADV2. The German method ($\overline{V}_{x,German}$) overestimates the highest measured value for $\overline{V}_x$ at ADV1 (x/D_t = 1.4) during the 50% power step with a factor of 2.56 (Table 6.8).

Table 6.9: Overview of the ratio for the relative near-bed flow velocity $\overline{V}_{hor}/\overline{V}_x$ and $\overline{V}_{hor,Dutch}/\overline{V}_{hor}$ for Test 19 (BT2, L_{BT}/D_t = 4.94) measured by ADV1-4 and Ott2 at 50% and 90% power.

	ADV1 $x/D_t = 1.40$ [-]	ADV2 $x/D_t = 2.94$ [-]	ADV3 $x/D_t = 4.81$ [-]	ADV4 $x/D_t = 6.81$ [-]	Ott2 $x/D_t = 7.90$ [-]	Average [-]
$\overline{V}_{hor} / \overline{V}_x$ 50% [-]	1.22	1.26	1.38	1.35	-	1.3
$\overline{V}_{hor} / \overline{V}_x$ 90% [-]	1.24	1.2	1.41	1.4	-	1.31
$\overline{V}_{hor,Dutch} / \overline{V}_{hor}$ 50% [-]	2.7	2.24	5.72	7.38	6.83	4.97
$\overline{V}_{hor,Dutch} / \overline{V}_{hor}$ 90% [-]	3.02	2.63	7.25	7.83	4.5	5.04

Test 9, BT1, L_{BT}/D_t = 5.24, h_t/D_t = 3.03

In Figure 6.5, Test 9 is plotted for $\overline{V}_x$ and $\overline{V}_{hor}$ together with the German method, Dutch method and measurement test S4 by Schmidt (1998). An overview of the flow velocity values is listed in Table 6.10. Similar to the previous measurement tests, a significant discrepancy between the German method ($\overline{V}_{x,German}$) and measured values for $\overline{V}_x$ in Gent is observed. Although for increasing values of L_{BT}/D_t the German method approaches the measurements more. Likewise, the Dutch method overestimates the measured values for $\overline{V}_{hor}$ for every measurement point. For S4, the measurement of Schmidt (1998) with L_{BT}/D_t = 5.44 and h_t/D_t = 2.42, the flow velocity starts at a comparable value to the German method close to the quay. However, strongly increases to the highest observed flow velocity value for $\overline{V}_{x,Schmidt}$ of 0.35 V_0 at x/D_t = 1 after which it declines again not showing a similar trend in the decay in flow velocity as the Dutch method and Gent measurements. Thus, the measurements by Schmidt (1998) do not reflect the strong dependency on quay wall clearance (L_{BT}) as observed for the German method.
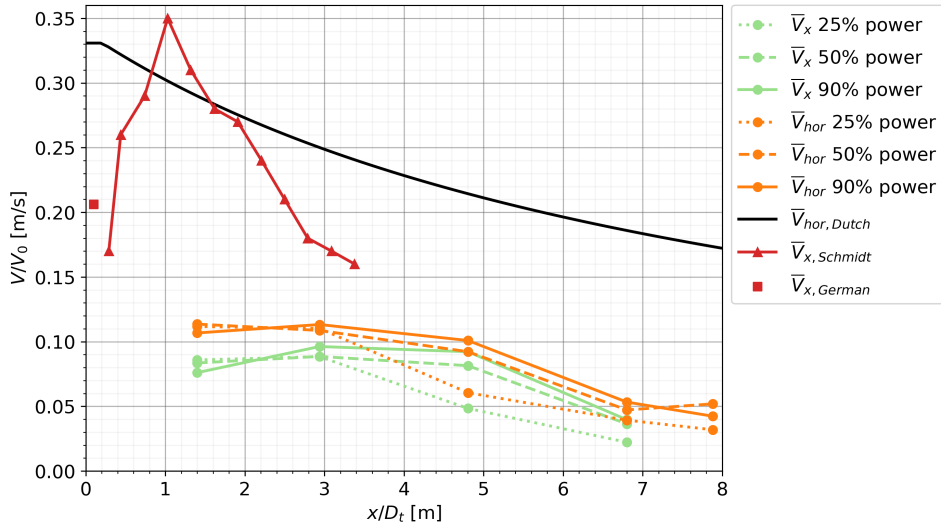
Figure 6.5: Decay of the relative near-bed flow velocities in x-direction from the quay wall for Test 9, BT1 L_{BT}/D_t = 5.24, h_t/D_t = 3.03. $\overline{V}_x$ and $\overline{V}_{hor}$ at 25%, 50% and 90% power are compared with $\overline{V}_{x,German}$ and $\overline{V}_{hor,Dutch}$. In addition, $\overline{V}_x$ is compared to measurement S5 by Schmidt (1998) ($\overline{V}_{x,Schmidt}$) with L_{BT}/D_t = 5.44 and h_t/D_t = 2.42.

Table 6.10: Overview of the relative near-bed flow velocities ($\overline{V}_x/V_0$ and $\overline{V}_{hor}/V_0$) for Test 9 (BT1, L_{BT}/D_t = 5.24, h_t/D_t = 3.03) measured by ADV1-4 and Ott2 at 25%, 50% and 90% power compared with $\overline{V}_{hor,Dutch}/V_0$, $\overline{V}_{x,German}/V_0$ and $\overline{V}_{x,Schmidt}/V_0$ for measurement S4 (L_{BT}/D_t = 5.44, h_t/D_t = 2.42).

	$x/D_t = 0$ [-]	ADV1 $x/D_t = 1.40$ [-]	ADV2 $x/D_t = 2.94$ [-]	ADV3 $x/D_t = 4.81$ [-]	ADV4 $x/D_t = 6.81$ [-]	Ott2 $x/D_t = 7.90$ [-]
$\overline{V}_x/V_0$ 25% [-]	-	0.09	0.09	0.05	0.02	-
$\overline{V}_x/V_0$ 50% [-]	-	0.08	0.09	0.08	0.04	-
$\overline{V}_x/V_0$ 90% [-]	-	0.08	0.1	0.09	0.04	-
$\overline{V}_{hor}/V_0$ 25% [-]	-	0.11	0.11	0.06	0.04	0.03
$\overline{V}_{hor}/V_0$ 50% [-]	-	0.11	0.11	0.09	0.05	0.05
$\overline{V}_{hor}/V_0$ 90% [-]	-	0.11	0.11	0.1	0.05	0.04
$\overline{V}_{hor,Dutch}/V_0$ [-]	0.33	0.29	0.25	0.21	0.18	0.17
$\overline{V}_{x,German}/V_0$ [-]	0.21	-	-	-	-	-
$\overline{V}_{x,Schmidt}/V_0$ [-]	0.17	0.28	0.17	-	-	-

In Table 6.11 the ratio of $\overline{V}_{hor}$ over $\overline{V}_x$ and $\overline{V}_{hor,Dutch}$ over $\overline{V}_{hor}$ is determined for 25%, 50% and 90% power. Showing that $\overline{V}_{hor}$ is between 9-77% larger than $\overline{V}_x$ with an average of 30%. The Dutch method ($\overline{V}_{hor,Dutch}$) differs from the measured values of $\overline{V}_{hor}$ with a factor ranging between 2.12-5.44. The largest difference between the two is mainly observed at ADV4 and Ott2. The German method ($\overline{V}_{x,German}$) overestimates the highest measured value for $\overline{V}_x$ at ADV2 (x/D_t = 2.94) during the 90% power step with a factor of 2.1 (Table 6.8).

Table 6.11: Overview of the ratio for the relative near-bed flow velocity $\overline{V}_{hor}/\overline{V}_x$ and $\overline{V}_{hor,Dutch}/\overline{V}_{hor}$ for Test 9 (BT1, L_{BT}/D_t = 5.24) measured by ADV1-4 and Ott2 at 25%, 50% and 90% power.

	ADV1 $x/D_t = 1.40$ [-]	ADV2 $x/D_t = 2.94$ [-]	ADV3 $x/D_t = 4.81$ [-]	ADV4 $x/D_t = 6.81$ [-]	Ott2 $x/D_t = 7.90$ [-]	Average [-]
$\overline{V}_{hor}$ / $\overline{V}_x$ 25% [-]	1.3	1.25	1.25	1.77	-	1.39
$\overline{V}_{hor}$ / $\overline{V}_x$ 50% [-]	1.36	1.23	1.13	1.3	-	1.25
$\overline{V}_{hor}$ / $\overline{V}_x$ 90% [-]	1.4	1.18	1.09	1.34	-	1.25
$\overline{V}_{hor,Dutch}$ / $\overline{V}_{hor}$ 25% [-]	2.59	2.27	3.54	4.73	5.44	3.71
$\overline{V}_{hor,Dutch}$ / $\overline{V}_{hor}$ 50% [-]	2.55	2.3	2.32	3.94	3.34	2.89
$\overline{V}_{hor,Dutch}$ / $\overline{V}_{hor}$ 90% [-]	2.72	2.21	2.12	3.49	4.09	2.93

Test 18, BT1&2, L_{BT}/D_t = 6.12, h_t/D_t = 3.03

In Figure 6.6 the flow velocities for the German method ($\overline{V}_{x,German}$), Dutch method ($\overline{V}_{hor,Dutch}$) and the results from the Gent measurements are plotted for Test 18 while their values are listed in Table 6.12. The German method at x/D_t = 0 results in a comparable value for $\overline{V}_x$ measured at ADV1 and ADV2 while the Dutch method significantly overestimates the measured values for $\overline{V}_{hor}$. In addition, $\overline{V}_{hor}$ measured in Gent declines faster than the Dutch method after ADV2 for increasing values of x/D_t.
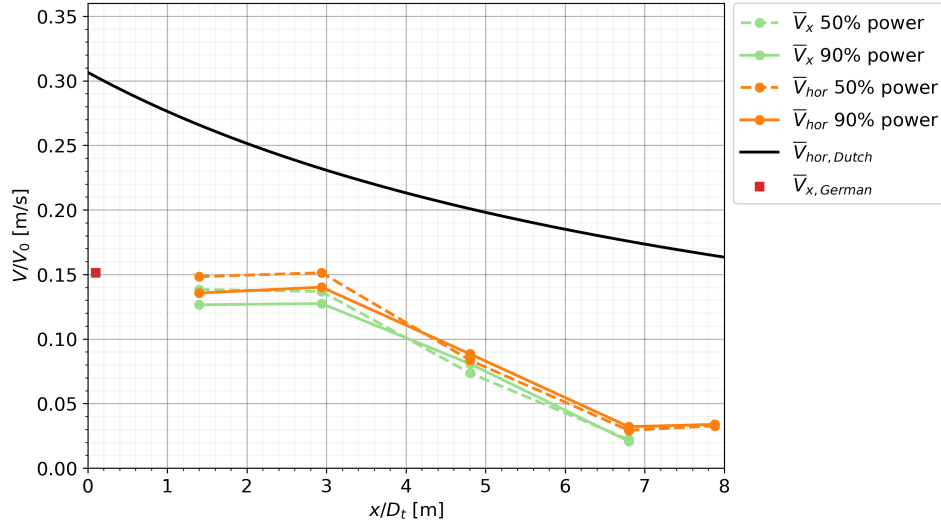
Figure 6.6: Decay of the relative near-bed flow velocities in x-direction from the quay wall for Test 18, BT1&2 L_{BT}/D_t = 6.12. $\overline{V}_x$ and $\overline{V}_{hor}$ at 50% and 90% power are compared with $\overline{V}_{hor,Dutch}$ and $\overline{V}_{x,German}$ respectively.

Table 6.12: Overview of the relative near-bed flow velocities ($\overline{V}_x/V_0$ and $\overline{V}_{hor}/V_0$) for Test 18 (BT1&2, L_{BT}/D_t = 6.12) measured by ADV1-4 and Ott2 at 50% and 90% power compared with $\overline{V}_{hor,Dutch}/V_0$ and $\overline{V}_{x,German}/V_0$.

	$x/D_t = 0$ [-]	ADV1 $x/D_t = 1.40$ [-]	ADV2 $x/D_t = 2.94$ [-]	ADV3 $x/D_t = 4.81$ [-]	ADV4 $x/D_t = 6.81$ [-]	Ott2 $x/D_t = 7.90$ [-]
$\overline{V}_x/V_0$ 50% [-]	-	0.14	0.14	0.07	0.02	-
$\overline{V}_x/V_0$ 90% [-]	-	0.13	0.13	0.08	0.02	-
$\overline{V}_{hor}/V_0$ 50% [-]	-	0.15	0.15	0.08	0.03	0.03
$\overline{V}_{hor}/V_0$ 90% [-]	-	0.14	0.14	0.09	0.03	0.03
$\overline{V}_{hor,Dutch}/V_0$ [-]	0.31	0.27	0.23	0.2	0.17	0.16
$\overline{V}_{x,German}/V_0$ [-]	0.15	-	-	-	-	-

In Table 6.13 the ratio of $\overline{V}_{hor}$ over $\overline{V}_x$ as well as the ratio of the Dutch method ($\overline{V}_{hor,Dutch}$) over the measured values for $\overline{V}_{hor}$ for Test 18 are determined. Showing that $\overline{V}_{hor}$ is between 7-54% higher than $\overline{V}_x$ with an average value of 18%. The Dutch method results in 1.53-6 times higher flow velocities than the measured values for $\overline{V}_{hor}$. The largest difference is observed at ADV4 and Ott2 while for ADV2 at 50% power the Dutch method is only a factor of 1.53 higher than the measured values for $\overline{V}_{hor}$. The German method ($\overline{V}_{x,German}$) overestimates the highest measured value for $\overline{V}_x$ at ADV1 (x/D_t = 1.4) during the 50% power step with a factor of 1.07 (Table 6.12).

Table 6.13: Overview of the ratio for the relative near-bed flow velocity $\overline{V}_{hor}/\overline{V}_x$ and $\overline{V}_{hor,Dutch}/\overline{V}_{hor}$ for Test 18 (BT1&2, L_{BT}/D_t = 6.12) measured by ADV1-4 and Ott2 at 50% and 90% power.

	ADV1 x/D$_t$ = 1.40 [-]	ADV2 x/D$_t$ = 2.94 [-]	ADV3 x/D$_t$ = 4.81 [-]	ADV4 x/D$_t$ = 6.81 [-]	Ott2 x/D$_t$ = 7.90 [-]	Average [-]
$\overline{V}_{hor}$ / $\overline{V}_x$ 50% [-]	1.07	1.11	1.14	1.32	-	1.16
$\overline{V}_{hor}$ / $\overline{V}_x$ 90% [-]	1.07	1.1	1.09	1.54	-	1.2
$\overline{V}_{hor,Dutch}$ / $\overline{V}_{hor}$ 50% [-]	1.79	1.53	2.4	6	5.02	3.35
$\overline{V}_{hor,Dutch}$ / $\overline{V}_{hor}$ 90% [-]	1.96	1.65	2.27	5.48	4.85	3.24

Test 20, BT1, L$_{BT}$/D$_t$ = 7.30, h$_t$/D$_t$ = 3.03

The determined flow velocities for Test 20 together with the Dutch method ($\overline{V}_{hor,Dutch}$), German method ($\overline{V}_{x,German}$) and T1 (L_{BT}/D_t = 7.28 and h_t/D_t = 2.18) measurement by Schmidt (1998) ($\overline{V}_{x,Schmidt}$)are plotted in Figure 6.7 and listed in Table 6.14. L_{BT}/D_t = 7.30 of Test 20 is just above the upper limit of L_{BT}/D_t = 7.28 for the applicability of the German method. However, as the difference in minimal the comparison can still be assumed reliable. Close to the quay, the German method and measurement T1 by Schmidt (1998) comply with each other at 0.11 V_0. Moving further from the quay $\overline{V}_{x,Schmidt}$ increases for T1 following the black line of the Dutch method for $\overline{V}_{hor,Dutch}$ between x/D$_t$ = 2-3.5. The German method approaches the measured values for $\overline{V}_x$ very well at ADV1 and ADV2. The Dutch method overestimates the measured values for $\overline{V}_{hor}$ for every values of x/D_t. The difference between the Dutch method and ADV4 and Ott2 is most significant with the Dutch method not resembling the same decay in flow velocities as the measurements in Gent.
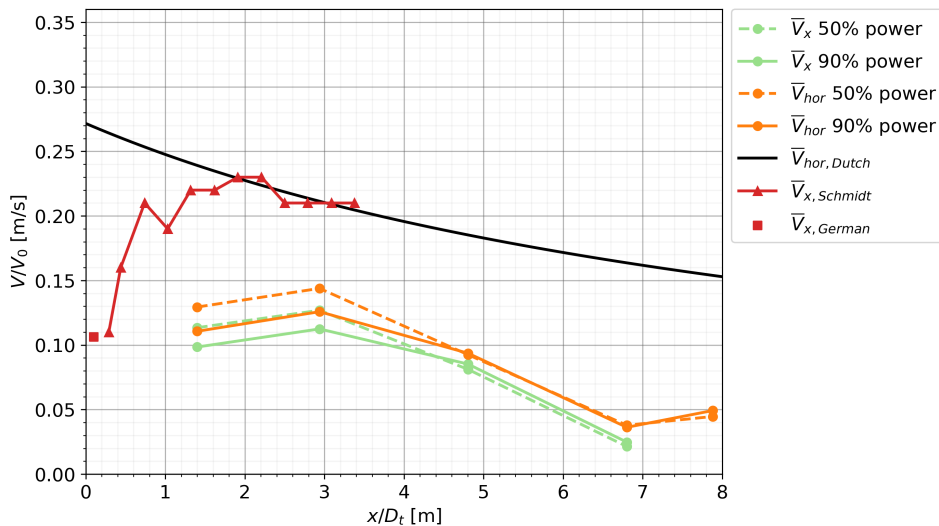

Figure 6.7: Decay of the relative near-bed flow velocities in x-direction from the quay wall for Test 20, BT1 L_{BT}/D_t = 7.30, h_t/D_t = 3.03. $\overline{V}_x$ and $\overline{V}_{hor}$ at 50% and 90% power are compared with $\overline{V}_{x,German}$ and $\overline{V}_{hor,Dutch}$. In addition, $\overline{V}_x$ is compared to measurement T1 by Schmidt (1998) ($\overline{V}_{x,Schmidt}$) with L_{BT}/D_t = 7.28 and h_t/D_t = 2.18.

Table 6.14: Overview of the relative near-bed flow velocities ($\overline{V}_x/V_0$ and $\overline{V}_{hor}/V_0$) for Test 20 (BT1, L_{BT}/D_t = 7.30, h_t/D_t = 3.03) measured by ADV1-4 and Ott2 at 25%, 50% and 90% power compared with $\overline{V}_{hor,Dutch}/V_0$,$\overline{V}_{x,German}/V_0$ and $\overline{V}_{x,Schmidt}/V_0$ for measurement T1 (L_{BT}/D_t = 7.28, h_t/D_t = 2.18).

	$x/D_t = 0$ [-]	ADV1 $x/D_t = 1.40$ [-]	ADV2 $x/D_t = 2.94$ [-]	ADV3 $x/D_t = 4.81$ [-]	ADV4 $x/D_t = 6.81$ [-]	Ott2 $x/D_t = 7.90$ [-]
$\overline{V}_x/V_0$ 50% [-]	-	0.11	0.13	0.08	0.02	-
$\overline{V}_x/V_0$ 90% [-]	-	0.1	0.11	0.09	0.02	-
$\overline{V}_{hor}/V_0$ 50% [-]	-	0.13	0.14	0.09	0.04	0.04
$\overline{V}_{hor}/V_0$ 90% [-]	-	0.11	0.13	0.09	0.04	0.05
$\overline{V}_{hor,Dutch}/V_0$ [-]	0.27	0.24	0.21	0.19	0.16	0.15
$\overline{V}_{x,German}/V_0$ [-]	0.11	-	-	-	-	-
$\overline{V}_{x,Schmidt}/V_0$ [-]	0.11	0.22	0.21	-	-	-

In Table 6.15 the ratio of $\overline{V}_{hor}$ over $\overline{V}_x$ and $\overline{V}_{hor,Dutch}$ over the measured values for $\overline{V}_{hor}$ is determined for Test 20. The difference between $\overline{V}_{hor}$ and $\overline{V}_x$ ranges between 10-77% with an average of 25%. The Dutch method is between 1.47-4.51 times higher than the measured values for $\overline{V}_{hor}$. With the biggest factor between the two at ADV4 and Ott2 whereas close to the quay the smallest difference is observed. The German method ($\overline{V}_{x,German}$) underestimates the highest measured value for $\overline{V}_x$ at ADV2 (x/D_t = 2.94) during the 50% power step with a factor of 0.85 (Table 6.12).

Table 6.15: Overview of the ratio for the relative near-bed flow velocity $\overline{V}_{hor}/\overline{V}_x$ and $\overline{V}_{hor,Dutch}/\overline{V}_{hor}$ for Test 20 (BT1, L_{BT}/D_t = 7.30) measured by ADV1-4 and Ott2 at 50% and 90% power.

	ADV1 $x/D_t = 1.40$ [-]	ADV2 $x/D_t = 2.94$ [-]	ADV3 $x/D_t = 4.81$ [-]	ADV4 $x/D_t = 6.81$ [-]	Ott2 $x/D_t = 7.90$ [-]	Average [-]
$\overline{V}_{hor} / \overline{V}_x$ 50% [-]	1.14	1.13	1.14	1.77	-	1.3
$\overline{V}_{hor} / \overline{V}_x$ 90% [-]	1.12	1.12	1.1	1.46	-	1.2
$\overline{V}_{hor,Dutch} / \overline{V}_{hor}$ 50% [-]	1.85	1.47	2	4.32	3.45	2.62
$\overline{V}_{hor,Dutch} / \overline{V}_{hor}$ 90% [-]	2.16	1.68	1.98	4.51	3.12	2.69

Test 21, BT1&2, L_{BT}/D_t = 7.99, h_t/D_t = 3.03

For Test 21 the flow velocities determined from the measurements in Gent are plotted in Figure 6.8 and listed in Table 6.16 along with the Dutch ($\overline{V}_{hor,Dutch}$) and German ($\overline{V}_{x,German}$) method. Test 21 has a value for L_{BT}/D_t = 7.99 falling outside of the applicability range for the German method. As observed for the other measurements with a large value for L_{BT}/D_t, the German methods results in similar values for $\overline{V}_x$ as measured in Gent. However, for L_{BT}/D_t = 7.99 the German method slightly underestimates the highest values for $\overline{V}_x$ measured at ADV1 and ADV2. The Dutch method overestimates $\overline{V}_{hor}$ at every measurement point with the smallest discrepancy found between the Dutch method and measured values for $\overline{V}_{hor}$ at ADV2.
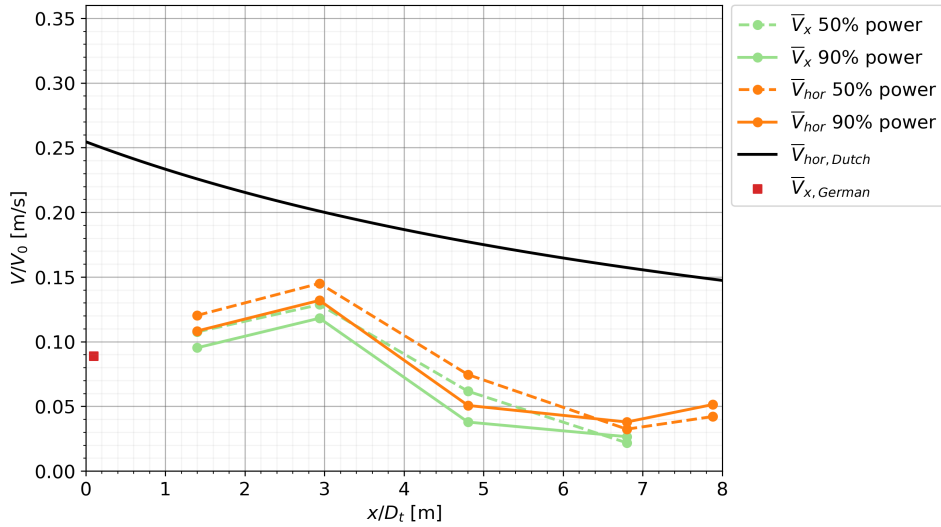
Figure 6.8: Decay of the relative near-bed flow velocities in x-direction from the quay wall for Test 21, BT1&2 L_{BT}/D_t = 7.99. $\overline{V}_x$ and $\overline{V}_{hor}$ at 50% and 90% power are compared with $\overline{V}_{hor,Dutch}$ and $\overline{V}_{x,German}$ respectively.

Table 6.16: Overview of the relative near-bed flow velocities ($\overline{V}_x/V_0$ and $\overline{V}_{hor}/V_0$) for Test 21 (BT1&2, L_{BT}/D_t = 7.99) measured by ADV1-4 and Ott2 at 50% and 90% power compared with $\overline{V}_{hor,Dutch}/V_0$ and $\overline{V}_{x,German}/V_0$.

	x/D$_t$ = 0 [-]	ADV1 x/D$_t$ = 1.40 [-]	ADV2 x/D$_t$ = 2.94 [-]	ADV3 x/D$_t$ = 4.81 [-]	ADV4 x/D$_t$ = 6.81 [-]	Ott2 x/D$_t$ = 7.90 [-]
$\overline{V}_x/V_0$ 50% [-]	-	0.11	0.13	0.06	0.02	-
$\overline{V}_x/V_0$ 90% [-]	-	0.1	0.12	0.04	0.03	-
$\overline{V}_{hor}/V_0$ 50% [-]	-	0.12	0.15	0.07	0.03	0.04
$\overline{V}_{hor}/V_0$ 90% [-]	-	0.11	0.13	0.05	0.04	0.05
$\overline{V}_{hor,Dutch}/V_0$ [-]	0.25	0.23	0.2	0.18	0.16	0.15
$\overline{V}_{x,German}/V_0$ [-]	0.09	-	-	-	-	-

In Table 6.17 the ratio of $\overline{V}_{hor}$ over $\overline{V}_x$ and $\overline{V}_{hor,Dutch}$ over the measured values for $\overline{V}_{hor}$ is determined for Test 21. $\overline{V}_{hor}$ is between 12-48% larger than $\overline{V}_x$ with an average value of 24%. The Dutch method is between 1.38-4.86 times larger than the measured values for $\overline{V}_{hor}$ in Gent. Especially at ADV4 and Ott2 the discrepancy between the two is significantly large although with increasing values for L_{BT}/D_t the difference between the Dutch method and the measurements becomes less. The German method ($\overline{V}_{x,German}$) underestimates the highest measured value for $\overline{V}_x$ at ADV2 (x/D$_t$ = 2.94) during the 50% power step with a factor of 0.70 (Table 6.12).

Table 6.17: Overview of the ratio for the relative near-bed flow velocity $\overline{V}_{hor}/\overline{V}_x$ and $\overline{V}_{hor,Dutch}/\overline{V}_{hor}$ for Test 21 (BT1&2, L_{BT}/D_t = 7.99) measured by ADV1-4 and Ott2 at 50% and 90% power.

	ADV1 x/D$_t$ = 1.40 [-]	ADV2 x/D$_t$ = 2.94 [-]	ADV3 x/D$_t$ = 4.81 [-]	ADV4 x/D$_t$ = 6.81 [-]	Ott2 x/D$_t$ = 7.90 [-]	Average [-]
$\overline{V}_{hor}$ / $\overline{V}_x$ 50% [-]	1.12	1.13	1.21	1.48	-	1.23
$\overline{V}_{hor}$ / $\overline{V}_x$ 90% [-]	1.14	1.12	1.34	1.43	-	1.25
$\overline{V}_{hor,Dutch}$ / $\overline{V}_{hor}$ 50% [-]	1.88	1.38	2.38	4.86	3.52	2.8
$\overline{V}_{hor,Dutch}$ / $\overline{V}_{hor}$ 90% [-]	2.09	1.52	3.49	4.15	2.88	2.83

6.4. Relative turbulence intensity

In the German and Dutch method, the turbulence intensities are not taken into account in determining the flow velocity load on the bed. As previously described, the flow velocity load is determined by the mean flow velocity in x-direction (German) or horizontal direction (Dutch). However, as the turbulence intensities are for a large part responsible for the hydraulic load on the bed, the relative turbulence intensities for the measurement tests considered in this chapter during 90% power are plotted together with the mean turbulence intensity of 0.3 determined from the field measurements by Blokland (1996) in Figure 6.9. It can be concluded that the measurements in Gent have a larger mean relative turbulence intensity for every measurement position compared to the mean relative turbulence intensity determined from the measurements by Blokland (1996). This can be explained due to the low sampling frequency of the measurement instruments that Blokland (1996) used during his field measurements. Similar to the Ott meter not being able to accurately measure the standard deviations during the measurements in Gent. It must be noted however that the average relative turbulence intensity by Blokland (1996) is extrapolated over the distance x from the quay wall to be compared with the Gent measurements. Furthermore, for the measurements by Schmidt (1998), which forms the basis of the German method, no values for the standard deviations were published in his research.
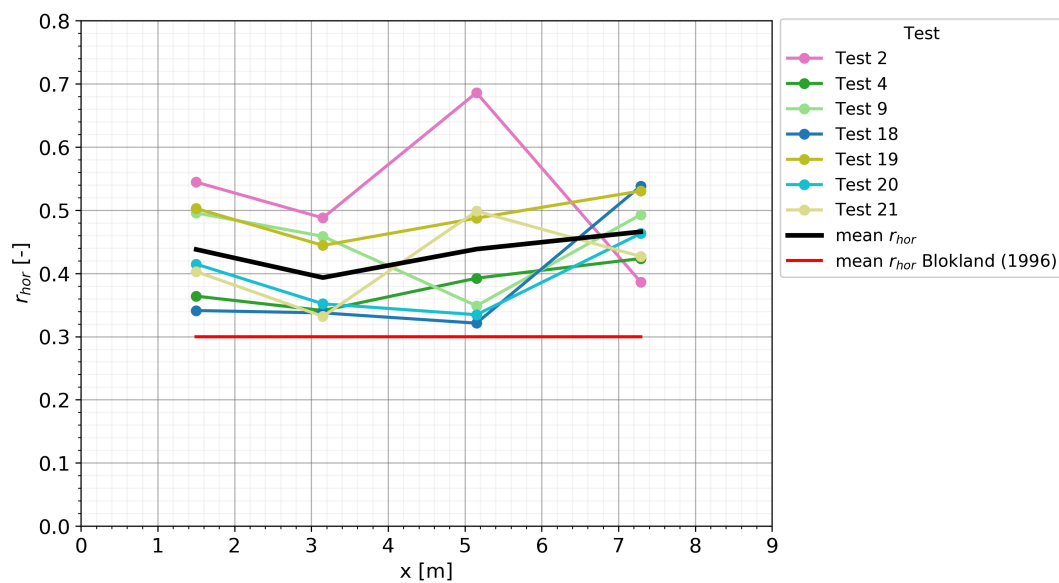
Figure 6.9: Relative turbulence intensity of the considered measurement tests in this chapter during 90% power compared to the mean relative turbulence intensity measured by Blokland (1996).

6.5. Flow velocity dependency on total distance travelled by the jet

The Dutch method gives a relation between the total travelled distance ($x_s = L_{BT} + h_t + x$) by the jet and the mean horizontal near-bed flow velocity ($\overline{V}_{hor,Dutch}$) for ($L_{BT}+x$)/h_t > 1.8 (Equation 6.3). Where L_{BT} is the quay wall clearance of the bow thruster, x the distance perpendicular to the quay wall where the flow velocities are determined and h_t the height of the bow thruster axis above the bed (Figure 6.10). In Figure 6.11 and 6.12 the Dutch method is plotted together with the measurement tests discussed in this chapter. Where $\overline{V}_{hor}/V_0$ is plotted against x_s/D_t, the total distance travelled x_s per measurement test divided by the diameter of a single bow thruster D_t. The condition of ($L_{BT}+x$)/h_t > 1.8 for Equation 6.3 is satisfied for approximately x_s/D_t > 8.5 from which the Dutch method starts to decay for larer values of x_s/D_t (Figure 6.11 and 6.12).
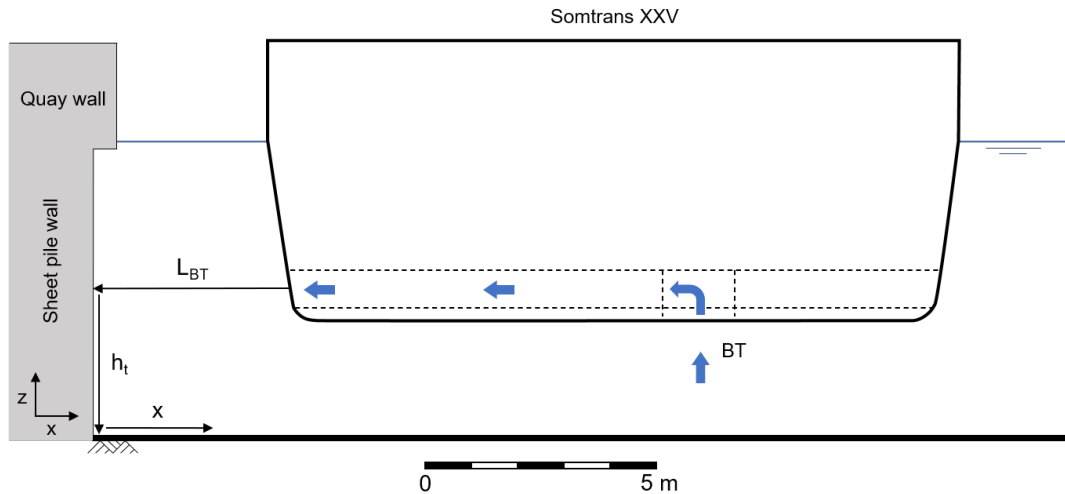
Figure 6.10: Illustration of the total distance travelled by the jet (x_s). Defined as the sum of the bow thruster quay wall clearance (L_{BT}), the height of the bow thruster axis above the bed (h_t) and the perpendicular distance x from the quay wall where the measurement point is located.

As concluded from the previous section, the Dutch method overestimates the values for $\overline{V}_{hor}$ at every power step. Analyzing the dependency on x_s for the Dutch method and the measurements in Gent leads to the observation that the Dutch design method does not correctly incorporates the dependency of the flow velocities on the distance x from the quay wall. As according to the dependency of the Dutch method on the total travelled distance x_s it is expected that the flow velocity of the considered tests would comply with each other for a similar value of x_s/D_t. However, the overlapping of the tests for comparable values of x_s/D_t is not observed. Thus, the Dutch design method leads to an overestimation of the flow velocity as the strong decline in flow velocity observed during the measurements in Gent for increasing values of x from the quay wall is not correctly included in the Dutch method. The assumption of a summation of L_{BT}, h_t and x to determine the decay in flow velocity is therefore not correct (based on the results from Gent) as the flow velocity decay is not equally dependent on L_{BT} and x (h_t was constant throughout the measurements). A more accurate definition for the flow velocity decay based on x would lead to a better formulae to determine the near-bed flow velocities at various distances x from the quay wall.
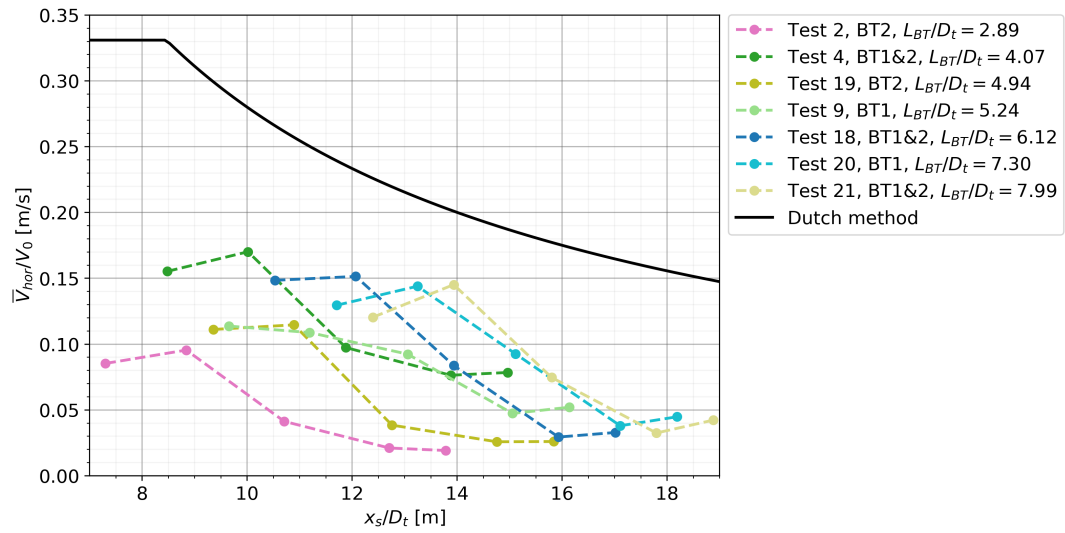
Figure 6.11: Comparison between the measurement tests ($\overline{V}_{hor}$) during 50% power based on the total distance travelled by the jet (x_s) in relation to the Dutch method ($\overline{V}_{hor,Dutch}$).
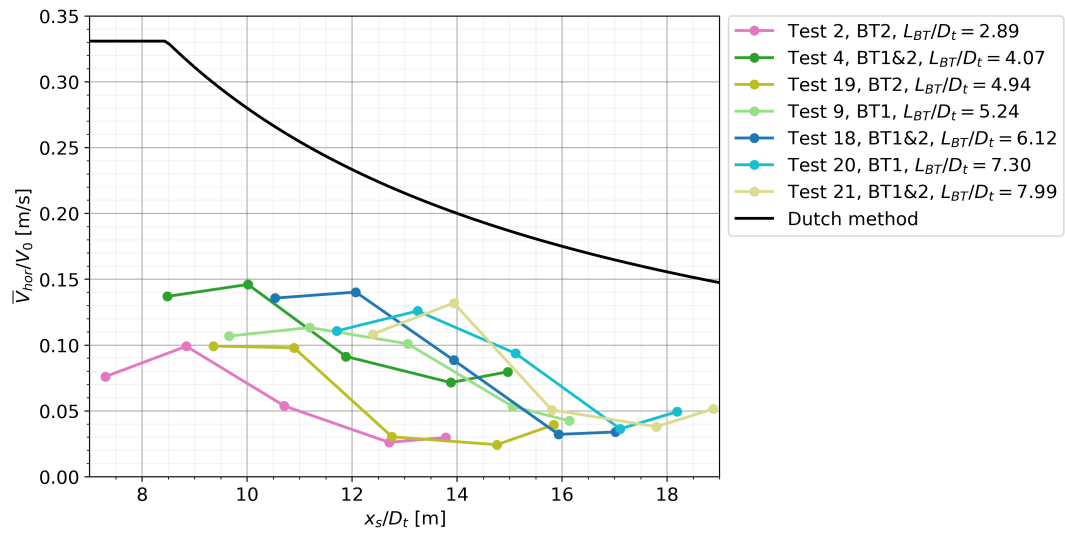
Figure 6.12: Comparison between the measurement tests ($\overline{V}_{hor}$) during 90% power based on the total distance travelled by the jet (x_s) in relation to the Dutch method ($\overline{V}_{hor,Dutch}$).

6.6. Conclusions

Comparison of the near-bed flow velocity in horizontal ($\overline{V}_{hor}$) and x-direction ($\overline{V}_x$)

For every test the mean flow velocity near the bed is determined in x-direction ($\overline{V}_x$) and in horizontal direction ($\overline{V}_{hor}$) complying with the definitions used for the German ($\overline{V}_{x,German}$) and Dutch method ($\overline{V}_{hor,Dutch}$). Measuring in horizontal direction (resultant of x and y component) results in 5-77% higher mean flow velocities in respect to only measuring in x-direction with an average of 25%. Showing that measuring in x-direction results in an average underestimation of the flow velocity near the bed of 25%.

German method ($\overline{V}_x$)

The German method only determines a value for the flow velocity at the intersection between the quay wall and the bed. The decay in flow velocity over increasing values x/D_t from the quay is therefore not resolved. However, as the German method is based on the upper limit of the measurements for $\overline{V}_x$ conducted by Schmidt (1998) (up to position 2 the intersection of the quay wall and the bed Figure 6.1) it can be compared to the highest measured flow velocities for $\overline{V}_x$ at ADV1 and ADV2. The German method shows a strong dependency on L$_{BT}$ rapidly declining in values for $\overline{V}_{x,German}$ with an increasing quay wall clearance of the bow thruster (L$_{BT}$). Declining from 0.66 V$_0$ for L$_{BT}$/D_t = 2.89 (Test 2) towards 0.09 V$_0$ for L$_{BT}$/D_t =7.99 (test 21). For values of L$_{BT}$/D_t of 5.24 or smaller (Test 2, 4, 19 and 9) the German method overestimates the measurement results with a factor 6 (Test 2), 2.13 (Test 4) , 2.56 (Test 19) and 2.1 (Test 9). At L$_{BT}$/D_t = 6.12 (Test 18) the German method ($\overline{V}_{x,German}$) corresponds well with the upper limit of $\overline{V}_x$ measured at ADV1 and ADV2 overestimating with only 7%. Increasing further towards L$_{BT}$/D_t = 7.30 and 7.99 (Test 20 and 21) the German method underestimates the measured values for $\overline{V}_x$ with 15 and 30% respectively.

Near-bed measurements by Schmidt (1998)

The near-bed measurements (R5, S4 and T1) by Schmidt (1998) show a rapid increase in $\overline{V}_{x,Schmidt}$ for increasing values of x/D_t. This is inline with the fifth zone of the wall jet reflecting on the bed, after which dynamic pressures are transformed back to kinetic energy while moving away from the quay wall (Section 2.3). At approximately x/D_t = 1 the maximum flow velocities are found by Schmidt (1998) after which the flow velocities rapidly decrease towards x/D_t = 3.4, the furthest measurement point of Schmidt (1998). Contrary to the measurements in Gent where for most of the tests higher flow velocities were measured at ADV2 (x/D_t = 2.94) than at ADV1 (x/D_t = 1.4). Leading to the conclusion that the flow velocity is still increasing between ADV1 and ADV2 for the Gent measurements. T1 is an exception to this previous descibred pattern, displaying a relatively constant flow level between x/D_t = 1.2 and 3.4. In magnitude, only during Test 4 (Gent) R5 from Schmidt (1998) complies reasonably well with the measured values for $\overline{V}_x$ at $x/D_t \approx 3$. Comparing the near-bed measurements by Schmidt (1998) to the German method results only in a similar maximum for R5 (L$_{BT}$/D_t = 4.07, h$_t$/D_t = 2.91). For larger quay wall clearances (L$_{BT}$) Schmidt (1998) measured higher values for $\overline{V}_{x,Schmidt}$ at a distance x from the quay wall than $\overline{V}_{x,German}$ at the intersection of the quay wall and the bed. An explanation for this can be found in the transition of kinetic energy to dynamic pressures as the jet approaches the bed decelerating the flow. Therefore, the total load of the jet at the intersection of the bed and the quay wall can be higher, but the measured values of $\overline{V}_{x,German}$ lower than measured for $\overline{V}_{x,Schmidt}$ as the flow velocity accelerates again after reflection on the bed (Figure 2.8).

Dutch method ($\overline{V}_{hor}$)

Comparing the Dutch method ($\overline{V}_{hor,Dutch}$) to the measured values for $\overline{V}_{hor}$ in Gent results in an overestimation of the flow velocity for every test. The Dutch method results in a value for the maximum measured $\overline{V}_{hor}$ at a certain distance x from the quay wall dependent on the total distance traveled by the jet based on the sum of L$_{BT}$, h$_t$ and x (the distance from the quay wall). However, the strong decline in $\overline{V}_{hor}$ after ADV2 observed during the measurements in Gent is not reflected by the Dutch method. Resulting in an overall increase in mismatch between the Dutch method and the measurement results for ADV3 and ADV4 until Ott2 when the difference between $\overline{V}_{hor,Dutch}$ and $\overline{V}_{hor}$ becomes less. When plotting the tests as function of the total travelled distance of the jet (x$_s$) the magnitudes of $\overline{V}_{hor}$ for the measurements do not overlap each other for similar values of x$_s$, showing that the decline in $\overline{V}_{hor}$ is not

equally dependent on L_{BT} and x (h_t was constant throughout the tests). Therefore, the Dutch method does not correspond to the flow velocity decay profile observed during the measurement tests in Gent. A more accurate definition for the flow velocity decay based on x would lead to a better formulae to determine the near-bed flow velocities at various distances x from the quay wall. In terms of magnitude, the Dutch method ($\overline{V}_{hor,Dutch}$) is on average 3.7 times larger than $\overline{V}_{hor}$ of the considered tests in this chapter over every measurement point. With Test 4 (BT1&2) having the smallest difference with a factor of 2.47 followed by Test 20 (BT1) with a factor of 2.48. However, this high average is mainly caused by the significant difference in $\overline{V}_{hor,Dutch}$ and $\overline{V}_{hor}$ at the measurement points furthest from the quay wall (ADV3, ADV4 and Ott2). When only considering the highest measured values for $\overline{V}_{hor}$ at ADV2 the Dutch method is on average 2.1 times higher than the measurements in Gent with the smallest discrepancy between the Dutch method and ADV2 for Test 21 during 50% power where the Dutch method is 1.38 times higher than the measured value of $\overline{V}_{hor}$.

7

Discussion & measurement accuracy

In this chapter, the main discussion points for the field measurements (Section 7.1), the pre-processing (Section 7.2) and the measurement results (Section 7.3) are elaborated. Highlighting the limitations of the measurement set-up and programme, assumptions made in the data analyses and uncertainties in the measurement results.

7.1. Field measurements

Spatial resolution of the measurement points in x-direction

Field measurements induce limitations on the number of measurement instruments and position of the instruments with respect to the quay wall, the bed and the vessel. Based on the recommendations by Cantoni (2020) a higher spatial resolution for the measurements was adopted in the set-up. The velocity was measured at five locations with a spacing varying from 1.5 to 2 m. The three ADCPs, also measuring the flow velocity although not analysed in this research, have a resolution of 0.2 m in the direction of the velocity component in which they measured. Even though the higher spatial resolution results in more accurate measurements of the decay in flow velocity, the highest flow velocities induced by the bow thruster jet could still be missed by the single point measurement locations of the ADVs and Ott meters. In the measurements by Blokland (1996) the highest flow velocities were measured at 0.8 D_t (x = 2 m) while Schmidt (1998) measured the highest flow velocities for his near-bed measurements at 0.9 D_t (x = 6.1 cm). Both measuring higher mean flow velocities than observed in the field measurements in Gent. The highest flow velocities in Gent were measured at 2.94 D_t (x = 3.15 m, second measurement point) closely followed by the first measurement point at 1.4 D_t (x = 1.5 m). Showing a discrepancy between the locations where the maximum flow velocity is measured near the quay wall in comparison to Blokland (1996) and Blokland (1996). Leading to the thought that either the highest flow velocities are not measured during the field measurements in Gent at the ADV and Ott meter measurement locations or there is a discrepancy between the measured flow velocities in Gent and those measured by Schmidt (1998) and Blokland (1996). In addition, to accurately compare the measured mean flow velocities with the German method an extra measurement point should be placed directly at the intersection of the bed and the quay wall. Also measuring the dynamic pressure fluctuations at this point to capture the total load (flow velocity and pressure) on the bed at the intersection of the quay wall and the bed where most scour occurs according to literature. Providing valuable information on the conversion of kinetic energy to dynamic pressure (and vice versa) in this area as discussed in Section 2.3 for the relevant zones of the flow field. To conclude, the spatial resolution in x-direction adopted in the measurement set-up in Gent resulted in adequate measurements of the velocity decay profile. However, in comparison to literature there is a discrepancy between the locations were the maximum flow velocity is measured which is recommended to be further researched.

Spatial resolution of the measurement points in y-direction
The instruments measuring the flow velocity were placed on a horizontal frame in line with each other in x-direction perpendicular to the quay wall. By moving the vessel with respect to the measurement frame in y-direction extra spatial points were created to capture the maximum flow velocities when the jet reflects under an angle with the quay wall as highlighted by the CFD model by Van Blaaderen (2005). For BT1, BT2 and BT1&2 the flow velocities are measured at y_t = 3.5 m, 2 m, 1.75 m, 0 m, -1.5 m, -1.75 m, -2 m, -3.5 m and 3.75 m. However, not every value of y_t is measured for every bow thruster due to time considerations during the measurements. Therefore, for the comparison between the bow thrusters not always the same value for y_t could be used. In addition, for the vessel positions with L = 3 and 5 m the vessel was not moved along the quay wall resulting in only one value for y_t for these measurements. Thus, more measurements with varying values for y_t are recommended to research the entire flow field over the bed in x- and y-direction. For instance measuring the flow velocity around the bow thruster axis with y_t varying from -5 to 5 m and a spacing of 1 m.

Measurement points location in z-direction
The ADVs measured between 0.24 - 0.36 m in z-direction above the bed while the Ott meters measured at 0.24 m above the bed. Leaving a gap between the bed and the position were the flow velocity is measured. Therefore, the highest flow velocities could be occurring closer to the bed below the measurement locations in z-direction. The relatively high measurement location above the bed of the ADVs and Ott meter is considered one of the most credible reasons that the measured flow velocities are lower than expected. Especially due to the fact that the bed protection, on which the horizontal frame was placed, consists out of asphalt mattresses leading to a lower boundary layer compared to a bed protection made out of rock. However, the measurement frame is made out of scaffolding of 0.05 m thick creating a rougher bed surface increasing the boundary layer. Leaving the question open whether or not the highest flow velocities could have occurred below the measurement points of the ADVs and Ott meters. During the field measurements by Blokland (1996) the flow velocities were measured at a comparable height above the bed of 0.2-0.3 m. Thus, the difference in measured mean horizontal flow velocities between Blokland (1996) and the measurement in Gent can not be attributed to this. Schmidt (1998) measured the flow velocities in a scale model for which the height above the bed where the flow is measured is unknown.

Measurement frames and fixation of the instruments
The horizontal and vertical measurement frames were placed by a diving team and checked for movements halfway through the measurement programme. For the horizontal measurement frame no significant movements were observed. However, the fixation of the vertical measurement frame was slightly loosened and had to be fixated again to the quay wall. The vertical frame was placed against the white stairs (Figure 3.18) resulting in approximately 0.8 m between the heart of the sheet pile wall and the vertical measurement frame (Figure 3.17). Therefore, the flow from the bow thruster reflects not only on the sheet pile wall but also partially against the vertical measurement frame. How this effects the near-bed flow velocities is unknown. In addition, the shape of the sheet pile wall results in a non-uniform reflection on the quay wall. The effect of the sheet pile wall configuration on the jet has not been studied before but could lead to different outcomes compared to a jet reflecting on a straight wall as used in the scale model by Schmidt (1998).

The ADVs and ADCPs are fixed to the horizontal measurement frame by wooden frames as illustrated in Figure 3.23 and 3.24 for the ADVs and Figure 3.26 for the ADCPs. After the frame was retrieved from the bed, rotations of the measurement heads of ADV2, ADV3 and ADV4 were observed in the order of 10-20°. The rotations of ADV2 and ADV3 were around the z axis which does not influence the results of the absolute horizontal flow velocity as these are not dependent on the orientation of the head of the ADV in the horizontal plane. For the analyses of the results of the flow direction, which can be determined from the x and y flow components, the rotation must be kept in mind. The rotation of ADV4 was around the x-axis influencing the y and z velocities. Nonetheless, as the x component is the main component of the horizontal flow velocity (Chapter 6) the effect of the rotation on the horizontal flow velocity at ADV4 is assumed to be small.

Measurement programme test redundancy

In the measurement programme only a few tests were repeated twice or had very similar parameters that they can be considered equivalent to each other. For BT2 Test 5 and Test 8 had the same parameters resulting in a good comparison between the two the determine the redundancy in the data by checking whether the same flow velocities and decay pattern is measured during both tests. In Figure 7.1 the tests are compared for 25% and 90% power leading to similar flow velocities at 90% power with the exception of the first measurement point were a clear mismatch in the flow velocity is observed. Comparing the tests for 25% power, both the first and the second measurement point do not correspond well with each other. However, overall similar magnitudes and a comparable decay pattern are observed for Test 5 and Test 8.
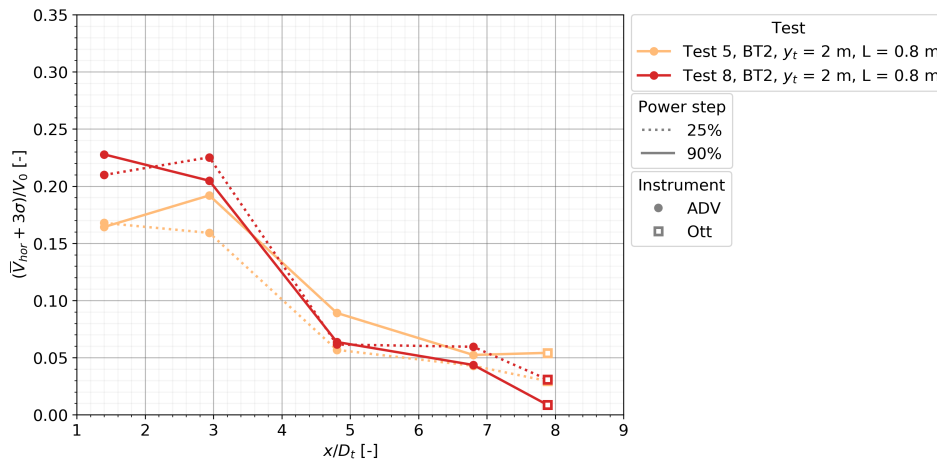
Figure 7.1: Comparison Test 5 and Test 8 at 25% and 90% power.

In Figure 7.2 Test 10 and Test 17 are compared with each other for BT1&2 at 50% power. The value for y_t for the two tests differ slightly with 0.25 m. Nevertheless, the flow velocities correspond reasonably well with each other. Based on 7.2 and 7.1 can be concluded that for the power steps of 50% and 90% the tests resemble each other rather well. Giving confidence that similar flow velocities and decay patterns are measured when a test would be repeated. In addition, by dividing the flow velocities by the efflux velocity V_0 the different power steps of a single test can be used to compare the similarities of the flow velocities and decay pattern as function of V_0. Resulting in very comparable flow velocities observed in Figure 7.1 during Test 9 for 25% and 90% power. Thus, the measurements divided by V_0 as illustrated throughout Chapter 5 and 6 for 25%, 50% and 90% power can be regarded as repetitions of the same test to evaluate their redundancy.
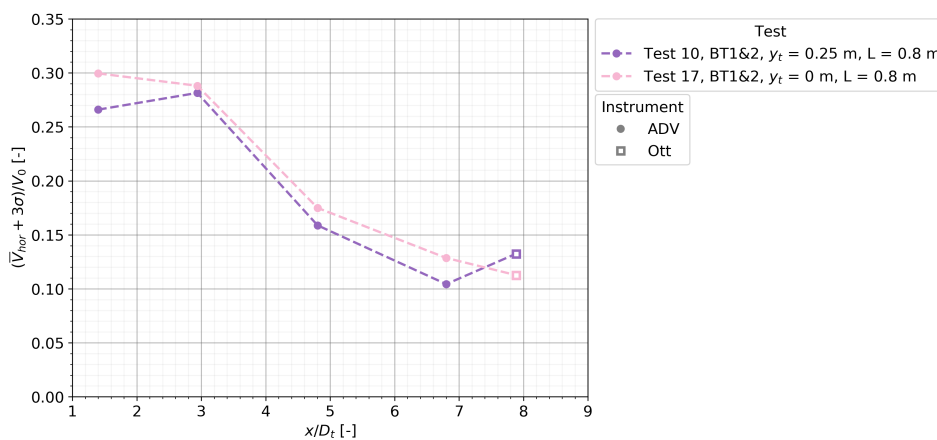
Figure 7.2: Comparison Test 10 and Test 17 at 50% power.

Measurement test duration

In Section 3.7 a measurement duration of 2 min for each power step of the tests was determined based on the characteristic time scale T_c of a turbulent fluctuation at the bed. In 2 min approximately 100 turbulent swirls would pass the measurement instruments giving an adequate measurement of the turbulent flow. However, this is based on the maximum flow velocity near the quay wall. For the instruments further away from the quay the number of turbulent swirls that pass the instrument will be less. To check whether the statistical parameters stay constant over a longer test duration, Test 1 at 50% power is analyzed which measured for a duration of 8 min as illustrated in Figure 7.3 for ADV2 (x = 3.15 m) and Figure 7.4 for ADV4 (x = 7.29 m). For every minute the mean horizontal flow velocity ($\overline{V}_{hor}$) and the standard deviation (σ_{hor}) is determined for ADV2 (Table 7.1) and ADV4 (Table 7.1). These values are then compared with the average values over the whole test duration of 8 min. From Figure 7.3 and Table 7.1 can be concluded that many turbulent swirls pass ADV2 while in the first minute a slightly lower mean flow velocity and standard deviation is observed but overall the statistical values stay rather constant for every minute of the measurement test. However, From Figure 7.4 and Table 7.2 is concluded that the turbulent swirls pass ADV4 at a much slower rate resulting in more variation in $\overline{V}_{hor}$ and σ_{hor}. For ADV4 the magnitudes of the statistical parameters are influenced by whether they measured a peak or a through in the flow velocity during that minute. Therefore, measuring for 2 min results in enough time to give an adequate representation of the magnitudes of $\overline{V}_{hor}$ and σ_{hor} close to the quay wall where the largest flow velocities are measured. However, further away from the quay wall a longer measurement duration is advised to increase the confidence in the measured values for $\overline{V}_{hor}$ and σ_{hor}.
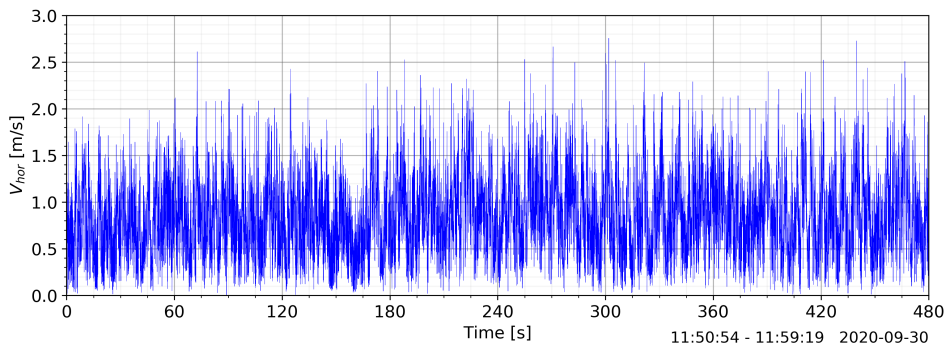
Figure 7.3: Test 1 ADV2 at 50% power during 8 minutes.

Table 7.1: Mean horizontal flow velocity ($\overline{V}_{hor}$) and standard deviation (σ_{hor}) of the 8 minutes measurement of Test 1 ADV2 at 50% power.

Minutes	$\overline{V}_{hor}$	σ_{hor}
Min 1	0.73	0.38
Min 2	0.79	0.40
Min 3	0.73	0.40
Min 4	0.89	0.43
Min 5	0.88	0.44
Min 6	0.84	0.46
Min 7	0.83	0.42
Min 8	0.83	0.43
Average	**0.81**	**0.42**
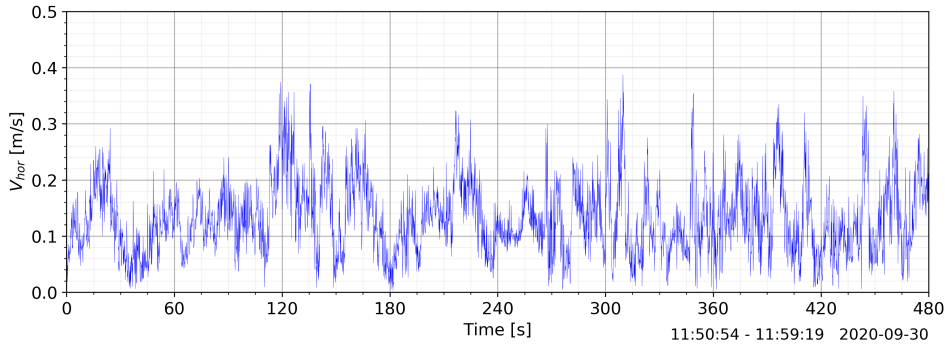
Figure 7.4: Test 1 ADV4 at 50% power during 8 minutes.

Table 7.2: Mean horizontal flow velocity ($\overline{V}_{hor}$) and standard deviation (σ_{hor}) of the 8 minutes measurement of Test 1 ADV4 at 50% power.

Minutes	$\overline{V}_{hor}$	σ_{hor}
Min 1	0.11	0.056
Min 2	0.13	0.053
Min 3	0.16	0.077
Min 4	0.13	0.059
Min 5	0.12	0.050
Min 6	0.12	0.071
Min 7	0.13	0.068
Min 8	0.13	0.068
Average	**0.13**	**0.065**

7.2. Pre-processing of the data

In Chapter 4 the data is pre-processed using several techniques to filter out incorrect data points and noise to increase the confidence level of the retrieved data. In this section the focus is on the filtering on outliers by means of a standard deviation filter (Section 4.1.4) and the noise correction method applied to the standard deviation (Section 4.1.6).

Filtering on outliers with a standard deviation filter
The clear band of outliers observed for the horizontal flow velocity in the range of 4-8 m/s in Figure 7.5 are filtered out from the ADV data sets by means of a standard deviation filter based on ±2σ (Equation 7.1). This approach results in an adequate filtering of the outliers as illustrated by the red dots in Figure 7.5 for Test 4 at 50% power measured with ADV1. However, filtering on 2σ above and below the mean flow velocity might result in maximum flow velocity points being filtered out from the data which are not considered as outliers. In addition, the maximum horizontal flow velocity load on the bed is defined as $V_{max} = \overline{V}_{hor} + 3\sigma_{hor}$ which might seem contradicting to the standard deviation filtering on ±2σ. Nevertheless, there is a significant difference between the standard deviation filter and the definition for V_{max}. The outliers influence the standard deviation of the unfiltered data resulting in values for σ_{hor} on average of 1.3 m/s while σ_{hor} decreases towards an average of 0.35 m/s when the outliers are filtered out. Therefore, there is a large difference in σ_{hor} before and after filtering of the outliers. Although, a different approach could have been chosen for the standard deviation filter by applying a filter with a higher value for σ twice, making sure the maximums in the flow velocity data sets are not filtered out together with the outliers. In Appendix C.2 a comparison is made between the applied 2σ standard deviation filter in this research and a 4σ standard deviation filter implemented twice as filtering on 4σ once does not filter out every outlier. The comparison shows that the influence of both filters on the mean flow velocity and standard deviation are almost identical with a maximal difference of 2% between the two filters. To conclude, applying the 4σ would have been a better choice in respect to

possibly filtering out maximum flow velocities and confusion with the definition for V_{max}. However, the choice for 2σ shows a minimal difference for the mean horizontal flow velocity and standard deviation of the measurement tests. An overview of the standard deviation filter results and comparison is given in Appendix C.2 for ADV1 and ADV2 as the filter is not applied to ADV3 and ADV4 due to no outliers being present in the data set as result of the lower sampling rate internally averaging the data points.

$$\overline{V} - 2\sigma < V_{data} < \overline{V} + 2\sigma \qquad\qquad (7.1)$$
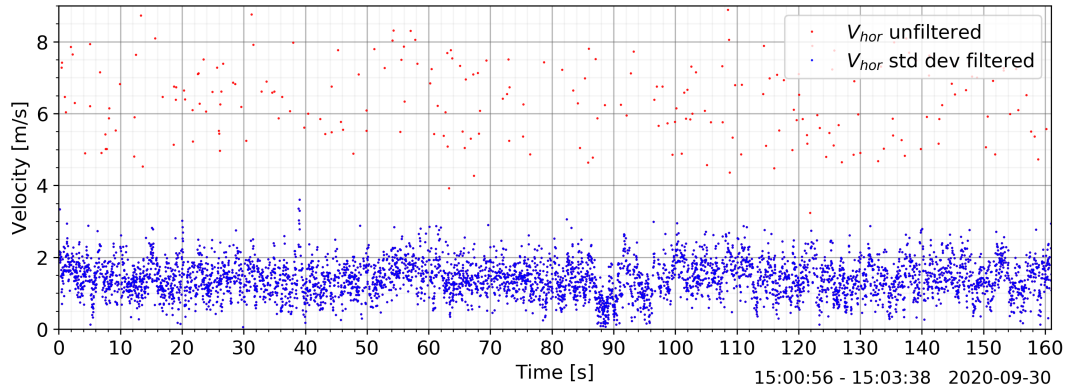
Figure 7.5: Plot of the horizontal flow velocity before and after filtering on standard deviation for Test 4 at 50% power measured with ADV1. In this figure the 2σ filter is applied as used for every measurement test in Section 4.1.4.

Noise correction method

During the zero measurements non-zero standard deviations were measured near the bed by the ADVs while the expectation was that the flow velocities and their fluctuations would be close to zero. Therefore, the measurement data is analyzed in a spectral domain for which a constant energy level is observed while moving towards the higher frequencies. This constant level in the higher frequencies is also observed for the spectral analyses of the measurement tests when the bow thruster was activated (Section 4.1.7). As during the zero measurements there were no vessels sailing through the Moervaart, this constant energy level is assumed to be a constant resulting noise level induced by the ADVs. According to (Durgesh et al., 2014) the resulting noise induced by the ADV is called Doppler noise which is similar to white noise. Measuring with a large velocity range and high sampling frequency leads to high Doppler noise energy levels Huang et al. (2020). To correct for the Doppler noise a correction is applied to measure the determine the correct statistical parameters induced by the bow thruster jet. The variance of the noise level is subtracted from total variance determined for a measurement test leading to a reduction of the standard deviation in the order of 10%. An overview of the standard deviation correction per test is listed in Section C.5. This correction results in lower values for $V_{max} = \overline{V}_{hor} + 3\sigma_{hor}$ as σ is reduced for every measurement test. The optimal settings for the ADV should be analyzed on before hand for further measurements to reduce the effect of the Doppler noise as much as possible. Measuring in a laboratory flume before measuring in the field could help optimize the ADV settings on beforehand. Besides, there are various algorithms available in literature which performance could be tested on the measurement results from Gent to check whether the noise reduction method applied in this thesis correctly reduces σ_{hor}.

7.3. Measurement results

Dimensionless parameters (efflux velocity V_0 and thruster diameter D_t)
The relative flow velocity is determined from the measurement results in Chapter 5 by dividing the measured near-bed flow velocity over the theoretical efflux velocity V_0 determined according to Equation 2.3. The distance from the quay in perpendicular direction (x) from the quay wall were the measurement instruments are positioned are divided by the thruster diameter D_t (= 1.07 m) of a single bow thruster of the Somtrans XXV. The dimensionless parameters lead to a comparison between the decay of the measured flow velocities between the bow thruster outlet and the bed where the flow is measured. In addition, the results for the magnitude of the flow as proportion of V_0 can be compared to results from previous measurements and current guidelines (Chapter 6). However, as the actual efflux velocity is not measured during the measurement tests in Gent, it is based on literature which did not base the relation for the efflux velocity (V_0) on measurements with a 4-channel bow thruster as used in this research. Therefore, using V_0 based on Equation 2.3 could lead to discrepancies with the actual efflux velocity of a 4-channeled bow thruster. In addition, the definition of the efflux velocity V_0 is not clear. Whether V_0 represents an average velocity or maximum flow velocity. Thus, using V_0 to compare the measured flow velocities with previous research and guidelines should be done with care and attention should be payed how V_0 is defined. Field measurements during which both the efflux velocity and the near-bed flow velocities are measured would provide the highest measurement accuracy and confidence in the measured data. Besides, V_0 is determined for BT1&2 based on the principle of quadratic superposition (Equation 5.3) as presented in the PIANC (2015) guidelines. When comparing the measurement results divided by V_0 between tests where one bow thruster is used (BT1 or BT2) and tests where two bow thrusters (BT1&2) are activated, a clear difference in the highest values for the flow velocity is observed. BT1&2 induce significantly higher flow velocities as function of V_0 than BT1 or BT2. This raises the question whether the principle of quadratic superposition for determining V_0 for BT1&2 is accurate as similar flow velocities as function of V_0 are expected for the different bow thrusters.

To compare the distance from the quay wall where the flow velocity is measured to previous research and guidelines, the distance x from the quay wall is divided by the bow thruster diameter D_t. This is a common used method in literature to make the distance x from the quay wall dimensionless. However, a clear definition for the use of D_t when two bow thrusters are activated simultaneously is not found in literature. It is arguable that when using two bow thruster simultaneously the distance from the quay wall (x) should be divided by two times D_t assuming that the two bow thruster are forming one large bow thruster. In Figure 7.6 for Test 17 and 18 where BT1&2 were activated simultaneously x is divided by two times D_t resulting in a shift of the decay profiles towards the quay wall while the distance between the measurement points becomes twice as small. Leading to a much steeper decay in flow velocity between ADV2 and ADV3 in comparison to when x is divided by one D_t for Test 17 and 18 as illustrated in Figure 7.7. The flow decay profiles do not overlap each other for the different bow thrusters as observed in Figure 7.7. Drawing the conclusion that using two times D_t for BT1&2 does not correspond to an accurate representation of the flow velocity decay profile in comparison to BT1 and BT2. Therefore, in this research BT1, BT2 and BT1&2 are divided by the diameter of a single bow thruster (D_t = 1.07 m) to make the plots dimensionless. Research on the use of D_t for comparing different research is recommended. Not only to decide how D_t should be applied when using two bow thrusters but also to check the validity of D_t to compare different research. For instance, by measuring flow velocities in a scale model at fixed locations x with a varying bow thruster diameter D_t.
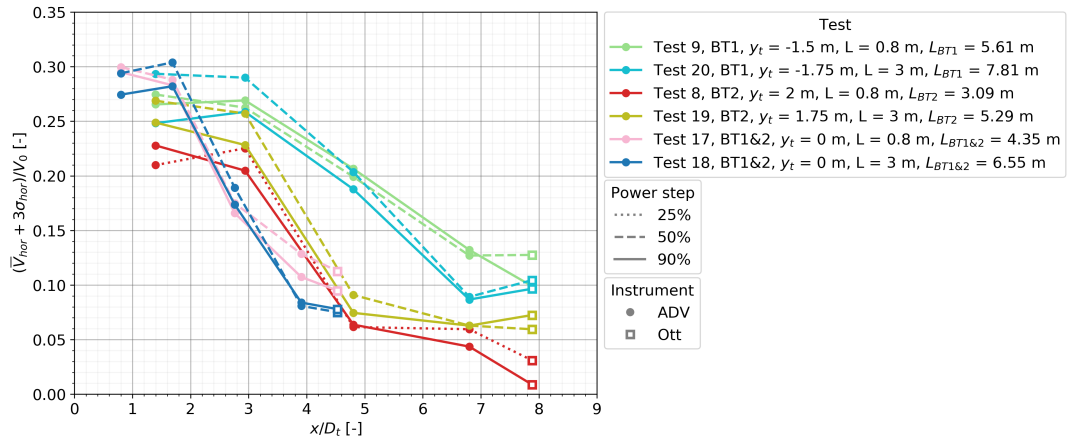
Figure 7.6: Dimensionless comparison of increasing the quay wall clearance from L = 0.8 to 3 m for BT1, BT2 and BT1&2. For BT1&2 two times D_t = 1.07 is used while for BT1 and BT2 only one time D_t = 1.07 is used to make x dimensionless.
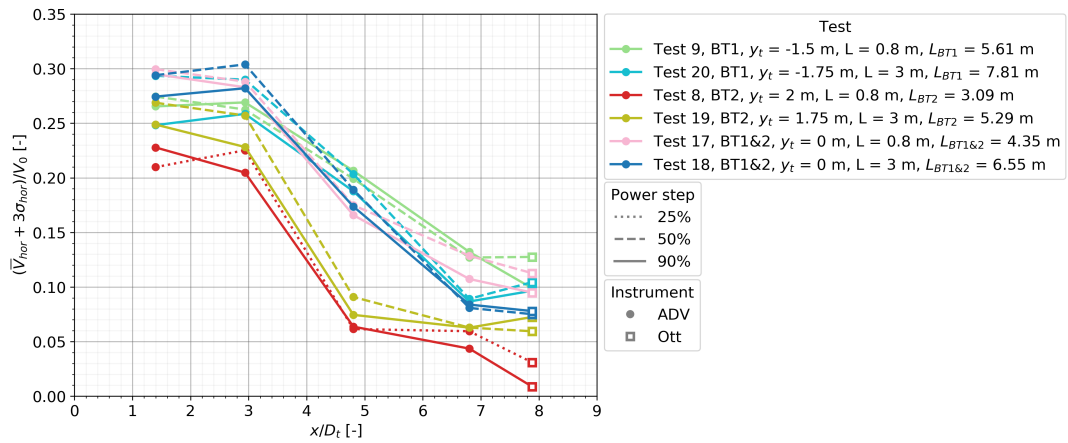
Figure 7.7: Dimensionless comparison of increasing the quay wall clearance from L = 0.8 to 3 m for BT1, BT2 and BT1&2. Using D_t = 1.07 for BT1, BT2 and BT1&2 to make x dimensionless as used throughout this thesis.

Reflection of the jet on the quay wall in y-direction

In Section 5.3 the influence of the distance y_t between the bow thruster axis and the measurement instruments is discussed on the flow velocity decay in perpendicular x-direction from the quay wall. From the measurement results is observed that the decay profile in x-direction is not similar for every measurement test as illustrated in Figure 7.8. Where for every bow thruster two tests are plotted which represent the highest measured values for V_{max} at the different measurement points from the quay wall (x). From Figure 7.8 can be concluded that the highest values for V_{max} per measurement instrument are not measured during one single test with a single value for y_t. For BT1 the highest values for V_{max} at ADV1-4 are measured during Test 9 (y_t = -1.5 m) while the highest value for Ott2 is measured during Test 3 (y_t = -3.5 m). For BT2 the highest values for V_{max} at ADV1-3 are measured during Test 2 (y_t = 0 m) while for ADV4 and Ott2 these are measured during Test 15 (y_t = -2 m). Showing significantly higher values than for Test 2 at ADV4 and Ott2. When BT1&2 are activated simultaneously the highest values for V_{max} are measured at ADV1 and ADV2 during Test 4 (y_t = -1.75 m) while for ADV3, ADV4 and Ott2 the highest values are measured by Test 16 for which y_t = -3.75 m. Although, Test 4 shows a similar pattern and values for V_{max} as Test 16. From these tests can be observed that the highest flow velocities further away from the quay wall are measured for larger values of y_t in negative y-direction indicating that the jet reflects under an angle towards the stern of the vessel (negative y-direction). As a result, the upper limit for the flow velocity per bow thruster and quay wall clearance (L_{BT}) should be a combination of the highest measured value for V_{max} at every specific measurement point. This is not adopted in this research in which the upper limit is defined as one single measurement test which

measured the highest flow velocities close to the quay wall at ADV1 and ADV2 for one specific value of y_t. For BT1 this is Test 9, for BT2 this is Test 2 and for BT1&2 this is Test 4. These tests are then used in Chapter 6 to compare the measured mean flow velocities to previous research and guidelines. Nevertheless, for BT1 and BT1&2 this difference in upper limit does not lead to significant differences in flow velocities as Test 9 (BT1) and Test 4 (BT1&2) measured either the upper limit per measurement instrument or similar values to this upper limit. However, for BT2 Test 2 and Test 15 show a significant difference between the measured flow velocities for ADV4 and Ott2.
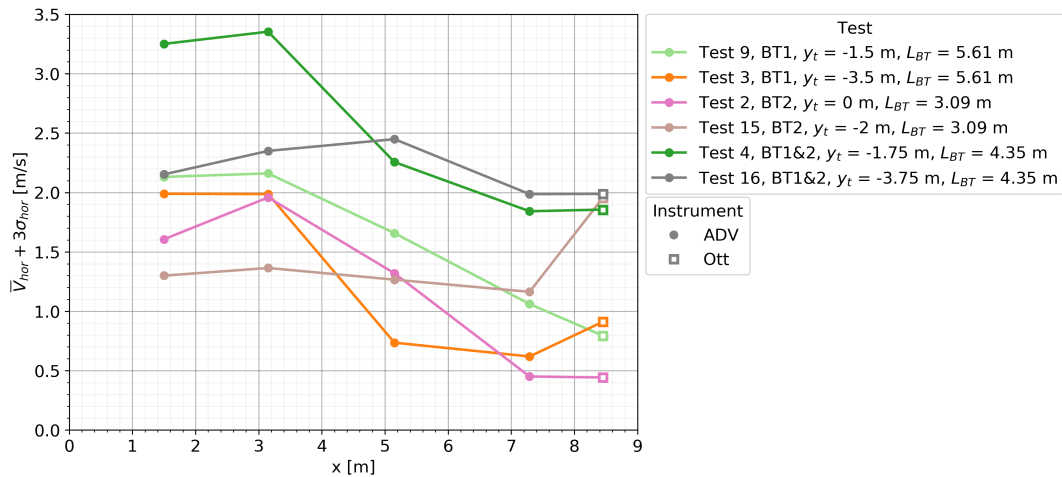
Figure 7.8: Comparison Test 10 and Test 17 at 50% power.

Influence inflow of the bow thruster inlet on the measured near-bed flow velocities
Close to the bow thruster inlet, several tests measure higher flow velocities at Ott2 (x = 8.45 m) than at the previous measurement point, ADV4 (x = 7.29), as illustrated in Figure 7.9 for the mean horizontal flow velocity. Similar to the observations in the research by Cantoni (2020), this is most likely caused by the bow thruster inlet drawing in water to the inlet increasing the mean flow velocity locally. When viewing the Somtrans XXV from above including the matrix of measurement points where the flow velocity is measured for BT1&2 in Figure 7.10, the close proximity of Ott2 near the bow thruster inlets of BT1 and BT2 is observed. For example, Test 17 in teh color pink shows higher flow velocities at Ott2 for both 50% and 90% power (Figure 7.9). When looking at Figure 7.10 for Test 17, Ott2 is positioned in close proximity of the inlet of BT1 agreeing with the theory that the bow thruster inlet causes higher mean flow velocities at Ott2. Whether this applies for every measurement that shows higher mean flow velocities for Ott2 in Figure 7.9 is uncertain. The reflection of the jet on the quay wall as described in the previous paragraph could also be the reason for Ott2 measuring higher mean flow velocities. Therefore, more data is required from the flow field around the bow thruster inlets to determine the area that is affected by the bow thruster inlets. In addition, measuring with an ADV in this area would provide more information on the effect of the inlet on the turbulence which is expected to reduce due to suction of the bow thruster inlet drawing in water. Researching the ADCP measurement data could also provide more knowledge on the flow pattern in this area.
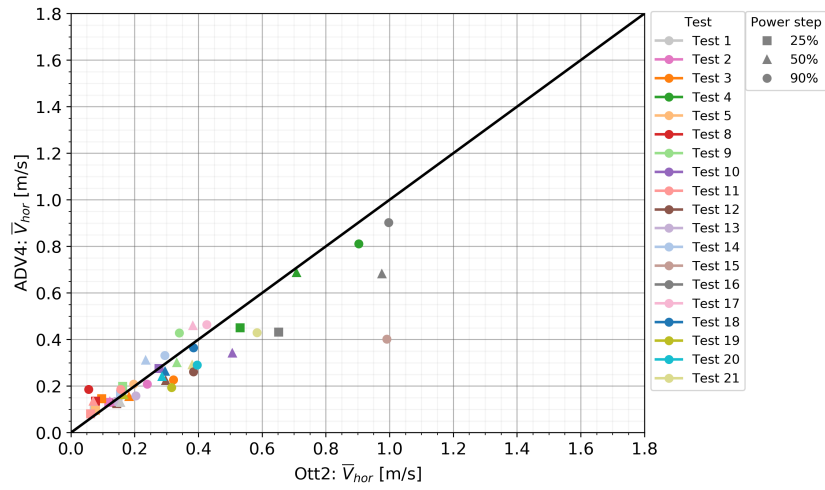
Figure 7.9: Mean horizontal flow velocity ($\overline{V}_{hor}$) of ADV4 compared to Ott2 for 25%, 50% and 90% power. ADV4 is located at x = 7.29 m while Ott2 is positioned at x = 8.45 from the sheet pile wall (quay wall).
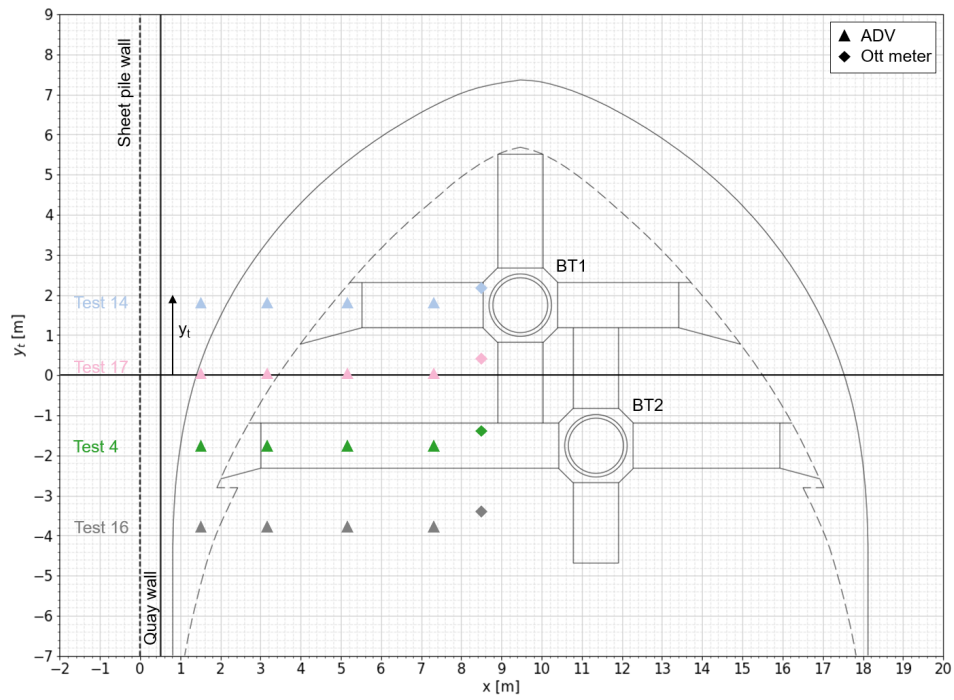
Figure 7.10: Measurement point matrix for ADV1-4 and Ott2 created by moving the vessel in y-direction along the quay wall with respect to the measurement frame. The vessel was moved to y_t = 1.75 m (Test 14), y_t = 0 m (Test 17), y_t = -1.75 m (Test 4) and y_t = -3.75 m (Test 16) in respect to the axis of BT1&2 defined in between BT1 and BT2.

8
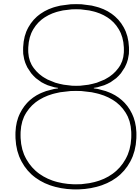
Conclusions & and recommendations

8.1. Conclusions

In this section, an answer is provided to the main research question together with the sub-questions. The main research question of this master thesis is as follows:

"How does the absolute horizontal velocity near the bed induced by the reflected flow of a 4-channel bow thruster on a vertical quay wall decay in perpendicular direction to the quay wall?"

The results from the measurements in Gent show a clear flow velocity decay pattern for almost every measurement while moving in perpendicular direction to the quay wall. The flow velocities were measured at five positions from the quay wall ranging between a spatial resolution of 1.5 m (near the quay) and 2 m (further from the quay). Close to the quay, the highest flow velocities are measured by the first two sensors which generally measure comparable values for the flow velocity resulting in a rather constant level close to the quay wall. Contradicting the research by Blokland (1996) and Schmidt (1998) who concluded that the highest flow velocities are measured in close proximity of the quay wall (within 2 m when their results are applied to this thesis). Moving further from the quay in x-direction, a sharp decline in flow velocities is observed towards the third sensor, displaying that a large proportion of the flow has dissipated between the second and third sensor. This decay pattern is observed for every power step and quay wall clearance of the bow thruster (L_{BT}). Advancing further in perpendicular direction to the quay, the strong decay in flow velocity starts to decline towards a more constant level. However, at the last sensor large deviations in the flow velocity are observed for which higher values than the previous sensor are not uncommon. Contradicting the pattern of the flow velocity decaying while moving away from the quay wall. An explanation can be found in the close proximity of the bow thruster inlets with respect to the last sensor, drawing in water while increasing the flow velocities locally. For two measurements, when the vessel was displaced along the quay with respect to the measurement frame, the above described profile was not observed due to the jet being skewed towards the back (stern) of the vessel. For the standard deviations, a similar decay pattern is observed as for the flow velocities leading to a constant relative turbulence intensity for every sensor. During the berthing manoeuvre measurements, the vessel was moving over the sensors contrary to the moored measurements when the vessel is fixed in a certain position to the quay wall. For the berthing measurements, a similar flow velocity decay profile is observed although lower maximum flow velocities were measured. Giving confidence in the similarities between the moored and berthing manoeuvre measurements. In addition, when the bed protection design is based on the moored measurements a small safety factor is present in the design.

From a design perspective, the measurements at full power are the most interesting as they result in the highest flow velocities and standard deviations. Therefore, an overview of these measurements results for the maximum horizontal flow velocity, defined as the mean horizontal flow velocity plus three times the standard deviation ($\overline{V}_{hor} + 3\sigma$), is illustrated in Figure 8.1 with the bandwidth for the maxima

and minima around the average values per sensor. Close to the quay wall, at the first two sensors, the maximum horizontal flow velocity reaches up to 3.4 m/s with an average of 2.1 m/s. After which the strong decline in the velocity decay profile is observed moving towards the last two sensors where an average maximum flow velocity of 0.85 m/s is observed with values reaching up to 2.0 m/s. Showing a decrease in average maximum horizontal flow velocities of 60% between the first two and the last two sensors.
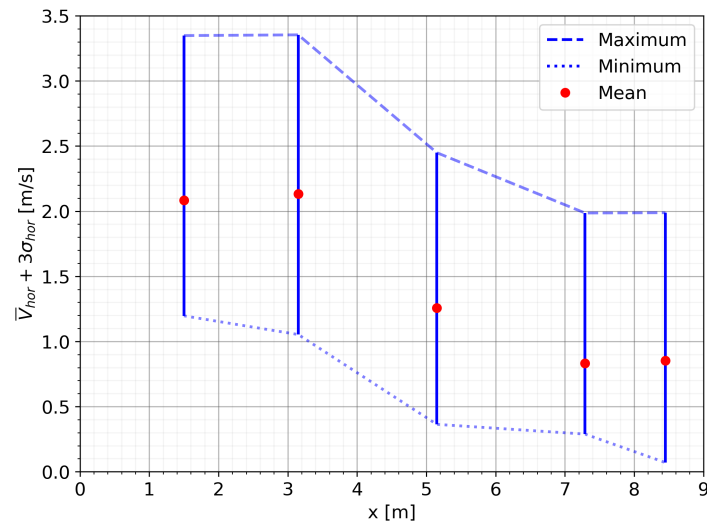
Figure 8.1: Decay profile for the maximum horizontal flow velocity defined as the mean horizontal flow velocity ($\overline{V}_{hor}$) plus three times the standard deviation (σ_{hor}) for the measurements during the 90% power step. The red dot represents the average value per sensor (measurement instrument) while the dashed blue line represents the maximum and the blue dotted line the minimum measured values.

Influence of main variables: applied power (P_t), y_t and quay wall clearance (L_{BT})
During the measurements, three main parameters were changed to study their effect on the decay of the horizontal flow velocity near the bed in perpendicular direction to the quay wall: applied power (P_t), y_t and bow thruster quay wall clearance (L_{BT}).

The applied bow thruster power was increased in three steps measuring the flow velocity at 25%, 50% and 90% power where 90% power corresponded with the bow thruster propeller rotating at its maximum RPM providing the maximum thrust that the engine could deliver. Increasing from 25% power to 50% power results in significantly higher mean flow velocities and standard deviations observed at every sensor. The spreading between the measurement results become larger showing a wider range in mean flow velocities and standard deviations. Rising in power from 50% towards 90% leads to less substantial growth in flow velocities and standard deviations compared with the previous increase in power step. However, the flow velocities, standard deviations and range of these statistical parameters continues to grow. In magnitude, increasing from 25% towards 50% leads to an increase in the mean flow velocity from approximately 0.60 m/s towards 0.90 m/s near the quay wall (on average). Further away from the quay at the last two sensors mean flow velocities increase from 0.20 m/s towards 0.30 m/s (on average). During the 90% power step, the flow velocities close to the quay wall slightly increase towards an average of 1 m/s whereas furthest away from the quay at the last two sensors the flow velocity rises towards 0.40 m/s. As a function of V_0, average values for the mean flow velocity are around 0.1 V_0 close to the quay decreasing to 0.04 V_0 at 8.5 m from the quay wall. The standard deviations increase substantially for every power step with the highest values found close to quay wall with an average of 0.24 m/s for 25% power increasing to 0.4 m/s at 90% power, growing with a total of 43%.

The vessel was moved parallel with the quay during the measurements to create a matrix of measurement points in x- and y-direction over the bed while being moored to the quay wall. By moving the vessel with respect to the horizontal measurement frame the distance between the bow thruster axis and the centerline of the horizontal measurement frame, y_t, is altered to analyse the influence of y_t on the maximum horizontal flow velocities and flow velocity decay profile. Besides, when the jet reflects under an angle from the quay wall the maximum flow velocities of the jet are captured by the instruments during measurements with different values for y_t. Overall the highest flow velocities close to the quay wall can be expected at y_t equals -1.5 m (BT1), -1.75 m (BT1&2) or 0 m (BT2). Further away from the quay wall, the highest or comparable flow velocities are measured for y_t = -2 m and -3.75 m. To conclude, generally higher maximum flow velocities are located towards the stern in negative y-direction. In addition, for increasing distance in x-direction from the quay wall higher maximum flow velocities are located further away from the bow thruster axis towards the stern (negative y-direction).

The vessel has two bow thrusters (BT1 and BT2) with different quay wall clearances L_{BT}, in addition, when activating BT1&2 at the same time there is a combination of the two bow thrusters and their quay wall clearances. Therefore, the average of these two quay wall clearances (L_{BT1} and L_{BT2}) is defined as the quay wall clearance of BT1&2 activated simultaneously ($L_{BT1\&2}$). In order to better analyze the effect of the quay wall clearance, the bow of the vessel is moved from 0.8 m between the port side of the vessel and the quay towards 3 m and 5 m. Resulting in a range of bow thruster quay wall clearances (L_{BT}) between 3.09 m and 8.55 m. For small quay wall clearances (L_{BT} = 3.09 m) an overall increase in flow velocities is observed when L_{BT} is increased while for L_{BT} = 5.61 m and larger, the flow velocities decrease for growing values of L_{BT}. Observing that when one bow thruster is used the highest flow velocities are measured for a quay wall clearance of L_{BT1} = 5.61 m while for two bow thrusters the highest flow velocities are at $L_{BT1\&2}$ = 4.35 m.

Performance measurement set-up
The measurements in Gent were conducted with four different types of measurement instruments (Acoustic Doppler Velocimeters, Acoustic Doppler Current Profilers, Ott meters and pressure sensors) resulting in a complex set-up both in software and hardware. Especially the Acoustic Doppler Velocimeter (ADV) and Acoustic Doppler Current Profiler (ADCP) require experience with the installation of the sensors and determining the correct settings. Perpendicular to the quay wall, the high spatial resolution of the ADVs in combination with the Ott meters resulted in an adequate velocity decay profile. In addition, moving the vessel parallel to the quay wall to create a matrix of measurement points made it possible to capture the maximum flow velocities of the jet even when the jet reflected under an angle from the quay wall. The accuracy of the measured flow velocity by the ADVs was checked by placing an Ott meter next to one of the ADVs resulting in similar mean flow velocities. However, a discrepancy was found between the standard deviations which can be attributed to the low sampling frequency of the Ott meter. Giving redundancy and confidence in the measurement data. The combination of a vertical (at the quay wall) and horizontal measurement frame (on the bed) resulted in a good representation of the pressure fluctuations over the quay wall and the bed including the critical reflection points of the jet. However, not every pressure sensor measured in the direction of the flow making a comparison between the different positions of the pressure sensors rather difficult. For the ADVs, the nominal velocity range and sampling frequency were set too high leading to outliers (spiking) and Doppler noise (comparable to white noise). In addition, from the flow velocity and pressure spectra is concluded that most of the energy is located between 0 and 10 Hz. Thus, sampling at a maximum frequency of 20 Hz (f_{nyq}= 10 Hz) would capture all the turbulent fluctuations of the jet. Lastly, the test duration of two minutes per power step was sufficient to base the mean flow velocity and standard deviation on. However, further away from the quay a larger deviation in these parameters is observed for a measurement duration of eight minutes due to the turbulent fluctuations passing the sensor at a smaller velocity resulting in a larger uncertainty in the mean flow velocity and standard deviation.

Relative turbulence intensity
Overall, a constant relation is observed between the decay in mean horizontal flow velocity and standard deviation while moving in perpendicular direction to the quay wall. Resulting in moderately constant values for the relative turbulence intensity (r_{hor}) ranging between 0.3 and 0.6 with an average of 0.44 over every measurement position and power step. Especially close to the quay wall the relative turbulence intensity stays within the range of 0.3-0.6 while during the 50% power step the most constant values are observed. During the 90% power step, the relative turbulence intensity deviates the most from the range of 0.3-0.6. Averaging the relative turbulence intensity per sensor over the power steps results in a range between 0.40 - 0.47 showing that there is no sensor that deviates significantly from the others for the relative turbulence intensity. Resulting in an average calculation value for the maximum horizontal flow velocity near the bed of 2.3 times the mean horizontal flow velocity.

Guidelines and previous research
For the last sub-question, the results from the measurements in Gent for the measured flow velocity magnitude and decay profile are compared to the German and Dutch method, based on research by Schmidt (1998) and Blokland (1996) respectively, to place the measurements results into perspective with current literature. Both methods are used as guidelines to determine an upper limit for the mean near-bed flow velocity induced by a reflected bow thruster jet. However, the German method determines the mean flow velocity in x-direction ($\overline{V}_{x,German}$) whereas the Dutch method in horizontal direction ($\overline{V}_{hor,Dutch}$). The difference in components results in 5-77% higher measured mean flow velocities in horizontal direction ($\overline{V}_{hor}$) with an average of 25%. Therefore, when only focusing on the measured flow velocities in x-direction the bed load is underestimated.

The German method only determines a value for $\overline{V}_{x,German}$ at the intersection of the quay wall and the bed which are thus compared with the highest measured value for $\overline{V}_x$ by the sensors close to the quay wall. The German method is highly dependent on the bow thruster quay wall clearance L_{BT}. Overestimating the measured values of $\overline{V}_x$ for small quay wall clearances ($L_{BT} < 5.24\ D_t$) with a factor ranging between 2.1-6 times the measured values for $\overline{V}_x$. For larger quay wall clearances the German method complies well with the measurement for $L_{BT} = 6.21\ D_t$ while underestimating $\overline{V}_x$ for $L_{BT} = 7.30$ and $7.99\ D_t$ with 15 and 30% respectively. Near-bed measurements by Schmidt (1998) between x = 0.3 - 3.4 D_t from the quay wall correspond well with the German method for a small quay wall clearance ($L_{BT} = 4.07\ D_t$) while overestimating the measurements of $\overline{V}_x$ for every quay wall clearance. In addition, the near-bed measurements by Schmidt (1998) show a much quicker decline in mean flow velocities for increasing distances from the quay wall.

Comparing the Dutch method with the measurement results for $\overline{V}_{hor}$ leads to a large overestimation of the mean flow velocity. On average, the Dutch method results in 3.7 times larger mean flow velocities than measured in Gent. The highest measured mean flow velocity induced by both bow thrusters activated together (BT1&2) still differs a factor of 2.47 with the Dutch method. The largest difference between the measured mean flow velocities and the Dutch method is found for the sensors located furthest away from the quay wall between x = 5 - 8.5 m. When only considering the first two sensors positioned near the quay wall, at x = 1.5 and 3 m, the Dutch method overestimates $\overline{V}_{hor}$ with an average factor of 2.1. Therefore, while moving away from the quay wall the Dutch method results in a larger overestimation of the measured mean flow velocity. The reason for this can be found in the total travelled distance by the jet (x_s) used to determine the mean flow velocity. This distance x_s is the sum of the quay wall clearance (L_{BT}), the height of the bow thruster axis above the bed (h_t, stayed constant throughout the measurements) and the position of the sensor from the quay wall (x). Based on the measurements, the decline in mean flow velocity is not equally dependent on L_{BT} and x. After approximately x = 3 m a strong decline in $\overline{V}_{hor}$ is observed regardless of the quay wall clearance (L_{BT}) which is not reflected by the Dutch method. Therefore, for increasing distance x from the quay wall the discrepancy between the measurement results and the Dutch method grows. Leading to the conclusion that according to the measurement results the summation of L_{BT} and x to determine and compare the flow velocities for different measurements is not correct. The decline in $\overline{V}_{hor}$ depends more on x than on L_{BT}. Thus, an improved definition for x in the formulae should be determined leading to a less conservative value for the mean horizontal flow velocity.

8.2. Recommendations

To develop further knowledge on the reflecting jet of a 4-channel bow thruster on a vertical quay wall the following recommendations are proposed consisting of four parts. First of all, further analysing of the extensive data set retrieved from the measurements in Gent is advised. Secondly, the data can be used to validate a numerical model and the measurement set-up used in Gent can be reproduced by means of a scale model to validate the results. Thirdly, recommendations for new full-scale measurements are proposed to further research the complex flow pattern of the bow thruster jet based on the experience gained from the measurements in Gent and any new knowledge gaps found by the numerical and scale model. Fourthly, combining the knowledge of the three different methodologies to update the current design guidelines on the design of bed protections.

Further analysing of the data set from the full-scale measurements in Gent

During the full-scale measurements in Gent four different types of measurement instruments were used to measure the flow velocities near the bed and pressure fluctuations over the quay wall and the bed. Consisting out of Acoustic Doppler Velocimeters, Acoustic Doppler Current Profilers, Ott meters and pressure sensors. This resulted in a unique and extensive data set. However, the ADCPs data was not analysed in this thesis. Furthermore, the flow direction measured by the ADVs is not researched for the measurements in Gent. Therefore, further analysis of the following aspects is recommended:

- **Acoustic Doppler Velocimeter (ADCP)**
  Three ADCPs were positioned at the end of the horizontal measurement frame. The first one directed towards the quay wall to measure the decay in flow velocity up to the ADCP, the second pointed upwards to measure the inflow velocities of the bow thruster inlet and the last ADCP looking further into the channel to detect any flow velocities present further from the quay wall than the position of the ADCPs. The ADCPs are able to spatially measure the flow in the direction of the beams while the ADVs only measure at one point. Therefore, analysing this data can provide valuable information on the flow field induced by the bow thruster jet near the bed. In addition, the influence of the bow thruster inlet on the flow field can be researched.

- **Direction of the flow over the bed**
  The ADVs measured in x, y, and z direction from which the flow direction of each data point can be determined. The flow field can be resolved in the direction perpendicular to the quay wall, by the high spatial resolution of the ADVs, and along the quay wall, due to the vessel being displaced with respect to the measurement frame. Resulting in a large matrix of measurement locations over the bed. In addition, the data on flow direction by the ADCPs can be used to complement to the ADV data.

Validating the measurement results by means of a numerical and scale model

The full-scale measurements in Gent were limited in spatial resolution of the measurement points and the possibility of varying the keel clearance (only one keel clearance researched). Furthermore, not many vessel configurations could be researched as moving the vessel to different positions took up a great amount of time. Resulting in a limited redundancy of the data as only a few tests are repeated more than once. Reproducing the measurement set-up conditions in Gent into a scale model can provide valuable information on the flow field while providing redundancy in the data by repeating the measurements several times and measuring in constant conditions for a longer duration. Furthermore, in a scale model a higher resolution of measurement points can be created while it is also having the possibility of measuring more quay wall clearances and keel clearances.

A numerical model can be validated on the measurement data from Gent to determine the influence of various parameters and boundary conditions on the flow velocity field. Analysing the sensitivity of the flow velocity on quay wall clearance, keel clearance and increased bow thruster power while also investigating at what distance from the bow thruster axis the highest flow velocities occur. By researching the same measurement set-up with three different methodologies (Full-scale measurements, scale model and numerical model) the complex flow field of the reflected bow thruster jet can be precisely analysed while validating the measured flow velocities of the measurements in Gent researched in this thesis. For the CROW joint research program, as discussed in Section 1.4, a road map is made by Charlotte van der Vorm-Hoek in which further research by means of a scale and numerical model on

the reflected bow thruster jet is further elaborated (Van der Vorm, 2020).

New full scale measurements

If new full-scale measurements are planned, the limitations and lessons learned from the measurements in Gent should be taken into account as listed below:

- **Acoustic Doppler Velocimeter (ADV) set-up**
  The ADV is a complicated measurement instrument for which experience is necessary to properly set-up the measurement instrument prior to the full-scale measurements. Therefore, testing the ADV thoroughly on beforehand is recommended. During the measurements in Gent, the nominal velocity range was set to high. An analysis of the expected flow velocities near the bed should be conducted to determine a reasonable nominal velocity range. Furthermore, the external sampling frequency should be set as low as possible. For a velocity range larger than 1 m/s the ADV samples internally with 125 Hz, thus a lower external sampling rate results in more internal averaging of the output data points resulting in a higher confidence level in the data. In addition, from the measurements was concluded that a sampling frequency above 20 Hz is unnecessary. As a result of the large nominal velocity range and high sampling frequency outliers (spikes) and Doppler noise is encountered in the measurement data which should be avoided.

- **Calibration of the measurement instruments**
  Prior to the full-scale measurements, the instruments should be tested and calibrated preferably in a wave flume where the flow velocities can be regulated and no external disturbances are present. During the zero measurements in Gent, the ADVs measured background noise or background flow velocity fluctuations. To check whether this was induced by the instrument itself (most likely) or was induced by the flow near the bed, the ADVs should be calibrated beforehand.

- **Fixation of the measurement instruments**
  Some ADVs rotated during the measurements leading to slight alterations in the x, y, and z directions of the flow velocity data. To prevent this, the ADVs should be mounted stiffly to the wooden structures used to mount the ADVs. Furthermore, a different (more robust) fixation of the ADVs could be thought of. In addition, a set-up could be designed similar to Blokland (1996) where the ADVs could be mounted upside down in order to measure more closely to the bed. As the highest flow velocities might be occurring below the ADV sampling volume height of 0.35 m, the height in z-direction where the flow was measured in Gent.

- **Free flow measurements**
  During the measurements in Gent, the efflux velocity of the bow thruster was measured by directing the flow from the bow thrusters towards the starboard channel, see Appendix E for the free flow set-up. In this way, the jet could spread into the Moervaart uninfluenced by lateral restrictions. The efflux velocity was measured by placing a vertical measurement frame on a small motorboat holding the boat in place by ropes from the Somtrans measuring the efflux velocity as close as possible near the bow thruster outlet. However, this set-up did not work properly as the large forces on the frame prevented stable measurements on a fixed location from the bow thruster outlet. Therefore, a more robust set-up should be designed for which the instruments can be fixed to either the vessel or the bed in order to accurately measure the efflux velocity and compare this with current guidelines. Furthermore, field measurements were both the efflux velocity and the near-bed flow velocities are measured results in the full flow field being analysed from the moment the jet exists the thruster channel to the location at the bed where the presence of the jet can not be measured anymore.

Updating current guidelines on bed protections

The measurement results showed discrepancies with the currently used guidelines to determine the near-bed flow velocities which are used as a hydraulic load for the design of bed protections. Not only did the measurements result in higher mean flow velocities than expected by the guidelines, the dependency of the guidelines on the quay wall clearance and the total travelled distance by the jet (x_s) was not reflected by the measurements results. However, it must be noted that the guidelines were not developed for a 4-channel bow thruster. Furthermore, the measurements were the guidelines are based on did not use two bow thrusters simultaneously. Thus, when a better understanding of the complex flow field of a reflected jet is obtained by means of combining the knowledge acquired

throughout full-scale measurements, scale models and numerical models the current guidelines as stated in PIANC (2015) can be modified and updated accordingly.

A
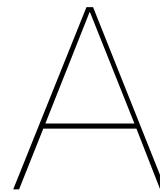
Somtrans XXV

This appendix provides additional technical information about the Somtrans XXV and the Verhaar Omega 31130-4k bow thruster are given. In Figure A.1 the bollard pull thrust is plotted against the direction of the bow thruster in kN provided by the Verhaar manufacturer.

	MAX. THRUST [N] 400 kW	MAX. THRUST [N] 450 kW	MAX. THRUST [N] 500 kW
Front	40.259	44.174	47.564
	39.384	43.214	46.530
	38.071	41.773	44.979
	35.883	39.372	42.394
45°	38.071	41.773	44.979
	40.259	44.174	47.564
	41.572	45.614	49.115
	42.885	47.055	50.666
StB	43.760	48.015	51.700
	42.885	47.055	50.666
	41.572	45.614	49.115
	40.259	44.174	47.564
135°	38.071	41.773	44.979
	35.883	39.372	42.394
	38.071	41.773	44.979
	39.384	43.214	46.530
Aft	40.259	44.174	47.564
	39.384	43.214	46.530
	38.071	41.773	44.979
	35.883	39.372	42.394
225°	38.071	41.773	44.979
	40.259	44.174	47.564
	41.572	45.614	49.115
	42.885	47.055	50.666
Port	43.760	48.015	51.700
	42.885	47.055	50.666
	41.572	45.614	49.115
	40.259	44.174	47.564
315°	38.071	41.773	44.979
	35.883	39.372	42.394
	38.071	41.773	44.979
	39.384	43.214	46.530

BOLLARD PULL THRUST PLOT IN kN [OMEGA 31130]

Figure A.1: Bollard pull thrust in kN of the Verhaar Omega 31130-4K channel bow thruster. The Somtrans XXV Verhaar bow thruster has 394 kW, slightly less than the 400 kW listed in the max thrust table. Looking at the max thrust for 400 kW this results in a maximum thrust of 43.76 kN when used in port or starboard direction.
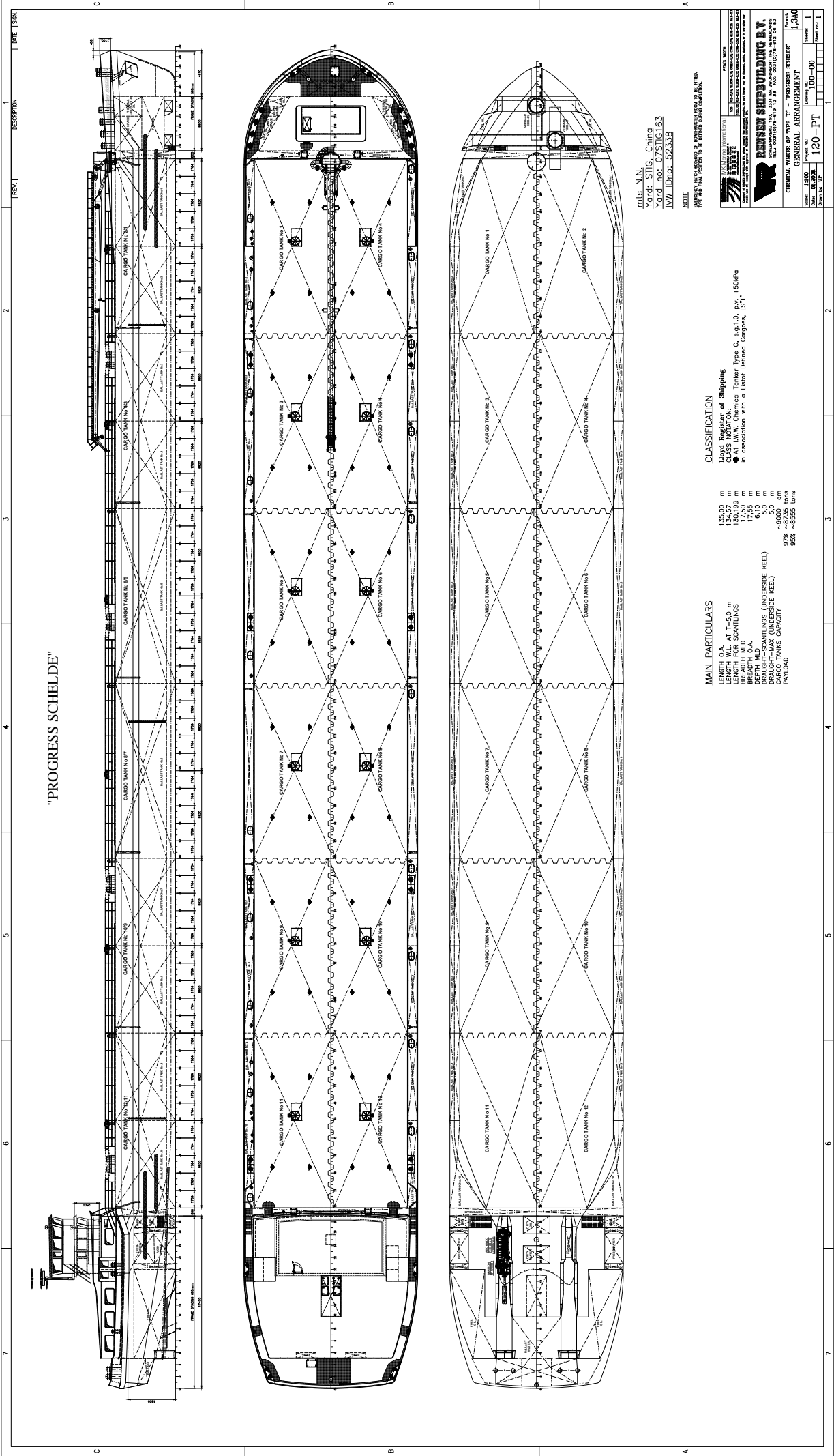
"PROGRESS SCHELDE"

CARGO TANK No 3/1
CARGO TANK No 5/3
CARGO TANK No 6/5
CARGO TANK No 8/7
CARGO TANK No 9/9
CARGO TANK No 12/11

BALLAST TANK No1
BALLAST TANK No2
BALLAST TANK No3
BALLAST TANK No4
BALLAST TANK No5

CARGO TANK No 1
CARGO TANK No 3
CARGO TANK No 5
CARGO TANK No 7
CARGO TANK No 9
CARGO TANK No 11

CARGO TANK No 4
CARGO TANK No 6
CARGO TANK No 8
CARGO TANK No 10
CARGO TANK No 12

CARGO TANK No 1
CARGO TANK No 3
CARGO TANK No 5
CARGO TANK No 7
CARGO TANK No 9
CARGO TANK No 11

CARGO TANK No 2
CARGO TANK No 4
CARGO TANK No 6
CARGO TANK No 8
CARGO TANK No 10
CARGO TANK No 12

CLASSIFICATION

Lloyd Register of Shipping
CLASS NOTATION:
● A1 IWW. Chemical Tanker Type C., s.g.1.0, p.v. +50kPa
in association with a List of Defined Cargoes, LST"

MAIN PARTICULARS

LENGTH O.A.	135,00	m
LENGTH W.L. AT T=5,0 m	134,57	m
LENGTH FOR SCANTLINGS	130,199	m
BREADTH MLD	17,50	m
BREADTH O.A.	17,55	m
DEPTH MLD	6,10	m
DRAUGHT-SCANTLINGS (UNDERSIDE KEEL)	5,0	m
DRAUGHT-MAX (UNDERSIDE KEEL)	5,0	m
CARGO TANKS CAPACITY	~9000	qm
PAYLOAD	97% ~8735	tons
	95% ~8555	tons

NOTE

EMERGENCY HATCH 600x600 OF BOWTHRUSTER ROOM TO BE FITTED.
TYPE AND FINAL POSITION TO BE DEFINED DURING COMPLETION.

REV.   DATE   DESCRIPTION   SIGN.

B

Measurement instruments

B.1. ADV - Nortek Vector
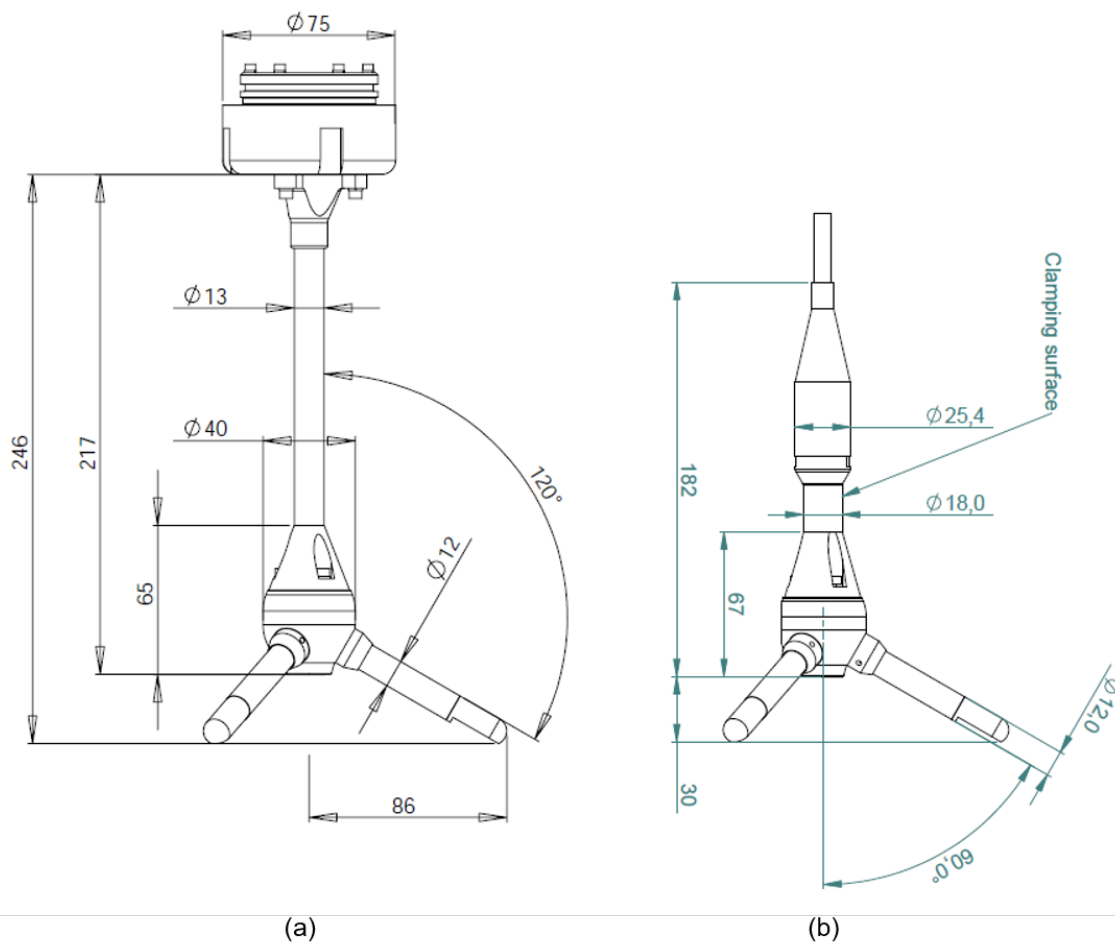
Figure B.1: Technical drawing of the Nortek Vector ADV. The dimensions are given in millimeters for the fixed head (a) and flexible head (b) Vector (Nortek Manuals, 2005)

C
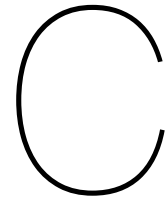
Post-processing

C.1. SNR and correlation filter

In this section, the flow velocity is plotted against time for Test 14 25% power after filtering on SNR and correlation. The flow velocity plots are grouped per ADV (1-4) and power step of 25% for V_x, V_y and V_z.
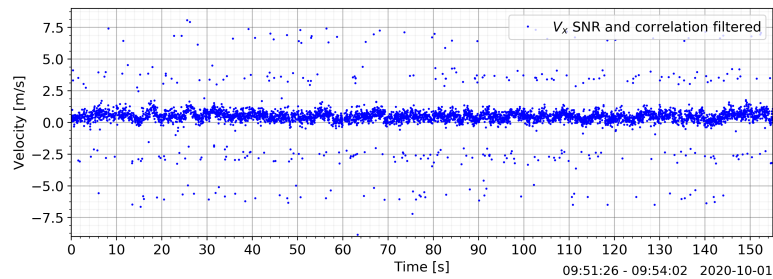
(a)
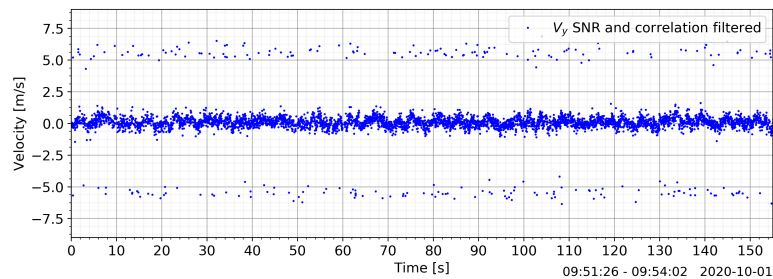
(b)
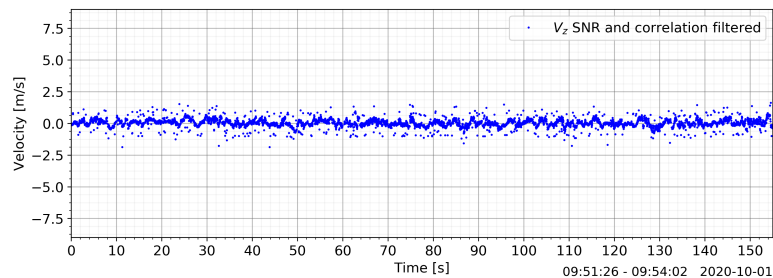
(c)

Figure C.1: Test 14 25% power ADV1. V_x (a), V_y (b) and V_z (c) velocity components after filtering on SNR and correlation.

159
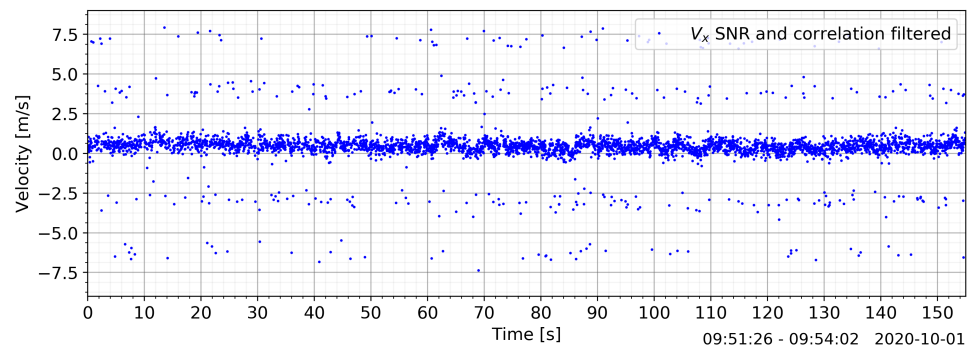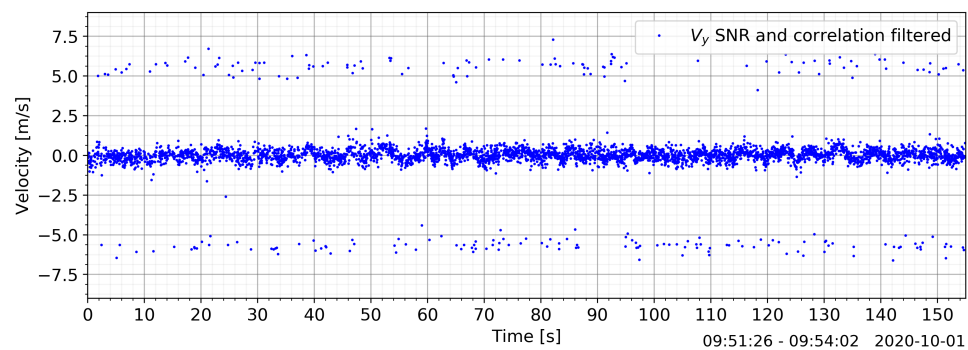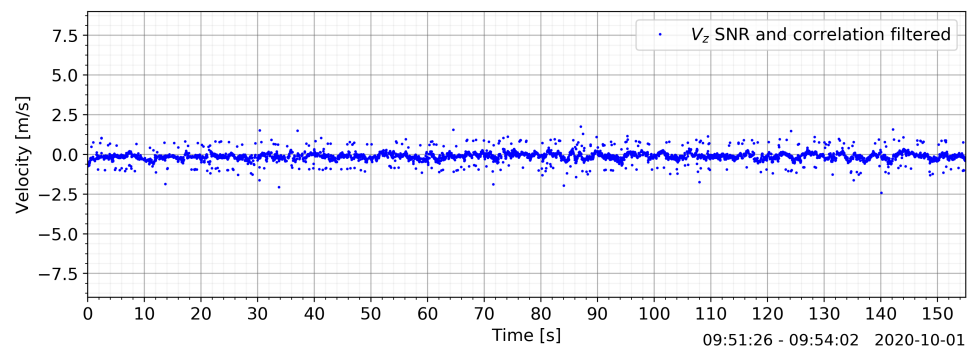
Figure C.2: Test 14 25% power ADV2. V_x (a), V_y (b) and V_z (c) velocity components after filtering on SNR and correlation.
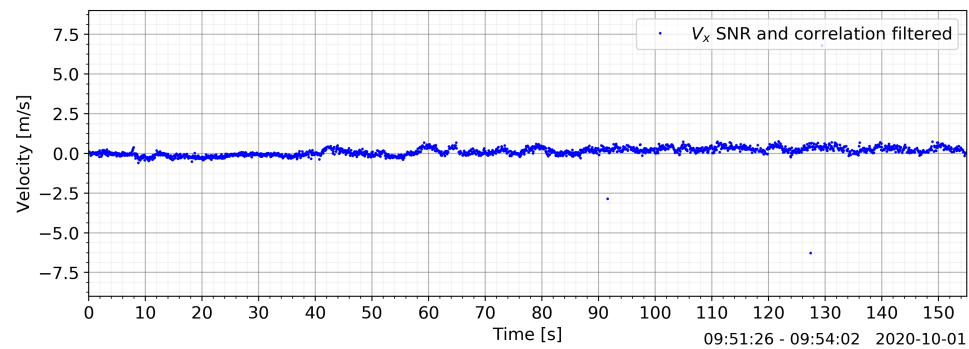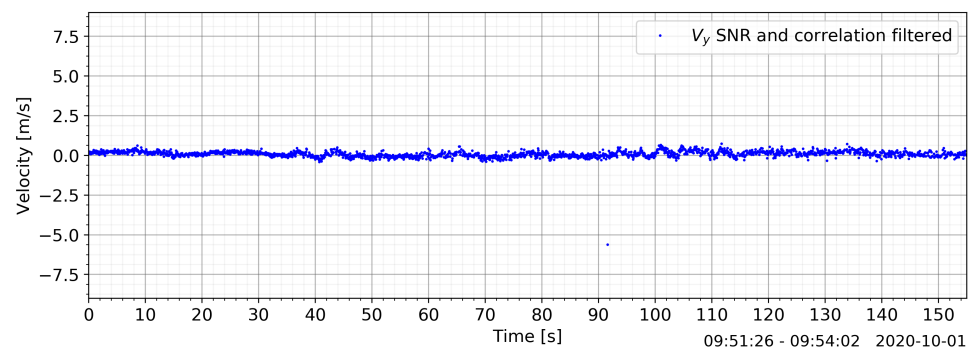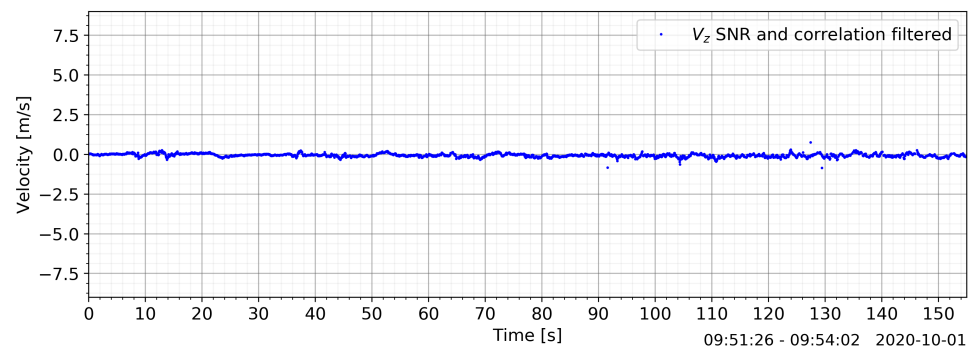
Figure C.3: Test 14 25% power ADV3. V_x (a), V_y (b) and V_z (c) velocity components after filtering on SNR and correlation.
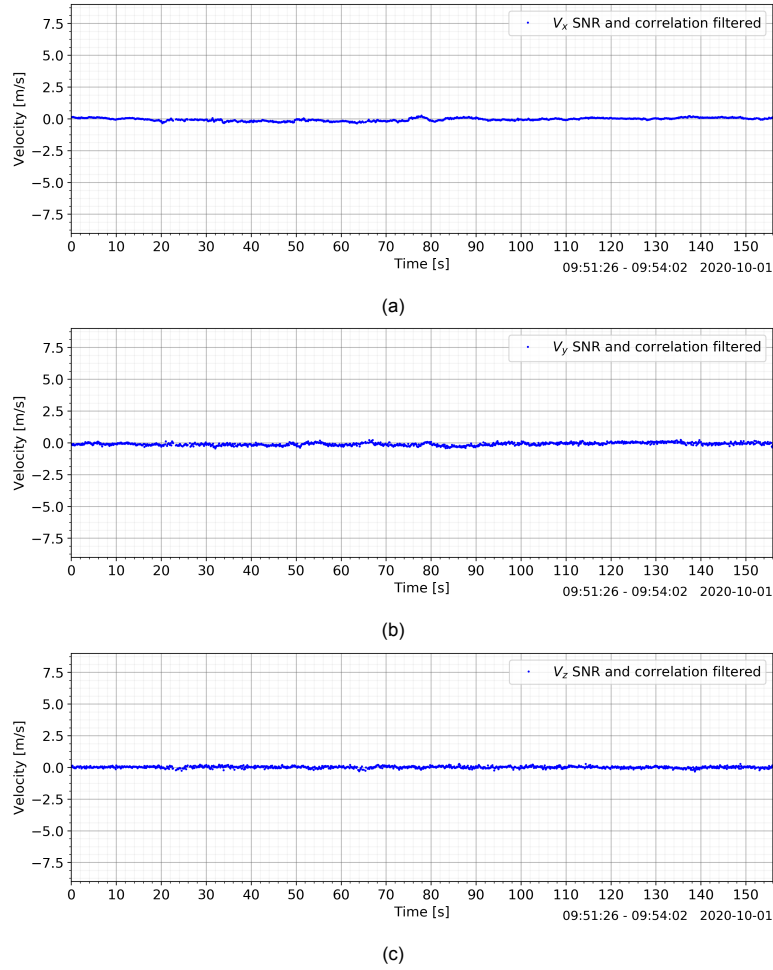
Figure C.4: Test 14 25% power ADV4. V_x (a), V_y (b) and V_z (c) velocity components after filtering on SNR and correlation.

C.2. Standard deviation filter

In Section 4.1.4 the outliers observed in the ADV data sets are filtered by means of a standard deviation filter where the data points that fall outside the range of ±2σ above and below $\overline{V}$ are filtered out (Equation C.1). This results in an average decrease in $\overline{V}_{hor}$ of 31.5% and an average decrease in σ_{hor} of 73.5% for the measurement tests in Gent measured by ADV1 and ADV2. As this filter is not applied for ADV3 and ADV4 (Section 4.1.4). However, to check the validity of the choice for 2σ the outcome of the filter for 2σ is compared to applying a 4σ filter (Equation C.2) two times to the data set. 4σ complies better with the assumption of only filtering out the highest outliers where filtering on 2σ could lead to non-outliers being filtered out as well. However, as illustrated in Figure C.5 applying the 4σ filter to Test 4 at 50% power for ADV1 (as example) does not filter out every outlier in the range of 4-8 m/s (blue dots observed in the outliers). Therefore, the filter is applied twice while making sure that with the ±4σ range only outliers are filtered out. This results in Figure C.6 where all the outliers are correctly filtered out. When comparing these results for the 2σ filter in Figure C.7 both filters seem to correctly filter out the outliers. To be sure they have filterd the same outliers from the data set, the mean horizontal flow velocity ($\overline{V}_{hor}$) and standard deviation (σ_{hor}) before filtering is compared to the resulting mean flow velocity after filtering, $\overline{V}_{hor,std2}$ and $\overline{V}_{hor,std4}$, as well as the resulting standard deviation $\sigma_{hor,std2}$ and $\sigma_{hor,std4}$ in Table C.1 and C.2 for ADV1 and ADV2 respectively. Where std2 is the 2σ filter and std4 the 4σ filter applied twice. The percentage of filtered mean flow velocity for std2 is given in the column labeled as 1-$\frac{\overline{V}_{hor,std2}}{\overline{V}_{hor}}$ while the difference between the std2 and std4 filter is represented in percentage

in the $\frac{\overline{V}_{hor,std2}}{\overline{V}_{hor,std3}}$ column. In a similar way this is presented for the standard deviations. From the tables can be concluded that filtering the data with the std2 or std4 filter results in almost identical mean flow velocities and standard deviations varying at most 2% from each other. Therefore, both filters can correctly be applied to the ADV data sets.

$$\overline{V} - 2\sigma < V_{data} < \overline{V} + 2\sigma \qquad (C.1)$$

$$\overline{V} - 4\sigma < V_{data} < \overline{V} + 4\sigma \qquad (C.2)$$
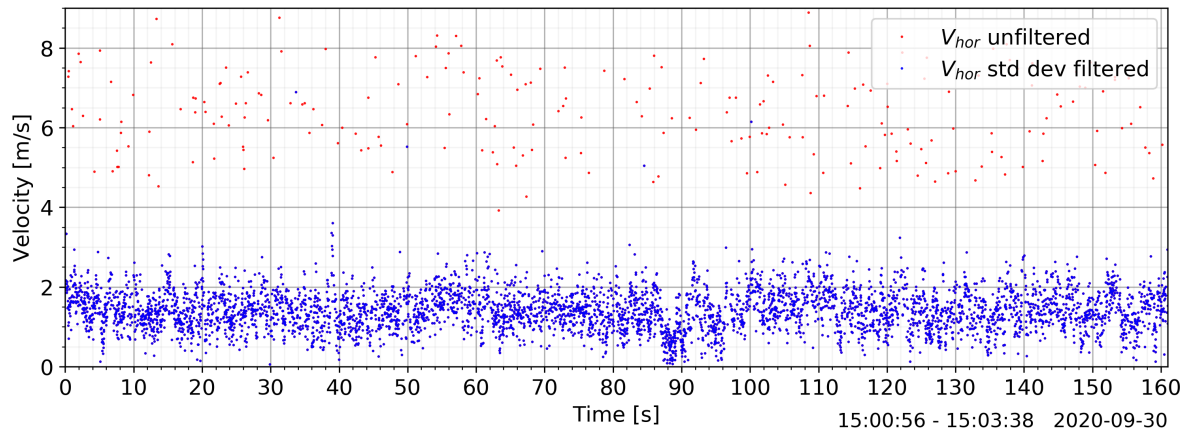
Figure C.5: Plot of the horizontal flow velocity before and after filtering on standard deviation for Test 4 at 50% power measured with ADV1. In this figure the 4σ filter is applied once resulting in several outliers not being filtered out (blue dots).
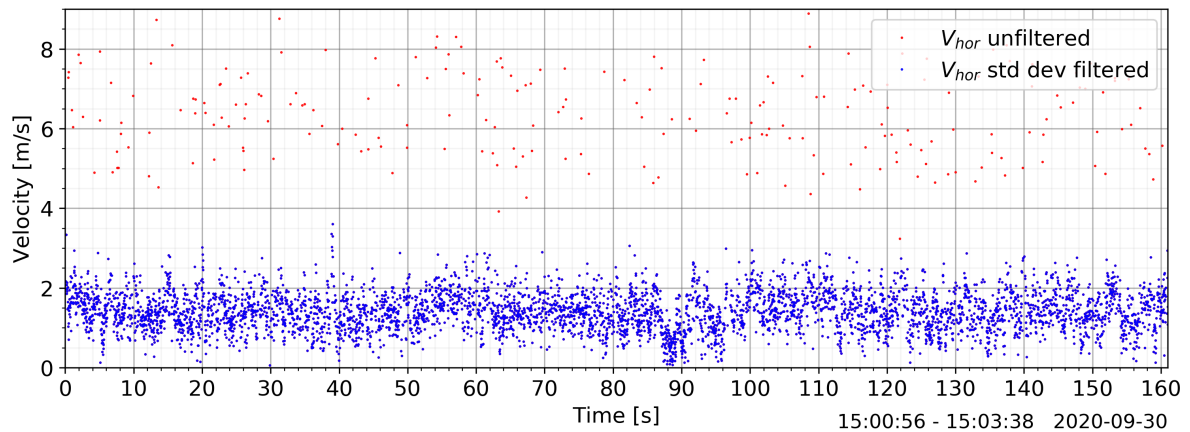
Figure C.6: Plot of the horizontal flow velocity before and after filtering on standard deviation for Test 4 at 50% power measured with ADV1. In this figure the 4σ filter is applied twice resulting in all the outliers being filtered out.
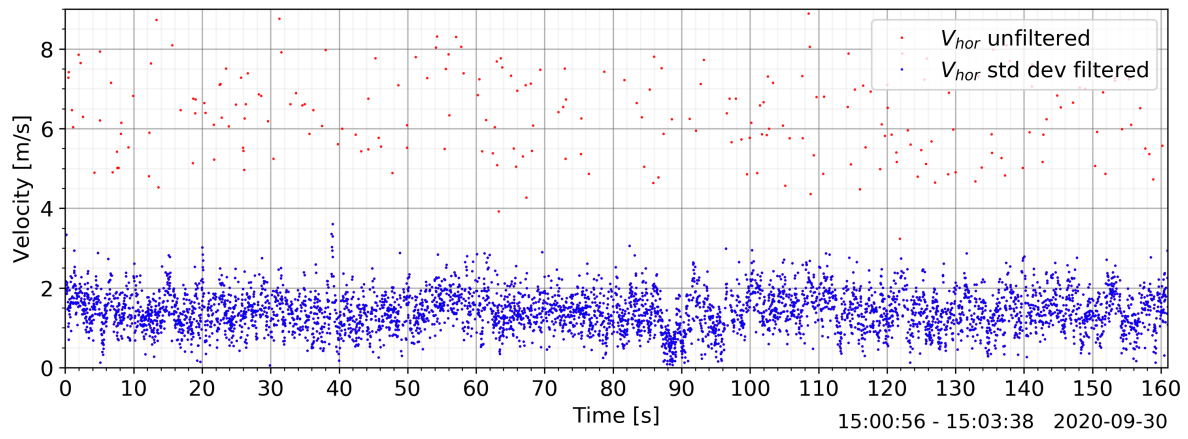
Figure C.7: Plot of the horizontal flow velocity before and after filtering on standard deviation for Test 4 at 50% power measured with ADV1. In this figure the 2σ filter is applied as used for every measurement test in Section 4.1.4.

Table C.1: Overview of the mean horizontal flow velocity ($\overline{V}_{hor}$) and standard deviation (σ_{hor}) before and after applying the standard deviation filter for 2σ and 4σ on the data set of ADV1.

Test	Power_step	$\overline{V}_{hor}$ [m/s]	$\overline{V}_{hor,std2}$ [m/s]	$\overline{V}_{hor,std4}$ [m/s]	$1-\frac{\overline{V}_{hor,std2}}{\overline{V}_{hor}}$ [%]	$\frac{\overline{V}_{hor,std2}}{\overline{V}_{hor,std4}}$ [%]	σ_{hor} [m/s]	$\sigma_{hor,std2}$ [m/s]	$\sigma_{hor,std4}$ [m/s]	$1-\frac{\sigma_{hor,std2}}{\sigma_{hor}}$ [%]	$\frac{\sigma_{hor,std2}}{\sigma_{hor,std4}}$ [%]
Test 1	25%	0.77	0.51	0.51	33.09	100.09	1.23	0.28	0.28	76.88	100.57
	50%	0.99	0.77	0.77	22.81	99.27	1.17	0.39	0.39	66.61	99.14
Test 2	25%	0.91	0.57	0.57	36.94	99.96	1.39	0.31	0.3	78.06	100.45
	50%	0.82	0.54	0.55	33.79	99.71	1.3	0.33	0.33	74.58	100.55
	90%	0.84	0.61	0.62	27.71	98.51	1.18	0.36	0.37	69.44	98.42
Test 3	25%	0.68	0.5	0.5	26.57	100.13	1.06	0.26	0.26	75.71	100.47
	50%	1.04	0.77	0.78	25.82	99.29	1.26	0.39	0.39	69.29	99.34
	90%	1.07	0.8	0.81	24.89	99.49	1.27	0.41	0.41	67.62	100.15
Test 4	25%	0.94	0.77	0.77	18.16	99.96	1.02	0.31	0.31	69.57	100.09
	50%	1.63	1.4	1.4	14.12	99.76	1.17	0.49	0.49	57.98	100.25
	90%	1.83	1.55	1.56	14.93	99.4	1.28	0.57	0.58	55.41	99.14
Test 5	25%	0.56	0.37	0.37	33.18	100.06	1.05	0.22	0.21	79.51	102.06
	90%	0.8	0.51	0.51	36.52	99.75	1.33	0.29	0.29	78	100.07
Test 8	25%	0.82	0.41	0.41	50.2	99.82	1.57	0.25	0.25	84.03	100
	90%	1.03	0.71	0.73	30.43	98.26	1.35	0.38	0.39	71.59	98.35
Test 9	25%	0.95	0.57	0.57	40.02	99.9	1.48	0.3	0.3	80.03	100.26
	50%	1.07	0.73	0.73	32.33	99.4	1.41	0.37	0.37	73.82	99.84
	90%	1.14	0.86	0.87	24.85	99.04	1.31	0.44	0.45	66.16	99.5
Test 10	25%	1.1	0.87	0.87	21.09	100.05	1.18	0.33	0.33	72.14	100.01
	50%	1.36	1.07	1.08	21.13	98.97	1.29	0.46	0.47	64.17	98.92
Test 11	25%	0.62	0.32	0.32	47.74	100.8	1.35	0.19	0.19	85.65	103.23
	50%	0.83	0.47	0.47	42.67	99.96	1.46	0.26	0.26	82.23	99.91
	90%	0.83	0.51	0.51	38.4	99.99	1.4	0.28	0.28	80.12	100.24
Test 12	25%	0.88	0.43	0.43	51.87	99.98	1.64	0.25	0.25	84.55	100.02
	50%	0.97	0.56	0.56	42.57	98.98	1.55	0.33	0.33	78.7	98.97
Test 13	90%	0.99	0.68	0.68	31.54	99.08	1.37	0.38	0.38	72.24	99.29
	25%	0.84	0.33	0.33	60.44	100	1.74	0.22	0.22	87.61	100
	90%	0.83	0.49	0.48	41.68	100.32	1.44	0.26	0.26	81.78	102.53
Test 14	25%	1.05	0.63	0.63	40.06	99.89	1.56	0.31	0.31	80.08	100
	50%	1.22	0.9	0.9	26.54	99.29	1.37	0.41	0.41	69.95	99.53
	90%	1.34	1.04	1.05	22.42	99.14	1.34	0.49	0.49	63.58	99.5
Test 15	90%	0.75	0.49	0.49	34.53	99.57	1.24	0.3	0.29	76.14	100.93
Test 16	25%	0.76	0.49	0.49	35.55	100.09	1.27	0.26	0.25	79.8	100.93
	50%	0.94	0.75	0.75	20.43	99.7	1.1	0.4	0.4	63.92	100
	90%	1.08	0.87	0.87	19.88	100	1.16	0.45	0.45	61.32	100.27
Test 17	50%	1.62	1.35	1.35	16.86	99.83	1.25	0.47	0.47	62.54	100.09
	90%	1.96	1.67	1.67	14.72	99.94	1.32	0.57	0.56	57.22	100.16
Test 18	50%	1.61	1.34	1.34	16.63	100.09	1.28	0.46	0.46	64.17	99.15
	90%	1.79	1.54	1.54	13.83	100.02	1.25	0.53	0.54	57.17	99.54
Test 19	50%	1.07	0.71	0.71	33.83	99.78	1.46	0.36	0.36	75.36	100.03
	90%	1.1	0.8	0.8	27.34	99.65	1.32	0.42	0.42	68.51	100.22
Test 20	50%	1.07	0.83	0.83	22.82	99.51	1.2	0.38	0.38	68.25	99.43
	90%	1.14	0.89	0.9	22.2	99.13	1.21	0.4	0.4	67.01	98.96
Test 21	50%	1.31	1.09	1.08	17.07	100.43	1.2	0.42	0.42	65.19	100
	90%	1.41	1.23	1.23	13.09	100.16	1.15	0.52	0.52	54.59	99.97

Table C.2: Overview of the mean horizontal flow velocity ($\overline{V}_{hor}$) and standard deviation (σ_{hor}) before and after applying the standard deviation filter for 2σ and 4σ on the data set of ADV2.

Test	Power_step	$\overline{V}_{hor}$ [m/s]	$\overline{V}_{hor,std2}$ [m/s]	$\overline{V}_{hor,std4}$ [m/s]	$1-\frac{\overline{V}_{hor,std2}}{\overline{V}_{hor}}$ [%]	$\frac{\overline{V}_{hor,std2}}{\overline{V}_{hor,std4}}$ [%]	σ_{hor} [m/s]	$\sigma_{hor,std2}$ [m/s]	$\sigma_{hor,std4}$ [m/s]	$1-\frac{\sigma_{hor,std2}}{\sigma_{hor}}$ [%]	$\frac{\sigma_{hor,std2}}{\sigma_{hor,std4}}$ [%]
Test 1	25%	0.88	0.59	0.59	33.15	100.22	1.32	0.3	0.3	77.41	100.88
	50%	1.06	0.79	0.79	25.47	99.73	1.28	0.41	0.41	67.87	99.9
Test 2	25%	1.06	0.65	0.65	39.28	99.86	1.56	0.33	0.33	78.81	99.94
	50%	0.92	0.59	0.59	35.33	99.75	1.39	0.34	0.34	75.72	100.53
	90%	1.04	0.77	0.78	25.47	99.13	1.26	0.4	0.4	68.58	98.99
Test 3	25%	0.78	0.51	0.51	34.64	100.14	1.28	0.25	0.25	80.47	100.17
	50%	0.99	0.68	0.68	30.92	100.2	1.37	0.34	0.34	74.84	100.07
	90%	1.15	0.87	0.87	24.91	99.72	1.31	0.37	0.37	71.41	99.74
Test 4	25%	1.25	1.01	1.01	18.74	100.11	1.18	0.32	0.32	72.85	100.34
	50%	1.75	1.5	1.49	14.41	100.14	1.23	0.47	0.47	62.12	99.95
	90%	1.95	1.61	1.62	17.28	99.7	1.38	0.56	0.56	59.77	99.45
Test 5	25%	0.61	0.38	0.37	38.7	100.38	1.21	0.2	0.2	83.09	101.58
	90%	0.92	0.61	0.61	33.55	99.94	1.34	0.31	0.31	76.67	100.51
Test 8	25%	0.92	0.44	0.44	52.47	99.8	1.7	0.25	0.26	85.21	97.19
	90%	1.08	0.7	0.7	35.34	100.1	1.5	0.32	0.32	78.89	100.3
Test 9	25%	1.02	0.55	0.55	46.63	100	1.7	0.29	0.29	82.8	99.99
	50%	1.08	0.68	0.68	37.68	99.97	1.56	0.34	0.34	78.22	100.36
	90%	1.22	0.89	0.89	27.56	99.6	1.42	0.42	0.42	70.26	99.5
Test 10	25%	1.25	0.91	0.91	27.62	100.01	1.41	0.32	0.31	77.61	100.01
	50%	1.53	1.18	1.18	22.96	99.89	1.42	0.45	0.45	68.33	100.22
Test 11	25%	0.7	0.34	0.34	51.25	100.6	1.47	0.2	0.19	86.49	102.61
	50%	0.82	0.48	0.47	41.88	100.24	1.44	0.26	0.25	82.08	101.22
	90%	0.91	0.59	0.59	34.93	100.15	1.38	0.27	0.27	80.15	100.35
Test 12	25%	0.94	0.43	0.43	53.93	99.92	1.76	0.25	0.25	85.69	99.15
	50%	0.97	0.47	0.48	51.01	99.57	1.73	0.27	0.28	84.27	95.57
	90%	0.96	0.59	0.6	38.17	99.63	1.49	0.34	0.34	77.01	100.04
Test 13	25%	0.66	0.29	0.29	55.19	101.53	1.49	0.18	0.17	87.77	107.12
	90%	0.79	0.43	0.43	46.27	100.02	1.49	0.24	0.23	84.22	100.12
Test 14	25%	1.12	0.59	0.61	47.6	96.79	1.77	0.3	0.43	83.12	69.43
	50%	1.21	0.85	0.85	29.51	99.74	1.45	0.39	0.39	72.73	99.82
	90%	1.47	1.1	1.1	24.92	100.12	1.45	0.47	0.47	67.72	99.6
Test 15	90%	0.91	0.54	0.54	39.92	100.09	1.48	0.28	0.28	80.83	100.72
Test 16	25%	0.91	0.61	0.61	32.8	100.06	1.35	0.31	0.3	77.27	100.41
	50%	1.07	0.78	0.79	27.61	98.86	1.33	0.42	0.42	68.61	99.75
	90%	1.24	0.96	0.96	22.46	99.74	1.3	0.45	0.46	65.09	99.76
Test 17	50%	1.56	1.29	1.28	17.33	100.14	1.25	0.43	0.43	65.58	99.67
	90%	1.95	1.62	1.61	16.85	100.36	1.38	0.51	0.51	63.15	99.88
Test 18	50%	1.7	1.33	1.33	21.66	100.28	1.47	0.46	0.46	68.59	99.41
	90%	1.86	1.55	1.55	16.62	99.88	1.32	0.53	0.53	59.73	99.98
Test 19	50%	1.09	0.71	0.71	34.48	100.08	1.51	0.32	0.32	78.8	100.34
	90%	1.1	0.77	0.77	30.46	99.99	1.39	0.36	0.36	74.42	100.19
Test 20	50%	1.25	0.89	0.9	28.61	99.96	1.43	0.33	0.33	76.72	100.02
	90%	1.3	0.98	0.98	24.04	100	1.35	0.37	0.37	72.27	99.86
Test 21	50%	1.56	1.28	1.28	18.05	99.81	1.29	0.44	0.45	65.6	99.36
	90%	1.72	1.46	1.46	14.94	100.22	1.3	0.5	0.51	61.08	99.5

C.3. Statistical analyses flow velocities: in x- and y-component

Histograms of the x- and y-components of the flow velocity for Test 14 at 50% power. The histograms have a uniform bin width of 0.05 m/s and have been normalized. The histograms of the flow velocity components confirm to the normal distribution plotted in orange in the figures. Concluding that the

statistical parameters can be used to determine the maximum flow velocities.

(a) ADV2: x-component
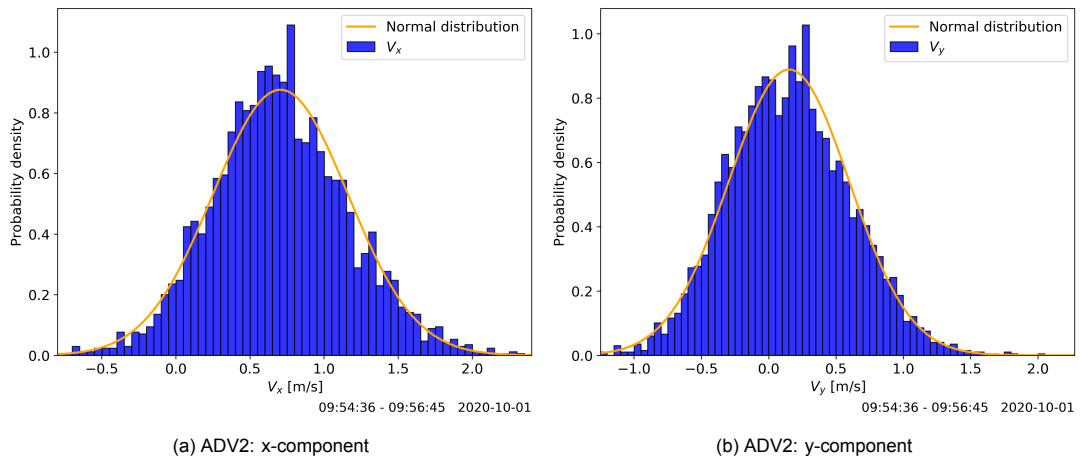
(b) ADV2: y-component

Figure C.8: Histograms for the x- and y-component of the flow velocity for Test 14 50% power ADV2 including the corresponding normal distribution in orange.

(a) ADV3: x-component
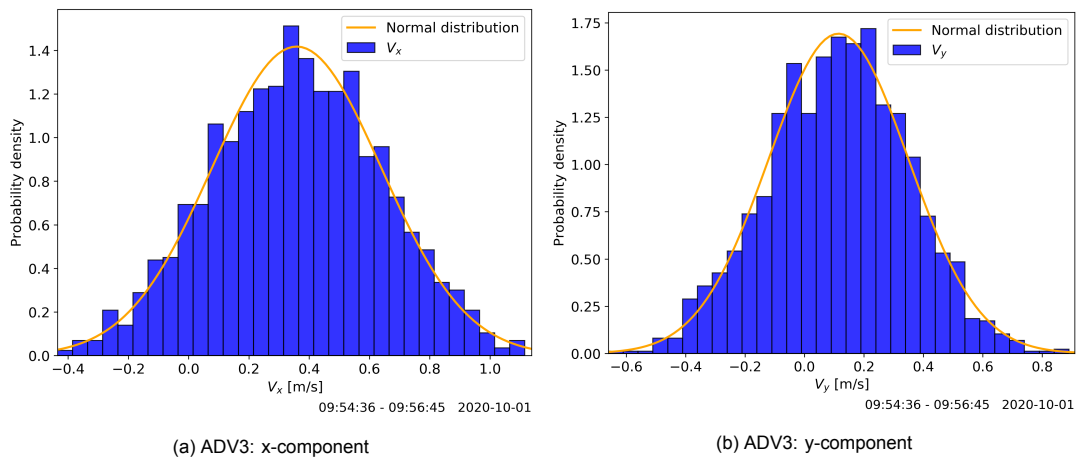
(b) ADV3: y-component

Figure C.9: Histograms for the x- and y-component of the flow velocity for Test 14 50% power ADV3 including the corresponding normal distribution in orange.

(a) ADV4: x-component
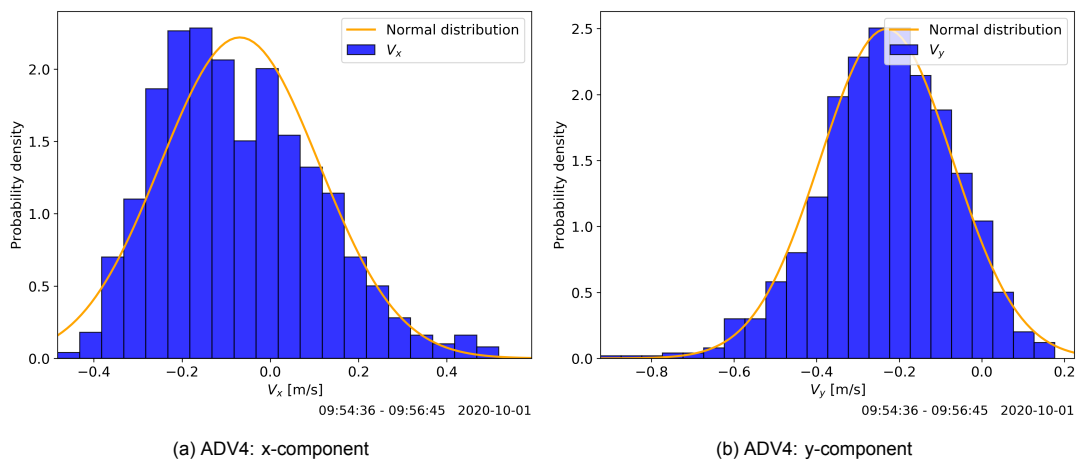
(b) ADV4: y-component

Figure C.10: Histograms for the x- and y-component of the flow velocity for Test 14 50% power ADV4 including the corresponding normal distribution in orange.

C.4. Variance density spectrum

C.4.1. Butterworth band pass filter

To filter out certain frequencies from the signal the Butterworth band pass filter is applied. This filter can be used as low-pass, high-pass or band pass filter. The Butterworth filter passes signals with a frequency lower or higher (low-pass or high-pass) than a certain cutoff frequency while attenuating signals with frequencies higher or lower (low-pass or high-pass) than the cutoff frequency (Figure C.11). The band pass filter is a combination of a low-pass and high-pass filter. The Butterworth filter is commonly used because of its flat frequency response (no ripples) in the passband which rolls off towards zero in the stopband (Figure C.12) (Jirafe, 2019). Within Python, the Butterworth function defined in SciPy (2021a) is used to filter the signals in this thesis.
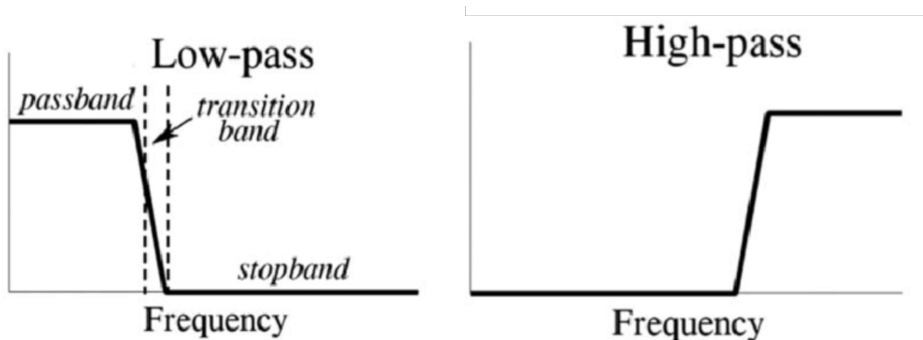
Figure C.11: Illustration of a low-pass and high-pass filter (Jirafe, 2019)
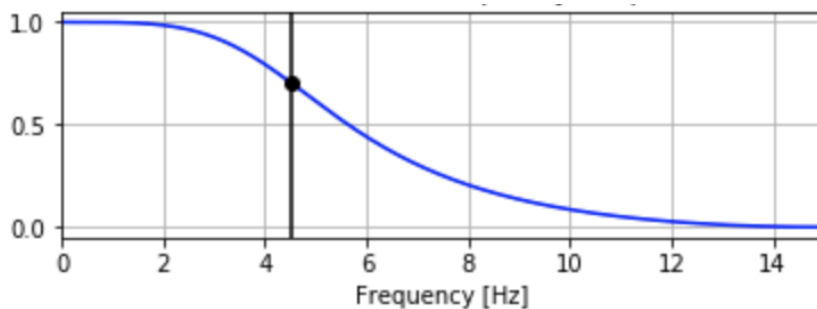
Figure C.12: Butterworth filter frequency response (Jirafe, 2019)

C.4.2. ADV1-4 horizontal flow velocity spectra
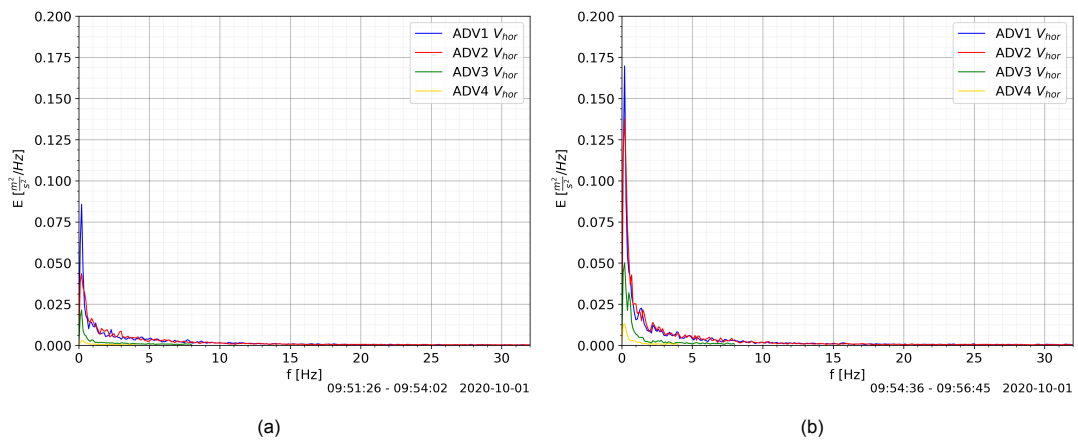
Figure C.13: Variance density spectrum of Test 14 at 25% (a) and 50% (b) power for V_{hor} ADV 1-4. $\Delta f = 0.1$, BT1&2, Vessel position 4 (L^{BT} = 4.35 m and y_t = 1.75 m).
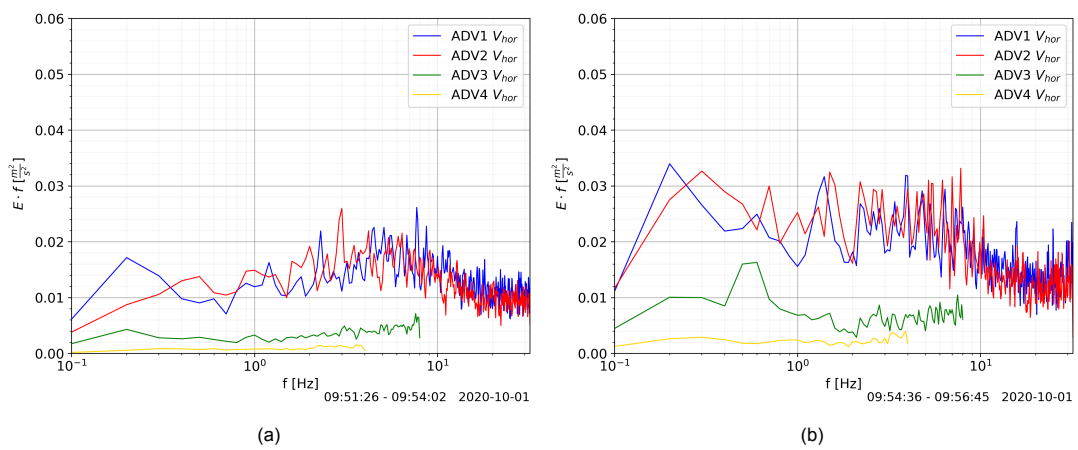
Figure C.14: Logarithmic x-axis plot of the variance density spectrum of Test 14 at 25% (a) and 50% (b) power for V_{hor} ADV 1-4. $\Delta f = 0.1$, BT1&2, Vessel position 4 (L^{BT} = 4.35 m and y_t = 1.75 m).
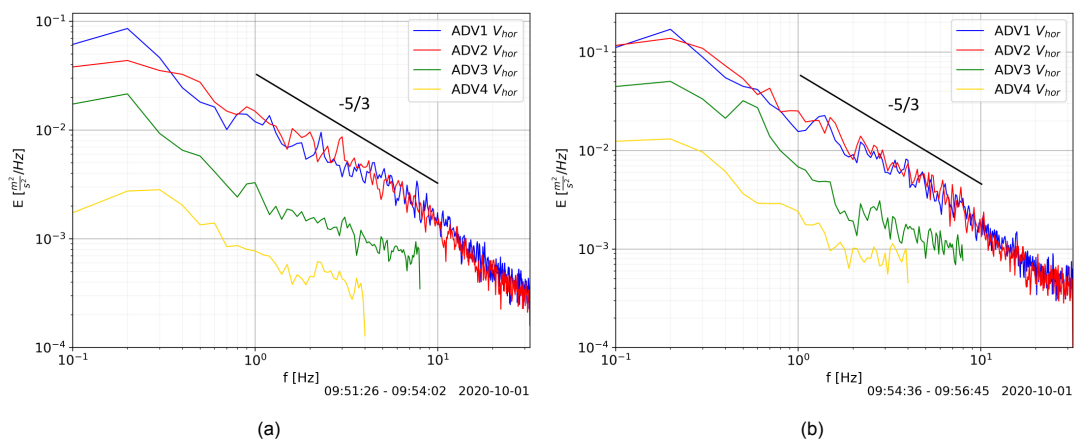
Figure C.15: Logarithmic plot of the variance density spectrum of Test 14 at 25% (a) and 50% (b) power for V_{hor} ADV 1-4. $\Delta f = 0.1$, BT1&2, Vessel position 4 (L^{BT} = 4.35 m and y_t = 1.75 m).

C.5. ADV1-4 standard deviation corrections

The noise correction method explained in Section 4.1.7 is applied to every measurement test to get an impression of the standard deviation correction in percentage compared to the original standard deviation (σ). An overview for the percentage of decreased standard deviation (σ) is listed in Table C.3 for 25%, 50% and 90% power. Overall the corrections for 50% and 90% power are below 10% (with some exceptions) while for 25% power higher corrections percentages are observed. This is due to the lower variance levels for 25% power resulting in the noise level being a bigger portion of the total variance. Looking back to Figure 4.21 this can be interpreted as the blue variance area being much smaller while the constant noise level stays relatively equal. On average, the noise reduction is 8.5% for ADV1, 8.0% for ADV2, 13.3% for ADV3 and 9.3 % for ADV4.

Table C.3: Overview of the standard deviation corrections for the moored tests at 25%, 50% and 90% power based on the constant noise level for V_{hor}. The percentage indicates how much the standard deviation (σ) is reduced compared to the original measured standard deviation (σ).

Test	**Power step**	σ_{ADV1}[%]	σ_{ADV2}[%]	σ_{ADV3}[%]	σ_{ADV4}[%]
Test 1	25%	15.4	14.13	26.48	17.54
	50%	6.44	5.09	11.98	10.46
Test 2	25%	11.17	7.89	8.9	3.13
	50%	9.58	8.26	10.99	11.65
	90%	7.67	4.93	4.1	7.72
Test 3	25%	19.72	21.23	9.9	7.02
	50%	6.13	7.56	11.43	12.97
	90%	3.91	4.62	11.52	4.69
Test 4	25%	14.83	15.66	6.28	2.77
	50%	4.26	2.96	5.48	4.21
	90%	1.11	0.87	3.43	3
Test 5	25%	25.82	32.68	31.3	15.67
	90%	7.63	5.05	15.64	12.17
Test 8	25%	12.6	10.27	32.57	11.92
	90%	2.86	4.87	22	11.52
Test 9	25%	10.98	7.39	15.73	7.3
	50%	7.02	5.96	9.12	3.97
	90%	4.12	3.74	8	4.27
Test 10	25%	12.63	10.3	5.45	3.67
	50%	4.15	3.41	6.61	3.81
Test 11	25%	27.7	20.92	30.62	30.51
	50%	13.45	10.96	20.21	25.35
	90%	11.97	10.69	22.6	18.18
Test 12	25%	10.58	9.97	21.65	13.11
	50%	5.3	7.24	12.21	7.29
	90%	4.3	4.48	8.23	7.01
Test 13	25%	10.85	19.59	52.99	40.3
	90%	9.81	14.86	41.95	26.71
Test 14	25%	6.2	5.63	13.66	8.72
	50%	4.83	4.15	8.02	9.69
	90%	2.6	2.02	8.55	7.39
Test 15	90%	9	8	7.73	2.71
Test 16	25%	18.79	11.92	7.07	3.05
	50%	7.84	5.47	4.59	4.01
	90%	4.4	2.57	2.91	3.52
Test 17	50%	3.22	3.6	6.6	2.7
	90%	0.96	1.18	4.83	3.21
Test 18	50%	4.22	2.83	4.91	4.89
	90%	1.57	1.54	5.9	5.48
Test 19	50%	6.45	7.44	16.39	8.24
	90%	3.78	4.66	14.21	4.24
Test 20	50%	8.57	8.8	6.99	6.81
	90%	7.42	7.56	8.11	6.39
Test 21	50%	7.68	5.27	5.31	5.4
	90%	5.15	3.92	6.72	3.96

C.6. Resampling ADV2 and ADV4 to Ott meter 1 and 2
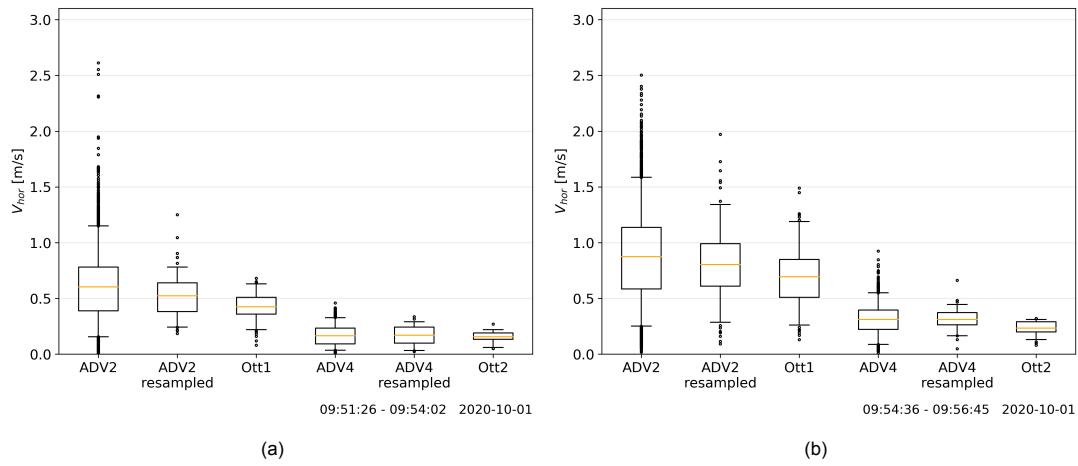
Figure C.16: Boxplot of Test 14 25% and 50% power for ADV2 and ADV4 resampled to Ott meter 1 and 2 sampling frequency.

C.7. Pressure sensors

C.7.1. zero measurement: Wednesday the 30th of September
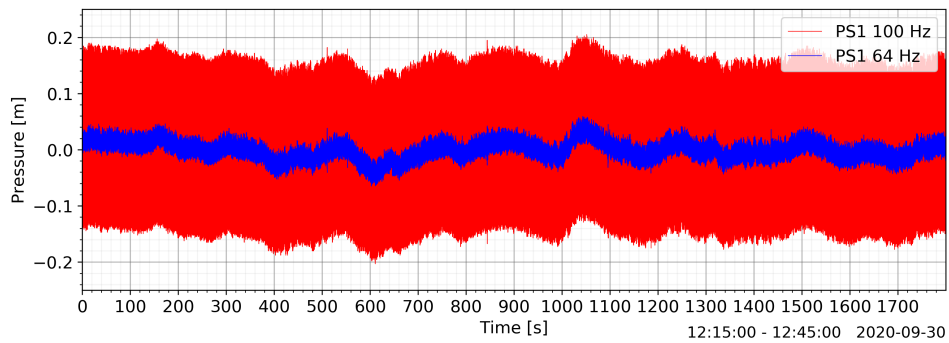
(a) High frequency pressure sensor 1 (PS1)
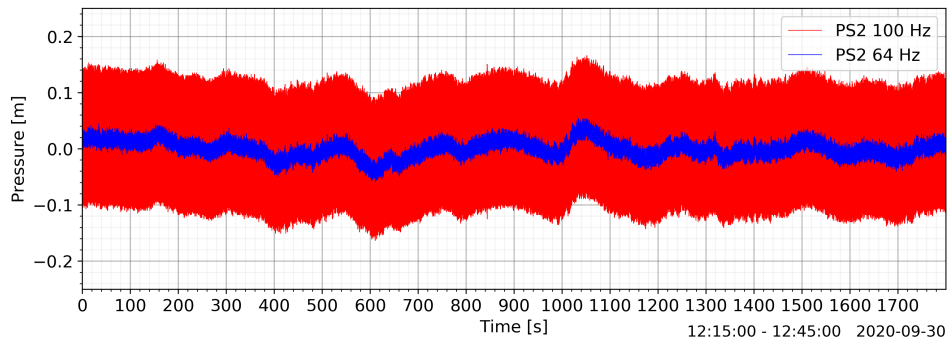
(b) High frequency pressure sensor 2 (PS2)
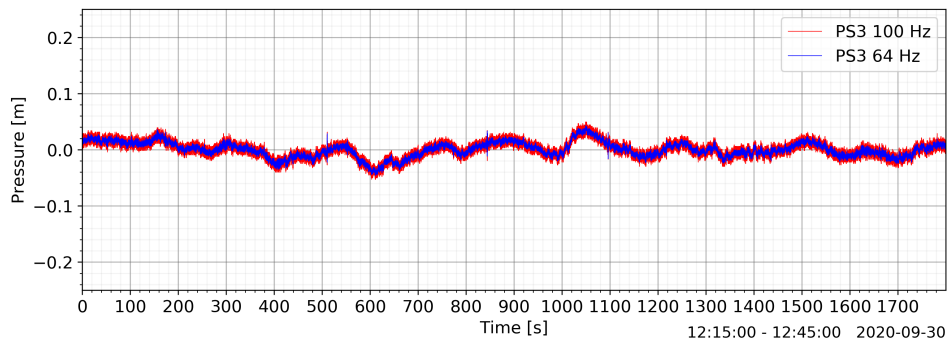
(c) High frequency pressure sensor 3 (PS3)
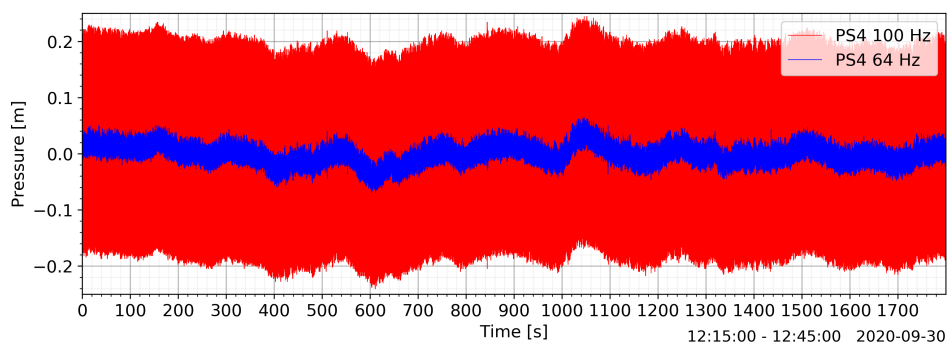
(d) High frequency pressure sensor 4 (PS4

Figure C.17: Zero measurement Wednesday 30th of September 12:15-12:45 for the high frequency pressure sensors PS1 (a), PS2 (b), PS3 (c) and PS4 (d). In red the unfiltered signal at 100 Hz and in blue the low-pass Butterworth filtered pressure signal.
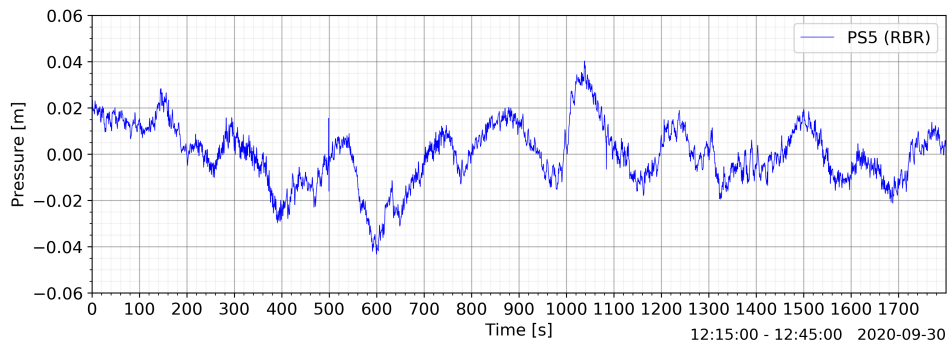
(a) RBR solo pressure sensor (PS5)
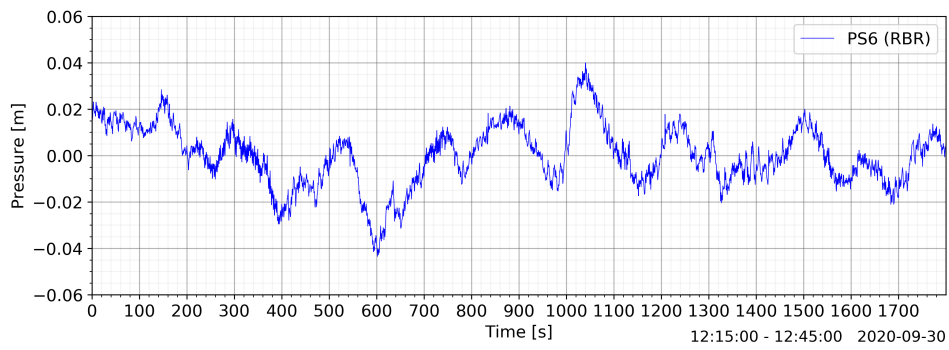
(b) RBR solo pressure sensor (PS6)

Figure C.18: Zero measurement Wednesday 30th of September 12:15-12:45 for PS5 (a) and PS6 (b).
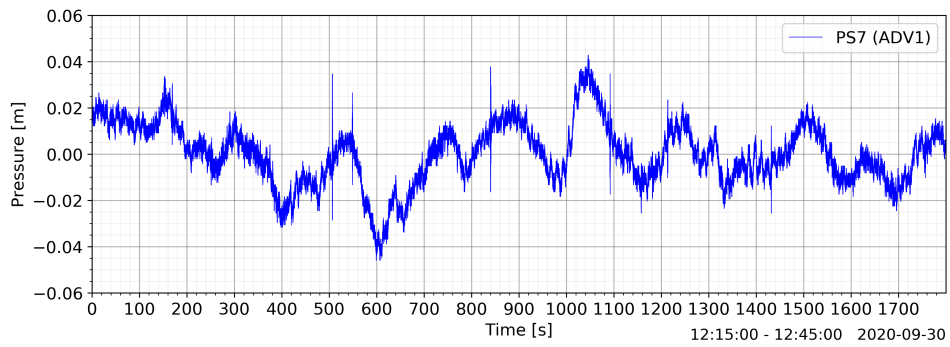
(a) Pressure sensor corresponding to ADV1 (PS7)
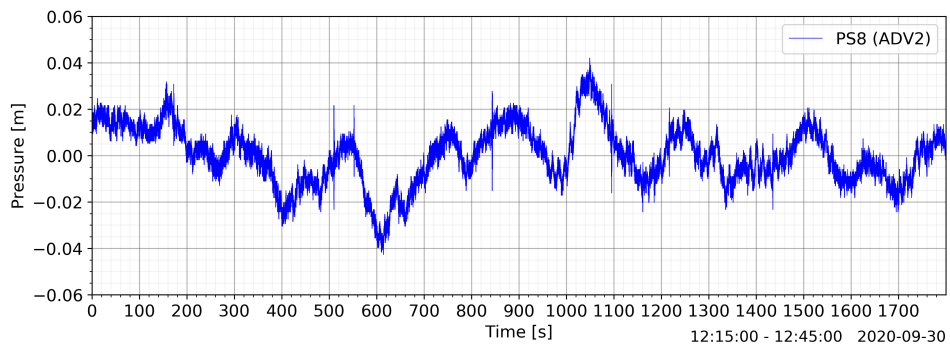
(b) Pressure sensor corresponding to ADV2 (PS8)
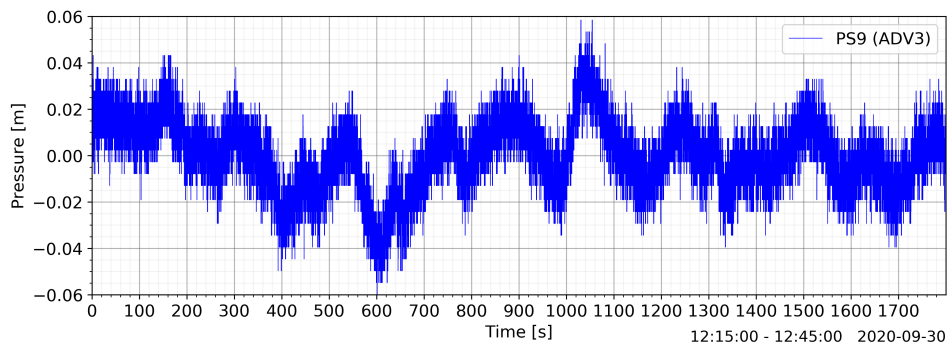
(c) Pressure sensor corresponding to ADV3 (PS9)
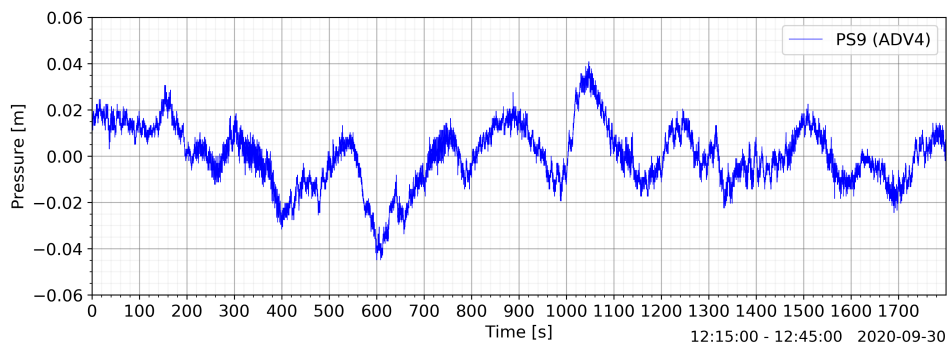
(d) Pressure sensor corresponding to ADV4 (PS9)

Figure C.19: Zero measurement Wednesday 30th of September 12:15-12:45 for ADV pressure sensors PS7 (a), PS8 (b), PS9 (c) and PS10 (d). For PS9 can be observed that the signal bandwidth is larger than for PS7 and PS8 which might be due to a disturbance of some kind.

C.7.2. Comparison flow velocity (ADV) to to pressure fluctuations (ADV)

To check the consistency between measured flow velocities and pressure fluctuations, the measured horizontal flow velocity (V_{hor}) of ADV1-4 and the pressure fluctuations (Δp) of ADV pressure sensors (PS7-10) are compared. The pressure fluctuations are converted to corresponding flow velocities according to Bernoulli (Equation C.3). Although the ADVs measured the flow velocity at a different location than the pressure (Figure 3.21), a comparison between the two could give valuable information on the relation between pressure fluctuations and flow velocities within a turbulent jet.

$$\Delta p = \frac{V_{hor}^2}{2g} \tag{C.3}$$

The pressure measurements of PS7-10 are first reduced by the hydrostatic pressure corresponding to the water depth at which the measurement frame is positioned at the bed. The pressure is averaged over 1 min before the measurements of Test 14 started, this average pressure is then subtracted from the measured pressure fluctuations during Test 14 after which the pressure fluctuations are converted to flow velocity with Equation C.3.

In Figure C.20 the time series for V_{hor} ADV1 and the velocity corresponding to the pressure fluctuations (V_p) of PS7 are plotted at 64 Hz. At 25% and 50% power a mismatch between the V_{hor} and V_p is observed. The fluctuations in V_{hor} are not represented in V_p and the average flow velocities around which V_p fluctuates are higher than for V_{hor} at 25% and 50% power. The mismatch is greater for 25% power than for 50% power. At 90% power V_{hor} and V_p match both in average velocity and fluctuation. The time series for PS8 (ADV2), PS9 (ADV3) and PS10 (ADV4) are given in Figure C.21, C.22 and C.23.
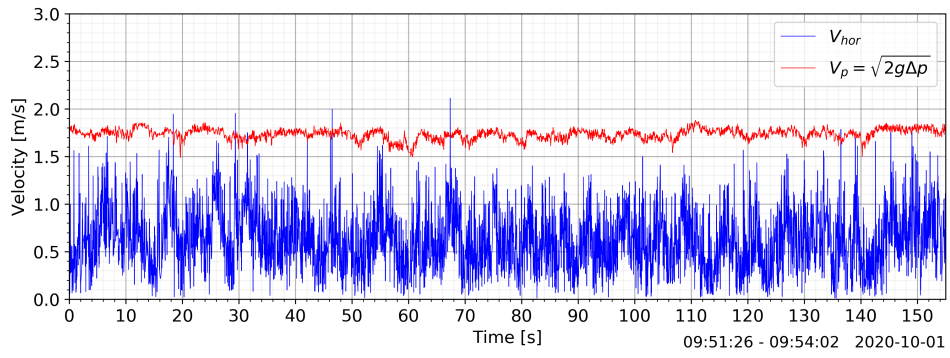
(a) ADV1 and PS7 Test 14 25% power
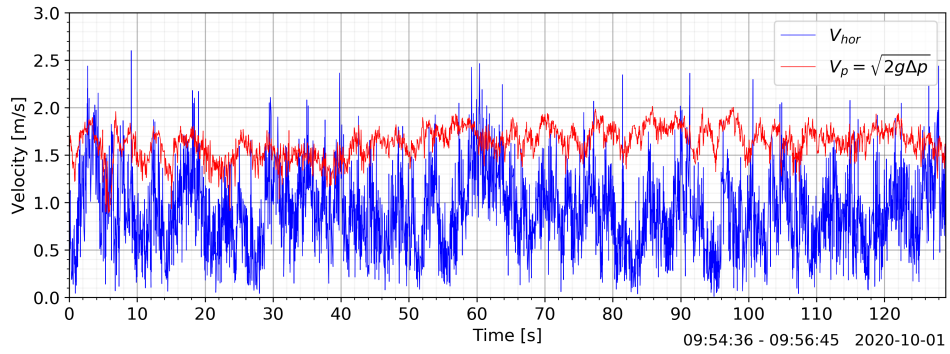
(b) ADV1 and PS7 Test 14 50% power
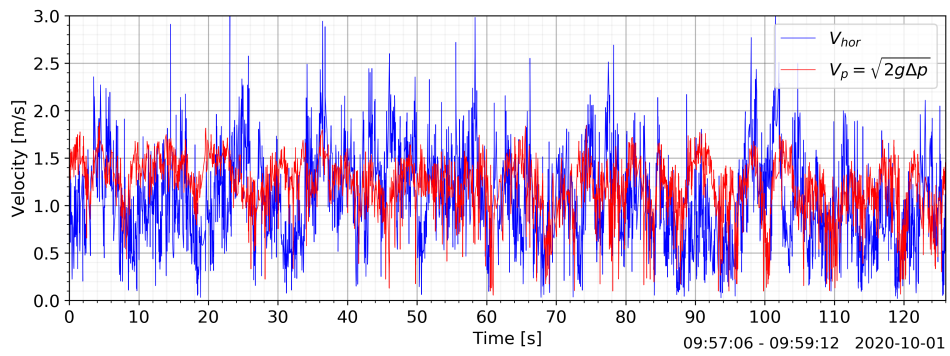
(c) ADV1 and PS7 Test 14 90% power

Figure C.20: ADV1 measured horizontal flow velocity (V_{hor}) and velocity corresponding to pressure fluctuations of PS7 (ADV1) for Test 14 power step 25% (a), 50% (b) and 90% (c).
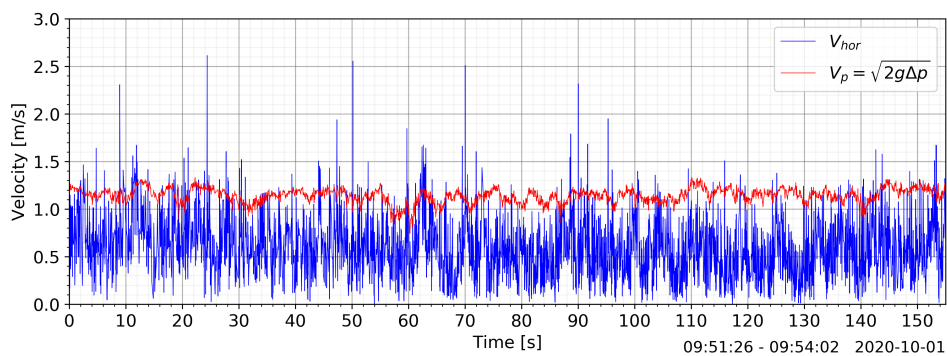
(a) ADV2 and PS8 Test 14 25% power
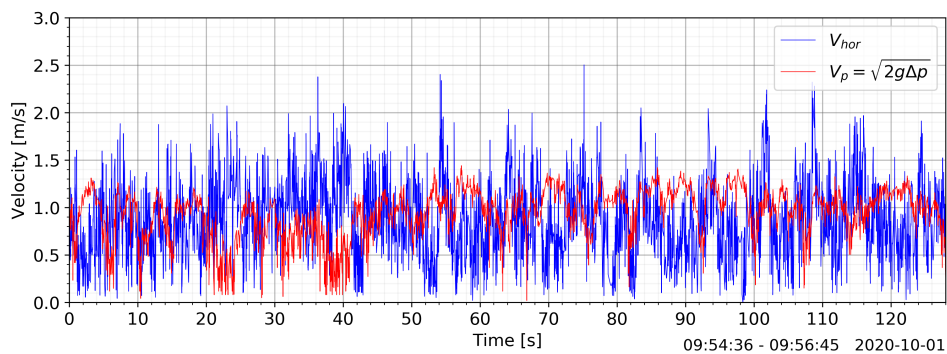
(b) ADV2 and PS8 Test 14 50% power
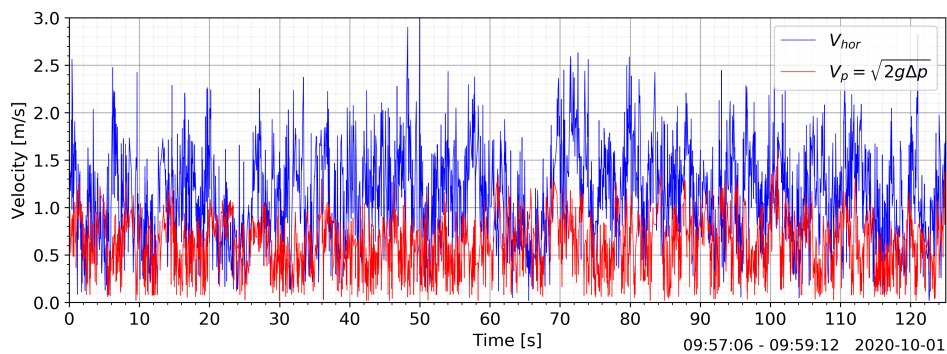
(c) ADV2 and PS8 Test 14 90% power

Figure C.21: ADV2 measured horizontal flow velocity (V_{hor}) and velocity corresponding to pressure fluctuations of PS8 (ADV2) for Test 14 power step 25% (a), 50% (b) and 90% (c).
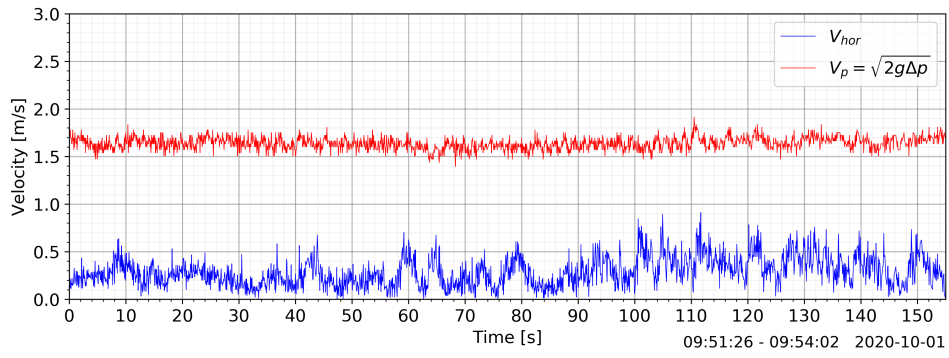
(a) ADV3 and PS9 Test 14 25% power
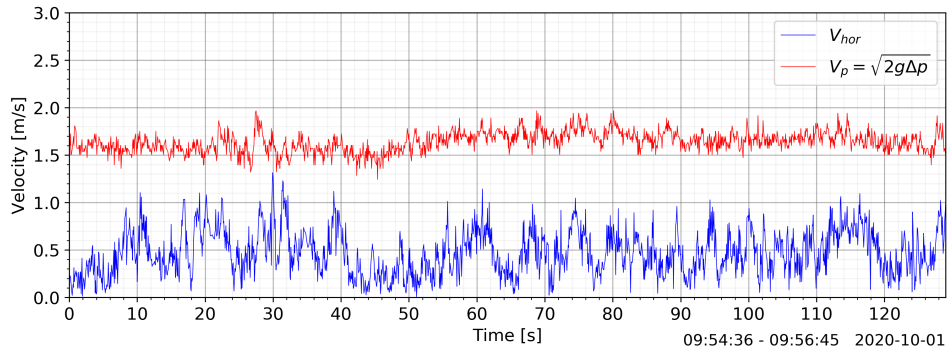
(b) ADV3 and PS9 Test 14 50% power
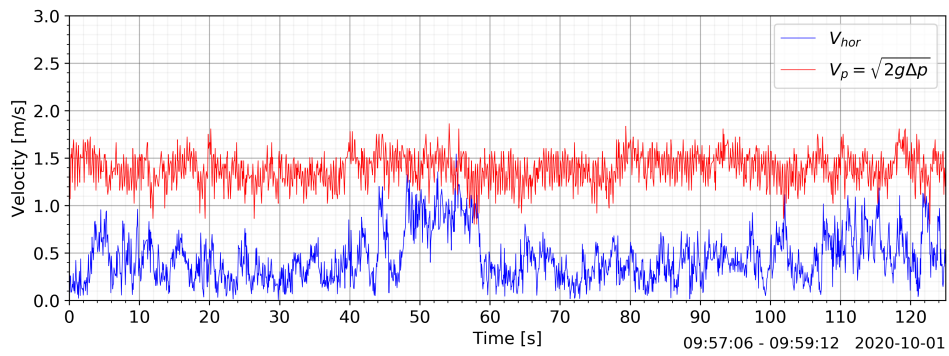
(c) ADV3 and PS9 Test 14 90% power

Figure C.22: ADV3 measured horizontal flow velocity (V_{hor}) and velocity corresponding to pressure fluctuations of PS9 (ADV3) for Test 14 power step 25% (a), 50% (b) and 90% (c).
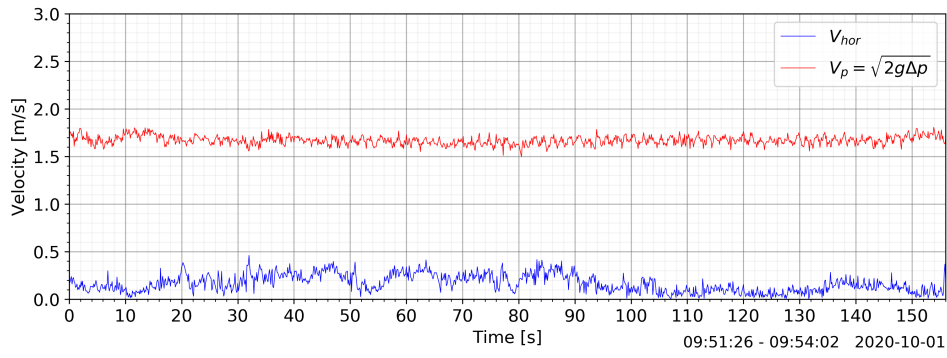
(a) ADV4 and PS10 Test 14 25% power
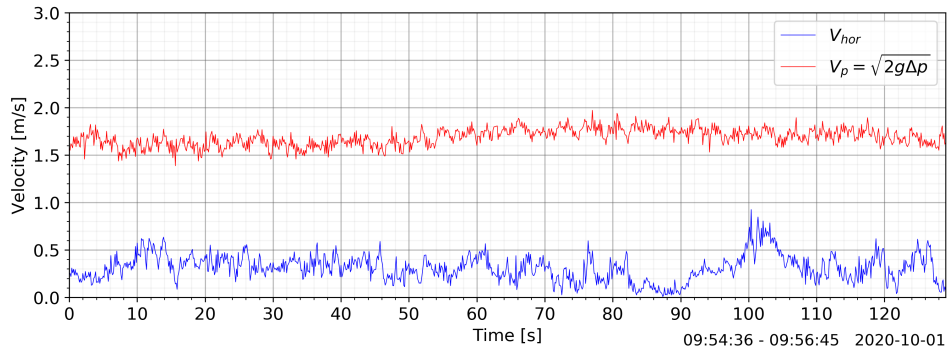
(b) ADV4 and PS10 Test 14 50% power
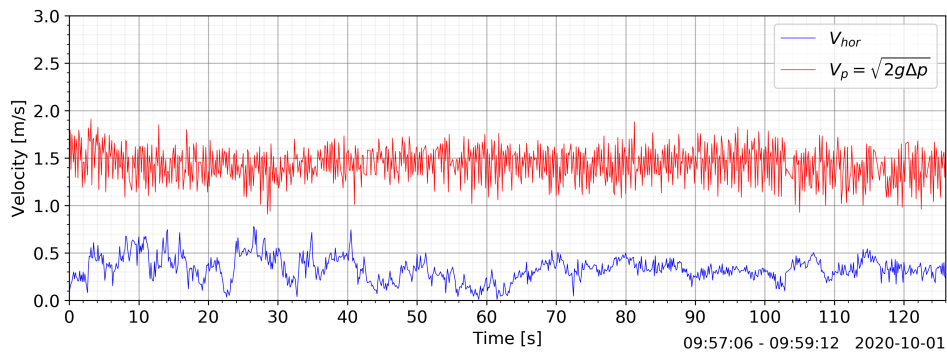
(c) ADV4 and PS10 Test 14 90% power

Figure C.23: ADV4 measured horizontal flow velocity (V_{hor}) and velocity corresponding to pressure fluctuations of PS10 (ADV4) for Test 14 power step 25% (a), 50% (b) and 90% (c).

D
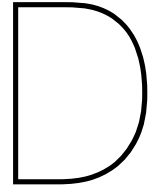
Results

In this appendix an overview is given of the results from Chapter 5. First the moored tests are listed including their characteristic parameters in Section D.1 after which the measurement points on the horizontal and vertical measurement frame are illustrated in Section D.2. Additional dimensionless plots of V_{max} are given in Section D.3. In Section D.4 the overview tables of the mean flow velocity ($\overline{V}_x$ and $\overline{V}_{hor}$), the standard deviation (σ_x and σ_{hor}), the maximum flow velocity load ($V_{x,max}$ and $V_{hor,max}$) and the relative turbulence intensity (r_x and r_{hor}) are presented for the flow in x and horizontal direction. In Section D.5 the statistical parameters of the flow in z-direction are presented. Lastly, in Section D.6 the standard deviations of the pressure sensors are listed.

D.1. Overview of the moored tests

Table D.1: Test data overview of the measurements were the Somtrans XXV was moored to the quay wall. Where L is the quay wall clearance between the port side of the vessel and the sheet pile wall, L_{BT} the quay wall clearance of BT1, BT2 or BT1&2 and y_t the distance in y-direction between the bow thruster axis and the instruments. The bow thruster axis of BT1&2 together is defined as the middle between BT1 and BT2.

Test	BT	Vessel position	L [m]	L_{BT} [m]	y_t [m]	Power step [%]
Test 1	2	1	0.8	3.09	0	25,50
Test 2	2	1	0.8	3.09	0	25,50,90
Test 3	1	1	0.8	5.61	-3.5	25,50,90
Test 4	1&2	1	0.8	4.35	-1.75	25,50,90
Test 5	2	2	0.8	3.09	2	25,90
Test 8	2	2	0.8	3.09	2	25,90
Test 9	1	2	0.8	5.61	-1.5	25,50,90
Test 10	1&2	2	0.8	4.35	0.25	25,50
Test 11	1	5	0.8	5.61	2	25,50,90
Test 12	1	4	0.8	5.61	0	25,50,90
Test 13	2	4	0.8	3.09	3.5	25,90
Test 14	1&2	4	0.8	4.35	1.75	25,50,90
Test 15	2	3	0.8	3.09	-2	90
Test 16	1&2	3	0.8	4.35	-3.75	25,50,90
Test 17	1&2	6	0.8	4.35	0	50,90
Test 18	1&2	7	3	6.55	0	50,90
Test 19	2	7	3	5.29	1.75	50,90
Test 20	1	7	3	7.81	-1.75	50,90
Test 21	1&2	8	5	8.55	0	50,90

Figure D.1: Illustration of the defined parameters listed in Table 5.1 and 5.2. Where L is the quay wall clearance between the port side of the vessel and the sheet pile wall, L_{BT1} and L_{BT2} the quay wall clearance of BT1 and BT2 and y_t the distance in y-direction between the center line of the horizontal measurement frame (the stairs used as reference line for the instruments) and the considered bow thruster axis. Where $L_{BT1\&2}$ is defined as the average value for L_{BT} of BT1 and BT2

D.2. Overview of the measurement points on the measurement frames
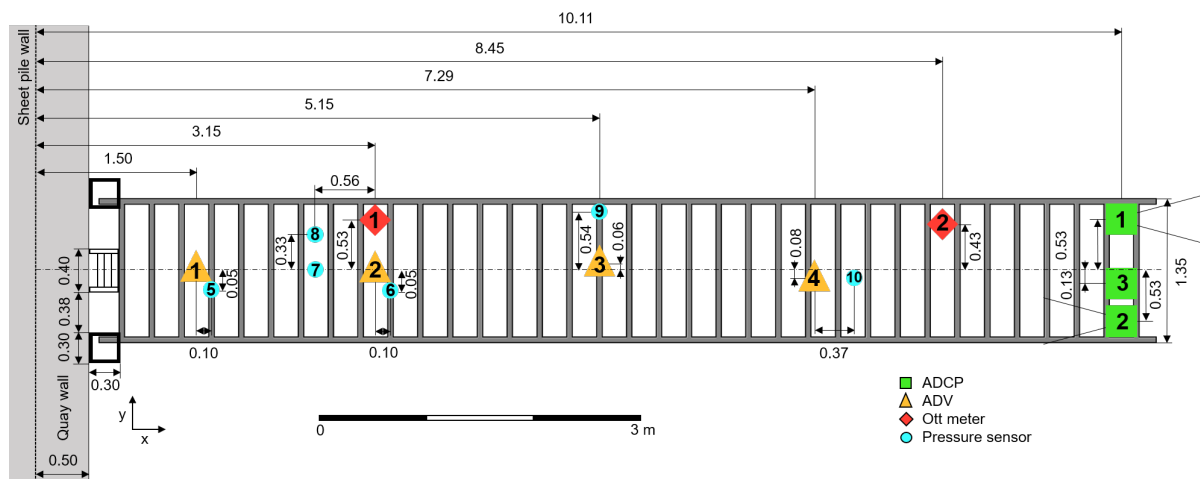
Figure D.2: Illustration of the horizontal measurement frame with respect to the quay wall aligned with the white stairs defined as the y = 0 reference line. On the measurement frame four ADVs (yellow triangles), three ADCPs (green squares), two Ott current meters (red rhombuses) and two RBR solo pressure sensors (blue circles) are mounted.

Table D.2: Overview of the measurement instruments mounted on the horizontal measurement frame including their x,y,z coordinates with respect to the reference system defined in Section 3.5.1. Distance x in D_t is defined as the dimensionless distance between the sheet pile wall and the instrument calculated by dividing the x-coordinate by the equivalent circular diameter of the bow thruster (D_t = 1.07 m)

Instrument	Sampling frequency [Hz]	x [m]	x in D_t [-]	y [m]	z [m]
ADV1	64	1.50	1.40	0	0.36
ADV2	64	3.15	2.94	0	0.36
ADV3	16	5.15	4.81	0.06	0.40
ADV4	8	7.29	6.81	-0.08	0.24
ADCP1	8	10.11	9.45	0.53	0.22
ADCP2	8	10.11	9.45	-0.53	0.22
ADCP3	16	10.11	9.45	-0.13	0.24
Ott meter 1	-	3.15	2.94	0.53	0.24
Ott meter 2	-	8.45	7.90	0.43	0.24
Pressure sensor 5 (RBR1)	2	1.60	1.50	-0.05	0.06
Pressure sensor 6 (RBR2)	2	3.25	3.04	-0.05	0.06
Pressure sensor 7 (ADV1)	64	2.59	2.42	0.33	0.07
Pressure sensor 8 (ADV2)	64	2.59	2.42	0	0.07
Pressure sensor 9 (ADV3)	16	5.15	4.81	0.54	0.07
Pressure sensor 10 (ADV4)	8	7.66	7.16	0.08	0.07

Figure D.3: Illustration of the vertical frame attached at the top to the white stairs near bollard 28 and at the bottom to the horizontal measurement frame. The center of the frame is aligned with the center of the white stairs (y=0). The water level is illustrated in blue which is approximately 6.4 m above the bed.

Table D.3: Overview of the programmable pressure sensors including their y and z coordinates with respect to the reference system defined in Section 3.5.1.

Instrument	Sampling frequency [Hz]	y [m]	z [m]
Pressure sensor 1	100	0.48	0.20
Pressure sensor 2	100	0	3.26
Pressure sensor 3	100	0	3.06
Pressure sensor 4	100	-0.48	0.20

D.3. Relative maximum flow velocity results
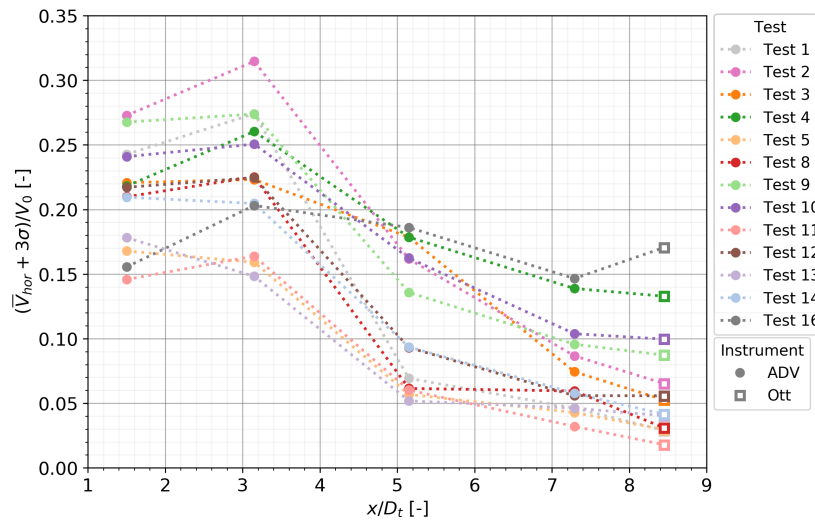
Figure D.4: Dimensionless plot of the maximum horizontal flow velocity for the moored measurement tests at 25% power. Where on the y-axis the maximum flow velocity (V_{max}) is divided by the efflux velocity (V_0) and on the x-axis the distance x from the quay wall over the bow thruster diameter (D_t)
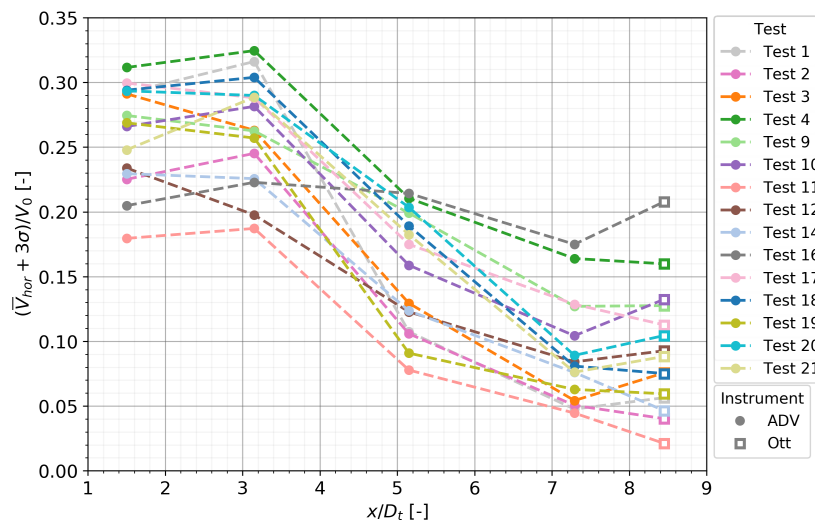
Figure D.5: Dimensionless plot of the maximum horizontal flow velocity for the moored measurement tests at 25% power. Where on the y-axis the maximum flow velocity (V_{max}) is divided by the efflux velocity (V_0) and on the x-axis the distance x from the quay wall over the bow thruster diameter (D_t)
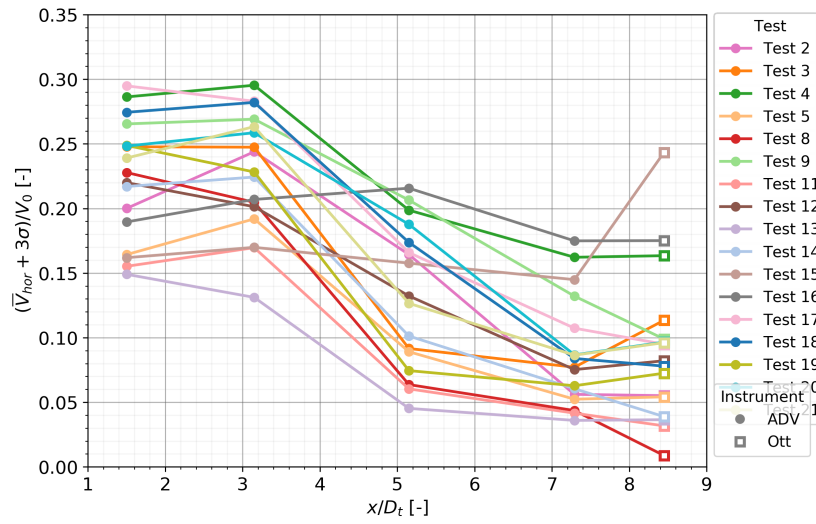
Figure D.6: Dimensionless plot of the maximum horizontal flow velocity for the moored measurement tests at 25% power. Where on the y-axis the maximum flow velocity (V_{max}) is divided by the efflux velocity (V_0) and on the x-axis the distance x from the quay wall over the bow thruster diameter (D_t)

D.4. Horizontal flow velocity statistical parameters

Table D.4: Overview of the mean flow velocities for ADV1-4 and Ott meter 1 and 2 at 25%, 50% and 90% power. For ADV1-4 both the mean flow velocity in x-direction ($\overline{V}_x$) and horizontal direction ($\overline{V}_{hor}$) are listed while Ott1 and Ott2 only measured the mean horizontal flow velocity ($\overline{V}_{hor}$).

Test	Power step	ADV1 x = 1.50 m		ADV2 x = 3.15 m		Ott1 x = 3.15 m	ADV3 x = 5.15 m		ADV4 x = 7.29 m		Ott2 x = 8.45 m
		$\overline{V}_x$ [m/s]	$\overline{V}_{hor}$ [m/s]	$\overline{V}_x$ [m/s]	$\overline{V}_{hor}$ [m/s]	$\overline{V}_{hor}$ [m/s]	$\overline{V}_x$ [m/s]	$\overline{V}_{hor}$ [m/s]	$\overline{V}_x$ [m/s]	$\overline{V}_{hor}$ [m/s]	$\overline{V}_{hor}$ [m/s]
Test 1	25%	0.4	0.51	0.5	0.6	0.41	0.13	0.17	0.06	0.1	0.07
	50%	0.64	0.77	0.63	0.81	0.75	0.21	0.27	0.08	0.13	0.15
Test 2	25%	0.45	0.57	0.54	0.66	0.52	0.27	0.32	0.1	0.13	0.12
	50%	0.42	0.54	0.47	0.61	0.65	0.2	0.26	0.08	0.13	0.12
	90%	0.44	0.61	0.62	0.79	0.68	0.37	0.43	0.15	0.21	0.24
Test 3	25%	0.32	0.5	0.43	0.53	0.52	0.36	0.42	0.1	0.15	0.1
	50%	0.46	0.77	0.59	0.7	0.72	0.21	0.32	0.1	0.15	0.18
	90%	0.47	0.8	0.76	0.89	0.83	0.18	0.3	0.13	0.23	0.32
Test 4	25%	0.6	0.77	0.99	1.04	0.92	0.48	0.56	0.39	0.45	0.53
	50%	1.09	1.4	1.47	1.54	1.39	0.78	0.88	0.58	0.69	0.71
	90%	1.16	1.55	1.57	1.66	1.78	0.94	1.04	0.69	0.81	0.9
Test 5	25%	0.21	0.37	0.29	0.39	0.32	0.1	0.14	0.06	0.1	0.08
	90%	0.3	0.51	0.45	0.63	0.58	0.26	0.36	0.11	0.21	0.2
Test 8	25%	0.24	0.41	0.33	0.45	0.37	0.11	0.16	0.09	0.14	0.08
	90%	0.49	0.71	0.6	0.72	0.68	0.09	0.26	0.14	0.19	0.06
Test 9	25%	0.44	0.57	0.45	0.56	0.61	0.25	0.31	0.11	0.2	0.16
	50%	0.53	0.73	0.57	0.69	0.9	0.52	0.59	0.23	0.3	0.33
	90%	0.61	0.86	0.77	0.91	1.1	0.74	0.81	0.32	0.43	0.34
Test 10	25%	0.79	0.87	0.85	0.93	0.82	0.41	0.47	0.21	0.28	0.28
	50%	0.96	1.07	1.11	1.21	1.09	0.53	0.63	0.27	0.34	0.51
Test 11	25%	0.19	0.32	0.24	0.35	0.19	0.09	0.14	0.05	0.08	0.06
	50%	0.31	0.47	0.36	0.49	0.35	0.13	0.24	0.06	0.14	0.07
	90%	0.32	0.51	0.48	0.61	0.5	0.13	0.24	0.11	0.19	0.16
Test 12	25%	0.3	0.43	0.32	0.44	0.36	0.15	0.2	0.08	0.12	0.14
	50%	0.41	0.56	0.32	0.49	0.46	0.25	0.32	0.13	0.22	0.3
	90%	0.5	0.68	0.44	0.61	0.54	0.33	0.41	0.14	0.26	0.38
Test 13	25%	0.21	0.33	0.18	0.3	0.16	0.07	0.16	0.02	0.13	0.15
	90%	0.35	0.49	0.27	0.44	0.18	0.12	0.23	0.04	0.16	0.2
Test 14	25%	0.51	0.63	0.49	0.6	0.43	0.21	0.28	0.1	0.16	0.16
	50%	0.76	0.9	0.73	0.87	0.69	0.38	0.47	0.16	0.31	0.23
	90%	0.81	1.04	0.96	1.13	0.88	0.34	0.44	0.19	0.33	0.29
Test 15	90%	0.33	0.49	0.35	0.56	0.75	0.46	0.54	0.3	0.4	0.99
Test 16	25%	0.33	0.49	0.5	0.63	0.6	0.51	0.59	0.35	0.43	0.65
	50%	0.5	0.75	0.63	0.8	0.9	0.74	0.85	0.58	0.68	0.98
	90%	0.55	0.87	0.78	0.99	0.96	0.94	1.04	0.78	0.9	1
Test 17	50%	1.26	1.35	1.22	1.32	1.28	0.66	0.73	0.39	0.46	0.38
	90%	1.56	1.67	1.55	1.66	1.56	0.79	0.87	0.38	0.46	0.43
Test 18	50%	1.25	1.34	1.24	1.37	1.34	0.67	0.76	0.2	0.26	0.3
	90%	1.44	1.54	1.45	1.59	1.6	0.92	1	0.24	0.36	0.38
Test 19	50%	0.58	0.71	0.58	0.73	0.74	0.18	0.24	0.12	0.16	0.17
	90%	0.64	0.8	0.66	0.79	0.8	0.17	0.24	0.14	0.19	0.32
Test 20	50%	0.72	0.83	0.81	0.92	1.01	0.52	0.59	0.14	0.24	0.29
	90%	0.79	0.89	0.9	1.01	1.2	0.68	0.75	0.2	0.29	0.4
Test 21	50%	0.97	1.09	1.16	1.31	1.34	0.56	0.67	0.2	0.29	0.38
	90%	1.08	1.23	1.34	1.5	1.59	0.43	0.58	0.3	0.43	0.58

Table D.5: Overview of the standard deviations (σ) to the mean flow velocities of ADV1-4 and Ott meter 1 and 2 at 25%, 50% and 90% power. For ADV1-4 both σ in x-direction (σ_x) and in horizontal direction (σ_{hor}) are listed while Ott1 and Ott2 only measured in horizontal direction (σ_{hor}) .

Test	Power_step	ADV1 x = 1.50 m		ADV2 x = 3.15 m		Ott1 x = 3.15 m	ADV3 x = 5.15 m		ADV4 x = 7.29 m		Ott2 x = 8.45 m
		σ_x [m/s]	σ_{hor} [m/s]	σ_x [m/s]	σ_{hor} [m/s]	σ_{hor} [m/s]	σ_x [m/s]	σ_{hor} [m/s]	σ_x [m/s]	σ_{hor} [m/s]	σ_{hor} [m/s]
Test 1	25%	0.24	0.24	0.27	0.26	0.16	0.06	0.06	0.04	0.04	0.02
	50%	0.38	0.37	0.41	0.4	0.28	0.14	0.14	0.05	0.06	0.07
Test 2	25%	0.28	0.27	0.32	0.31	0.21	0.18	0.17	0.11	0.1	0.07
	50%	0.3	0.3	0.32	0.32	0.29	0.15	0.14	0.06	0.06	0.05
	90%	0.33	0.33	0.39	0.39	0.25	0.3	0.3	0.08	0.08	0.07
Test 3	25%	0.18	0.21	0.21	0.2	0.14	0.16	0.16	0.08	0.08	0.06
	50%	0.31	0.36	0.34	0.33	0.19	0.16	0.17	0.06	0.06	0.1
	90%	0.33	0.4	0.37	0.37	0.21	0.13	0.15	0.13	0.13	0.2
Test 4	25%	0.25	0.27	0.29	0.28	0.17	0.25	0.24	0.18	0.18	0.14
	50%	0.43	0.47	0.48	0.47	0.28	0.35	0.34	0.27	0.26	0.25
	90%	0.52	0.57	0.58	0.57	0.37	0.42	0.41	0.34	0.34	0.32
Test 5	25%	0.13	0.16	0.14	0.14	0.09	0.04	0.05	0.04	0.04	0.02
	90%	0.22	0.27	0.31	0.31	0.19	0.12	0.12	0.06	0.07	0.08
Test 8	25%	0.17	0.22	0.22	0.23	0.12	0.05	0.05	0.05	0.06	0.03
	90%	0.36	0.37	0.32	0.31	0.15	0.07	0.08	0.05	0.05	0
Test 9	25%	0.27	0.26	0.28	0.28	0.21	0.14	0.13	0.1	0.1	0.09
	50%	0.36	0.34	0.34	0.33	0.29	0.25	0.23	0.18	0.17	0.16
	90%	0.44	0.42	0.44	0.42	0.36	0.3	0.28	0.24	0.21	0.15
Test 10	25%	0.3	0.29	0.3	0.29	0.21	0.24	0.23	0.17	0.16	0.15
	50%	0.47	0.44	0.46	0.45	0.33	0.28	0.27	0.2	0.2	0.23
Test 11	25%	0.12	0.14	0.15	0.16	0.12	0.05	0.06	0.03	0.03	0.01
	50%	0.21	0.22	0.23	0.24	0.11	0.07	0.09	0.04	0.05	0.02
	90%	0.21	0.24	0.26	0.25	0.15	0.07	0.08	0.05	0.05	0.03
Test 12	25%	0.21	0.23	0.22	0.23	0.16	0.1	0.09	0.04	0.05	0.05
	50%	0.3	0.31	0.24	0.26	0.24	0.16	0.15	0.08	0.1	0.1
	90%	0.37	0.36	0.33	0.34	0.3	0.23	0.22	0.1	0.11	0.09
Test 13	25%	0.16	0.19	0.12	0.15	0.03	0.02	0.03	0.02	0.03	0.02
	90%	0.22	0.24	0.18	0.21	0.06	0.04	0.04	0.03	0.04	0.03
Test 14	25%	0.29	0.29	0.29	0.29	0.13	0.13	0.13	0.07	0.08	0.05
	50%	0.4	0.39	0.4	0.39	0.28	0.23	0.22	0.1	0.12	0.06
	90%	0.46	0.48	0.48	0.47	0.31	0.25	0.24	0.1	0.12	0.05
Test 15	90%	0.25	0.27	0.25	0.27	0.28	0.26	0.24	0.25	0.25	0.32
Test 16	25%	0.19	0.21	0.29	0.28	0.22	0.24	0.25	0.2	0.21	0.19
	50%	0.3	0.37	0.42	0.41	0.34	0.36	0.36	0.29	0.3	0.3
	90%	0.35	0.43	0.49	0.45	0.32	0.48	0.47	0.35	0.36	0.33
Test 17	50%	0.47	0.45	0.44	0.43	0.31	0.3	0.28	0.23	0.23	0.21
	90%	0.57	0.56	0.53	0.52	0.35	0.35	0.34	0.26	0.25	0.22
Test 18	50%	0.46	0.44	0.48	0.46	0.28	0.34	0.32	0.15	0.16	0.13
	90%	0.55	0.53	0.55	0.54	0.36	0.33	0.32	0.16	0.2	0.17
Test 19	50%	0.35	0.34	0.31	0.3	0.18	0.11	0.11	0.07	0.08	0.07
	90%	0.4	0.4	0.36	0.35	0.23	0.11	0.12	0.09	0.1	0.09
Test 20	50%	0.37	0.35	0.33	0.31	0.25	0.26	0.24	0.1	0.11	0.13
	90%	0.39	0.37	0.37	0.36	0.29	0.27	0.25	0.12	0.13	0.13
Test 21	50%	0.41	0.38	0.45	0.43	0.3	0.34	0.33	0.12	0.13	0.14
	90%	0.52	0.49	0.52	0.5	0.43	0.29	0.29	0.16	0.18	0.17

Table D.6: Overview of the maximum flow velocity load (V_{max}) defined as $V_{max} = \overline{V} + 3\sigma$ for ADV1-4 and Ott meter 1 and 2 at 25%, 50% and 90% power. For ADV1-4 both V_{max} in x-direction ($V_{x,max}$) and in horizontal direction ($V_{hor,max}$) are listed while Ott1 and Ott2 only measured in horizontal direction ($V_{hor,max}$).

Test	Power_step	ADV1 x = 1.50 m		ADV2 x = 3.15 m		Ott1 x = 3.15 m	ADV3 x = 5.15 m		ADV4 x = 7.29 m		Ott2 x = 8.45 m
		$V_{x,max}$ [m/s]	$V_{hor,max}$ [m/s]	$V_{x,max}$	$V_{hor,max}$ [m/s]	$V_{hor,max}$ [m/s]	$V_{x,max}$	$V_{hor,max}$ [m/s]	$V_{x,max}$	$V_{hor,max}$ [m/s]	$V_{hor,max}$ [m/s]
Test 1	25%	1.13	1.23	1.31	1.39	0.9	0.3	0.35	0.17	0.24	0.15
	50%	1.77	1.86	1.86	2.02	1.6	0.64	0.69	0.23	0.3	0.36
Test 2	25%	1.29	1.39	1.5	1.6	1.14	0.82	0.82	0.42	0.44	0.33
	50%	1.32	1.44	1.43	1.57	1.52	0.65	0.68	0.27	0.32	0.26
	90%	1.43	1.61	1.8	1.96	1.43	1.27	1.32	0.38	0.45	0.44
Test 3	25%	0.88	1.12	1.07	1.13	0.93	0.83	0.91	0.35	0.38	0.27
	50%	1.4	1.86	1.61	1.68	1.29	0.69	0.83	0.29	0.35	0.48
	90%	1.46	1.99	1.88	1.99	1.46	0.56	0.74	0.53	0.62	0.91
Test 4	25%	1.34	1.57	1.84	1.87	1.43	1.23	1.28	0.94	1	0.95
	50%	2.37	2.81	2.91	2.93	2.24	1.82	1.9	1.38	1.48	1.44
	90%	2.71	3.25	3.31	3.35	2.89	2.2	2.26	1.71	1.84	1.86
Test 5	25%	0.59	0.85	0.71	0.81	0.6	0.24	0.29	0.18	0.22	0.15
	90%	0.97	1.32	1.37	1.54	1.15	0.62	0.72	0.29	0.42	0.43
Test 8	25%	0.74	1.07	0.99	1.14	0.72	0.25	0.31	0.26	0.3	0.16
	90%	1.55	1.83	1.57	1.64	1.12	0.3	0.51	0.3	0.35	0.07
Test 9	25%	1.25	1.36	1.29	1.39	1.25	0.66	0.69	0.43	0.49	0.44
	50%	1.61	1.75	1.57	1.68	1.75	1.26	1.27	0.78	0.81	0.81
	90%	1.94	2.13	2.09	2.16	2.18	1.65	1.66	1.05	1.06	0.79
Test 10	25%	1.7	1.73	1.76	1.8	1.45	1.13	1.17	0.71	0.75	0.72
	50%	2.36	2.4	2.5	2.54	2.07	1.37	1.43	0.88	0.94	1.2
Test 11	25%	0.54	0.74	0.68	0.83	0.55	0.23	0.31	0.14	0.16	0.09
	50%	0.93	1.15	1.05	1.2	0.67	0.33	0.5	0.17	0.28	0.13
	90%	0.97	1.25	1.26	1.36	0.95	0.35	0.48	0.27	0.33	0.25
Test 12	25%	0.93	1.1	0.99	1.14	0.83	0.44	0.47	0.21	0.28	0.28
	50%	1.31	1.49	1.04	1.26	1.18	0.73	0.78	0.36	0.54	0.59
	90%	1.6	1.77	1.41	1.62	1.45	1.04	1.06	0.44	0.6	0.66
Test 13	25%	0.7	0.91	0.53	0.75	0.24	0.13	0.26	0.07	0.23	0.2
	90%	1.01	1.2	0.81	1.05	0.38	0.24	0.36	0.13	0.29	0.29
Test 14	25%	1.38	1.51	1.36	1.47	0.81	0.61	0.67	0.31	0.42	0.3
	50%	1.96	2.07	1.94	2.04	1.53	1.06	1.12	0.47	0.69	0.42
	90%	2.2	2.46	2.41	2.55	1.82	1.1	1.15	0.49	0.69	0.44
Test 15	90%	1.07	1.3	1.1	1.36	1.59	1.24	1.27	1.06	1.16	1.96
Test 16	25%	0.91	1.12	1.37	1.46	1.25	1.24	1.34	0.96	1.05	1.23
	50%	1.4	1.85	1.88	2.01	1.9	1.84	1.94	1.43	1.58	1.88
	90%	1.61	2.15	2.25	2.35	1.91	2.37	2.45	1.84	1.99	1.99
Test 17	50%	2.66	2.71	2.55	2.6	2.21	1.55	1.58	1.1	1.16	1.02
	90%	3.28	3.35	3.15	3.21	2.62	1.85	1.88	1.15	1.22	1.08
Test 18	50%	2.62	2.66	2.66	2.75	2.17	1.67	1.71	0.64	0.73	0.68
	90%	3.1	3.12	3.1	3.2	2.69	1.91	1.97	0.73	0.95	0.88
Test 19	50%	1.62	1.72	1.52	1.64	1.29	0.5	0.58	0.34	0.4	0.38
	90%	1.86	2	1.74	1.83	1.49	0.51	0.6	0.4	0.5	0.58
Test 20	50%	1.84	1.87	1.79	1.85	1.75	1.3	1.3	0.43	0.57	0.67
	90%	1.95	1.99	2	2.08	2.08	1.49	1.51	0.56	0.7	0.78
Test 21	50%	2.21	2.24	2.52	2.61	2.23	1.59	1.65	0.55	0.69	0.8
	90%	2.66	2.71	2.89	2.99	2.89	1.3	1.44	0.79	0.98	1.09

Table D.7: Overview of the relative turbulence intensity r defined as the standard deviation divided by the mean flow velocity ($\sigma/\overline{V}$) for ADV1-4 and Ott meter 1 and 2 at 25%, 50% and 90% power. For ADV1-4 both r for the flow velocity in x-direction (r_x) and horizontal direction (r_{hor}) are listed.

Test	Power_step	ADV1 x = 1.50 m		ADV2 x = 3.15 m		Ott1 x = 3.15 m	ADV3 x = 5.15 m		ADV4 x = 7.29 m		Ott2 x = 8.45 m
		r_x [-]	r_{hor} [-]	r_x [-]	r_{hor} [-]	r_{hor} [-]	r_x [-]	r_{hor} [-]	r_x [-]	r_{hor} [-]	r_{hor} [-]
Test 1	25%	0.61	0.47	0.55	0.44	0.39	0.44	0.36	0.63	0.44	0.34
	50%	0.59	0.48	0.65	0.49	0.38	0.67	0.51	0.6	0.44	0.44
Test 2	25%	0.62	0.48	0.6	0.47	0.4	0.67	0.53	1.03	0.79	0.6
	50%	0.72	0.55	0.69	0.52	0.44	0.73	0.52	0.81	0.47	0.37
	90%	0.74	0.54	0.62	0.49	0.36	0.8	0.69	0.53	0.39	0.28
Test 3	25%	0.57	0.41	0.49	0.39	0.26	0.44	0.39	0.82	0.53	0.59
	50%	0.68	0.47	0.58	0.47	0.26	0.76	0.53	0.64	0.41	0.55
	90%	0.71	0.49	0.49	0.41	0.25	0.69	0.49	1.03	0.58	0.61
Test 4	25%	0.41	0.34	0.29	0.27	0.18	0.51	0.43	0.46	0.4	0.27
	50%	0.39	0.34	0.33	0.3	0.2	0.45	0.39	0.46	0.38	0.35
	90%	0.44	0.36	0.37	0.34	0.21	0.44	0.39	0.49	0.42	0.35
Test 5	25%	0.63	0.43	0.5	0.37	0.28	0.43	0.33	0.62	0.42	0.32
	90%	0.73	0.53	0.68	0.49	0.33	0.45	0.33	0.59	0.34	0.4
Test 8	25%	0.7	0.53	0.68	0.51	0.32	0.46	0.31	0.57	0.41	0.35
	90%	0.73	0.52	0.54	0.43	0.22	0.79	0.31	0.4	0.29	0.09
Test 9	25%	0.62	0.46	0.62	0.5	0.35	0.57	0.41	0.93	0.48	0.58
	50%	0.67	0.47	0.59	0.47	0.32	0.47	0.39	0.78	0.56	0.49
	90%	0.73	0.5	0.57	0.46	0.33	0.41	0.35	0.77	0.49	0.44
Test 10	25%	0.38	0.33	0.36	0.31	0.25	0.58	0.49	0.78	0.57	0.53
	50%	0.48	0.41	0.42	0.37	0.3	0.54	0.43	0.76	0.58	0.45
Test 11	25%	0.61	0.43	0.62	0.46	0.62	0.54	0.41	0.57	0.33	0.16
	50%	0.68	0.47	0.65	0.48	0.32	0.55	0.36	0.72	0.37	0.31
	90%	0.67	0.48	0.55	0.42	0.29	0.57	0.34	0.46	0.26	0.21
Test 12	25%	0.7	0.53	0.7	0.52	0.43	0.64	0.44	0.58	0.43	0.33
	50%	0.74	0.56	0.74	0.53	0.53	0.64	0.48	0.62	0.47	0.33
	90%	0.73	0.54	0.74	0.55	0.56	0.7	0.54	0.73	0.44	0.24
Test 13	25%	0.77	0.58	0.67	0.5	0.15	0.32	0.2	0.64	0.25	0.13
	90%	0.64	0.49	0.67	0.47	0.36	0.33	0.19	0.74	0.27	0.15
Test 14	25%	0.57	0.46	0.6	0.48	0.3	0.65	0.46	0.72	0.51	0.31
	50%	0.53	0.44	0.56	0.44	0.4	0.59	0.46	0.64	0.4	0.26
	90%	0.57	0.46	0.5	0.42	0.35	0.74	0.53	0.55	0.36	0.17
Test 15	90%	0.76	0.55	0.71	0.48	0.38	0.57	0.45	0.84	0.63	0.32
Test 16	25%	0.57	0.43	0.58	0.44	0.36	0.48	0.43	0.57	0.48	0.29
	50%	0.61	0.49	0.67	0.51	0.37	0.49	0.43	0.49	0.44	0.31
	90%	0.64	0.49	0.62	0.46	0.33	0.5	0.45	0.45	0.4	0.33
Test 17	50%	0.37	0.34	0.36	0.32	0.24	0.45	0.38	0.59	0.51	0.55
	90%	0.37	0.34	0.34	0.31	0.23	0.45	0.39	0.68	0.54	0.51
Test 18	50%	0.37	0.33	0.38	0.34	0.21	0.5	0.42	0.74	0.59	0.43
	90%	0.39	0.34	0.38	0.34	0.23	0.36	0.32	0.7	0.54	0.43
Test 19	50%	0.59	0.47	0.54	0.41	0.24	0.61	0.46	0.6	0.48	0.43
	90%	0.63	0.5	0.55	0.44	0.29	0.65	0.49	0.62	0.53	0.28
Test 20	50%	0.51	0.42	0.4	0.34	0.24	0.5	0.4	0.71	0.45	0.45
	90%	0.49	0.41	0.41	0.35	0.25	0.39	0.33	0.61	0.46	0.32
Test 21	50%	0.43	0.35	0.39	0.33	0.22	0.62	0.48	0.59	0.45	0.36
	90%	0.48	0.4	0.39	0.33	0.27	0.68	0.5	0.54	0.43	0.29

D.5. Vertical flow velocity statistical parameters

In Table D.8 the mean and standard deviation of the flow in the vertical z-direction is listed. The mean flow velocity is for every ADV either close to zero or in negative z-direction towards the bed.

Table D.8: Overview of the mean flow velocities and standard deviations in vertical z-direction for ADV1-4 at 25%, 50% and 90% power.

Test	Power step	ADV1 x = 1.50 m		ADV2 x = 3.15 m		ADV3 x = 5.15 m		ADV4 x = 7.29 m	
		$\overline{V}_z$ [m/s]	σ_z [m/s]	$\overline{V}_z$ [m/s]	σ_z [m/s]	$\overline{V}_z$ [m/s]	σ_z [m/s]	$\overline{V}_z$ [m/s]	σ_z [m/s]
Test 1	25%	0	0.19	-0.06	0.2	0.01	0.2	-0.01	0.07
	50%	0.02	0.26	-0.05	0.28	-0.05	0.28	0	0.07
Test 2	25%	0.02	0.21	-0.08	0.23	-0.12	0.23	-0.01	0.08
	50%	0	0.2	-0.08	0.22	-0.09	0.22	0	0.07
	90%	-0.02	0.24	-0.12	0.25	-0.08	0.25	-0.01	0.08
Test 3	25%	-0.09	0.17	-0.06	0.16	-0.15	0.16	-0.02	0.08
	50%	-0.21	0.31	-0.1	0.21	-0.09	0.21	-0.01	0.09
	90%	-0.22	0.28	-0.15	0.23	0.01	0.23	-0.03	0.12
Test 4	25%	0.06	0.24	-0.12	0.2	-0.15	0.2	0.02	0.13
	50%	-0.01	0.41	-0.17	0.33	-0.31	0.33	0.05	0.19
	90%	-0.09	0.42	-0.06	0.37	-0.42	0.37	0.07	0.25
Test 5	25%	0.01	0.14	-0.13	0.13	0.01	0.13	0	0.06
	90%	-0.03	0.22	-0.48	0.26	0.03	0.26	0.02	0.07
Test 8	25%	0.05	0.16	-0.15	0.14	-0.03	0.14	-0.01	0.08
	90%	0.1	0.33	-0.15	0.2	-0.08	0.2	0.02	0.06
Test 9	25%	-0.05	0.19	-0.08	0.16	-0.1	0.16	-0.01	0.09
	50%	-0.06	0.28	-0.08	0.25	-0.27	0.25	0	0.12
	90%	-0.13	0.33	-0.09	0.28	-0.34	0.28	-0.02	0.17
Test 10	25%	-0.07	0.25	-0.23	0.19	-0.17	0.19	0.01	0.12
	50%	-0.12	0.32	-0.36	0.31	-0.21	0.31	0.04	0.15
Test 11	25%	0.03	0.12	-0.13	0.1	-0.01	0.1	0	0.06
	50%	0.12	0.2	-0.25	0.18	-0.02	0.18	0.02	0.06
	90%	0.16	0.23	-0.28	0.18	-0.02	0.18	0.03	0.06
Test 12	25%	0	0.18	-0.02	0.17	-0.05	0.17	0	0.07
	50%	0.03	0.27	-0.03	0.23	-0.1	0.23	0.02	0.09
	90%	0.05	0.3	-0.06	0.26	-0.13	0.26	0.04	0.1
Test 13	25%	-0.05	0.1	-0.03	0.06	-0.02	0.06	0.01	0.05
	90%	-0.13	0.18	-0.27	0.17	-0.02	0.17	0.02	0.05
Test 14	25%	0.04	0.23	-0.13	0.17	-0.06	0.17	0.02	0.08
	50%	0.13	0.31	-0.19	0.3	-0.17	0.3	0.03	0.12
	90%	0	0.37	-0.29	0.37	-0.13	0.37	0.03	0.11
Test 15	90%	-0.11	0.26	-0.08	0.18	-0.19	0.18	0.02	0.19
Test 16	25%	-0.15	0.18	-0.09	0.23	-0.23	0.23	0.01	0.15
	50%	-0.25	0.28	-0.1	0.33	-0.34	0.33	0.02	0.23
	90%	-0.29	0.31	-0.13	0.42	-0.56	0.42	0.03	0.26
Test 17	50%	-0.1	0.37	-0.34	0.29	-0.35	0.29	0.01	0.17
	90%	-0.16	0.46	-0.42	0.35	-0.41	0.35	0.03	0.2
Test 18	50%	-0.23	0.38	-0.22	0.33	-0.35	0.33	0.04	0.14
	90%	-0.23	0.43	-0.16	0.4	-0.48	0.4	0.07	0.19
Test 19	50%	-0.22	0.3	-0.16	0.22	-0.03	0.22	0	0.08
	90%	-0.28	0.32	-0.13	0.26	-0.04	0.26	0.02	0.08
Test 20	50%	-0.16	0.29	-0.11	0.23	-0.3	0.23	-0.03	0.12
	90%	-0.17	0.3	-0.08	0.26	-0.42	0.26	0.07	0.16
Test 21	50%	-0.24	0.38	-0.08	0.36	-0.34	0.36	0.03	0.14
	90%	-0.39	0.47	-0.06	0.45	-0.24	0.45	0.06	0.16

D.6. Pressure sensors standard deviation

Table D.9: Overview of the standard deviations (σ) for PS1-4 (high frequency pressure sensors) and PS7-10 (ADV pressure sensors) at 25%, 50% and 90% power.

Test	Power step	σ_{PS1}[m]	σ_{PS2}[m]	σ_{PS3}[m]	σ_{PS4}[m]	σ_{PS7}[m]	σ_{PS8}[m]	σ_{PS9}[m]	σ_{PS10}[m]
Test 1	25%	0.039	0.27	0.254	0.039	0.021	0.018	0.017	0.015
	50%	0.068	0.504	0.422	0.064	0.027	0.023	0.018	0.016
Test 2	25%	0.034	0.268	0.24	0.037	0.012	0.01	0.011	0.007
	50%	0.049	0.496	0.544	0.048	0.02	0.021	0.013	0.011
	90%	0.1	0.786	0.779	0.104	0.031	0.023	0.016	0.017
Test 3	25%	-	-	-	-	0.017	0.015	0.018	0.016
	50%	-	-	-	-	0.021	0.022	0.025	0.021
	90%	-	-	-	-	0.016	0.021	0.028	0.024
Test 4	25%	-	-	-	-	0.022	0.02	0.028	0.023
	50%	-	-	-	-	0.023	0.021	0.04	0.025
	90%	-	-	-	-	0.037	0.037	0.047	0.038
Test 5	25%	-	-	-	-	0.008	0.007	0.011	0.008
	90%	-	-	-	-	0.026	0.021	0.016	0.016
Test 8	25%	-	-	-	-	0.013	0.01	0.013	0.011
	90%	-	-	-	-	0.017	0.015	0.016	0.015
Test 9	25%	-	-	-	-	0.02	0.018	0.022	0.021
	50%	-	-	-	-	0.018	0.02	0.027	0.015
	90%	-	-	-	-	0.029	0.029	0.05	0.038
Test 10	25%	-	-	-	-	0.016	0.014	0.019	0.014
	50%	-	-	-	-	0.02	0.019	0.031	0.014
Test 11	25%	0.011	0.015	0.014	0.019	0.008	0.007	0.011	0.009
	50%	0.019	0.023	0.024	0.035	0.012	0.009	0.012	0.01
	90%	0.025	0.042	0.039	0.055	0.016	0.013	0.016	0.019
Test 12	25%	0.021	0.136	0.14	0.024	0.011	0.01	0.012	0.011
	50%	0.048	0.319	0.312	0.055	0.016	0.015	0.01	0.011
	90%	0.067	0.483	0.486	0.086	0.024	0.023	0.021	0.023
Test 13	25%	0.015	0.013	0.012	0.017	0.007	0.006	0.009	0.007
	90%	0.019	0.022	0.023	0.033	0.014	0.012	0.014	0.015
Test 14	25%	0.022	0.119	0.129	0.027	0.009	0.009	0.011	0.008
	50%	0.052	0.29	0.289	0.062	0.026	0.023	0.018	0.016
	90%	0.071	0.394	0.413	0.098	0.034	0.03	0.023	0.025
Test 15	90%	0.053	0.028	0.03	0.045	0.017	0.018	0.034	0.027
Test 16	25%	0.021	0.012	0.011	0.015	0.009	0.008	0.016	0.012
	50%	0.05	0.021	0.022	0.028	0.022	0.022	0.037	0.03
	90%	0.062	0.032	0.034	0.038	0.026	0.022	0.064	0.039
Test 17	50%	0.05	0.132	0.116	0.067	0.025	0.023	0.04	0.022
	90%	0.066	0.2	0.188	0.103	0.033	0.031	0.056	0.033
Test 18	50%	0.039	0.097	0.103	0.06	0.022	0.02	0.029	0.012
	90%	0.052	0.142	0.145	0.086	0.029	0.027	0.042	0.028
Test 19	50%	0.021	0.049	0.048	0.051	0.011	0.01	0.011	0.008
	90%	0.03	0.077	0.077	0.074	0.019	0.016	0.012	0.01
Test 20	50%	0.034	0.076	0.071	0.033	0.013	0.014	0.027	0.011
	90%	0.046	0.097	0.094	0.051	0.022	0.022	0.045	0.041
Test 21	50%	0.038	0.081	0.082	0.049	0.029	0.026	0.032	0.016
	90%	0.058	0.128	0.135	0.084	0.053	0.047	0.048	0.044

E
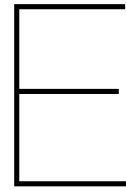
Free flow set-up

In Figure E.1 an overview of the free flow measurement frame attached to the back of a smaller vessel is illustrated. The same measurement instruments are used for the free flow measurements as for the measurements of the near-bed flow velocity. In Figure E.2 the cross-sectional view of the free flow measurement set-up is illustrated. In the set-up the bow of the smaller vessel was placed near the bow thruster outlet to measure the efflux velocity of the free bow thruster jet. However, during the measurements with 25% power the vessel could not be kept in a constant position with respect to the Somtrans XXV. Therefore, the measurements were nut further conducted. A new better set-up which should be thought of which can place the measurement instruments at a stable location with respect to the bow thruster outlet.
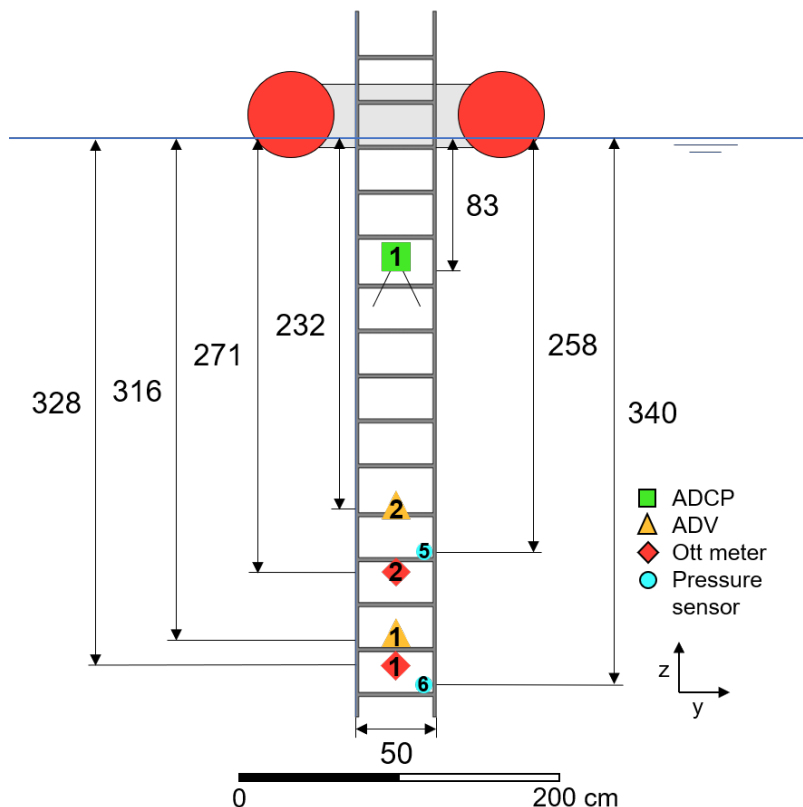

Figure E.1: Illustration of the measurement frame for the free flow measurements attached to the back of the smaller vessel.
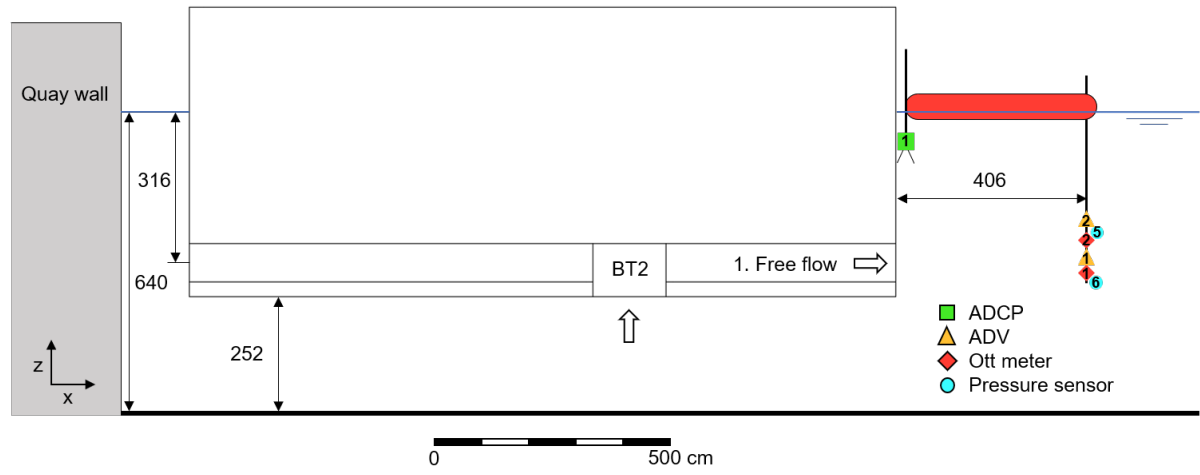
Figure E.2: Cross-section of the Somtrans XXV with the smaller vessel including the free flow measurement frame near the out flow point of the bow thruster jet.

Bibliography

Albertson, M., Dai, Y., Jensen, R., and Rouse, H. (1950). Diffusion of submerged jets. *Transcript of the A.S.C.E.*, Paper No.2409, 115, 639-697.

BAW (2010). BAW Code of Practice: Principles for the Design of Bank and Bottom Protection for Inland Waterways (GBB). *Federal Waterways Engineering and Research Institute,Karlsruhe*.

Berger, W., FelKel, K., Hager, M., Oebius, H., and Schale, E. (1985). Courant provoque par les bateaux protection des berges et solution pour eviter l'erosion du lit du Haut Rhin. *Proceedings of the 25th Congress on P.I.A.N.C., Edinburgh, 1981, Section I-1.*

Bergh, H. and Cederwall, K. (1981). Propeller Erosion in Harbours. *Bulletin No. TRITA-VBI-107.* Hydraulics Laboratory, Royal Institute of Technology, Stockholm ,Sweden.

Bevel, P. (2010). The fourier transform. Retrieved from `https://www.thefouriertransform.com/`.

Blaauw, H. and van de Kaa, E. (1978). Erosion of bottom and sloping banks caused by the screw race of manoeuvring ships. *Publ.no.202.*

Blokland, T. (1996). Bodembeschermingen belast door schroefstralen. Huidige ontwerpmethodiek. *Gemeentewerken Rotterdam, Ingenieursbureau havenwerken, Rapport 61.00-R94.038.*

Bok, A. (1996). De stabiliteit van de bodembescherming voor een kademuur bij het gebruik van boegschroeven. Master's thesis, TU Delft.

Calizo Manaois, J. (2011). Pumpjets in de binnenvaart. Master's thesis, TU Delft.

Cantoni, I. (2020). Bowthruster-induced flow on the bottom of a vertical quay wall. Master's thesis, TU Delft.

CIRIA, CUR, CETMEF (2007). "the rock manual. the use of rock in hydraulic engineering" (2nd edition). *Manual on the Use of Rock.*

De Jong, M. and Van Velzen, G. (2015). Propeller jets, knowledge gap 7. Deltares.

Durgesh, V., Thomson, J., Richmond, M., and Polagye, B. (2014). Noise correction of turbulent spectra obtained from acoustic doppler velocimeters. *Flow Measurement and Instrumentation Volume 37, 29–41, ISSN 0955-5986.*

Fuehrer, M., Pohl, H., and Römisch, K. (1987). Propeller jet erosion and stability criteria for bottom protection of various constructions. *Proceedings of P.I.A.N.C.,Bulletin No. 58, 1987.* Edinburgh.

Fuehrer, M. and Römisch, K. (1977). Effects of modern ship traffic on inland and ocean waterways and their structures. *PIANC 24th congress*, section 1-3.

Fuehrer, M., Römisch, K., and Engelke, G. (1981). Criteria for dimensioning the bottom and slope protections and for applying the new methods of protecting navigation canals. *PIANC XXVth Congress*. Edinburgh.

Goring, D. and Nikora, V. (2002). Despiking acoustic doppler velocimeter data. *Journal of Hydraulic Engineering-asce - J HYDRAUL ENG-ASCE*, 128.

Hamill, G. (1987). Characteristics of the screw wash of a manoeuvring ship and the resulting bed scour. *Thesis submitted to the Queen's University of Belfast for the degree of Doctor of Philosophy.*

Hamill, G., McGarvey, J., and Hughes, D. (2003). Determination of the efflux velocity from a ship's propeller. *Maritime Engineering 157 Issue MA2*.

Hamill, G. A. and Kee, C. (2016). Predicting axial velocity profiles within a diffusing marine propeller jet. *Ocean Engineering*, 124:104–112.

Hoffmans, G. and Verheij, H. (2011). Jet scour. *Maritime Engineering Vol 164*.

Holthuijsen, L.H. (2007). Waves in oceanic and coastal waters. *Delft University of Technology and UNESCO-IHE*.

Huang, C., Qiao, F., and Ma, H. (2020). Noise reduction of acoustic doppler velocimeter data based on kalman filtering and autoregressive moving average models. *Acta Oceanol. Sin. 39, 106–113*, 128.

Jirafe, N. (2019). How to filter noise with a low pass filter — python. Retrieved from `https://docs.scipy.org/doc/scipy/reference/generated/scipy.signal.butter.html`.

Katopodes, N. (2019). Chapter 8 - turbulent flow. *Free-Surface Flow,Butterworth-Heinemann*, 128:566–650.

Kolmogorov, A. (1941). The local structure of turbulence in incompressible viscous fluid for very large reynolds numbers. *In Dokl. Akad. Nauk SSSR, vol. 30, no. 4, pp. 299-303*.

Lam, W., Hamil, G. A., Song, Y. C., Robinson, D. J., and Raghunathan, S. (2011a). A review of the equations used to predict the velocity distribution within a ship's propeller jet.

Lam, W., Hamil, G. A., Song, Y. C., Robinson, D. J., and Raghunathan, S. (2011b). A review of the equations used to predict the velocity distribution within a ship's propeller jet. *Ocean Engineering*, 38(1):1–10.

Lindner, B. (2021). Doppler effect. Retrieved from `https://www.natuurkunde.nl/artikelen/1540/toepassingen-van-dopplereffect`. Natuurkunde.

Looye, N. (2021). Schaalvergroting Binnenvaart. *Rijkswaterstaat*.

Maklin, C. (2019). Fast fourier transform. Retrieved from `https://towardsdatascience.com/fast-fourier-transform-937926e591cb`.

Matplotlib (2021). Boxplot. Retrieved from `https://matplotlib.org/3.1.1/api/_as_gen/matplotlib.pyplot.boxplot.html`.

NI (2021). Understanding ffts and windowing. Retrieved from `https://www.ni.com/nl-nl/innovations/white-papers/06/understanding-ffts-and-windowing.html`.

Nielsen, B. (2005). Bowthruster-Induced Damage: A physical model study on bowthruster-induced flow. Master's thesis, TU Delft.

Nortek Manuals (2005). Vector current meter. Nortek AS.

Nortek Manuals (2018a). The comprehensive manual for velocimeters. Nortek AS.

Nortek Manuals (2018b). Signature operations. Nortek AS.

Nortek Manuals (2018c). Signature principles of operation. Nortek AS.

Nortek Manuals (2018d). The Comprehensive Manual for ADCPs. Nortek AS.

OECD (2015). The impact of mega-ships.

O'Reilly (2021). Frequency and the fast fourier transform. Retrieved from `https://learning-oreilly-com.tudelft.idm.oclc.org/library/view/elegant-scipy/9781491922927/ch04.html`.

OTT-HydroMet (2021). Ott c31. Retrieved from `https://www.ott.com/products/water-flow-3/ott-c31-958/`.

Panteia (2017). Middenllange termijn prognoses voor de binnenvaart.

Patwardhan, S. and Ramesh, O. (2014). Scaling of pressure spectrum in turbulent boundary layers. *J. Phys.: Conf. Ser. 506 012011*.

PIANC (2015). Guidelines for protecting berthing structures from scour caused by ships. *Report No. 180*. ISBN 9782872232239.

RBR (2021). Rbrsolo3 depth logger. Retrieved from `https://rbr-global.com/products/compact-loggers/rbrsolo-d`.

Roubos, A. and Verhagen, H. (2007). Uncertainties in the design of bed protections near quay walls. *4th International Conference Port Development and Coastal Environment: PDCE 2007, 25-27 September 2007, Varna, Bulgaria*.

Römisch, K. (1975). Der Propellerstrahl als erodierendes Element bei An- unde Ablegemanövern im Hafenbecken. *Seewirtschaft,7,7,S. 431-434*.

Schiereck, G. and Verhagen, H. (2016). Introduction to bed, bank and shore protection. *Delft Academic Press*.

Schmidt, E. (1998). Ausbreitungsverhalten und Erosionswirkung eines Bugpropellerstrahls vor einer Kaiwand. *Dissertation am Leichtweiss-Institut für Wasserbau der Technischen Universität Braunschweig*.

SciPy (2021a). Scipy documentation: Butterworth filter. Retrieved from `https://docs.scipy.org/doc/scipy/reference/generated/scipy.signal.butter.html`.

SciPy (2021b). Scipy documentation: Hann window. Retrieved from `https://docs.scipy.org/doc/scipy/reference/generated/scipy.signal.windows.hann.html`.

SciPy (2021c). Scipy documentation: Simpson rule. Retrieved from `https://docs.scipy.org/doc/scipy/reference/generated/scipy.integrate.simpson.html`.

STS-sensors (2018). Programmable submersible level transmitters: Ptm/n - programmable 4-20 ma.

UNCTAD (2020). Review of maritime transport 2019. Retrieved from `https://unctad.org/webflyer/review-maritime-transport-2020`.

Van Blaaderen, E. (2005). Modelling bowthruster induced flow near a quay wall. Master's thesis, TU Delft.

Van der Hout, A. (2017). Verkenning schroefstraalbelastingen. Deltares.

Van der Hout, A. (2018). Veldmetingen schroefstraalbelastingen. Deltares.

van der Laan, T. (2005). Het ontwikkelen van een model voor boegschroefstralen bij verticale kademuren. Master's thesis, TU Delft.

Van der Vorm, C. (2020). Roadmap bottom protection design.

Van Manen, J. (1956). Recent research on propellers in nozzles. *NSP, Publication 136*. Wageningen, The Netherlands.

Verhagen, H. (2001). Bowthruster and the stability of a riprap revetment. *Section of Hudraulic Engineering, Delft University of Technology, Netherlands*.

Verheij, H. (1983). The stability of bottom and banks subjected to the velocities in the propeller jet behind ships. *8th Int. Harbour Congress, Antwerp*.

Verheij, H. (1985). Propeller jets and bed stability. *Report M1115 parts VI and Xa, Deltares, Delft*.

Verheij, H. (2020). Overview relevant formulas propeller induced flow velocities and impact on bed material. *Unpublished memo based on PIANC report 180*.

Veth propulsion (2020). Veth jet. Retrieved from `https://www.vethpropulsion.com/products/bow-thrusters/veth-jet/`.

Wei, M. and Chiew, Y. M. (2019). Impingement of propeller jet on a vertical quay wall. *Ocean Engineering*, 183:73–86.

Welch, P. (1967). The use of the fast fourier transform for the estimation of power spectra: A method based on time averaging over short, modified periodograms. *IEEE Trans. Audio Electroacoust. vol. 15, pp. 70-73*.

WHOI (2020). Acoustic Doppler Current Profiler (ADCP). Retrieved from `https://www.whoi.edu/what-we-do/explore/instruments/instruments-sensors-samplers/acoustic-doppler-current-profiler-adcp/`. Woods Hole Oceanographic Institution.

WL (1985). Aantasting van dwarsprofielen van vaarwegen.Schroefstralen en de stabiliteit van bodem en oevers onder invloed van de stroomsnelheden in de schroefstraal. *Waterloopkundig Laboratorium, M1115, deel VII en Xa*.

Wright, D. (2021). Emperical rule. Retrieved from `https://www.drdawnwright.com/empirical-rule-and-z-score-probability/`.